Untersuchungen zum Katalysemechanismus von Methyl-Coenzym M Reduktase (MCR) aus methanogenen Archaea

DISSERTATION

zur

Erlangung des Doktorgrades

der Naturwissenschaften

(Dr. rer. nat.)

dem

Fachbereich Biologie

der Philipps-Universität Marburg/Lahn

vorgelegt von

Meike Goenrich

aus Hanau

Marburg/Lahn, September 2004

Die Untersuchungen zur vorliegenden Arbeit wurden von Oktober 2001 bis September 2004 am Max-Planck-Institut für terrestrische Mikrobiologie unter der Leitung von Professor Dr. R. K. Thauer durchgeführt.

Vom Fachbereich Biologie der Philipps-Universität Marburg als Dissertation angenommen am:

29. September 2004

Tag der mündlichen Prüfung: **19. November 2004**

Erstgutachter: Professor Dr. R. K. Thauer

Zweitgutachter: Professor Dr. W. Buckel

Die in dieser Dissertation beschriebenen Ergebnisse wurden in folgenden Originalpublikationen veröffentlicht:

Goenrich M, Mahlert F, Duin EC, Bauer C, Jaun B, Thauer RK (2004) Probing the reactivity of Ni in the active site of methyl-coenzyme M reductase with substrate analogues. J Biol Inorg Chem **im Druck**

Goenrich M, Duin EC, Mahlert F, Thauer RK (2004) Temperature dependence of methyl-coenzyme M reductase (MCR) activity and of the formation of the MCR-red2 state induced by coenzyme B. J Biol Inorg Chem **eingereicht**

Finazzo C, Harmer J, Bauer C, Jaun B, Duin EC, Mahlert F, Goenrich M, Thauer RK, Van Doorslear S, Schweiger A (2003) Coenzyme B induced coordination of coenzyme M via its thiol group to Ni(I) of F_{430} in active methyl-coenzyme M reductase. J Am Chem Soc **125**(17):4988-4989

Duin EC, Signor L, Piskorski R, Mahlert F, Clay MD, Goenrich M, Thauer RK, Jaun B, Johnson MK (2004) Spectroscopic investigation of the nickel-containing porphinoid cofactor F_{430}. Comparison of the free cofactor in the +1, +2 and +3 oxidation states with the cofactor bound to methyl-coenzyme M reductase in the silent, red and ox forms. J Biol Inorg Chem **9**:563-576

Weitere Ergebnisse zu Nebenprojekten, die in dieser Dissertation nicht aufgegriffen wurden, sind in folgenden Publikationen veröffentlicht worden:

Goenrich M, Bartoschek S, Hagemeier CH, Griesinger C, Vorholt JA (2001) A glutathione-dependent formaldehyde activating enzyme Gfa from *Paracoccus denitrificans* detected and purified via 2D proton exchange NMR spectroscopy. J Biol Chem **277**(5): 3069-3072

Goenrich M, Bursy J, Hübner E, Linder D, Schwartz AC, Vorholt JA (2001) The methylene tetrahydromethanopterin dehydrogenase MtdB and the methylene tetrahydrofolate dehydrogenase FolD from *Hyphomicrobium zavarzinii* ZV580. Arch Microbiol **177**(4): 299-303

Acharya P, Goenrich M, Hagemeier CH, Demmer U, Vorholt JA, Thauer RK, Ermler U (2004) How an enzyme binds the C_1-carrier tetrahydromethanopterin: Structure of the tetrahydromethanopterin-dependent formaldehyde-activating enzyme Fae from *Methylobacterium extorquens* AM1. EMBO J **eingereicht**

Once you have tasted the secrets,
you will have a strong desire
to understand them.

William Eamon
aus: “Science and the Secrets of Nature”

Für meine Familie

Inhaltsverzeichnis

Abkürzungsverzeichnis

BES	2-Bromoethansulfonat
BPS	3-Bromopropansulfonat
CH_3-S-CoM	2-(Methylthio)ethansulfonat; Methyl-Coenzym M
CoM-S-S-CoB	Heterodisulfid aus 2-Mercaptoethansulfonat und 7-Mercapto-N-heptanoyl-O-phospho-L-threonin
EPR	Elektronenparamagnetische Resonanz
F_{430}	Faktor 430
F_{430}M	Pentamethylester von Faktor 430
FPLC	Fast protein liquid chromatography
HS-CoB	7-Mercapto-N-heptanoyl-O-phospho-L-threonin; Coenzym B
HS-CoM	2-Mercaptoethansulfonat; Coenzym M
MCD	Magnetischer zirkularer Dichroismus
MCR	Methyl-Coenzym M Reduktase
MCR-BPS	MCR mit dem EPR-Signal BPS
MCR-ox	MCR mit den EPR-Signalen ox1, ox2 und/oder ox3
MCR-ox1	MCR mit dem EPR-Signal ox1
MCR-ox2	MCR mit dem EPR-Signal ox2
MCR-ox3	MCR mit dem EPR-Signal ox3
MCR-red1	MCR mit den EPR-Signalen red1a, red1c und/oder red1m
MCR-red1a	MCR-red1c oder MCR-red1m nach Ultrafiltration in Abwesenheit von Coenzym M oder Methyl-Coenzym M
MCR-red1c	MCR-red1 in Gegenwart von Coenzym M
MCR-red1m	MCR-red1 in Gegenwart von Methyl-Coenzym M
MCR-red1/2	MCR mit den EPR-Signalen red1 und red2
MCR-red2	MCR mit dem EPR-Signal red2
OD_x	Optische Dichte bei der Wellenlänge x nm
Q_{10}	Faktor, mit dem die Rate ansteigt, wenn die Temperatur um 10°C zunimmt
U	Unit = µmol Umsatz x min^{-1}

I Zusammenfassung

Die Bildung von Methan erfolgt in allen methanogenen Archeaen durch die Reduktion von Methyl-Coenzym M (CH_3-S-CoM) mit Coenzym B (HS-CoB) zu CH_4 und dem Heterodisulfid CoM-S-S-CoB. Diese Reaktion, die mit Umkehr der Stereokonfiguration der Methylgruppe erfolgt, wird in einem ternären Komplex-Mechanismus von Methyl-Coenzym M Reduktase (MCR) katalysiert. Das sauerstofflabile Enzym ist aus drei verschiedenen Untereinheiten zusammengesetzt, die in einem $\alpha_2\beta_2\gamma_2$ Hexamer angeordnet sind und zwei strukturell verknüpfte aktive Zentren ausbilden, in denen je ein Molekül des Nickelporphinoids Faktors F_{430} als prosthetische Gruppe wirkt. Im aktiven Enzym befindet sich F_{430} in der Oxidationsstufe Ni(I) und läßt sich durch seine paramagnetische Eigenschaft mittels Elektronenparamagnetischer Resonanz (EPR)-Spektroskopie detektieren. Derzeit lassen sich für MCR fünf EPR-aktive und zwei EPR-inaktive (silent) Zustände definieren: die enzymatisch aktiven Zustände MCR-red1 und MCR-red2, sowie die enzymatisch inaktiven Zustände MCR-ox1, MCR-ox2, MCR-ox3, MCR-ox1-silent und MCR-silent. Von den beiden Ni(II)-Formen ohne EPR Signal (MCR-ox1-silent und MCR-silent) liegen detaillierte Kristallstrukturen vor, die zusammen mit biochemischen Eigenschaften zur Formulierung von zwei alternativen Katalysemechanismen geführt haben: Mechanismus I favorisiert einen nukleophilen Angriff von Ni(I) auf die Methylgruppe von CH_3-S-CoM, was zur Bildung einer Methyl-Ni(III)F_{430}-Zwischenstufe führt. Dagegen postuliert Mechanismus II die Entstehung eines Methylradikals aufgrund eines Angriffs von Ni(I) auf den Thioetherschwefel von CH_3-S-CoM.

In der vorliegenden Arbeit wurde die Wirkung von Methyl-Coenzym M- und Coenzym B-Substratanaloga auf die enzymatische Akivität und den Nickel-Redoxzustand von MCR untersucht, um tiefere Einblicke in den Katalysemechanismus dieses Enzyms zu erhalten. Neben Aktivitätsmessungen wurden dazu im wesentlichen EPR-spektroskopische Untersuchungen durchgeführt.

Analoga des Substrats CH_3-S-CoM wurden aufgrund ihrer Wirkung in drei Gruppen unterteilt: (i) Reversible Inhibitoren wie Ethyl-Coenzym M, Propyl-Coenzym M, Allyl-Coenzym M und Coenzym M (HS-CoM), in deren Gegenwart der Ni(I)-Zustand erhalten blieb. Von den vier Inhibitoren wurde nur Ethyl-Coenzym M reduziert, allerdings mit einer katalytischen Effizienz, die geringer als 1% der Effizienz mit Methyl-Coenzym M war; (ii) Irreversible Inhibitoren wie 2-Bromoethansulfonat, 3-Bromopropionat, Cyano-Coenzym M, Seleno-Coenzym M und Trifluoromethyl-Coenzym M, die nach Zugabe zu aktiver MCR das Ni(I)-EPR-Signal auslöschten und bei Anwesenheit von HS-CoB zur Induktion eines isotropen

Radikalsignals führten. Die Reaktivität des Ni(I)-Zustandes gegenüber dieser Gruppe von Inhibitoren wurde in Gegenwart von HS-CoB um das 10-fache gesteigert; und (iii) Irreversible Inhibitoren wie 3-Bromopropansulfonat, 3-Iodopropansulfonat und 4-Bromobutyrat, in deren Gegenwart das EPR Signal von aktiver MCR in das MCR-BPS-Signal umgewandelt wurde. Das MCR-BPS-Signal ist denen der MCRox-Signale ähnlich und wurde wie diese in Gegenwart von 2-Bromoethansulfonat nicht ausgelöscht. Messungen des magnetischen zirkularen Dichroismus (MCD) identifizierten Nickel im MCR-ox1-Zustand als High Spin Ni(II), welches axial mit einem Thiyl-Radikal koordiniert ist. Analog dazu könnte das MCR-BPS-Signal von einem Alkyl-Ni(III)-Zustand stammen.

Ein weiterer Schwerpunkt der Arbeit beschäftigt sich mit dem MCR-red2-Zustand, der im Enzym in Gegenwart von HS-CoM und HS-CoB induziert wird und durch ein rhombisches EPR-Signal charakterisiert ist. Eine solche Induktion wurde neben HS-CoB ebenfalls für die zwei HS-CoB-Analoga HS-CoB_6 und Methyl-CoB beobachtet. Durch den Einsatz von ^{33}S-markiertem Coenzym M konnte eindeutig gezeigt werden, dass im MCR-red2-Zustand der Thioetherschwefel von HS-CoM axial mit dem Ni(I) aus F_{430} koordiniert ist. Das Ausmaß der MCR-red2 Induktion durch HS-CoM und HS-CoB zeigte sich in den Untersuchungen abhängig von der Temperatur. Unterhalb von 20^{o}C wandelte sich der red2-Zustand mit sinkender Temperatur mehr und mehr in den red1-Zustand um. Oberhalb von 20^{o}C allerdings lagen nur maximal 50% des Enzyms im red2-Zustand vor, was u. a. dafür spricht, dass sich jeweils nur eines der beiden aktiven Zentren von MCR im red2-Zustand befindet.

Die vorliegenden Ergebnisse sind weitgehend konform mit einem Reaktionsmechanismus, in welchem der erste Schritt des Katalysezyklus eine nukleophile Substitution unter Bildung einer Methyl-Ni(III)-Zwischenstufe darstellt. Dafür sprechen: (i) die Inversion der Stereokonfiguration bei der Reduktion der Methylgruppe von Methyl-Coenzym M; (ii) die niedrige katalytische Effizienz des Enzyms gegenüber Ethyl-Coenzym M als Substrat; (iii) die um einen Faktor 20 höhere apparente Affinität des Enzyms zu 3-Bromopropansulfonat im Vergleich zu 2-Bromoethansulfonat; und (iv) die Induktion des MCR-BPS-Signals durch 3-Bromopropansulfonat, das als ein von einem Alkyl-Ni(III) stammenden Signal gedeutet wird. Der Befund, dass jeweils nur eine der beiden aktiven Zentren des Enzyms in Gegenwart von HS-CoM und HS-CoB in den MCR-red2-Zustand überführt werden kann, weist auf eine Halbseitenreaktivität („Half-of-the-sites reactivity“) von MCR hin, was für eine phasenversetzte Kopplung der beiden aktiven Zentren, ähnlich wie in einem Zweitaktmotor, spricht.

Diese Ergebnisse wurden in vier Publikationen beschrieben, die den Ergebnisteil dieser Arbeit ausmachen. Drei weitere Publikationen zu Nebenprojekten sind als Anhang beigefügt.

II Einleitung

Methan entsteht als Endprodukt im mikrobiologischen Remineralisationsprozess von organischem Material in anaeroben Habitaten, wie marinen und terrestrischen Sedimenten, den Verdauungstrakten von Insekten oder Pansen von Wiederkäuern. Derzeit werden dadurch jährlich ca. 10^9 t des brennbaren Gases (1% des photosynthetisch fixierten Kohlenstoffs) gebildet. Davon gelangen ungefähr 2/3 durch Diffusion in aerobe Zonen und werden dort von methanotrophen Bakterien zu Kohlendioxid oxidiert. Das übrige Drittel entweicht in die Atmosphäre, wo es schließlich auf photochemischen Wege in Kohlendioxid umgewandelt wird (Thauer 1998).

Auch in anaeroben Habitaten antrophogenen Ursprungs findet biologische Methanbildung statt, beispielsweise in Reisfelder, Faultürmen in der Abwasserreinigung oder Mülldeponien. Bedingt durch den exponentiellen Anstieg der Weltbevölkerung und durch die fortschreitende Industrialisierung, nahm sowohl die Anzahl solcher oben aufgeführten Biotope als auch die Massentierhaltung deutlich zu. Damit einhergehend stieg die atmosphärische Methankonzentration in den letzten 160 Jahren von 0,8 ppm auf rund 1,7 ppm an. Da es sich bei Methan um ein hochpotentes Treibhausgas handelt (21 mal wirksamer als Kohlendioxid), trägt dieser Zusammenhang zur globalen Erwärmung bei (Conrad 1996).

In anaeroben Habitaten werden Biopolymere von fermentativen Bakterien zu CO_2, H_2, Formiat und Acetat abgebaut. Diese Produkte sind wiederum die Substrate für methanogene Archaea, die sich auf die Verwertung von C_1-Verbindungen, wie etwa CO_2, Formiat, Methanol, Methylthiole und Methylamine, aber auch Acetat, spezialisiert haben. Diese Substrate stellen die einzige Energie- und Kohlenstoffquelle der *Methanoarchaea* dar (Thauer 1998; Wolfe 2004).

Abbildung 1 zeigt die Methanbildung aus H_2 und CO_2, wie sie beispielsweise in *Methanothermobacter marburgensis* vorkommt. Dabei dient CO_2 als terminaler Elektronenakzeptor und H_2 als primärer Elektronendonor. Im Verlauf des Stoffwechsels wird CO_2 zunächst, gebunden als C_1-Einheit an Methanofuran (MFR), Tetrahydromethanopterin (H_4MPT) und Coenzym M (2-Mercaptoethansulfonat; HS-CoM), auf die Oxidationsstufe einer Methylgruppe reduziert (Thauer 1998; Ferry 1999). Das gebildete Methyl-Coenzym M (2-(Methylthio)ethansulfonat; CH_3-S-CoM) stellt in allen methanogenen Archaea das erste gemeinsame Intermediat im methanogenen Stoffwechsel dar.

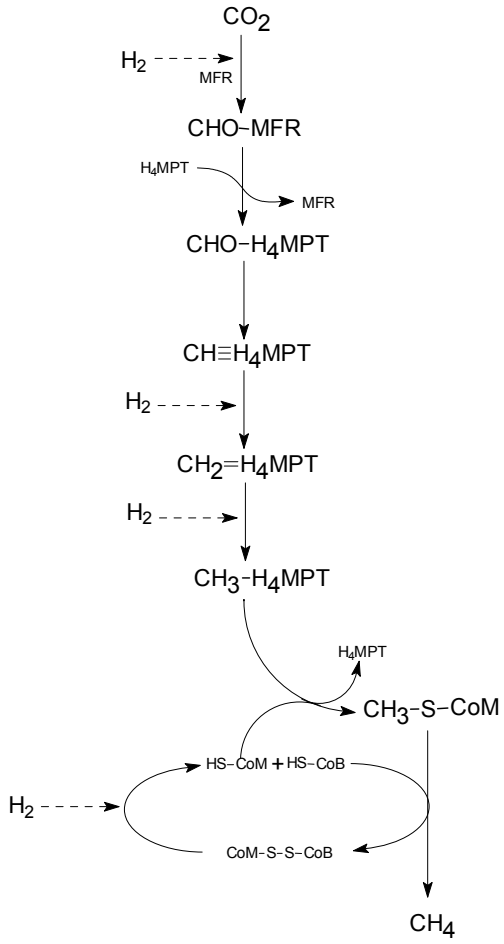

Abb. 1: Stoffwechselweg der Methanbildung aus H_2 und CO_2 in *Methanothermobacter marburgensis*. Abkürzungen: MFR: Methanofuran; H_4MPT: Tetrahydromethanopterin; HS-CoM: Coenzym M; HS-CoB: Coenzym B.

Im darauffolgenden methanbildenden Schritt reagiert Methyl-Coenzym M mit Coenzym B (7-Mercapto-N-heptanoyl-O-phospho-L-threonin; HS-CoB) zu Methan und dem Heterodisulfid (CoM-S-S-CoB) (Bobik et al. 1987; Ellermann et al. 1988). Die beiden Thiole Coenzym M und Coenzym B werden anschließend in einer von Heterodisulfid-Reduktase katalysierten Reduktion wieder regeneriert, während Methan als Endprodukt der Methanogenese in die Umgebung diffundiert (Hedderich and Thauer 1988).

Die exergone Reaktion ($\Delta G°' = -30$ kJ/mol) von Methyl-Coenzym M mit Coenzym B zu Methan und dem Heterodisulfid wird in allen methanogenen Archaea in einem ternären Komplex-Mechanismus durch die Methyl-Coenzym M Reduktase (MCR) katalysiert (Abb. 2) (Ellermann et al. 1987; Noll et al. 1987; Bonacker et al. 1993).

Die Umkehr dieser Reaktion spielt vermutlich eine bedeutende Rolle bei der anaeroben Methanoxidation (AMO) in marinen Sedimenten (Hallam et al. 2003; Krüger et al. 2003).

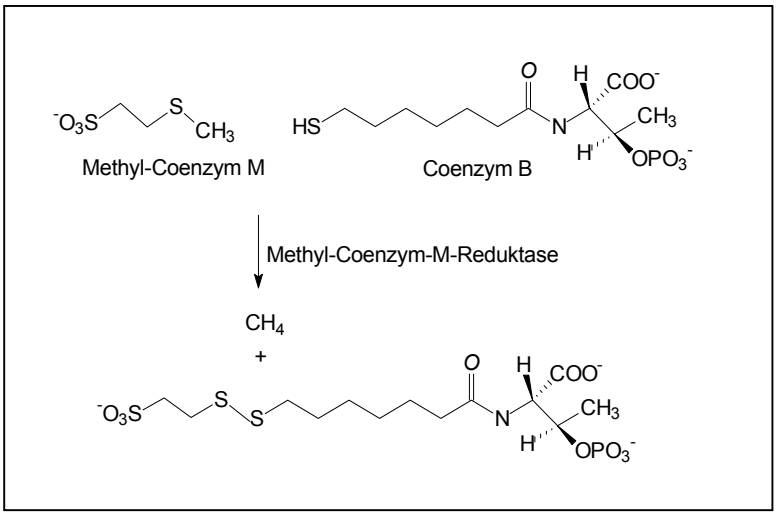

Abb. 2: Die Methanbildende Reaktion katalysiert von Methyl-Coenzym M Reduktase (MCR) in methanogenen Archaea (Ellermann et al. 1987; Noll et al. 1987).

Das Methanbildende Enzym MCR besitzt eine molekulare Masse von ca. 300 kDa. Das Protein besteht aus drei Untereinheiten (α, β, γ), die in hexamerer Konfiguration ($\alpha_2\beta_2\gamma_2$) angeordnet sind (Abb. 3) (Ellefson and Wolfe 1981; Ankel-Fuchs et al. 1986; Ankel-Fuchs and Thauer 1986; Hartzell and Wolfe 1986; Jetten et al. 1990; Rospert et al. 1990; Rospert et al. 1991b).

Abb. 3: Struktur von Methyl-Coenzym M Reduktase (MCR) aus *Methanothermobacter marburgensis* (Ermler et al. 1997). Das Enzym besteht aus sechs Untereinheiten: α (rot), α' (orange), β (grün), β' (hellgrün), γ (blau), γ' (hellblau). Das Heterohexamer $\alpha_2\beta_2\gamma_2$ bindet zwei Moleküle F_{430} (gelb), die 50 Å voneinander entfernt am Ende eines 50 Å langen Kanals liegen. Die Kanäle setzen sich aus den Untereinheiten α, α', β und γ, beziehungsweise α', α, β' und γ', zusammen.

In *Methanothermobacter marburgensis* (Rospert et al. 1990; Brenner et al. 1993), *Methanothermus fervidus* (Lehmacher and Klenk 1994), *Methanococcus jannaschii* (Bult et al. 1996) und *Methanothermobacter thermoautotrophicum* ΔH (Smith et al. 1997) wurde zusätzlich ein Isoenzym von MCR, die Methyl-Coenzym M Reduktase II (MCR II), nachgewiesen. Die Expression für MCR I und MCR II codierende Gene wird durch verschiedene Wachstumsbedingungen reguliert (Bonacker et al. 1992; Nölling et al. 1995); ein biochemischer Grund für die Existenz des Isoenzyms von MCR ist jedoch noch weitgehend unklar.

MCR enthält als prosthetische Gruppe zwei nicht-kovalent, jedoch fest gebundene Moleküle des Faktors 430 (F_{430}) (Abb. 4) (Ellefson et al. 1982).

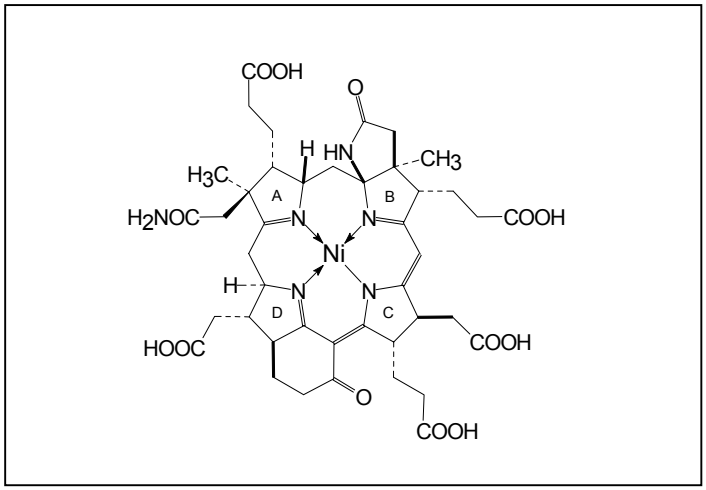

Abb. 4: Struktur von Faktor 430 (F_{430}), der prosthetischen Gruppe von Methyl-Coenzym M Reduktase (Färber et al. 1991). Faktor F_{430} besitzt ein zyklisches Tetrapyrrolsystem mit Nickel als Zentralatom (Diekert et al. 1980; Pfaltz et al. 1982).

Die Kristallstruktur von MCR aus *M. marburgensis* zeigt, dass je ein Moleküle F_{430} am Ende eines 50 Å langen Substratkanals liegt (Abb. 5). Am Aufbau der beiden 50 Å voneinander entfernten aktiven Zentren sind jeweils vier Untereinheiten (α, α´, β, γ, bzw. α', α, β' und γ') beteiligt. An der Proteinoberfläche besitzt der Substratkanal einen Durchmesser von 25 Å und wird dann in einer Tiefe von ca. 30 Å enger. Über eine Länge von ca. 16 Å über dem Nickel hat er einen Durchmesser von nur 8 Å. Oberhalb der Tetrapyrrolebene ragen zwei Tyrosinreste mit ihren Hydroxylgruppen in den Kanal hinein und dürften so für die Katalyse der Enzymreaktion von Bedeutung sein (Ermler et al. 1997; Grabarse et al. 2001a; Grabarse et al. 2001b).

In allen bekannten Strukturen wird das Zentralatom Nickel der prosthetischen Gruppe F_{430} von der dem Substratkanal abgewandten Seite mit dem Sauerstoffatom der Amidgruppe von Glutamin$^{\alpha 147}$ axial ligiert. Der axiale Ligand auf der Vorderseite von F_{430} hängt von dem jeweiligen Zustand des Enzyms ab. Im sogenannten MCR-ox1-silent-Zustand (siehe unten)

fungiert dort die Thiolgruppe von Coenzym M als axialer Ligand von Nickel (Abb. 5A). Direkt über F_{430} erweitert sich der Substratkanal und formt eine Bindungstasche für Methyl-Coenzym M. Diese Tasche ist so eng, daß das Substrat seine Orientierung nicht mehr verändern kann. Damit die Thiolgruppe (bzw. Methylgruppe von Methyl-Coenzym M) über dem Nickel positioniert werden kann, muß das Substrat mit der Sulfonatgruppe zuerst in den Substratkanal eintauchen. Darüber hinaus muß Methyl-Coenzym M als Erstes der beiden Substrate in den Substratkanal gelangen, da durch die Bindung von Coenzym B dieser komplett verschlossen wird. Die Threoninphosphatgruppe von Coenzym B wird mit der Proteinmatrix verankert, während der aliphatische Arm in der engsten Stelle des Kanals (Durchmesser 6 Å) bindet. Die Thiolgruppe von Coenzym B kann sich somit dem Nickel von F_{430} nur bis zu einem Abstand von 8 Å nähern und bleibt auch von der Thiolgruppe von Coenzym M in einem Abstand von 6 Å fixiert. Bei gleichzeitiger Bindung von Methyl-Coenzym M und Coenzym B im aktiven Zentrum bleibt, im Gegensatz zur Situation mit gebundenem Coenzym M und Coenzym B, kein Platz mehr für auch nur ein einziges Molekül Wasser. Die Reduktion von Methyl-Coenzym M mit Coenzym B läuft somit unter vollständigem Ausschluß von H_2O im Proteininneren ab (Ermler et al. 1997; Grabarse et al. 2001a; Grabarse et al. 2001b). Die zweite dargestellte Struktur von MCR-silent (siehe unten) zeigt schließlich den Produktkomplex von MCR, in dem das Heterodisulfid gebildet ist und die Sulfonatgruppe von Coenzym M den axialen Liganden des somit hexakoordinierten Nickels von F_{430} bildet (Abb. 5B).

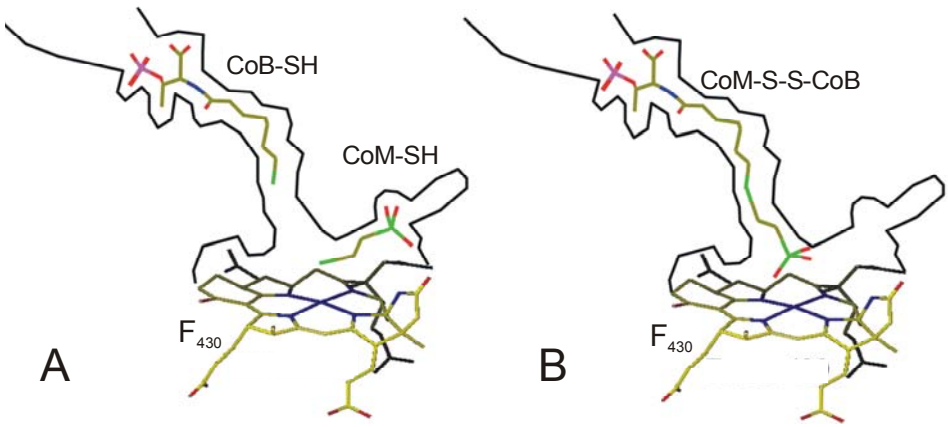

Abb. 5: Schematische Darstellung des aktiven Zentrums von inaktiver Methyl-Coenzym M Reduktase (MCR): A MCR im Komplex mit Coenzym M (2-Mercaptoethansulfonat) und Coenzym B (N-7-Mercaptoheptanoylthreoninphosphat); **B**: MCR im Komplex mit dem Heterodisulfid aus Coenzym M und Coenzym B. Die schematische Darstellung wurde aus zwei Kristallstrukturen von enzymatisch inaktiver MCR abgleitet (Ermler et al. 1997). Es wird angenommen, dass Methyl-Coenzym M (2-(Methylthio)ethansulfonat) in ähnlicher Weise wie Coenzym M bindet. Die Bindung des Coenzym B-Restes ist fast deckungsgleich, wohingegen sich die Konformation von Coenyzm M und dessen Ligandierung zum Nickel deutlich zwischen beiden Komplexen A und B unterscheidet. Das gasförmige Produkt Methan konnte nicht in der Struktur identifiziert werden. Farbcode: Schwefel in grün, Kohlenstoff in gelb, Stickstoff und Nickel in blau und Sauerstoff in rot.

Kristallstrukturen von MCR des mesophilen Archaeon *Methanosarcina barkeri*, sowie auch des hyperthermophilen Organismus *Methanopyrus kandleri*, ergaben im Grunde die gleiche Architektur des aktiven Zentrums. Unterschiede zwischen den drei Enzymen bestanden vor allem an der Proteinoberfläche, wodurch eine Anpassung an die optimale Wachstumstemperatur und an unterschiedliche intrazelluläre Salzkonzentrationen gewährleistet werden könnte (Grabarse et al. 2000).

In der Umgebung des Reaktionszentrums von MCR aus *M. marburgensis* wurden fünf modifizierte Aminosäuren nachgewiesen: 1-*N*-Methyl-Histidin$^{\alpha 257}$, 5-Methyl-Arginin$^{\alpha 271}$, 2-Methyl-Glutamin$^{\alpha 400}$, *S*-Methyl-Cystein$^{\alpha 452}$ und Thioglycin$^{\alpha 445}$, dessen Carbonylsauerstoff durch Schwefel ersetzt ist. Das Thioglycin könnte über den Stickstoff der Seitengruppe von Asn$^{\alpha 481}$ in Wechselwirkung mit der Thiolgruppe von Coenzym B treten und so möglicherweise als Redoxmediator eine Rolle im Katalysemechanismus spielen. Mittels ^{13}C markiertem Methionin konnte gezeigt werden, daß die Methylgruppen der vier weiteren Aminosäuren aus Methionin stammen und wahrscheinlich *S*-Adenosylmethionin-abhängig in das Protein eingeführt werden (Selmer et al. 2000). Bislang wurde Thioglycin auch in MCR II aus *M. marburgensis*, sowie in MCR aus *Methanosarcina barkeri*, *Methanococcus voltae* und *Methanopyrus kandleri* eindeutig nachgewiesen und darüber hinaus in MCR aus *Methanoculleus thermophilicus* starke Hinweise für dessen Existenz gefunden (Jörg Kahnt, persönliche Mitteilung). Damit scheint diese außergewöhnliche Aminosäure in jeder phylogenetischen Gruppe der *Methanoarchaea* präsent zu sein. Die Bedeutung der Modifikationen ist allerdings weiterhin ungeklärt.

Trotz der detaillierten strukturellen Informationen ließ sich hieraus noch kein endgültiger Reaktionsmechanismus formulieren. Ein Grund hierfür ist, daß bisherige Kristallstrukturen lediglich die Situation eines enzymatisch inaktiven Pseudo-Substratkomplexes mit dem Methyl-Coenzym M-Analog Coenzym M und Coenzym B oder eines Pseudo-Produktkomplexes von MCR mit Heterodisulfid zeigten (siehe auch Abb. 5). Die Struktur des enzymatisch aktiven Zustands von MCR fehlt bislang.

Für die Formulierung eines Katalysemechanismus sind zudem die chemischen Eigenschaften der prosthetischen Gruppe F_{430} von erheblicher Relevants. Durch Denaturierung mit Perchlorsäure oder Trichloressigsäure kann F_{430} von MCR getrennt werden. F_{430} selbst tritt in den Oxidationszuständen Ni(I), Ni(II) und Ni(III) auf. Bedingt durch deren paramagnetische Eigenschaften sind Ni(I)- und Ni(III)-Zustände mittels Elektronenparamagnetischer Resonanz (EPR)-Spektroskopie detektierbar, während der stabile Ni(II)-Zustand EPR-„silent“ ist. Die

einzelnen Oxidationsstufen lassen sich ebenfalls durch ihr Absorptionsspektrum von ultravioletten und sichtbaren Licht voneinander unterscheiden (Jaun 1993). Enzymatisch aktive MCR zeigt dabei die gleichen Eigenschaften und Spektren wie proteinfreier Ni(I)F_{430}, wodurch ein definierter Katalysemechanismus für MCR mit F_{430} im Ni(I)-Zustand beginnen würde (Jaun and Pfaltz 1986; Holliger et al. 1993; Goubeaud et al. 1997).

Freier F_{430} im Ni(II)-Zustand kann in wäßriger alkalischer Lösung in Gegenwart von Ti(III)Citrat zu Ni(I)F_{430} reduziert werden (Holliger et al. 1993). Ein Großteil der Erkenntnisse bezüglich der chemischen Eigenschaften von freiem F_{430} stammen jedoch aus Untersuchungen mit dessen Pentamethylester (F_{430}M). Dabei werden die beiden Acetat- und drei Propionat-Seitenketten mit Methylgruppen verestert. Dieses Derivat ist in nichtkoordinierenden, organischen Lösungsmitteln löslich. F_{430}M, isoliert im stabilen Ni(II)-Zustand, kann mit einem geeigneten Reduktionsmittel in Ni(I)F_{430}M überführt werden (Jaun and Pfaltz 1986). Das Standardredoxpotential E_0' des Ni(II)/Ni(I)-Paares liegt bei –650 mV (Jaun and Pfaltz 1986; Holliger et al. 1993) und ist damit im gleichen Bereich, wie das Cob(II)alamin/Cob(I)alamin-Redoxpaar in Corrinoiden mit –640 mV (Lexa and Saveant 1983; Daas et al. 1995).

Ni(I)F_{430}M kann mit Methyltosylat und Methyljodid methyliert und in einen Methyl-Ni(II)F_{430}M-Zustand überführt werden (Jaun and Pfaltz 1988; Lin and Jaun 1991). Im Falle von Methyltosylat entsteht zunächst wahrscheinlich Methyl-Ni(III)F_{430}M als Zwischenprodukt, da die Methylgruppe von Methyltosylat nur heterolytisch abgespalten werden kann (Jaun 1993). Dieser Zustand ist jedoch so labil, daß er sich nicht darstellen läßt. Die Methylierung von Ni(I)F_{430}M zu Methyl-Ni(III)F_{430}M stellt eine nukleophile Substitution dar, die mit einer Inversion der Stereokonfiguration einher geht (Lin and Jaun 1991). Aus dem bekannten Redoxpotential des Ni(III)F_{430}M/Ni(II)F_{430}M-Paares (Jaun 1990) wurde das Redoxpotential des Methyl-Ni(III)/Methyl-Ni(II)-Paares auf weit über 0 mV geschätzt. Damit reagiert jeder Elektronendonor mit einem Potential negativer als 0 mV mit dieser Methyl-Ni(III)F_{430}M-Zwischenstufe und reduziert diese sofort zu Methyl-Ni(II)F_{430}M. In dieser Hinsicht unterscheidet sich F_{430}M von den Corrinoiden, denn deren Methyl-Cob(III)alamin-Verbindungen sind sehr stabil. Das Redoxpotential des Methyl-Cob(III)alamin/Methyl-Cob(II)alamin-Paares liegt bei ca. –640 mV (Lexa and Saveant 1983).

Methyl-Ni(II)F_{430}M ist in aprotischen Lösungen eine recht stabile Verbindung, die aber bei Verfügbarkeit von Protonen in einer elektrophilen Substitutionsreaktion zu Ni(II)F_{430}M und Methan protonolysiert (Lin and Jaun 1992), wobei die vorliegende Stereokonfiguration erhalten bleibt. Im Vergleich dazu reagiert Methyl-Cob(II)alamin in einer homolytischen Spaltung zu einem Methylradikal und Cob(I)alamin (Hogenkamp et al. 1985). Durch diesen Unterschied läßt

sich auch erklären, warum F_{430} ein guter Katalysator für die Methylgruppen-Reduktion ist, während die Corrinoide in der Katalyse des Methylgruppentransfers eine wichtige Rolle spielen. Allerdings reduziert freier Ni(I)F_{430} keine Methylthioether und damit auch nicht Methyl-Coenzym M zu Methan. Dazu muß die Methylgruppe zunächst durch Elektronenabzug am Schwefel aktiviert werden. Dieses könnte durch eine Protonierung oder durch eine radikalische Aktivierung der Thioetherfunktion mittels eines Sauerstoff- oder Thiylradikals erfolgen (Jaun and Pfaltz 1988). Zur Formulierung eines Katalysemechanismus von MCR ist eine Arbeit von besonderer Bedeutung, die zudem Übereinstimmungen mit den oben bereits beschriebenen Beobachtungen anhand von F_{430}M zeigt. So findet während der von MCR katalysierten Reduktion von Ethyl-Coenzym M zu Ethan ebenfalls eine Umkehr der Stereokonfiguration statt (Ahn et al. 1991).

Die aktuelle Diskussion um den Reaktionsmechanismus von MCR konzentriert sich hauptsächlich auf zwei Varianten. Basierend auf den strukturellen Erkenntnissen von MCR und den Eigenschaften von freiem F_{430} favorisiert ein Mechanismus (Mechanismus I; Abb. 6) als ersten Schritt der Katalyse einen nukleophilen Angriff des Ni(I) der prosthetischen Gruppe auf die Methylgruppe von Methyl-Coenzym M. Das dadurch entstehende Methyl-Ni(III) reagiert anschließend mit dem Coenzym M-Thiolat zu Methyl-Ni(II) und einem Coenzym M-Thiylradikal. Wie für freien F_{430} beobachtet, entsteht Methan in diesem Mechanismus durch die Protonolysis von Methyl-Ni(II) in einer elektrophilen Substitution. Das Coenzym M-Thiylradikal wiederum bildet zusammen mit dem Coenzym B-Thiolatanion ein Heterodisulfidanionradikal, welches als Reduktant stark genug ist, um Ni(II)F_{430} im letzten Zyklusschritt zurück zu Ni(I)F_{430} zu reduzieren (Ermler et al. 1997; Grabarse et al. 2001a; Grabarse et al. 2001b). Die Schwachpunkte dieses Mechanismus liegen zum einen darin, daß wie im Falle von freiem F_{430}, Ni(I)F_{430} nicht ausreichend nukleophil ist, um die Methylgruppe von unaktiviertem Methyl-Coenyzme M in einer nukleophilen Substitutionsreaktion anzugreifen (Jaun 1993) und zum anderen daran, daß noch völlig unklar ist, ob ein Methyl-Ni(III) ausreicht, um Coenzym M-Thiolat zu Coenzym M-Thiylradikal zu oxidieren. Jedoch liefert die nukleophile Substitution im ersten Katalyseschritt eine mögliche Erklärung für die Umkehr der Stereokonfiguration bei der Reduktion der Ethylgruppe von Ethyl-Coenzym M zu Ethan (Ahn et al. 1991).

Ausgehend von quantenchemischen Berechnungen geht der zweite Mechanismus (Mechnismus II; Abb. 6) in einem ersten, geschwindigkeitsbestimmenden Schritt des

Katalysezyklus von einem Angriff des $Ni(I)F_{430}$ auf den Thioetherschwefel des Methyl-Coenzym M aus. Das dadurch entstandene freie Methylradikal wird durch den Transfer eines Wasserstoffatoms der Thiolgruppe von Coenzyme B sofort in Methan umgewandelt. Zurück bleibt das Coenzym B-Thiylradikal, welches im zweiten Schritt des Reaktionsmechanismus unter der Rückführung von $Ni(II)F_{430}$ zu $Ni(I)F_{430}$ mit Coenzym M zum Heterodisulfid CoM-S-S-CoB reagiert (Ghosh et al. 2001; Pelmenschikov et al. 2002; Pelmenschikov and Siegbahn 2003). Für diesen Mechanismus spricht vor allem das errechnete Energieprofil. Besonders der erste Reaktionsschritt mit einer Aktivierungsbarriere von +85 kJ mol^{-1} erscheint deutlich attraktiver als die für die nukleophile Substitution am Beginn von Mechanismus I mit +190 kJ mol^{-1} (Pelmenschikov et al. 2002). Allerdings kann dieser Mechanismus nicht die von Ahn et al. (1991) beschriebene Inversion der Stereokonfiguration erklären.

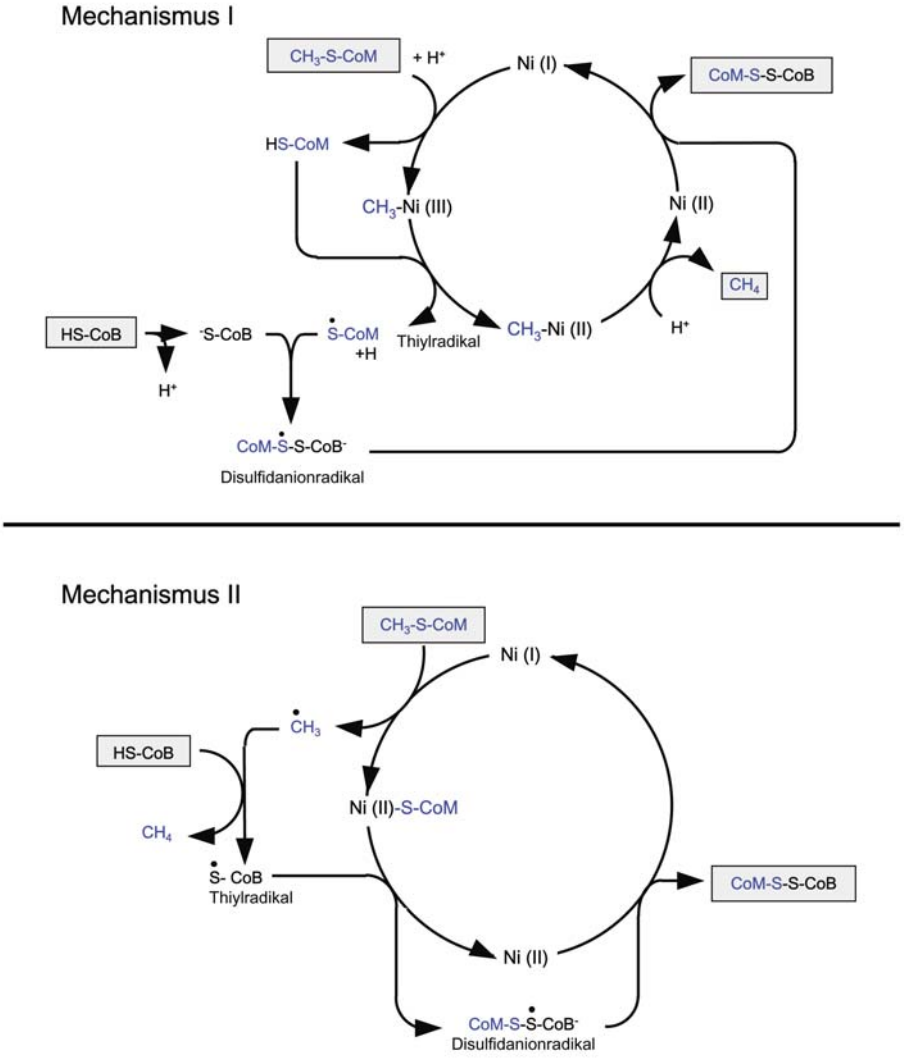

Abb. 6: Katalysemechanismus I (Ermler et al. 1997; Grabarse et al. 2001a; Grabarse et al. 2001b) und Katalysemechnismus II (Ghosh et al. 2001; Pelmenschikov et al. 2002; Pelmenschikov and Siegbahn 2003).

Indizien, die für oder gegen einen der beiden Katalysemodelle sprechen, erhält man jedoch nur aus experimentellen Daten, die man durch Untersuchungen am intakten Enzym gewinnt.

Die EPR-spektroskopischen Eigenschaften von F_{430} machen es beispielsweise möglich, unterschiedliche Oxidationszustände von F_{430} in MCR zu detektieren. Bisher wurden für MCR aus *M. marburgensis*, neben mehreren inaktiven Ni(II)-Zuständen, verschiedene EPR-aktive Zustände definiert: MCR-red1, MCR-red2, MCR-ox1, MCR-ox2 MCR-ox3 und MCR-BPS (Albracht et al. 1986; Albracht et al. 1988; Rospert et al. 1992; Mahlert et al. 2002a; Mahlert et al. 2002b), von denen die MCR-red-Zustände enzymatisch aktiv sind (Rospert et al. 1991a; Goubeaud et al. 1997). Diese Zustände sind inzwischen hinsichtlich ihrer EPR-Signale, ihrer Absorptionsspektren, ihrer Aktivität und zum Teil auch ihres Oxidationszustands charakterisiert worden (Tab. 1). Bedauerlicherweise können die EPR-Spektren nicht *per se* dem Ni(I) ($d^9 = S$ ½) oder Ni(III) ($d^7 = S$ ½) Oxidationszustand zugeordnet werden. Die Bedingungen, unter denen die Signale und Zustände *in vivo* oder *in vitro* induziert werden können, sind im Folgenden beschrieben:

Tab. 1: Spektroskopische Parameter für die verschiedenen EPR detektierbaren Zustände von Methyl-Coenzym M Reduktase (Albracht et al. 1986; Albracht et al. 1988; Rospert et al. 1992; Mahlert et al. 2002a; Mahlert et al. 2002b), freiem F_{430} (Holliger et al. 1993) und dem Pentamethylester von F_{430} (Jaun and Pfaltz 1986; Jaun 1993). n.b. = nicht bestimmt.

	Zustand	Anisotropie des EPR-Signals	*g*-Werte des EPR-Signals			Absorptionsmaxima im UV/vis (nm)	
			g_z	g_y	g_x		
			g_z		g_{xy}		
MCR-	silent Ni(II)	-	-	-	-	420	445 (Schulter)
	red1 Ni(I)	axial	2,240		2,052	386	725
	red2 Ni(I)	rhombisch	2,284	2,231	2,175	415	
	ox1 Ni(I)/Ni(III)?	axial	2,226		2,148	420	
	ox2 Ni(I)/Ni(III)?	axial	2,240		2,122	n.b.	
	ox3 Ni(I)/Ni(III)?	axial	2,217		2,137	n.b.	
	BPS Ni(I)/Ni(III)?	axial	2,227		2,119	n.b.	
F_{430}	Ni(I)	axial	2,244		2,061	376	710
F_{430}M	Ni(I)	axial	2,250		2,065	382	754
	Ni(III)	axial	2,211		2,020	368	595, 890, 1020

Im **MCR-silent**-Zustand befindet sich das Zentralatom der prosthetischen Gruppe im Ni(II)-Oxidationszustand und somit zeigt das Enzym keinerlei EPR-Signal. Werden Zellen von *M. marburgensis* nach Wachstum bei 65°C auf 80% H_2/20% CO_2 auf 8°C gekühlt und unter weiterer Begasung geerntet, so liegt MCR in einem MCR-silent-Zustand vor (Ankel-Fuchs and Thauer 1986; Rospert et al. 1991a). Nach Zellaufschluß ist das Enzym im Zellextrakt weitgehend inaktiv und zeigt nur eine kleine Restaktivität, die auf Spuren aktiver Enzymzustände zurückzuführen ist (Brenner et al. 1993).

Aktive MCR zeigt das axiale EPR-Signal **MCR-red1**. In Abwesenheit der Substrate wird dieses als **MCR-red1a**-Zustand (a für *a*bwesend) bezeichnet. Charakteristisch für diesen Zustand ist die aufgelöste Superhyperfeinstruktur des EPR-Signals aufgrund der Interaktion des Elektronenspins (S = 1/2) von Ni(I) mit dem Kernspin (I = 1) der vier benachbarten Stickstoffatome des Tetrapyrrolringsystems von F_{430}. Die gleiche Aufspaltung zeigt MCR-red1 in Gegenwart von Methyl-Coenzym M, welcher als **MCR-red1m**-Zustand (m für *M*ethyl-Coenzym M) bezeichnet wird. Enthält das aktive Enzym statt Methyl-Coenzym M den kompetitven Inhibitor Coenyzm M, so befindet sich das Enzym im sogenannten **MCR-red1c**-Zustand (c für *C*oenzym M). Das entsprechende EPR-Signal ist ähnlich dem von MCR-red1m, besitzt jedoch nur gering aufgelöste Superhyperfeinaufspaltung (Mahlert et al. 2002a). MCR-red1 kann auch *in vitro* durch Aktivierung von MCR-ox1 bei pH 9 und 60°C in Gegenwart von Ti(III)Citrat und Methyl-Coenzym M induziert werden (Goubeaud et al. 1997).

In Anwesenheit sowohl von Coenzym M als auch Coenzym B wandelt sich das axiale red1-Signal teilweise in das rhombische EPR-Signal **MCR-red2** um. Durch Zugabe von Methyl-Coenzym M kann MCR-red2 zurück zu MCR-red1m umgewandelt werden. Die Zugabe von Coenzym B zu MCR im red1m- oder red1a-Zustand bewirkt dagegen keinerlei sichtbare Änderung des EPR-Signals (Mahlert et al. 2002a). Als Oxidationsstufe für F_{430} in MCR-red2 wird ebenso wie für MCR-red1 Ni(I) angenommen. Zumal beide Zustände reversibel ineinander überführt werden können, wobei eine Änderung des Redoxzustandes ausgeschlossen werden kann (Rospert et al. 1991a). *In vivo* werden MCR-red1 und MCR-red2 durch Begasen der Kultur mit 100% H_2 vor der Ernte erhalten (Rospert et al. 1991a). Zeitabhängig wird dabei zunächst das MCR-red1-Signal induziert. Nach ca. 15 min geht dann die Intensität des MCR-red1-Signals zurück und es bildet sich das MCR-red2-Signal. Beide Signale sind gegenüber Sauerstoff sehr labil. Nach Zellaufschluß läßt sich eine hohe MCR-Aktivität detektieren, die allerdings proportional zum Verlust der EPR-Signale abnimmt. Aktivität und EPR-Signal können jedoch durch Zugabe von Coenzym M zum Zellextrakt stabilisiert werden (Rospert et al. 1991a). Wird das Enzym in Gegenwart von Coenzym M gereinigt, verschwindet das rhombische red2-Signal

aufgrund des Verlustes von Coenzym B und übrig bleibt MCR im red1c-Zustand (Mahlert et al. 2002a).

Der **MCR-ox1**-Zustand wird durch Begasen der Kultur mit 80% N_2/20% CO_2 (Albracht et al. 1986) oder durch Zugabe von 30 mM Na_2S (Becker and Ragsdale 1998) direkt vor der Ernte induziert. Dieser Zustand ist relativ stabil gegenüber Sauerstoff. Nach Aufschluß der Zellen wird nur eine sehr geringe Restaktivität gefunden. MCR-ox1 kann in Gegenwart von Methyl-Coenzym M ohne erheblichen Verlust des EPR-Signals gereinigt werden (Goubeaud et al. 1997). *In vitro* erhält man diesen Zustand durch Zugabe von 40 mM Na_2S oder 0,5 mM Polysulfid zu MCR in Gegenwart von Coenzym M und Coenzym B (Mahlert et al. 2002b).

Der **MCR-ox2**-Zustand zeigt ein sehr ähnliches EPR-Signal wie MCR-ox1 und wird induziert durch Zugabe von 10 mM Na_2SO_3 zu einer wachsenden Kultur von *M. marburgensis* (Becker and Ragsdale 1998) oder zu gereinigtem Enzym im MCR-red2-Zustand (Mahlert et al. 2002b). Wie MCR-ox1 ist auch dieser Zustand stabil gegenüber Sauerstoff und läßt sich mit relativ hohen Spinausbeuten reinigen.

Ein weiterer enzymatisch inaktiver MCR-ox-Zustand wurde bislang nur *in vitro* induziert (Mahlert et al. 2002b). Dieses **MCR-ox3**-Signal erhält man durch Sauerstoffexposition von MCR im red1/2-Zustand.

MCR-BPS wird nur durch die Zugabe des Hemmstoffes 3-Bromopropansulfonat (BPS) zu aktivem Enzym in den MCR-red-Zuständen induziert (Rospert et al. 1992).

Der Valenzzustand von Nickel in den ox-Zuständen ist nicht eindeutig geklärt. EPR- und ENDOR-Spektren der ox-Zustände wurden so interpretiert, daß sie einen Ni(I)F_{430}-Zustand favorisieren (Telser et al. 2000; Telser et al. 2001). Zusätzliche Messungen der Absorption von Röntgenstrahlen (X-ray absorption; XAS) und Resonanz-Raman-Daten führten zu der Annahme, daß MCR-red1 und MCR-ox1 sich eher im Reduktionszustand des Porphinoidligandensystems als im Oxidationszustand von Nickel unterscheiden (Telser et al. 2000; Telser et al. 2001; Tang et al. 2002). Diese Hypothese wird jedoch nicht durch Redoxtitrationen (Piskorski and Jaun 2003) sowie optischen und Magnetisch Circuläre Dichroismus (MCD) spektroskopischen Daten (Duin et al. 2004) und aktuellen Berechnungen von Elektronedichtefunktionen (Craft et al. 2004b; Craft et al. 2004a) gestützt. Frühere Berechnungen von Elektronendichtefunktionen zeigten, daß die ox-Spektren auch mit Ni(III)F_{430} kompatibel sind (Wondimagegn and Ghosh 2001). Wiederum für Ni(I)F_{430} sprechen würde die Beobachtung, daß in einer MCR-ox1-silent-Präparation mittels Kryoreduktion neben dem red1- auch das ox1-Signal induziert werden kann (Telser et al. 2001). Allerdings bietet die strukturelle Situation im MCR-ox1-silent-Zustand mit gebundenem Coenzym M und Coenzym B im aktiven Zentrum Platz für ein Wassermolekül

(siehe oben und Ermler et al. 1997). Dieses könnte während der Behandlung mit γ-Strahlung als Elektronendonor fungieren und somit nicht zu der vermutete Kryoreduktion, sondern zu einer Kryooxidation des Nickels führen. *In vitro* wird MCR-ox1 in Gegenwart von Ti(III)Citrat in MCR-red1 umgewandelt (Goubeaud et al. 1997). Ti(III)Citrat ist ein starkes Reduktionsmittel, das sogar freien F_{430} in den Ni(I)-Zustand überführen kann (Holliger et al. 1993). Diese Beobachtung würde für MCR-ox1 wiederum den Ni(III)F_{430}-Valenzzustand favorisieren.

In der vorliegenden Arbeit werden verschiedene Wege beschrieben, die es ermöglichen, einen tieferen Einblick in die unterschiedlichen Zustände zu erhalten. Mit Hilfe von spektroskopischen Methoden wurde erstmals die Wirkungsweise verschiedener Substratanaloga nachgewiesen und im Hinblick auf ihre Bedeutung für einen postulierten Reaktionsmechanismus diskutiert. Ferner wurden Untersuchungen zum MCR-red2-Zustand durchgeführt, welcher eine Situation darstellt, wie sie parallel dazu in einem Übergangszustand des Reaktionsmechanismus vorliegen könnte. Erstmals konnte hierbei das Ligandenumfeld des Nickels eindeutig charakterisiert werden und der Nachweis erbracht werden, daß die zwei aktiven Zentren von MCR nicht unabhängig voneinander, sondern in einem Zweitaktermechanismus funktionieren könnten.

III Material und Methoden

1. Material

Chemikalien und Biochemikalien. Das für die Proteinbestimmung nach Bradford (Bradford, 1976) verwendete Farbstoffkonzentrat wurde von BioRad Laboratories (München) bezogen. Coenzym M (2-Mercaptoethanesulfonat) stammte von Merck (Darmstadt), 2-Bromoethansulfonsäure (BES) und 3-Bromopropionsäure von Fluka (Sigma-Aldrich; Taufenkirchen) und 4-Bromobutansäure von Aldrich (Sigma-Aldrich; Taufenkirchen).

Methyl-Coenzym M wurde aus Coenzym M (Natriumsalz, Merck) durch Methylierung mit Methyl-Jodid (Fluka) hergestellt (Gunsalus et al. 1978). 3 mmol Coenzym M wurden für 12 h mit 6 mmol Methyljodid in 5 ml 32%iger wäßriger Ammoniaklösung unter Stickstoffatmosphäre gerührt. Nach 12 h bei Raumtemperatur wurde die Lösung im Rotationsverdampfer evaporiert und anschließend bis zur völligen Trockenheit lyophylisiert. Das trockene, gelbe Pellet wurde in 10 ml destilliertem Wasser gelöst. In Anteilen von 5 ml wurde die Lösung auf eine Q-Sepharose-Säule (30 ml) aufgetragen. Für die Trennung wurde ein $(NH_4)_2CO_3$-Gradient von 0-1 M angelegt. Das Eluat wurde gesammelt und mit Dünnschichtchromatographie an Kieselgel 60 F_{254} (Merck, Darmstadt) auf den Gehalt an Methyl-Coenzym M überprüft. Der Laufpuffer der Chromatographie war Butanol/Essigsäure/Wasser (2:1:1). Methyl-Coenzym M eluierte von der Q-Sepharose-Säule zwischen 250 mM und 350 mM $(NH_4)_2CO_3$. Methyl-Coenzym M-haltige Fraktionen wurden gesammelt und für 48 h bei 60°C unter Vakuum evaporiert, um $(NH_4)_2CO_3$ und Spuren von Methyljodid zu entfernen. Ein trockenes weißes Pulver war das Endprodukt. Methyl-Coenzym M wurde mit $(NH_4)_2CO_3$ statt der üblicherweise verwendeten Salzsäure von Q-Sepharose eluiert, da Methyl-Coenzym M als protonierte Sulfonsäure und Wasser ein azeotropes Gemisch formen.

Ethyl-Coenzym M und Propyl-Coenzym M wurden analog dazu aus den jeweiligen Jodiden synthetisiert.

Coenzym B (*N*-7-Mercapto-*N*-heptanoyl-*O*-phospho-*L*-threonin) wurde durch Reduktion des symmetrischen Disulfids CoB-S-S-CoB mit $NaBH_4$ hergestellt (Kobelt et al. 1987; Ellermann et al. 1988). Das Disulfid selber wurde in einer Dreistufensynthese nach der Methode von Noll et al. (1987) synthetisiert und mir freundlicherweise von Jürgen Koch zur Verfügung gestellt.

N-6-Mercapto-*N*-hexanoyl-*O*-phospho-*L*-threonin (HS-CoB_6) und *N*-8-Mercapto-*N*-octanoyl-*O*-phospho-*L*-threonin (HS-CoB_8) wurden ebenfalls aus den synthetisierten Disulfiden hergestellt (Ellermann et al. 1988; Olson et al. 1991).

[2-^{33}S]-Coenzym M ($H^{33}S$-CoM), 2-(Allylsulfanyl)ethanesulfonat (Allyl-CoM), 2-(Trifluoromethylsulfanyl)ethansulfonat (Trifluoromethyl-Coenzym M; CF_3-CoM), 2-Thiocyanatoethansulfonat (Cyano-Coenzym M; NC-CoM) und 2-Selenolatoethansulfonat (Seleno-Coenzym M; HSe-CoM) wurden freundlicherweise von Dr. Carsten Bauer und Rafal Piskorski (ETH-Zürich) synthetisiert (Finazzo et al. 2003a; Goenrich et al. 2004).

3-Bromopropansulfonat (BPS), 3-Fluoropropansulfonat und 3-Iodopropansulfonat stammten aus den früheren Präparationen von Rospert et al. (1992).

Polysulfidlösungen bekannter Konzentration wurden aus elementarem Schwefel und Natriumsulfid bei pH 8,5 hergestellt (Klimmek et al. 1991; Schauder and Mueller 1993).

Säulen, Säulenmaterial und Membranen. Die verwendete FPLC-Fertigsäule, sowie das Chromatographiematerial (Q-Sepharose) wurden von Pharmacia (Freiburg) bezogen. Die Proteinkonzentrationssysteme Amicon und Centricon-Mikrokonzentratoren (30 und 100 kDa Ausschlussgröße) stammten von Amicon (Beverly, MA, USA).

Gase. Formiergas (95% N_2/5% H_2), das Wasserstoff-Kohlendioxid-Gemisch (80% H_2/20% CO_2), Wasserstoff (99,9995%), das Gasreinigungssystem Oxisorb© zum Entfernen von Sauerstoffspuren aus gekauften Gasen, sowie die verflüssigten Gase Stickstoff und Helium wurden von der Firma Messer Griesheim (Siegen) bezogen.

2. Anzucht von *Methanothermobacter marburgensis* und Reinigung von Methyl-Coenzym M Reduktase im MCR-red1c-Zustand

Wachstumsbedingungen. *Methanothermobacter marburgensis* (vormals *Methanobacterium thermoautotrophicum* Stamm Marburg (Wasserfallen et al. 2000)) (DSM 2133) wurde unter strikt anaeroben Bedingungen auf einem Mineralsalzmedium (Tab. 2) mit einem Gasgemisch aus 80% H_2/20% CO_2 als Energie- und Kohlenstoffquelle kultiviert (Schönheit et al. 1980). Die Kulturen wurden in 14 l Glasfermentern (New Brunswick, Michigan) in 10 l Medium bei 65°C gezogen. Die Gasflußrate betrug 1200 ml/min. Als Reduktionsmittel und Schwefelquelle wurde dem Gasgemisch 0,1% H_2S zugesetzt.

Tab. 2: Zusammensetzung des Mediums (10 l) für *Methanothermobacter marburgensis*. Zur Herstellung des Mediums wurde einfach entionisiertes Wasser verwendet.

	Komponenten	Menge	Endkonzentration
Medium	NH_4Cl	27,5 g	65 mM
	KH_2PO_4	90,0 g	50 mM
	Na_2CO_3	33,0 g	30 mM
	Resazurin (0,2%)	500 µl	20 µM
	Spurenelementlösung	15 ml	
	H_2O	ad. 10 l	
Spurenelementlösung			
	Nitrilotriessigsäure	30,0 g	160 µM
	H_2O	ad. 500 ml	
	mit 10 M NaOH auf pH 6,7 einstellen.		
	$MgCl_2$ x 6 H_2O	40,0 g	200 µM
	$FeCl_2$ x 4 H_2O	10,0 g	50 µM
	$NiCl_2$ x 6 H_2O	1,2 g	5 µM
	$CoCl_2$ x 6 H_2O	0,2 g	1 µM
	$NaMoO_4$ x 2 H_2O	0,2 g	1 µM
	H_2O	ad. 1000 ml	

Das Medium wurde mit 1200 upm gerührt. Nach ca. 1,5 h, in der das Medium durch das Begasen mit 80% H_2/20% CO_2/0,1% H_2S bei 65°C anaerobisiert wurde, wurde der Fermenter auf eine optische Dichte von ΔOD_{578} = 0,1-0,3 mit einer frischen, in der spätexponentiellen Phase geernteten Vorkultur inokuliert. Das Wachstum wurde durch Bestimmung der optischen Dichte bei 578 nm mit einem Spektralphotometer (Ultrospec 2000, Amersham Pharmacia Biotech, Freiburg) verfolgt. Die Mikroorganismen wuchsen nun mit einer Verdopplungszeit von ca. 2 h.

***In vivo* Induktion von MCR im aktiven red1-Zustand und Zellernte.** Die im folgenden beschriebene *in vivo*-Induktion des MCR-red1c-Zustandes und dessen Reinigung erfolgte weitgehend nach Angaben von Mahlert et al. (2002a). Um MCR in einem aktiven MCR-

red1-Zustand zu erhalten, wurde nach Erreichen einer ΔOD_{578} von 4,5 – 5 das Gas 30 min vor der Zellernte von 80% H_2/20% CO_2 auf 100% H_2 umgeschaltet, wodurch das MCR-red1- und zeitverzögert das MCR-red2-Signal induziert wurden. Die H_2S-Zufuhr wurde 5 min vorher abgestellt, um MCR-ox1-Kontaminationen zu vermeiden. Bevor das H_2-Gas in den Fermenter gelangte, wurde es über eine Oxisorb©säule geleitet, um Spuren von Sauerstoff zu entfernen. Nach 30 min wurde die Kultur innerhalb von 15-20 min auf 10°C abgekühlt und anschließend mit Hilfe einer Durchflußzentrifuge (Hettich, Contrifuge 17RS) unter H_2-Begasung anaerob geerntet. Durchschnittlich erhielt man dadurch zwischen 60-70 g Feuchtzellen. Sämtliche nun folgenden Reinigungsschritte wurden in einem Anaerobenzelt (Coy Instruments), gefüllt mit 95% N_2/5% H_2 durchgeführt.

Herstellung von Zellextrakt. Die Feuchtzellen wurden zunächst in 100 ml 10 mM Tris/HCl pH 7,6, versetzt mit 10 mM Coenyzm M, resuspendiert. Um zellfreien Extrakt zu erhalten, wurde die Zellsuspension in einem mit Eiswasser gekühlten Rosettengefäß mit Ultraschall (Ultraschall Desintegrator Sonoplus HD200 mit der Sonotrode TT 100, Bandelin, Berlin) mit einer Leistung von 200 W innerhalb von 35 min beschallt. Die effektive Beschallungsdauer betrug 28 min. Nicht aufgeschlossene Zellen, Zelltrümmer und Membranen wurden in einem Ultrazentrifugationsschritt bei 160 000 * *g* (Erdbeschleunigung *g*: 9,81 m s^{-1}) für 20 min entfernt (Sorvall Ultra pro 80 mit dem Rotor Ti-45, Sorvall, Bad Homburg).

Ammoniumsulfatfällungen. Der Überstand, im Folgenden als Zellextrakt bezeichnet, wurde einer fraktionierten $(NH_4)_2SO_4$-Präzipitation, bestehend aus einem 60%igen und 100%igen Schritt, unterzogen. Große Teile des Gesamtproteins vom Zellextrakt präzipitierten bei einer $(NH_4)_2SO_4$-Konzentration von 60% und wurden durch Ultrazentrifugation vom löslichen Protein getrennt. Nachdem der Überstand mit 100% $(NH_4)_2SO_4$ gefällt wurde, wurde das nach Zentrifugation erhaltene Pellet in 100 ml 50 mM Tris/HCl pH7,6, versetzt mit 10 mM Coenzym M, gelöst.

Anionenaustauschchromatographie an Q-Sepharose. Das resuspendierte Pellet nach der 100% $(NH_4)_2SO_4$-Fällung wurde auf eine Q-Sepharosesäule (High load, High performance; 3,58 cm^2 x 15 cm) aufgetragen, die zuvor mit 50 mM Tris/HCl pH 7,6 plus 10 mM Coenzym M equilibriert worden war. Die zur FPLC-Reinigung verwendeten Puffer wurden vor dem Anaerobisieren durch einen Membranfilter (0,45 µm; Pall Corporation, Michigan, USA) filtriert. Die verwendete Säule wurde über eine FPLC-Anlage (Amersham Pharmacia Biotech, Freiburg)

bei Raumtemperatur betrieben. Proteine wurden aufgrund ihrer Absorption bei 280 nm detektiert. Die Elution von MCR erfolgte in 120 ml Schritten bei einer Flussrate von 4 ml/min mit einem NaCl-Stufengradienten in 50 mM Tris/HCl pH 7,6 in Gegenwart von 10 mM Coenzym M: 360 mM; 400 mM; 440 mM, 480 mM; 520 mM; und 600 mM NaCl. MCR eluierte bei 480 mM NaCl in einem Volumen von 70-100 ml.

Das Eluat wurde anschließend mittels einer Amicon-Rührzelle (Ausschlussgröße 100 kDa) auf 3-5 ml ankonzentriert. Mit dieser Reinigungstrategie wurde MCR (ca. 150 mg) im MCR-red1-Zustand mit 0,7-0,9 Spin pro mol F_{430} in mehr als 50 Präparationen erhalten. Die spezifische Aktivität des gereinigten Enzyms betrug 10-30 U mg^{-1}, korrigiert für 1 Spin pro mol F_{430}. Gereinigte MCR wurde bei Raumtemperatur anaerob im Zelt gelagert, wobei nach 3-7 Tagen erste Aktivitätverluste auftraten.

3. Analytische Methoden

3.1 Bestimmung der Enzymaktivität

Die Aktivität von Methyl-Coenzym M Reduktase wurde anhand der zeitabhängigen Methanbildung von Methyl-Coenzym M und Coenzym B bzw. Ethanbildung von Ethyl-Coenzym M und Coenzym B bei 65°C bestimmt. Die Ansätze zur Bestimmung der katalytischen Effizienz von MCR wurden mit einem Volumen von 0,4 ml in 8 ml Serumflaschen, verschlossen mit Butylgummistopfen, durchgeführt. Dabei kamen zwei unterschiedliche Ansatzlösungen zur Anwendung. Der Ti(III)Citrat/B_{12}-Ansatz bestand aus 50 mM Kaliumphosphatpuffer pH 7,6, 10 mM Methyl-Coenzym M bzw. Ethyl-Coenzym M, 0,5 mM CoB-S-S-CoB, 10 mM Ti(III)Citrat, 0,3 mM Hydroxycobalamin und 10-200 µg gereinigter MCR. Der DTT(Dithiothreitol)-Ansatz dagegen bestand aus 50 mM Kaliumphosphatpuffer pH 7,6, 5 mM Methyl-Coenzym M, 1 mM Coenzym B, 10 mM DTT und 10-200 µg gereinigter MCR. Die Gasphase in den Flaschen bestand in allen Ansätzen aus 95% N_2/5% H_2. Die Reaktion wurde entweder durch einen Temperaturshift von 4°C auf 65°C oder durch Zugabe von MCR zum vorinkubierten Ansatz gestartet. In Intervallen von 0,5 bis 3 min wurden Gasproben von 0,2 ml entnommen und auf ihren Methan- bzw. Ethangehalt hin mittels Gaschromatographie analysiert (Bonacker et al. 1993; Goubeaud et al. 1997).

Dazu wurde ein Gaschromatograph GC 8000 (Carlo Erba, Mailand, Italien) mit Flammenionisationsdetektor (FID) verwendet (Tab. 3). Zur Kalibrierung dienten selbst hergestellte Gasgemische mit unterschiedlichen Methan- bzw. Ethankonzentrationen.

Tab. 3: Einstellungen und verwendete Materialien am Gaschromatographen GC 8000 (Carlo Erba, Mailand) für die Bestimmung von Methan und Ethan. Die Retentionszeit betrug dabei für Methan etwa 0,5 min und für Ethan etwa 0,6 min.

Detektor		FID
Säule		Edelstahlsäule (130 x 0,2 cm)
Material		Molekularsieb 0,5 nm
Temperatur	(Injektor)	80°C
	(Säule)	150°C
	(Detektor)	150°C
Trägergas		Stickstoff
Eingangsdruck		5 bar
Trägergasfluß		30 ml min^{-1}
Brenngas		Wasserstoff/Luft
Eingangsdruck	(H_2)	5 bar
	(Luft)	5 bar
Brenngasfluß	(H_2)	10 ml min^{-1}
	(Luft)	250 ml min^{-1}

Für die inhibitorischen Substratanaloga von Methyl-Coenzym M wurden K_i-Werte im Dixon-Plot bestimmt (Segel 1993). Dazu wird die Geschwindigkeit der Methanbildung aus Methyl-Coenzym M und Coenzym B in Abhängigkeit steigender Inhibitorkonzentrationen gemessen. Durch die Auftragung der reziproken Methanbildungsrate gegen die steigende Inhibitorkonzentration läßt sich im Dixon-Plot der K_i ablesen. Dieser ist definiert als die Inhibitorkonzentration, welche die Steigung der Geraden im Dixon-Plot verdoppelt.

3.2 Bestimmung des Proteingehaltes

Die Proteinbestimmung wurde mit dem BioRad-Microassay durchgeführt (BioRad Laboratories, 1990). Das Testprinzip beruht auf der Verschiebung des Absorptionsmaximums von Coomassie Brilliantblau R250 in saurer Lösung von 465 nm zu 595 nm durch die Bindung des Farbstoffes an Proteine (Bradford 1976). Dazu wurden 0,8 ml Probe bzw. Rinderserumalbumin als Standard (0-8 µg pro 0,8 ml) mit 0,2 ml BioRad-Proteinfarbstoffreagenz versetzt und die Extinktion der Lösung nach 20 min bei 595 nm gegen Wasser, versetzt mit 0,2 ml Farbstoffkonzentrat, als Referenzwert am Spektralphotometer bestimmt (Ultrospec 2000, Amersham Pharmacia Biotech, Freiburg).

3.3 Aufnahme von UV/Vis-Spektren

UV/Vis-Spektren von MCR wurden standardmäßig an einem Dioden-Array-Photometer (Specord S10 von Zeiss, Jena) bei Raumtemperatur bestimmt. Dazu wurden die Enzymproben (5-15 mg ml^{-1}; 0,5 - 1 ml) im Anaerobenzelt unter 95% N_2/5% H_2 in 1 ml Quarzküvetten (Helma) mit einer Schichtdicke von 1 cm überführt. Die Küvetten wurden entweder direkt im Anaerobenzelt gemessen oder für Temperaturmessungen mit einem Butylgummistopfen verschlossen, durch den eine Temperaturmeßelektrode gestochen wurde, und die Spektren außerhalb des Anaerobenzeltes aufgenommen. Als Referenz wurde anaerober Puffer verwendet.

Bestimmung des F_{430}-Gehaltes. Der Gehalt an F_{430} in den MCR-Präparationen wurde über das Absorptionsmaximum des proteingebundenen F_{430} bei 420 nm bestimmt: Es wurde der von Pfaltz et al. (1982) bestimmte, molare Extinktionskoeffizient von 22000 M^{-1} cm^{-1} für Ni(II)F_{430} verwendet. Vor der Messung wurden die anaeroben Proben kurz mit Sauerstoff in Kontakt gebracht oder mit 10 mM 2-Bromoethansulfonat (BES) versetzt, um Ni(I)F_{430} mit einem Absorptionsmaximum von 386 nm zu Ni(II)F_{430} zu oxidieren.

Unter der Annahme, daß MCR 2 mol F_{430} pro mol Enzym enthält, konnte der F_{430}-Gehalt der MCR-Präparationen auch aus der ermittelten Proteinkonzentration errechnet werden. Dabei wurde mit einem Molekulargewicht von MCR von 150 kDa pro mol Nickel gerechnet. Beide Methoden führten zu gleichen Ergebnissen.

4. Aufnahme und Auswertung der EPR-Spektren

4.1 Grundlagen der EPR-Spektroskopie

Im Allgemeinen werden bei spektroskopischen Messungen Energiedifferenzen zwischen Atom- oder Molekülzuständen gemessen, um Stoffe zu analysieren, zu quantifizieren oder Einsicht in deren Struktur zu bekommen. Die in einem EPR-Experiment untersuchten Energiedifferenzen stammen in erster Näherung von der Wechselwirkung ungepaarter Elektronen mit einem Magnetfeld B_0, welches von außen an die Probe angelegt wird. Diese Wechselwirkung beruht darauf, dass der quantenmechanische Drehimpuls, der Elektronenspin (m_s = +1/2 oder –1/2), ein magnetisches Moment (μ_e) besitzt. Dieses magnetische Moment verhält sich wie eine Kompassnadel im Erdmagnetfeld, und richtet sich parallel (höhere Energie) oder antiparallel (niedrigere Energie) zum äußeren Magnetfeld aus. Diese Aufspaltung wird auch als Elektonen-Zeemann-Aufspaltung bezeichnet (Abb. 7).

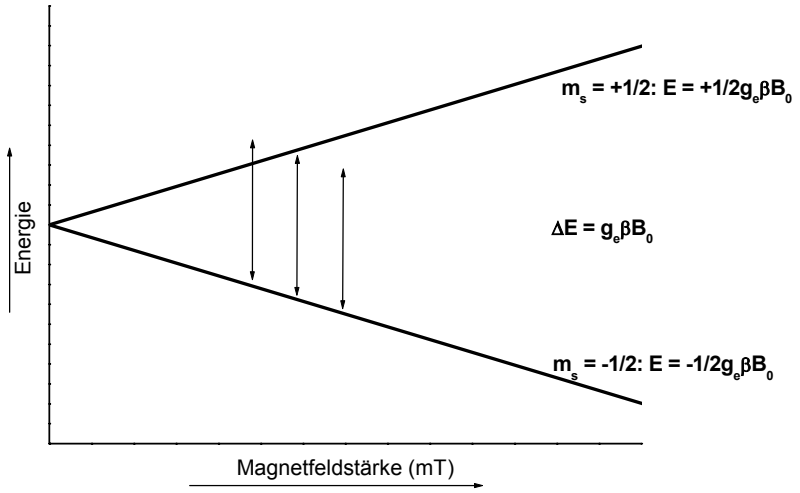

Abb. 7: Abhängigkeit der Energiedifferenz der beiden Spinzustände m_s = +/- ½ eines Elektrons von der Magnetfeldstärke des äußeren Feldes. Die drei vertikalen Pfeile stehen für die Energie, die mit dem Mikrowellen-Quantum assoziiert ist und verdeutlichen, daß es genau einen Wert für das magnetische Feld gibt, an dem die Absorption der Mikrowellen stattfinden kann.

Die Energiedifferenz zwischen den beiden Zuständen ist direkt proportional zu der Stärke des magnetischen Feldes:

$$E = \mu B \qquad \mu = +/- \frac{1}{2} g\beta \qquad (1)$$

$$\Delta E = 2\mu B = g\beta B \qquad (2)$$

wobei E die Energie (in Joule), B die Magnetfeldstärke (in Tesla), *g* ein Proportionalitätsfaktor, dessen Wert direkt proportional zum magnetischen Moment μ ist, und β das Bohrmagneton (Joule/Tesla), darstellt.

Werden nun Mikrowellen geeigneter Frequenz (und damit geeigneter Energie) eingestrahlt, so kommt es zu Absorptionseffekten. Diese treten genau dann auf, wenn die Energie der Mikrowellen genau der Energiedifferenz der beiden Zustände entspricht, und es dadurch zur Umkehr der Orientierung des Spins im magnetischen Feld kommt:

$$h\nu = g\beta B \qquad\qquad g = 0{,}7145\,\frac{\nu\,[\mathrm{MHz}]}{B\,[\mathrm{Gauss}]} \qquad\qquad (3)$$

wobei h das Plancksche-Wirkungsquantum ($6{,}6 * 10^{-34}$ J * s) und ν die Mikrowellen-Frequenz in Hertz ist. Der *g*-Wert ist spezifisch für die jeweilige Probe. Für ein freies Elektron (Radikal) ergibt sich:

$$g = g_e = 2{,}0023 \qquad\qquad (4)$$

Aus technischen Gründen erfolgt die Messung von EPR-Spektren bei konstanter Frequenz und variablen Magnetfeldstärken. Ferner wird dabei die erste Ableitung des eigentlichen Spektrums aufgezeichnet, um ein besseres Signal- und Rauschverhältnis zu erhalten.

Die Eignung dieses Meßverfahrens als spektroskopische Methode für eine „reale“ Probe rührt daher, daß neben dem eigenen magnetischen Moment des Elektrons (μ_e) noch ein magnetisches Orbitalmoment (μ_o) existiert. Dieses wird von dem Orbital, in dem sich das Elektron befindet (z.B. *s*-, *p*- oder *d*-Orbital), der Kerngröße und auch von der Symmetrie des Moleküls beeinflußt. Beide magnetischen Momente koppeln und ergeben das gesamte magnetische Moment ($\mu_{ges} = \mu_e + \mu_o$) des Systems (Spin-Bahn Kopplung). Aus Gleichungen (1) und (2) ergibt sich dadurch auch eine Verschiebung der *g*-Werte und damit aus Gleichung (3) eine Verschiebung der Resonanzfrequenz. Der Einfluss des magnetischen Bahnmomentes führt also zum Abweichen des *g*-Wertes von 2,0023.

Das magnetische Moment μ stellt im Prinzip einen Vektor dar. Das magnetische Moment μ_e des Elektrons koppelt nur mit dem Anteil von des magnetischen Moments μ_0, welcher parallel zum äußeren Magnetfeld steht. Ein Spin mit kugelsymmetrischer Umgebung zeigt ein isotropes EPR-Signal, da der Betrag des magnetischen Moments μ_o in jeder Richtung gleich ist. Ist die

magnetische Umgebung des Paramagneten axialsymmetrisch, so wird ein axiales, anisotropes EPR-Signal detektiert. Haben alle drei Raumrichtungen einen unterschiedlichen Betrag, so erhält man ein rhombisches Signal. Bei einer Probe, in der die räumliche Orientierung eines jeden Moleküls zufällig und jede Position gleich wahrscheinlich ist (Powder-Spektrum), ergeben sich für die drei genannten Beispiele die Spektren, wie sie in Abbildung 8 dargestellt sind.

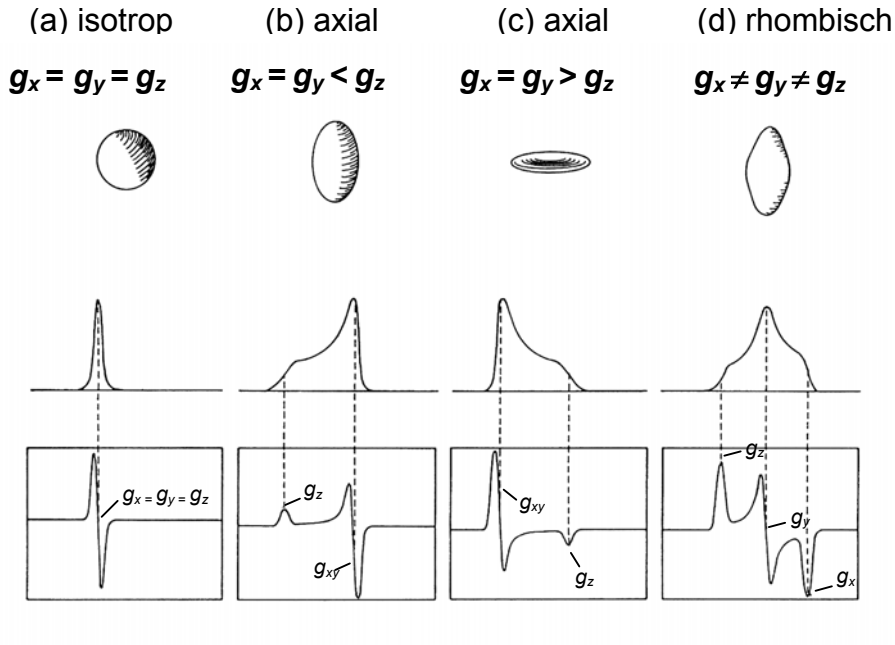

Abb. 8: Grundlegende EPR-Spektren von *S* = 1/2 Paramagneten. Die Säulen (a-d) zeigen von oben nach unten den Spektraltyp, die *g*-Anisotropie (dargestellt in Zahlen und einer graphischen Darstellung), sowie die idealisierten Spektren, zunächst in der Absorptionsform und dann in der 1. Ableitung des Spektrums. Entnommen aus: (Palmer 2000).

Neben den magnetischen Orbitalmomenten, kann der Spin auch mit weiteren räumlich benachbarten magnetischen Momenten interagieren. In der vorliegenden Arbeit ist vor allem das magnetische Moment hervorgerufen vom Kernspin $I = 1$ von ^{14}N von Bedeutung. Dieses ruft eine Superhyperfeinauflösung im EPR-Signals hervor, da sich, vereinfacht dargestellt, das magnetische Moment des Kerns im äußeren Magnetfeld B ausrichtet und sich das Magnetfeld B_k des Kerns entweder zu dem äußeren Magnetfeld B addiert oder subtrahiert. Im Falle von ^{14}N ist diese Aufspaltung dreifach, da der Kern, mit einem Kernspin von $I = 1$, drei verschiedene Orientierungen im Magnetfeld annehmen kann.

Die hier dargestellten physikalischen Zusammenhänge wurden aus dem Lehrbuch „Electron Paramagnetic Resonance“ von J.A. Weil, J.R. Bolton und J.E. Wertz (Weil et al. 1994)

und einem Skript von Gunnar Jeschke „Einführung in die ESR-Spektroskopie“ (http://www.mpip-mainz.mpg.de/~jeschke/vbook.pdf) entnommen.

4.2 Vorbereitung der Proben

Die EPR-Probenröhrchen bestanden aus hochreinem Quarzglas (99,99%) mit einem Innendurchmesser von 3 mm bei einer Wandstärke von 0,5 mm. Diese wurden nach Befüllen des Röhrchens mit 350 µl Probe mittels eines Plastikstabes und eines etwa 3 cm langen Latexschlauchs verschlossen. Für Raumtemperaturmessungen wurden Quarzröhrchen mit einer flachen Innenzelle verwendet, die nach Befüllen mit Parafilm (American National Can, Chicago, USA) verschlossen wurden. Die Anaerobisierung der Röhrchen und des Verschlußmaterials erfolgte durch Lagerung im Anaerobenzelt unter einer 95% N_2/5% H_2-Atmosphäre. Nach dem Verschließen der Röhrchen wurden die Proben entweder bereits im Anaerobenzelt in einem Ethanol-Flüssigstickstoffbad oder außerhalb des Zeltes in flüssigem Stickstoff (77 K) eingefroren. Nach dem Einfrieren wurde der Latexschlauch eingeschnitten, um das Entstehen eines Überdruckes beim späteren Auftauen des Röhrchens zu vermeiden. Bei Lagerung der Proben in flüssigem Stickstoff veränderten sich die EPR-Signale in ihrer Intensität nicht.

4.3 Aufnahme der EPR-Spektren

EPR-Spektren wurden bei 9,4 GHz (X-Band) in einem Bruker EMX-6/1 EPR-Spektrometer, bestehend aus einer EMX 1/3 Konsole, einer ER-041 X6 Brücke mit eingebautem ER-0410-116 Frequenzzähler, einem ER-070 Magneten und einem ER-4102st Standard-Resonator, bei einer Feld-Modulationsfrequenz von 100 kHz aufgezeichnet. Die Kühlung der Proben erfolgte entweder in einem Helium-Flußsystem in einem Kryostaten mit einem Temperatursensor (Oxford Instruments ESR 900 Cryostat) oder standardmäßig mit flüssigem Stickstoff in einem Finger-Dewar-Gefäß bei 77 K.

4.4 Interpretation und Quantifizierung von EPR-Spektren

Die Auswertung der EPR-Spektren erfolgte sowohl mit dem Programm WIN-EPR von Bruker als auch mit den von Simon Albracht entwickelten und zur Verfügung gestellten Computerprogrammen. Die Grundlagen der Quantifizierung und Simulation von EPR-Daten sind von Beinert und Albracht (1982) beschrieben worden. Dabei wird bei axialen Signalen g_z am Maximum der Absorptions-Typ-Linie und g_{xy} am unteren Drittel der Ableitungs-Typ-Linie

bestimmt. Bei rhombischen Signalen sind g_z und g_x an den Extrema der Absorptions-Typ-Linie und g_y am Schnittpunkt mit der 0-Linie definiert.

Differenzspektren wurden mit dem von Bruker oder S. Albracht entwickelten Computerprogrammen gebildet. Die endgültige graphische Darstellung der EPR-Spektren erfolgte mit Hilfe des Programms Origin (Microcal, Northhampton, MA).

Zur Bestimmung der Spinkonzentration wurde neben den Proben immer ein Standard gemessen. Eine 10 mM Cu(II)-Lösung (10 mM $CuSO_4$ x 5 H_2O, 2 M $NaClO_4$, 10 mM HCl) diente als Standard, der unter nicht-sättigenden Bedingungen, bei gleicher Temperatur und gleicher Modulationsamplitude wie die zu untersuchende Probe gemessen wurde. Da die Fläche unter dem ursprünglichen Spektrum proportional zu der Konzentration der absorbierenden Elektronen ist, erfolgt die quantitative Bestimmung der Spinkonzentration über die normierten Doppelintegrale (I_N) der gemessenen Spektren. Die Berechnungen wurden mit den von S. Albracht oder Brucker entwickelten Computerprogrammen durchgeführt. Das normierte Doppelintegral (I_N) berechnet sich unter Einbeziehung von Geräte- und Probeneigenschaften nach der von Aasa et al. (1975) erstellten Gleichung aus dem berechneten Doppelintegrals I_0 wie in der unten dargestellten Gleichung. Diese Korrekturen wurden bereits von den Computerprogrammen übernommen.

$$C_P = \frac{I_N(\text{Probe}) \text{ x } C_s}{I_N(\text{Standard})} \qquad I_n = \frac{I_0 \text{ x } d^2 \text{x } T \text{ x } 10^{dB/20}}{g_p^{av} \text{x } f \text{ x } a}$$

C_P	Spinkonzentration der Probe	dB	Mikrowellenenergie
C_S	Spinkonzentration des Standards	f	Röhrchen-Faktor
I_n	Normiertes Doppelintegral	a	Verstärkerstufe
I_0	gemessene Intensität	d	Abstand der Meßpunkte
T	Temperatur [K]		

VI Ergebnisse/Publikationen

Das folgende Kapitel beinhaltet vier Publikationen zur Thematik der vorliegenden Doktorarbeit, die im Zeitraum dieser Arbeit entstanden. Darin wurden die gewonnenen Ergebnisse zu Untersuchungen der Aktivität von Methyl-Coenzym M Reduktase und des Redoxzustandes des Nickels in der prosthetischen Gruppe F_{430} wiedergegeben. Diese aktuellen Daten tragen zu erweiterten Erkenntnissen bezüglich der MCR bei und ermöglichen so die erneute Diskussion um einen möglichen Katalysemechanismus für das Enzym, welche sich ausführlich im nachfolgenden Diskussionskapitel anschließt.

Die Publikation „Probing the reactivity of Ni in the active site of methyl-coenzyme M reductase with substrate analogues“ greift bereits früher publizierte Untersuchungen auf. Als klassischer Ansatz zur Aufklärung des Katalysemechanismus eines Enzyms dient die Beobachtung von Änderungen in der Enzymreaktivität durch Substrate mit veränderter Struktur, sogenannten Substratanaloga. Im Falle von MCR wurden die ersten solcher Versuche schon 1978 von Ralph Wolfe und Mitarbeitern (Gunsalus et al. 1978) durchgeführt und dabei Ethyl-Coenzym M als alternatives Substrat zu Methyl-Coenzym M, sowie 2-Bromoethansulfonat als potenter Inhibitor, identifiziert. Die erste Bestimmung von kinetischen Parametern dieser und einer ganzen Reihe weiterer Methyl-Coenzym M-Analoga wurden später in einer umfangreichen Studie von Christopher T. Walsh und Mitarbeitern durchgeführt (Wackett et al. 1987; Wackett et al. 1988). Hier wurden jedoch alle Aktivitätsmessungen in zellfreien Extrakten methanogener Archeaenkulturen vorgenommen, in denen ein Großteil der MCR bereits im inaktiven Zustand vorlag. Auch in einigen späteren Arbeiten mit Substratanaloga der MCR konnten Aktivitäten nur in partiell gereinigter und/oder teilweise inaktiver MCR gemessen werden. Die komplette Aufreinigung von zu mehr als 85%ig aktivem Enzym (Mahlert et al. 2002a) ermöglichte es schließlich, viele der in Wackett et al. (1988) aufgeführten Methyl-Coenzym M-Analoga noch einmal zu untersuchen. Neben den kinetischen Eigenschaften wurde zudem mittels EPR-Spektroskopie der Einfluß dieser Substratanaloga auf den Ni(I)-Zustand in der prosthetischen Gruppe F_{430} untersucht.

Zwei Analoga des Substrates Coenzym B sind u. a. Gegenstand einer weiteren Veröffentlichung „Temperature dependence of methyl-coenzyme M reductase (MCR) activity

and of the formation of the MCR-red2 state induced by coenzyme B". Wie bereits in der Einleitung dieser Arbeit erwähnt, wird das rhombische EPR-Signal MCR-red2 nur in Gegenwart von Coenzym M (einem Methyl-Coenzym M-Analog) und Coenzym B zu maximal 50% induziert (Mahlert et al. 2002a). Im Rahmen von Experimenten zur versuchten Umkehrbarkeit der von MCR katalysierten Reaktion durch hohe Methankonzentrationen, wurde eine solche MCR-Probe mitsamt des sie umgebenden, 0,5 cm starken Metallzylinders eingefroren. Trotz der Gegenwart von Coenzym M und Coenzym B zeigte diese Probe fast ausschließlich das axiale MCR-red1-Signal und nicht das rhombische MCR-red2-Signal. Dieses Phänomen führte nach umfangreichen Kontrollen zur Entdeckung der Temperaturabhängigkeit des red2-Signals.

Eine dritte Publikation „Coenzym B induced coordination of coenzym M via its thiol group to Ni(I) of F_{430} in active methyl-coenzyme M reductase" charakterisiert schließlich erstmals sicher das Umfeld des Nickels von F_{430} im MCR-red2-Zustand. Ausgangspunkt für diese Arbeit war die Frage nach einer Interaktion des Thioetherschwefels von Coenzym M (als Methyl-Coenzym M-Analog) mit dem Nickelzentralatom von F_{430} in einem der bekannten EPR-detektierbaren MCR-Zustände. Zu diesem Zweck wurde zunächst in der Arbeitsgruppe von Prof. Dr. Bernhard Jaun (ETH Zürich) Seleno-Coenzym M synthetisiert. Statt einer Selen-Nickel-Koordinierung führte jedoch die Zugabe dieses Analogs zu aktiver MCR zu einer Inaktivierung des Enzyms durch die Oxidation des Ni(I) zu Ni(II) (siehe dazu Goenrich et al. 2004a). Einen erfolgreichen Ansatz lieferte anschließend der Einsatz von ^{33}S-markiertem Coenzym M. Hier wurde eine Koordinierung von Nickel mit ^{33}S im MCR-red2-Zustand des Enzyms identifiziert.

Die vierte Publikation „Spectroscopic investigation of the nickel-containing porphinoid cofactor F_{430}. Comparison of the free cofactor in the +1, +2 and +3 oxidation states with the cofactor bound to methyl-coenzyme M reductase in the silent, red and ox forms" beschäftigt sich schließlich mit der Frage nach dem Oxidationszustand des Nickelzentralatoms in F_{430}, eine Frage, die unerläßlich ist für die endgültige Darstellung eines Katalysemechanismus von MCR. Hierzu wurde eine umfangreiche Studie über MCR im red1-, red2- und einigen silent-Zuständen durchgeführt, in deren Verlauf Messungen des magnetischen zirkularen Dichroismus bei variiernden Temperaturen und variierendem Magnetfeld (VTVH MCD) vorgenommen wurden, sowie Absorption- und EPR-Spektren gemessen wurden. Diese elektronischen und magnetischen Eigenschaften wurden zu Interpretationszwecken anschließend mit denen von pentamethyliertem F_{430} (F_{430}M) im Ni(I)-, Ni(II)- und Ni(III)-Zustand verglichen.

J Biol Inorg Chem (2004), published online as HTML version
DOI 10.1007/s00775-004-0552-1

ORIGINAL ARTICEL

Meike Goenrich · Felix Mahlert · Evert C. Duin
Carsten Bauer · Bernhard Jaun · Rudolf K. Thauer

Probing the reactivity of Ni in the active site of methyl-coenzyme M reductase with substrate analogues

Received: 17 March 2004 / Accepted: 21 April 2004 / Published online: 15 June 2004

Abstract Methyl-coenzyme M reductase (MCR) catalyses the reduction of methyl-coenzyme M (CH_3-S-CoM) with coenzyme B (HS-CoB) to methane and CoM-S-S-CoB. It contains the nickel porphinoid F_{430} as prosthetic group which has to be in the Ni(I) oxidation state for the enzyme to be active. The active enzyme exhibits an axial Ni(I) derived EPR signal MCR-red1. We report here on experiments with methyl-coenzyme M analogues showing how they affect the activity and the MCR-red1 signal of MCR from *Methanothermobacter marburgensis*.

Ethyl-coenzyme M was the only methyl-coenzyme M analogue tested that was used by MCR as a substrate. Ethyl-coenzyme M was reduced to ethane (apparent K_M = 20 mM; apparent Vmax = 0.1 U/mg) with a catalytic efficiency of less than 1% of that of methyl-coenzyme M reduction to methane (apparent K_M = 5 mM; apparent Vmax = 30 U/mg). Propyl-coenzyme M (apparent K_i = 2 mM) and allyl-coenzyme M (apparent K_i = 0.1 mM) were reversible inhibitors.

2-Bromoethanesulfonate ($[I]_{0.5V}$ = 2 µM), cyano-coenzyme M ($[I]_{0.5V}$ = 0.2 mM), 3-bromopropionate ($[I]_{0.5V}$ = 3 mM), seleno-coenzyme M ($[I]_{0.5V}$ = 6 mM) and trifluoromethyl-coenzyme M ($[I]_{0.5V}$ = 6 mM) irreversibly inhibited the enzyme. In their presence the MRC-red1 signal was quenched indicating the oxidation of Ni(I) to Ni(II). The rate of oxidation in the presence of coenzyme B increased over 10 fold in the presence of coenzyme B indicating that the Ni(I) reactivity was increased. Enzyme inactivated in the presence of coenzyme B showed an isotropic signal characteristic of a radical, that is spin coupled with one hydrogen nucleus. The coupling was also observed in D_2O. The signal was abolished upon exposure of the enzyme to O_2.

3-Bromopropanesulfonate ($[I]_{0.5V}$ = 0.1 µM), 3-iodopropanesulfonate ($[I]_{0.5V}$ = 1 µM), and 4-bromobutyrate also inactivated MCR. In their presence the EPR signal of MCR-red1 was converted to a Ni based EPR signal MCR-BPS that resembles in line shape the MCR-ox1 signal. The signal was quenched by O_2.

2-Bromoethanesulfonate and 3-bromopropanesulfonate, which both rapidly reacted with Ni(I) of MRC-red1, did not react with the Ni of MCR-ox1 and MCR-BPS: The Ni based EPR spectra of both inactive forms were not affected in the presence of high concentrations of these two potent inhibitors.

Keywords Methyl-coenzyme M reductase · Nickel enzymes · Factor 430 · Catalytic mechanism · EPR spectroscopy · Methanogenic archaea

Abbreviations H_3C-S-CoM: methyl-coenzyme M · HS-CoM: coenzyme M · HS-CoB: coenzyme B · MCR: methyl-coenzyme M reductase · MCR-red1: MCR exhibiting the EPR signals red1a, red1c or red1m · MCR-red1c: MCR-red1 in the presence of coenzyme M · MCR-red1m: MCR-red1 in the presence of methyl-coenzyme M · MCR-red1a: MCR-red1c or MCR-red1m after extensive washing by ultrafiltration in the absence of coenzyme M and methyl-coenzyme M · MCR-red2: MCR exhibiting both the red1 and red2 EPR signals · MCR-ox: MCR exhibiting the EPR signals ox1, ox2 or ox3 · BES: 2-bromoethanesulfonate · BPS: 3-bromopropanesulfonate

M. Goenrich · F. Mahlert · R. K. Thauer (✉)
Max-Planck-Institut für terrestrische Mikrobiologie
and Laboratorium für Mikrobiologie, Fachbereich Biologie,
Philipps-Universität, Karl-von-Frisch-Strasse,
35043 Marburg, Germany
E-mail: thauer@staff.uni-marburg.de
Fax: +49 6421178209

E. C. Duin
Department of Chemistry,
Auburn University, AL 36849, USA

C. Bauer · B. Jaun
Laboratorium für Organische Chemie,
Eidgenössische Technische Hochschule Zürich,
ETH Hoenggerberg HCI, 8093 Zürich, Switzerland

INTRODUCTION

Methyl-coenzyme M reductase (MCR) is a nickel enzyme found in all methanogenic archaea [1], in which it catalyses the methane forming step [2]. The nickel is bound within the prosthetic group F_{430}, which is a nickel porphinoid. The active enzyme contains F_{430} in the Ni(I) oxidation state as evidenced by EPR and UV/Vis spectroscopy [3-5]. It catalyses the reduction of methyl-coenzyme M (CH_3-S-CoM) with coenzyme B (HS-CoB) to methane (CH_4) and the heterodisulfide CoM-S-S-CoB.

CH_3-S-CoM + HS-CoB = CH_4 + CoM-S-S-CoB
$\Delta G^{o\prime}$ = - 25 kJ/mol

Indirect evidence is available that MCR is also involved in anaerobic methane oxidation of methane [6].

The crystal structure of the inactive MCR (with F_{430} in the Ni(II) oxidation state) from *Methanothermobacter marburgensis* has been resolved to 1.16 Å [7-10]. The $\alpha_2\beta_2\gamma_2$ heterohexamer of molecular mass 300 kDa forms two separate active sites with F_{430} as prosthetic group deeply buried within the protein and accessible from the outside only via a 50 Å long narrow channel through which methyl-coenzyme M can diffuse to the bottom. The channel is built such that the long aliphatic arm of coenzyme B can only reach into the channel to the extent where its terminal thiol group is still at a distance of 8 Å from the nickel. Once coenzyme B is bound methyl-coenzyme M can no longer enter the channel. Methyl-coenzyme M binding appears to facilitate that of coenzyme B thus ensuring that methyl-coenzyme M enters first [9, 10].

Active MCR exhibits a characteristic axial Ni(I) derived EPR signal designated MCR-red1 [3, 11-13]. In the absence of substrates this signal is referred to as MCR-red1a [5]. In this state the signal shows hyperfine splitting due to the interaction of the electron spin with the nuclear spins (S=1/2) of the four nitrogens of the tetrapyrrole ring system. The active enzyme in the presence of the substrate methyl-coenzyme M is referred to as MCR-red1m. The corresponding EPR signal shows improved resolution in comparison to MCR-red1a. Active MCR in the presence of coenzyme M, which inhibits the enzyme competitively to methyl-coenzyme M, is referred to as MCR-red1c. Its EPR signal shows less resolved hyperfine splitting than MCR-red1m but is otherwise unchanged. When both coenzyme M and coenzyme B are present the axial red1 signal is partially and reversibly converted into a strongly rhombic Ni(I) derived EPR signal designated MCR-red2. The red2 signal rather than the red1 signal broadens characteristically when $H^{33}S$-CoM is employed indicating coordination of the thiol group of coenzyme M to the Ni(I) center of F_{430} in the presence of coenzyme B [14, 15]. Apparently, binding of coenzyme B to active MCR induces a conformational change which is required for the Ni(I) to be able to interact with the thiol group of coenzyme M and a corresponding change is assumed to be required for Ni(I)F_{430} to react with methyl-coenzyme M. Methyl-coenzyme M is not reduced to methane by active MCR in the absence of coenzyme B, as shown in a single turnover experiment [5, 16]. Also free reduced F_{430} pentamethyl ester does not react with methyl-coenzyme M [17]. These findings indicate that either F_{430} or the substrate must be somehow activated for the reduction to occur. It was shown that methyl sulfonium ions such as *S*-methyl methyl-coenzyme M [18] are readily reduced to methane by free Ni(I)F_{430} pentamethyl ester, and photolytically generated Ni(I)/thiyl radical pairs reacted with methyl thioether functions to give disulfides and methane [19, 20]. These reactions could be considered as models of substrate activation.

Presently two catalytic mechanisms for the enzymatic conversion of methyl-coenzyme M to methane and CoM-S-S-CoB are favoured. Mechanisms I assumes that the first step in the catalytic cycle is a nucleophilic attack of the methyl group of methyl-coenzyme M by Ni(I) of the F_{430} prosthetic group yielding methyl-Ni(III), which reacts with the coenzyme M thiolate to methyl-Ni(II) and the coenzyme M thiyl radical. In this mechanism methane is generated by protonolysis of methyl-Ni(II) in an electrophilic substitution reaction [7, 9, 10]. Mechanism II assumes that the first step in the catalytic cycle is the attack of the thioether sulfur of methyl-coenzyme M by Ni(I) yielding a free methyl radical which reacts with the thiol group of coenzyme B to methane and the coenzyme B thiyl radical [21-23]. In favour of mechanism I is that it can explain the observed inversion of stereoconfiguration in ethyl-coenzyme M reduction to ethane [24] and that it involves a methyl-Ni(II) intermediate which has been shown to be an intermediate in the reduction of activated methylthioethers to methane by free reduced F_{430} pentamethyl ester [18, 25]. Arguments against mechanism I are that - at least in solution - Ni(I) in F_{430} is not a strong enough nucleophile to attack the methyl group of unactivated methyl-coenzyme M in a nucleophilic substitution reaction [17] and that it is unknown whether methyl-Ni(III) is a strong enough oxidant to oxidize the coenzyme M thiolate to the thiyl radical. In favour of mechanism II is mainly that the calculated energy profile, especially that of the first step, appears to be much more favourable than that calculated for mechanism I [22-23]. An argument against mechanism II is that inversion of stereoconfiguration (as observed in the case of ethyl-coenzyme M) would require hydrogen abstraction by the intermediate methyl radical before it has time to rotate inside the active site. Although Ahn et al. [24] observed only ca. 60% of the maximal enantiomeric excess possible on the basis of the optical purity of their starting material, it is difficult to judge whether the enzyme reaction did indeed in part proceed under racemization or if the partial loss of enantiomeric purity was due to the very harsh conditions needed to convert the resulting ethane to acetic acid.

The oxidation state of Ni in the enzymatically inactive MCR-ox states, which like MCR-red1 exhibit a Ni based EPR signal, is still an open question. The MCR-ox states are generated from MCR-red2 by the addition of polysulfide (MCR-ox1), sulfite (MCR-ox2) or O_2 (MCR-ox3) [26]. EPR and ENDOR results have been interpreted as indicating a Ni(I) oxidation state for the MCR-ox states [27, 28] and Raman data led to the proposal that MCR-red1 and MCR-ox1 differ in the reduction state of the porphinoid ligand system rather than in the Ni oxidation state [29-30]. However, this hypothesis is inconsistent with recently published experimental results [31] and density function calculations [32].

In the following communication we have probed for the reactivity of Ni in MCR-red1 and MCR-ox1 with analogues of methyl-coenzyme M to further our understanding of the catalytic mechanism of MCR and of the oxidation state of Ni in the inactive MCR-ox states. The reaction of ethyl-coenzyme, allyl-coenzyme M, 2-bromoethanesulfonate (BES) and 3-bromopropanesulfonate (BPS) with MCR-red1 and MCR-ox1 in the absence and presence of coenzyme B are described in greater detail.

Material and Methods

Methanothermobacter marburgensis (*Methanobacterium thermoautotrophicum,* strain Marburg [33]) is the strain deposited under DSM 2133 in the Deutsche Sammlung von Mikroorganismen und Zellkulturen (Braunschweig). Coenzyme M (2-mercaptoethanesulfonate) was obtained from Merck (Darmstadt); methyl-coenzyme M was synthesized from coenzyme M by methylation with methyl iodide (Fluka) [5, 34]. According to the same protocol ethyl-coenzyme M and propyl-coenzyme M were synthesized from their corresponding iodides. Coenzyme B (*N*-7-mercaptoheptanoylthreonine phosphate) was prepared from the symmetric disulfide CoB-S-S-CoB by reduction with $NaBH_4$ as previously described [35, 36]. 2-Bromoethanesulfonic acid (BES) and 3-bromopropionic acid were obtained from Fluka and 4-bromobutyric acid from Aldrich. 3-Bromopropanesulfonate (BPS), 3-fluoropropanesulfonate and 3-iodopropanesulfonate were from the same preparations used by Rospert et al. [37].

Purification of active MCR

M. marburgensis was grown at 65°C in a 13 L glass fermenter (New Brunswick) containing 10 L mineral medium stirred at 1200 rpm and gassed with 80% H_2/20% CO_2/0.1% H_2S at a rate of 1200 mL/min [5]. When an ΔOD_{578} of 4.5 was reached, the gas supply was switched to 100% H_2 for 30 min to induce the EPR signals MCR-red1 and red2 in the cells. After 30 min the cells were cooled to 10°C within 10 min under continuous gassing and harvested anaerobically by centrifugation using a flow-through centrifuge (Hettich, centrifuge 17 RS). Approximately 70 g of wet cells were obtained. From these cells only the MCR isoenzyme I was purified [38, 39]. All steps of the purification were performed in the presence of 10 mM coenzyme M and in an anaerobic chamber (Coy Instruments) filled with 95% N_2/5% H_2 as described previously [5]. During purification the enzyme lost its MCR-red2 signal due to the removal of coenzyme B. In one purification generally 150 mg active MCR in the red1c state (in 120 mL) were obtained. The spin concentration per mol F_{430} was higher than 0.8.

To obtain MCR-red1a the purified MCR-red1c was washed free of coenzyme M with 50 mM Tris/HCl pH 7.6 by ultrafiltration with Amicon Ultra Centrifugal Filter Devices with a 100 kDa cut of (Millipore, Bedford MA). The spin concentration per mol F_{430} generally decreased to values between 0.5 and 0.8 during the washing procedure. MCR-red1a was converted to MCR-red1m by addition of methyl-coenzyme M to a final concentration of 10 mM.

The protein concentration was determined by using the method of Bradford [40] with bovine serum albumin (Serva) as standard or by measuring the absorbance difference of oxidized enzyme (MCR-silent) at 420 nm using an ε = 44,000 $M^{-1}cm^{-1}$ for a molecular mass of 280,000 Da. Both methods yielded almost the same results.

MCR activity determination

Methyl-coenzyme M reductase activity was determined by following methane formation at 65°C gaschromatographically. The assays were performed in 8 mL serum bottles containing 0.4 mL assay solution and closed with a rubber stopper. Two different assay solutions were used. The DTT (dithiothreitol)-assay solution was composed of 50 mM potassium phosphate pH 7.6, 5 mM methyl-coenzyme M, 1 mM HS-CoB, 10 mM DTT and 10 – 200 µg of MCR. The Ti(III)/B_{12}-assay solution was composed of 50 mM potassium phosphate pH 7.6, 10 mM methyl-coenzyme M or ethyl-coenzyme M, 0.5 mM CoB-S-S-CoB, 10 mM Ti(III)citrate, 0.3 mM hydroxycobalamin and 10 – 200 µg of MCR. The gas phase was in both assays 95% N_2/5% H_2. The reaction was started by the addition of MCR or by raising the temperature from 4°C to 65°C. At intervals of 0.5 to 3 min, 0.2 mL gas samples were withdrawn and analyzed for methane and ethane by gas chromatography [3, 39].

EPR spectroscopy

Samples (0.35 mL) were analyzed for EPR spectra at 77 K in 0.3 cm (inner diameter) quartz tubes with 95% N_2/5% H_2 as gas phase and closed with a closed off rubber tube. The samples contained at least 1 – 4.7 mg

MCR (3.6 – 17 nmol) in 10 or 50 mM Tris/HCl pH 7.6. EPR spectra at X-band (9.4 GHz) were obtained with a Bruker EMX-6/1 EPR spectrometer composed of the EMX 1/3 console, ER 041 X6 bridge with built-in ER-0410-116 microwave frequency counter, ER-070 magnet and ER-4102st standard universal rectangular cavity. All spectra were recorded with a field modulation frequency of 100 kHz. Cooling of the sample was performed with liquid nitrogen in a finger dewar at 77 K.

EPR spin quantitations were carried out under non-saturating conditions using 10 mM copper perchlorate as the standard (10 mM $CuSO_4$; 2 M $NaClO_4$; 10 mM HCl). All signal intensities are expressed as spin per mol F_{430}. The programs of S.P.J. Albracht were used for computer simulations of the EPR signals [41].

Syntheses of allyl-coenzyme M, trifluoromethyl-coenzyme M, cyano-coenzyme M and seleno-coenzyme M

Sodium 2-(allysulfanyl)-ethanesulfonate (Allyl-coenzyme M)

Sodium 2-mercaptoethanesulfonate (1.64 g, 10 mmol) was dissolved under nitrogen at 0° C in a solution of sodium methoxide (from 10 mL of dry methanol and 252 mg [11 mmol] of sodium metal). Under vigorius stirring, allyl iodide (1.68 g, 10 mmol) was added dropwise at 0° C and the resulting precipitate was resuspended by adding another 5 mL of methanol. The reaction mixture was allowed to warm to room temperature, stirred overnight and evaporated to dryness. The product was isolated by repeated precipitation from 1-2 mL H_2O with acetone (3x, until a test for iodide with $AgNO_3$ was negative) to give 450 mg (23%, mp. >200˚C) of sodium 2-(allylsulfanyl)-ethanesulfonate. ^{1}H-NMR (d_6-DMSO, 400 MHz): δ 5.67 (ddt, J = 7.1, 9.9, 17.0, 1 H), 5.05 (dd, J = 1.4, 17.0, 1 H), 4.98 (d, J = 9.9, 1 H), 3.06 (d, J = 7.1, 2 H), 2.57 (s, 4 H). ^{13}C-NMR (d_6-DMSO, 125 MHz): δ 135.0, 117.5, 51.9, 34.1, 26.2. MS (ESI -Q1, m/z): monoisotopic mass calc. for $[C_5H_9O_3S_2]^{-1}$: 181.00; found: 180.7 (M^-, 100), 181.7 (M^-, 8), 384.8 (M_2Na^-, 52), 385.8 (M_2-Na, 10), 792.8 ($M_4Na_3^-$, 10), 793.8 ($M_4Na_3^-$, 4), 996.6 ($M_5Na_4^-$, 6), 997.6 ($M_5Na_4^-$, 4). Elemental analysis (C,H,S): calc. for $C_5H_9S_2O_3Na$ (204.25 gmol^{-1}): C 29.40, H 4.44, S 31.40; found: C 29.24, 29.32, H 4.45, 4.67, S 31.

Ammonium 2-(trifluoromethylsulfanyl)-ethanesulfonate (Trifluoromethyl-coenzyme M)

Sodium 2-mercaptoethanesulfonate (4.1 g, 25 mmol) was placed in a jacket-cooled photolysis apparatus under N_2, and ca. 90 mL of liquid NH_3 was condensed in at –45° C. Trifluoroiodomethane was condensed into a *Schlenk*-flask at –75° C and 3.1 mL (1.6 eq., 40 mmol) was rapidly transferred into the photolysis apparatus with a precooled (-80° C) pipette. The resulting homogeneous mixture was irradiated with a central high pressure mercury lamp for 4.5 h (negative Ellman test). The ammonia was allowed to evaporate over night, the residue was dissolved in 5 mL H_2O and repeatedly precipitated from acetone until a test for iodide was negative (4.71 g). The mixed Na^+/NH_4^+ salt (3.0 g) was converted into the ammonium form by acidification of a solution in 20 mL H_2O with 7 cm^3 of amberlite IR-120 (H^+-form) to pH=1, filtration, addition of conc. aq. NH_3 to reach pH=12, and lyophilisation (2.71 g, 64% overall yield). ^{1}H-NMR (d_6-DMSO, 400 MHz)*: δ 7.07 (4 NH, s), 3.15 (2H), 2.77 (2H), AA‘BB‘- system: $J_{AA} = J_{BB}$ = -13.0, $J_{AB1} = J_{AB3}$ = 6.1, $J_{AB2} = J_{AB4}$ = 11.25. ^{13}C-NMR (d_6-DMSO, 100 MHz): 133.6 (q, J = 3.0), 53.6 (s), 26.8 (s). ^{19}F-NMR (CD_3OD, F_3C-C_6H_5, 282 MHz): -41.8 (s). MS (ESI -Q1, m/z): monoisotopic mass calc. $[C_3F_3H_4O_3S_2]^{-1}$: 208.96; found: 208.8 (M^-, 100), 209.9 (M^-, 4), 210.8 (M^-, 10), 440.8 (M_2^-, 8), 442.8 (M_2^-, 1). Elemental analysis (C,H,N,F,S: calc. for $C_3H_8F_3NS_2O_3$ (227.23 gmol^{-1}): C 15.99, H 3.55, F 25.08, N 6.16, S 28.22, O 21.12; found: C 15.99, H 3.59, F 25.23, N 5.96, S 28.41, O 21.12.

Sodium 2-thiocyanato-ethanesulfonate (Cyano-coenzyme M)

Sodium 2-bromoethanesulfonate (614.1 mg, 2.91 mmol) and potassium thiocyanate (291.5 mg, 3.0 mmol) was suspended in dry DMF (12 mL) and stirred at 120° for 4 h. The solvent was evaporated under vacuum and the residue dissolved in 10 mL H_2O. The product was converted into the ammonium form by acidification with amberlite IR-120 (H^+-form) to pH=1, filtration, addition of conc. aq. NH_3 to reach pH=12, and lyophilisation. The resulting solid was suspended in 100 mL of diethyl ether, stirred for 24 h and filtered. Recrystallization from methanol gave 160 mg (29%) of pure product. ^{1}H-NMR (CD_3OD, 400 MHz): δ 3.38 (2 H), 3.21 (2 H, AA‘BB‘-system, J_{AA} = -16.3, J_{BB} = -15.4, J_{AB1} = 5.3, J_{AB2} = 11.3, J_{AB3} = 11.1, J_{AB4} = 5.1). ^{1}H-NMR (D_2O, 300 MHz): δ 3.23 (2 H), 3.18 (2 H, AA‘BB‘-system, J_{AA} = -10.3, J_{BB} = -11.9, J_{AB1} = 7.5, J_{AB2} =J_{AB3} = 4.7, J_{AB4} = 8.1). ^{13}C-NMR (CD_3OD, 125 MHz): δ 113.4, 52.4, 30.3. ^{13}C-NMR (D_2O, 75 MHz): δ 113.6, 50.0, 27.7. MS (ESI -Q1, m/z): monoisotopic mass calc. for $[C_3H_4S_2O_3N]^{-1}$: 165.96; found: 165.7 (M^-, 100), 167.5 (M^-, 10).

Disodium 2-selenolatoethanesulfonate (Seleno-coenzyme M)

All operations were carried out under N_2 with solvents that had been degassed by three freeze thaw cycles. To a solution of $NaBH_4$ (606 mg, 16 mmol) in 5 mL H_2O kept at 4° C, selenium metal (3 x 300 mg, 3 x 3.8 mmol) was carefully added in three portions. After 10 min, a solution of sodium 2-bromoethanesulfonate (1.60 g, 7.6 mmol) in H_2O (5 mL) was added dropwise and the resulting solution was stirred overnight at 25°. The solvent was removed by lyophilisation, the residue was ground into a

fine powder, washed with ethanol (200 mL) and dried in the vacuum giving 1.43 g (45%) of product. ^{1}H-NMR (D_2O/K_2DPO_4/NaOD, pH = 7.1, 500 MHz): δ 3.26 (2H), 2.93 (2 H), AA'BB'- system. ^{13}C-NMR (D_2O/K_2DPO_4/NaOD, pH = 7.1, 75 MHz): δ 54.7, 19.1 (t, J_{CSe} = 0.26). ^{77}Se-NMR (D_2O/K_2DPO_4/NaOD, pH = 7.1, 93 MHz): δ 201.9 (s). MS(ESI -Q1, m/z): monoisotopic mass calc. for $[C_2H_5SeSO_3]^{-1}$: 188.91; found: 185.2 (M^-, 20), 186.1 (M^-, 52), 187.0 (M^-, 93), 188.0 (M^-, 100), 189.0 (M^-, 46).

Results

Methanothermobacter marburgensis grows at 65°C on 80% H_2 / 20% CO_2 with a doubling time of approximately 2 hours to a cell concentration of 10 g (wet mass) per L [42] and contains approximately 7 mg MCR per g cells (wet mass) after growth under these conditions [36]. The MCR fraction obtained by ammonium sulfate precipitation between 70% and 100% consists of two MCR isoenzymes designated MCR I (Mcr) and MCR II (Mrt) [38, 39]. Isoenzyme I predominates (70%) in cells grown under conditions of H_2 limitation, which were used for mass cultivation of the organism in 13 L fermenters [43, 44]. The high cell yield and MCR concentration in the cells is the reason why almost all biochemical studies with purified active MCR have been performed with MCR I from *M. marburgensis*.

The following investigations were performed with isoenzyme I from *M. marburgensis*, which was purified and separated from isoenzyme II to apparent homogeneity in the active MCR-red1c state [5]. This state was induced in the cells by incubating them after growth under 100% H_2 at 65°C for 30 min before harvest of the cells. During purification all solutions contained 10 mM coenzyme M since in its absence MCR-red1 is very labile and almost impossible to purify. On the other hand coenzyme M is a competitive inhibitor to methyl-coenzyme M. Coenzyme M therefore had to be removed before assay of the enzyme. Complete removal was very difficult to achieve without considerable loss in activity. Thus in most of the MCR-red1 preparations used there was still some coenzyme M left.

The presence of some coenzyme M in all of the MCR preparations is the reason why in Table 1 apparent K_M and *V*max values are given for the substrates and apparent K_i values for the reversible inhibitors. Another reason is that it was not always possible to obtain initial velocities since the activity of the enzyme sometimes increased in the first minutes as shown for the kinetics of ethane formation from ethyl-coenzyme M and coenzyme B in Fig. 1A. In these cases the highest rate reached was used for the graphic determination of K_M and *V*max from Lineweaver-Burk plots and of K_i from Dixon plots.

For the irreversible inhibitors in Table 1 $[I]_{0.5V}$ values are given, which indicate the concentration of the inhibitor at which 50% of the activity in the absence of the inhibitor was observed under the experimental conditions. These inhibitors were found to inactivate MCR by reacting with the active site Ni(I) as revealed by EPR spectroscopy. Inhibition of methane formation from methyl-coenzyme M by the irreversible inhibitors is the result of both competitive binding and inactivation. Therefore, there are no K_i values for these inhibitors.

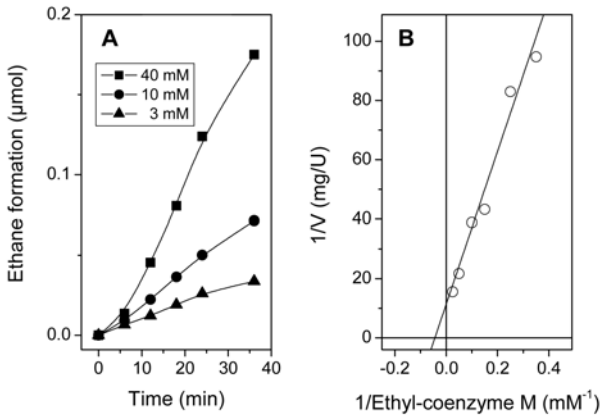

Fig. 1 Kinetics of ethyl-coenzyme M reduction to ethane catalysed by methyl-coenzyme M reductase (MCR) from *M. marburgensis*. A Kinetics of ethane formation in the presence of (■) 40 mM, 20 mM, (●) 10 mM, 6.7 mM, 4 mM and (▲) 3 mM ethyl-coenzyme M. B Reciprocal plots of the rates versus the ethyl-coenzyme M concentration. The 0.4-mL assay mixture contained 50 mM potassium phosphate pH 7.6, 0.5 mM CoB-S-S-CoB, 10 mM Ti(III)citrate, 0.3 mM hydroxycobalamin, 0.1 mg of purified MCR-red1c (<0.1 mM coenzyme M) and ethyl-coenzyme M in the concentrations indicated.

The specific activity of the preparations was generally near 30 U per mg protein under the standard assay conditions and the spin concentration determined from the EPR signal was above 80%. The standard assay mixture contained hydroxycobalamin and Ti(III)citrate for the continuous reduction of the product CoM-S-S-CoB [45], which is a very potent inhibitor of MCR activity, and for the reductive activation of the enzyme before start of the reaction. In some of the assays hydroxycobalamin and Ti(III) had to be left out since cobalamins very effectively catalyse the reductive dehalogenation of compounds such as 2-bromoethanesulfonate and 3-bromopropanesulfonate with Ti(III). In the absence of hydroxycobalamin and Ti(III), product formation relatively rapidly leveled off and there was no reductive activation of the enzyme before start of the reaction. Therefore the specific activities were much lower. In Table 1 the footnotes a and b indicate which assays contained cobalamin and Ti(III) and which did not.

Table 1 Effect of methyl-coenzyme M analogues on the activity and EPR spectroscopic properties of active methyl-coenzyme M reductase (MCR) from *Methanothermobacter marburgensis*.

		Kinetic properties	EPR signal		
			In the absence of coenzyme B	In the presence of coenzyme B	After oxidation with O_2
Substrates		**app. K_M (mM)**			
Methyl-coenzyme M[a]	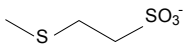	5 (30 U/mg) [c]	MCR-red1m	MCR-red1m	No signal
Ethyl-coenzyme M[a]	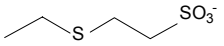	20 (0.1 U/mg) [c]	MCR-red1m	MCR-red1m	No signal
Inhibitors		**app. K_i (mM)**			
Allyl-coenzyme M[b]	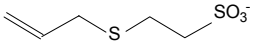	0.1	MCR-red1m	MCR-red1m	No signal
Propyl-coenzyme M[b]	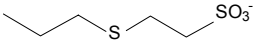	2	MCR-red1m	MCR-red1m	No signal
Coenzyme M[a]	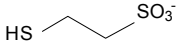	4	MCR-red1c	MCR-red2	MCR-ox3
		$[I]_{0.5V}$ (mM)			
2-Bromoethanesulfonate[b]	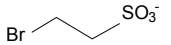	0.002	MCR-red1 **slowly** quenched	MCR-red1 **rapidly** quenched and radical with hyperfine structure induced	Radical without hyperfine structure induced
3-Bromopropionate	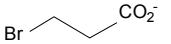	n.d.			
Cyano-coenzyme M[b]	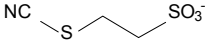	0.2			
Seleno-coenzyme M[b]	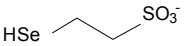	6			
Trifluoromethyl-coenzyme M[a]	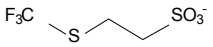	6			
3-Bromopropanesulfonate[b]	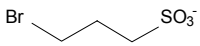	0.0001	MCR-red1 converted into MCR-BPS	MCR-red1 converted into MCR-BPS	Radical induced
3-Iodopropanesulfonate[b]	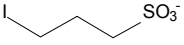	0.001			
4-Bromobutyrate	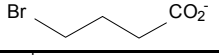	n.d.			

[a]Determined with Ti(III)/B_{12} assay; [b]Determined with DTT assay; [c]apparent V_{max}; n.d.= not determined

Substrate specificity

It is long known that MCR can catalyse the reduction of ethyl-coenzyme M with coenzyme B [46-48]. We found that ethyl-coenzyme M reduction proceeds with less than 0.1% of the catalytic efficiency of methyl-coenzyme M reduction (Table 1). The apparent K_M and Vmax for methyl-coenzyme M and ethyl-coenzyme M were obtained from kinetic analyses as shown for ethyl-coenzyme M in Fig. 1A. They were determined with the same enzyme preparation and under the same assay conditions. The only difference was that the enzyme concentration was much higher in the assays for ethyl-coenzyme M reduction. In the kinetic analysis the coenzyme B concentration (1 mM) was not varied since MCR has been shown to have a ternary complex catalytic mechanism [39]: reciprocal plots of the rates versus the methyl-coenzyme M concentration at different constant coenzyme B concentrations were intersecting with the intersecting point on the abscissa to the right of the ordinate. The K_M values obtained are thus independent on the coenzyme B concentration.

The apparent K_M for methyl-coenzyme M was found to be 5 mM and the apparent Vmax to be 30 U/mg (Table 1). In previous studies a lower K_M value for methyl-coenzyme M of 1 mM was obtained [39]. An explanation most probably is, that the apparent K_M given in Table 1 was determined with MCR-red1 purified in the presence of 10 mM coenzyme M whereas the lower K_M of 1 mM was determined with enzyme preparations partially purified in the presence of 12 mM methyl-coenzyme M. We observed that MCR-red1 purified in the presence of coenzyme M is much more stable than MCR-red1 purified in the presence of methyl-coenzyme M or generated from MCR-ox1 by reduction in the presence of methyl-coenzyme M. At equal spin concentrations, however, the specific activity of MCR-red1c is only half that of MCR-red1m and this difference in specific activity was not abolished, when most of the coenzyme M was

removed from the MCR-red1c sample by ultrafiltration and washing [5]. This is still not understood.

We also tested propyl-coenzyme M and allyl-coenzyme M as possible substrates. If they were reduced to propane and propene, respectively, this was at rates below the detection limit of the gaschromatographic method employed. Propyl-coenzyme M (apparent K_i = 2 mM) and allyl-coenzyme M (apparent K_i = 0.2 mM) reversibly inhibited methyl-coenzyme M reduction with coenzyme B (Table 1) indicating that they competed with methyl-coenzyme in binding to the active site. Binding to the active site was also evidenced by the finding that, when allyl-coenzyme M or propyl-coenzyme M were added to MCR-red1c, the hyperfine splitting became much more pronounced just as this was the case when methyl-coenzyme M or ethyl-coenzyme M were added. This is shown for methyl-coenzyme M and allyl-coenzyme M in Fig. 2A.

In line 1 of Fig. 2A the EPR spectrum of MCR-red1 in the presence of coenzyme M is given and in lines 2 and 3 the EPR spectra when additionally methyl-coenzyme M or allyl-coenzyme M were present. Fig. 2B shows the spectra of the enzyme supplemented subsequently with coenzyme B and Fig. 2C what happened when the solutions were finally exposed to air. When MCR-red1c was supplemented with coenzyme B the rhombic MCR-red2 signal was induced (Fig. 2B, line 1), which was converted to the MCR-ox3 signal upon exposure of MCR-red2 to air (Fig. 2C, line 1). In the presence of methyl-coenzyme M (Fig. 2, line 2) or allyl-coenzyme M (Fig.2, line 3) neither the red2 signal nor the ox3 signal were induced. Upon subsequent exposure of the enzyme solutions to air the MCR-red1 signal was quenched leaving behind only a small radical signal (Fig. 2C, lines 2 and 3).

The results obtained for allyl-coenzyme M are of special interest. Hydroxycobalamin and Ti(III) were found to chemically reduce allyl-coenzyme to a gaseous product, which was observed gas chromatographically. It thus could have been that allyl-coenzyme M inactivates the enzyme in the absence or presence of coenzyme B by oxidation of its active site Ni(I), which was, however not observed. Allyl-coenzyme M thus behaved quite differently from 2-bromoethanesulfonate and 3-bromopropanesulfonate, which both were also chemically reduced by hydroxycobalamin and Ti(III), but which inactivated MCR as indicated by the quenching of the MCR-red1 signal or convertion of the MCR-red1 signal to the MCR-BPS signal (see below).

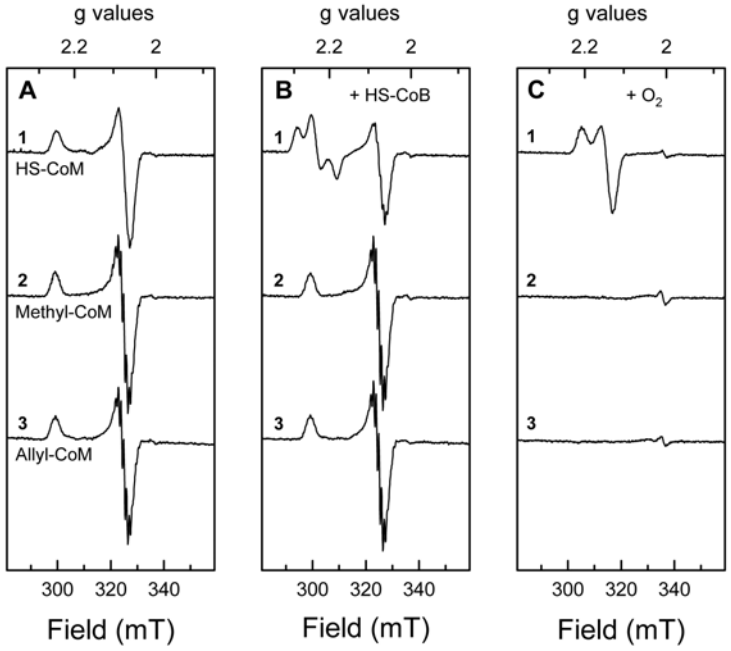

Fig. 2 EPR spectra of purified MCR-red1 after addition of coenzyme M, methyl-coenzyme M or allyl-coenzyme M (A) in the absence and (B) presence of coenzyme B and (C) after exposure to air. A (1) MCR-red1c = active methyl-coenzyme M reductase in the presence of 10 mM coenzyme M (g_z = 2.250; $g_{x,y}$ = 2.066); (2) MCR-red1m = active MCR in the presence of 10 mM methyl-coenzyme M (g_z = 2.252; $g_{x,y}$ = 2.068); (3) MCR-red1c after the addition of 10 mM allyl-coenzyme M. B Samples as in A but supplemented with 5 mM coenzyme B. In the case of (1) the rhombic MCR-red2 signal was induced (g_z = 2.288; g_y = 2.235; g_x = 2.179). C Samples as in B but after exposure to air. In the case of (1) the MCR-ox3 signal was induced (g_z = 2.217; $g_{x,y}$ = 2.137). The samples in 2 and 3 contained small amounts of MCR-ox1 signal, which has been substracted for better comparison. The concentration of purified enzyme in all samples was 4.7 mg (17 nmol) in 0.35 mL 50 mM Tris/HCl pH 7.6. Where indicated substrate and/or substrate analogues were added to the samples at room temperature and the samples were incubated at the same temperature for 5 min before freezing in liquid nitrogen. Spectra were recorded under the conditions: microwave frequency, 9434 MHz; microwave power incident to the cavity, 2.05 mW; temperature, 77 K; modulation amplitude, 0.6 mT.

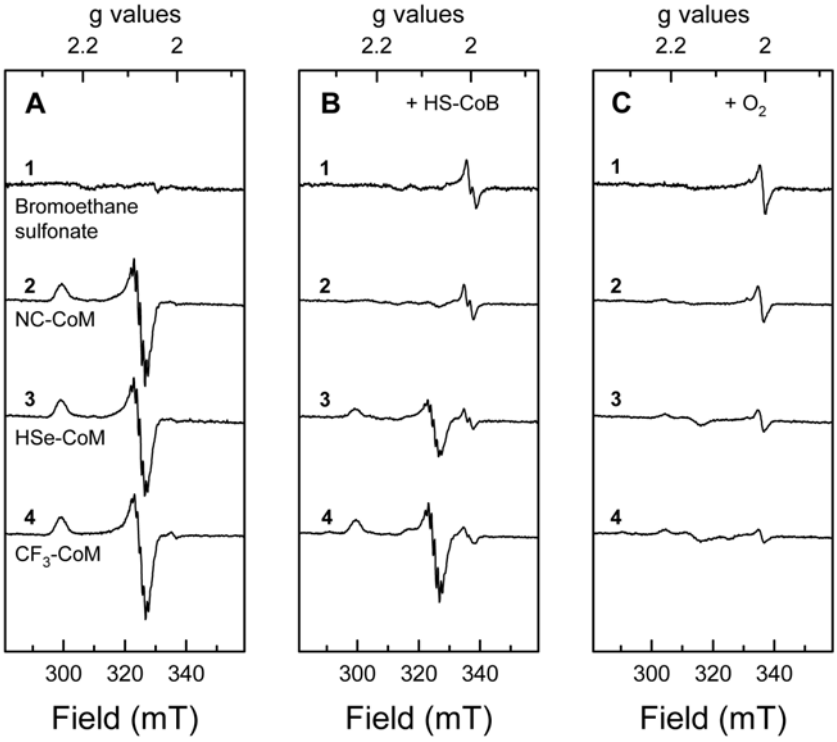

Fig. 3 Inactivation of MCR-red1a by 2-bromoethanesulfonate (BES), cyano-coenzyme M, seleno-coenzyme M and trifluoromethyl-coenzyme M (**A**) in the absence and (**B**) in the presence of coenzyme B and (**C**) after exposure to air. **A** EPR spectra of MCR-red1a after 5 min incubation in the presence of 10 mM analogues: (1) 2-bromoethanesulfonate; (2) cyano-coenzyme M; (3) seleno-coenzyme M; and (4) trifluoromethyl-coenzyme M. **B** Samples as in **A** but supplemented with 5 mM coenzyme B; the radical signal at g = 2.008 had a signal intensity of approximately 0.1 spin per mol F_{430} and showed a resolved hyperfine structure with I = 1/2. **C** Samples as in **B** but after exposure to air; the radical signal at g = 2.008 had a signal intensity of less than 0.1 spin per mol F_{430}. The concentration of purified enzyme in all samples was 4.7 mg (17 nmol) in 0.35 mL 10 mM Tris/HCl pH 7.6. Sample handling was performed at room temperature. Samples were frozen after 5 min. For EPR conditions see Fig. 2, microwave frequency, 9434 MHz. inactivated MCR as indicated by the quenching of the MCR-red1 signal or conversion of the MCR-red1 signal to the MCR-BPS signal (see below).

Inhibitors that quench the MCR-red 1 signal

2-Bromoethanesulfonate, cyano-coenzyme M, seleno-coenzyme M and trifluoromethyl-coenzyme M belong into this category (Table 1). When added to MCR-red1 in 10 mM concentrations, 2-bromoethanesulfonate quenched the MCR-red1 signal both in the absence and presence of coenzyme B (Fig. 3A and B, lines 1). The three other inhibitors oxidized the active site Ni(I) to Ni(II) only at significant rates in the presence of coenzyme B (Fig. 3B). The rate of inactivation was highest with 2-bromoethanesulfonate and lowest with trifluoromethyl-coenzyme M. The differences in inactivation rates reflected the differences in the $[I]_{0.5V}$ values (Table 1) but there was no linear correlation.

The finding that the inactivation of MCR-red1 by cyano-coenzyme M, seleno-coenzyme M and trifluoromethyl-coenzyme M was dependent on coenzyme B prompted us to investigate the effect of coenzyme B on the inactivation of MCR-red1 by 2-bromoethanesulfonate at low concentrations of the inhibitor. Indeed, at concentrations of 2-bromoethanesulfonate of 25 µM (Fig. 4A) and 250 µM (Fig. 4B), MCR-red1 inactivation was stimulated by coenzyme B (Fig. 4). The rate of inactivation by 2-bromoethanesulfonate at 25 µM was 2-3 fold lower than that at 250 µM, which is consistent with the observed $[I]_{0.5V}$ of 2 µM (Table 1). In the absence of coenzyme M, which competes with 2-bromoethanesulfonate for binding in the active site, the rate of inactivation was much higher than in its presence (Fig. 4A). Coenzyme M thus protected the enzyme from inactivation by 2-bromoethanesulfonate.

When MCR-red1 was inactivated by 2-bromoethanesulfonate, cyano-coenzyme M, seleno-coenzyme M or trifluoromethyl-coenzyme M in the presence of coenzyme B, a novel radical signal with doublet hyperfine structure was induced (Fig. 3B). Upon exposure of the inactivated enzyme to air the doublet was replaced by a new radical signal without resolved hyperfine structure (Fig. 3C). The hyperfine splitting of the radical signal is characteristic of coupling to a single hydrogen nucleus (S=1/2).

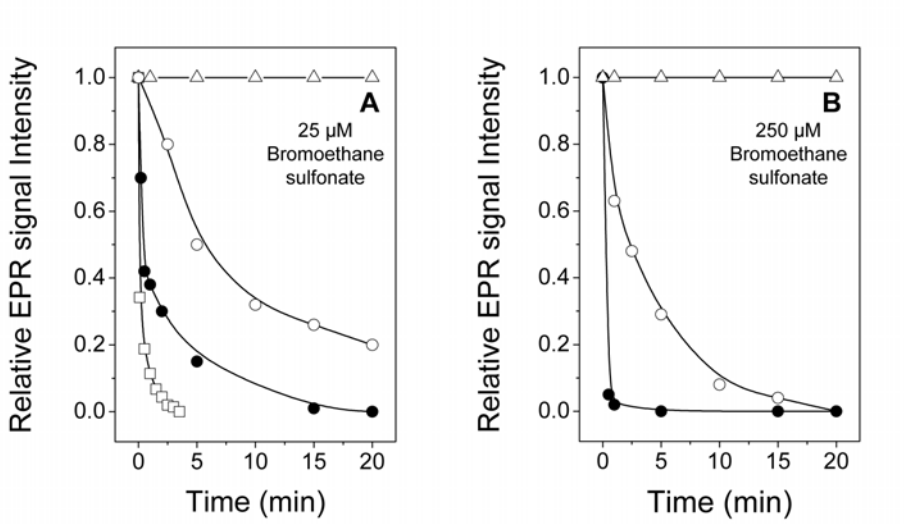

Fig. 4 Kinetics of MCR-red1c inactivation by 2-bromoethanesulfonate (BES) in the (○) absence or (●) presence of coenzyme B as followed by EPR spectroscopy. A (Δ) MCR-red1c in the absence of BES; (○) MCR-red1c in the presence of 25 µM BES; (●) MCR-red1c in the presence of 5 mM coenzyme B and 25 µM BES; (□) MCR-red1a (active MCR in the absence of coenzyme M) in the presence of 25 µM BES. B (Δ) MCR-red1c in the absence of BES; (○) MCR-red1c in the presence of 250 µM BES; (●) MCR-red1c in the presence of 5 mM coenzyme B and 250 µM BES. The experimental conditions were as described in Fig. 2. The concentration of purified enzyme in all samples was 2.5 mg (8.8 nmol) in 0.35 mL. The samples were incubated at room temperature for the times indicated, then frozen in liquid nitrogen and analysed for EPR signal intensities. The relative signal intensities of the red1 signal were determined by double integration of the EPR-signals. The intensity of the MCR-red1 signal in the absence of coenzyme B and BES was taken as 1. The kinetic labeled with □ was obtained by following the decrease of absorbance at 385 nm spectrophotometrically.

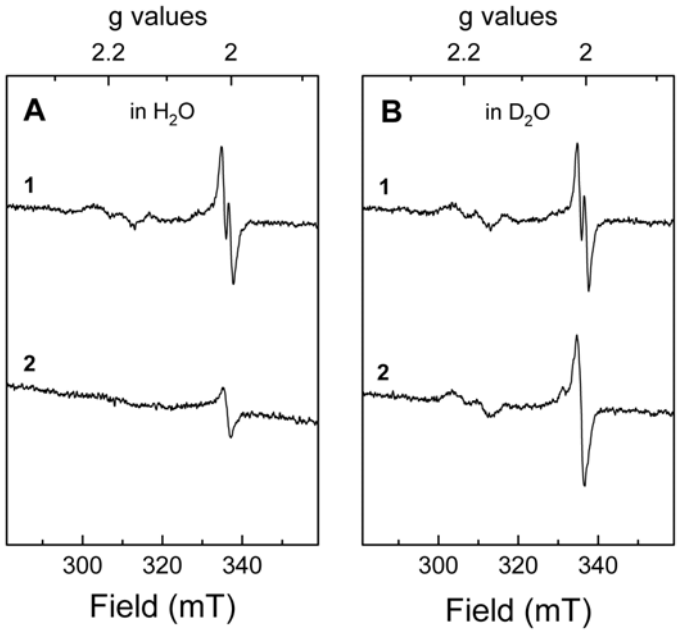

Fig. 5 EPR spectra of MCR-red1c in the presence of coenzyme B after inactivation by 2-bromoethanesulfonate (BES) in (A) H_2O or (B) in D_2O. A (1) MCR-red1c in the presence of 5 mM coenzyme B after the addition of 10 mM BES. (2) The same sample after exposure to air. B (1) MCR-red1c in the presence of 5 mM coenzyme B after the addition of 10 mM BES. (2) The same sample after exposure to air. The concentration of purified enzyme in all samples was 4.7 mg (17 nmol) in 0.35 mL 10 mM Tris/HCl pH 7.6. Sample handling was performed at room temperature. For EPR conditions see Fig. 2, microwave frequency, 9434 MHz.

We therefore repeated the experiment with 2-bromoethanesulfonate in D_2O. In Fig. 5A, line 1, the EPR spectrum of MCR in H_2O after the addition of 2-bromoethanesulfonate is shown and in Fig. 5B, line 1, the respective spectrum of MCR in D_2O. The spectra in H_2O and D_2O before (not shown) and after inactivation by 2-bromoethanesulfonate were almost identical indicating that, if the hyperfine splitting of the radical signal was derived from spin coupling to a hydrogen nucleus, this nucleus was not exchangeable by deuterons of D_2O.

3-Bromopropionate was found to also quench the MCR-red1 signal (result not shown). We did not determine, whether inactivation by this 2-bromoethanesulfonate analogue was coenzyme B dependent.

Inhibitors that convert the MCR-red1 signal to the MCR-BPS signal

3-Bromopropanesulfonate, 3-iodopropanesulfonate and 4-bromobutyrate belong into this category. All three compounds were found to irreversibly inhibit MCR, most of them at relatively low concentrations (Table 1). 3-Bromopropanesulfonate with an $[I]_{0.5V}$ < 0.1 µM is the most potent inhibitor of MCR known to date [49]. Via titration we found that MCR-red1 is completely inactivated when only twice the molar amount of the inhibitor is added. The EPR spectrum of the enzyme inactivated by 3-bromopropanesulfonate in the absence of coenzyme B is given in Fig. 6A, line 1. The signal, which was first described by Rospert et al. [37], has been designated the MCR-BPS signal. The EPR spectrum after inactivation in the presence of coenzyme B is shown in Fig. 6A, line 2. It differs from the MCR-BPS signal only very slightly in the *g* values. The MCR signal generated by 3-bromopropanesulfonate in the absence or presence of coenzyme B was quenched upon exposure of the enzyme to O_2 (Fig. 6A) but not by 10 mM 2-bromoethanesulfonate (not shown), which had absolutely no effect on the EPR signal. When the enzyme had been inactivated in the presence of coenzyme B, exposure to O_2 led to the induction of a novel radical signal (Fig. 6A, line 3). Almost identical spectra were obtained, when the enzyme was inactivated by 3-iodopropanesulfonate (not shown) and 4-bromobutyrate (Fig. 6B).

3-Bromopropanesulfonate has been reported to be a reversible inhibitor [49]. Reversible inhibition was concluded from investigations with enzyme preparations that contained low amounts of enzymatically inactive MCR-ox1, which is not affected by the inhibitor (see below). After removal of the excess 3-bromopropanesulfonate by gel filtration the enzyme regained some activity. We know now that MCR-ox1 was converted to active enzyme under the reducing assay conditions [26]. That 3-bromopropanesulfonate irreversibly inhibits MCR was already mentioned by Rospert et al. [37].

3-Fluoropropanesulfonate ($[I]_{0.5V}$ = 50 µM) has been reported to also inhibit MCR and to induce the MCR-BPS signal. We found that for full signal induction 50 mM 3-fluoropropanesulfonate had to be present. At 10 mM 3-fluoropropanesulfonate only approximately 30% of MCR-red1 was converted to MCR-BPS and this percentage did not increase during incubation at room temperature for many hours (not shown). The easiest interpretation of these findings is that the 3-fluoropropanesulfonate used was contaminated with minute amounts of 3-bromopropanesulfonate. It was synthesized starting from 1-fluoro-3-bromopropane via sulfitolysis [37].

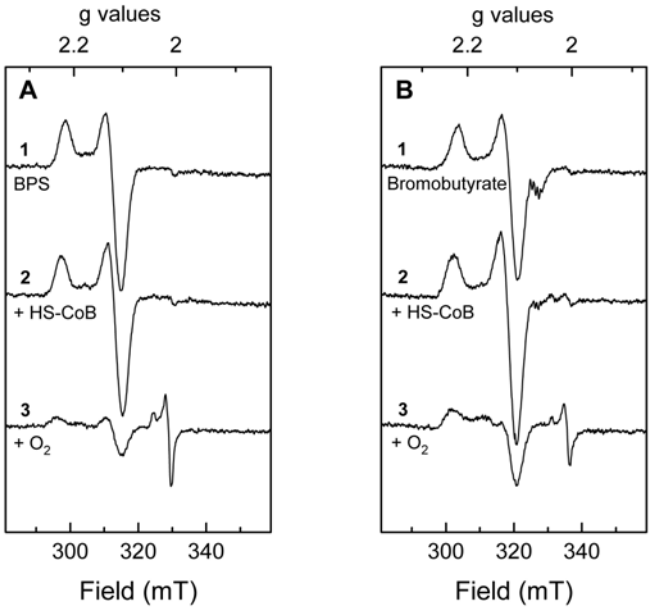

Fig. 6 Inactivation of MCR-red1c by (**A**) 3-bromopropanesulfonate (BPS) and (**B**) 4-bromobutyrate in the absence and presence of coenzyme B as followed by EPR spectroscopy. **A** (1) MCR-red1c after the addition of 10 mM BPS; the MCR-BPS signal was induced (g_z = 2.219; $g_{x,y}$ = 2.116); (2) Sample as in 1 but supplemented with 5 mM coenzyme B (g_z = 2.229; $g_{x,y}$ = 2.111); (3) Sample as in 2 but after exposure to air. A new signal appeared at g_z = 2.035 and $g_{x,y}$ = 2.007. The signal intensity was approximately 0.1 spin per mol F_{430}. **B** (1) MCR-red1c after the addition of 10 mM 4-bromobutyrate; (2) Sample as in 1 but supplemented with 5 mM coenzyme B; (3) Sample as in 2 but after exposure to air. The concentration of purified enzyme in all samples was 3.2 mg (11.4 nmol) in 0.35 mL. Sample handling was performed at room temperature. Samples were frozen after 5 min. For EPR conditions see Fig. 2, microwave frequency, (**A**) 9272 MHz, (**B**) 9434 MHz.

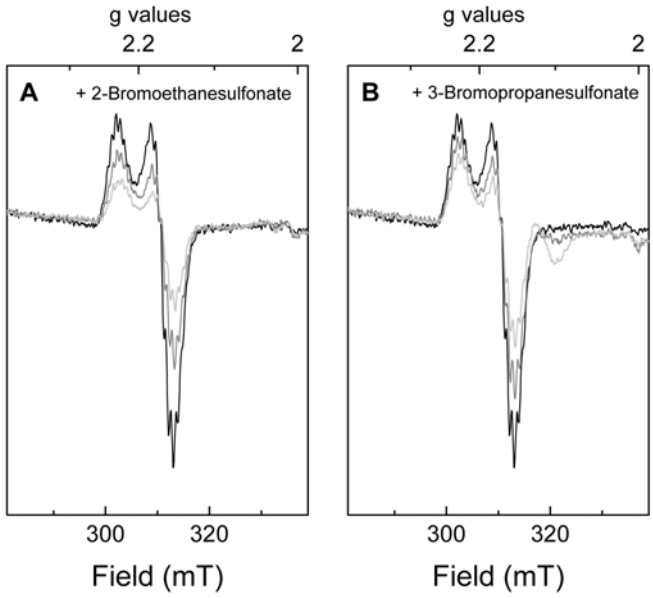

Fig. 7 EPR spectra of MCR-ox1 before and after the addition of (**A**) 2-bromoethanesulfonate (BES) and (**B**) 3-bromopropanesulfonate (BPS). In *black*: MCR-ox1 (g_z = 2.231; $g_{x,y}$ = 2.160) = MCR-red1c supplemented with 5 mM coenzyme B and subsequently with 1 mM polysulfide. In *grey*: MCR-ox1 two hours after the addition of (**A**) 10 mM BES or (**B**) 10 mM BPS. In *light grey*: the same samples fifty hours after the addition of BES or BPS. The concentration of purified enzyme in all samples was 1 mg (3.6 nmol) in 0.35 mL. For EPR conditions see Fig. 2, microwave frequency, 9434 MHz.

Effect of the inhibitors on MCR-ox1

MCR-ox1 is an enzymatically inactive form of MCR, which exhibits a nickel based EPR spectrum. It can be either generated *in vivo* by "oxidizing" the cells of *M. marburgensis* with CO_2 after growth on 80% H_2 /20% CO_2 [50, 51] or *in vitro* by "oxidizing" MCR-red1 in the presence of coenzyme M and coenzyme B with polysulfide [26]. MCR-ox1 can also be generated *in vivo* by incubation of *M. marburgensis* cells in the presence of high concentrations of sulfide or dithionite [4]. MCR-ox1 is relatively stable under oxic conditions and less stable under reducing conditions under which it is slowly converted to MCR-red1. It also reacts over 1000 fold slower with chloroform than MCR-red1 [26, 30]. We report here that MCR-ox1 is also relatively stable in the presence of 2-bromoethanesulfonate (Fig. 7A) or 3-bromopropanesulfonate (Fig. 7B; [30]). At 10 mM concentrations of the two inhibitors the intensity of the MCR-ox1 signal only decreased slowly. The slow decrease observed can be explained by a slow conversion of MCR-ox1 into MCR-red1 under the reducing assay conditions (10 mM coenzyme M). This interpretation is supported by the finding, that in the presence of 3-bromopropanesulfonate some MCR-BPS was formed after 50 hours incubation as indicated from the EPR spectrum.

It was previously reported that MCR-ox1 is slowly converted to MCR-BPS in the presence of 3-bromopropanesulfonate [30]. This result, which differs from ours, can be explained by the presence of Ti(III) in the assays of [30]. Ti(III) is known to reduce MCR-ox1 to MCR-red1 [3], which we have shown to react with 3-bromopropanesulfonate.

Discussion

In the results section it was shown that there are three types of methyl-coenzyme M analogues: (i) Analogues such as ethyl-coenzyme M and allyl-coenzyme M that are alternate substrates or reversible inhibitors; (ii) analogues such as 2-bromoethanesulfonate, that irreversibly inhibit the enzyme by oxidation of its active site Ni(I) to Ni(II); and (iii) analogues such as 3-bromopropanesulfonate that irreversibly inhibit the enzyme by reacting with the active site Ni(I) to a state that exhibits an Ni derived EPR signal similar in line shape to that of the inactive MCR-ox states.

Alternate substrates

MCR was shown to catalyze the reduction of ethyl-coenzyme M to ethane with a catalytic efficiency less than 0.1 % of that of methyl-coenzyme M reduction to methane. The large difference in catalytic efficiency was mainly due to differences in *V*max (0.1 U/mg versus 30 U/mg) and only partly due to differences in K_M (20 mM versus 5 mM). In 1978 it was reported that at a

concentration of 10 mM ethyl-coenzyme M was reduced to ethane at only 20% of the rate of methyl-coenzyme M reduction to methane (2 mU/mg versus 10 mU/mg) [34]. Wackett et al. [47] published an apparent K_M for ethyl-coenzyme M of 1.3 mM and a *V*max of 7.4 mU/mg to be compared with an apparent K_M for methyl-coenzyme M of 0.1 mM and *V*max of 11 mU/mg. Both results were obtained with cell extract, which was inactive (note the low specific activities) but which was slowly activated under the assay conditions in an ATP and H_2 dependent process. Thus the results can really not be compared.

In the introductory section it was indicated that presently two catalytic mechanisms are favored differing mainly in how methyl-coenzyme M is attacked by the active site´s Ni(I). Mechanism I assumes that the methylthioether bond is heterolytically cleaved in a nucleophilic substitution reaction at the methyl carbon [9, 10] and mechanism II by a homolytic substitution at sulfur [21-23]. For maximal reactivity, in mechanism I the methyl group of methyl-coenzyme M has to be positioned above the Ni(I) as shown in Fig. 8A and in mechanism II the thioether sulfur has to be positioned as shown in Fig. 8B. From Fig. 8 it can be deduced that when the rest **R** is a methyl group as in ethyl-coenzyme M rather than a hydrogen as in methyl-coenzyme M, the reacting carbon of ethyl-coenzyme M (**R** = CH_3) cannot be positioned above the Ni in the same distance as the reacting carbon of methyl-coenzyme M (**R** = H), whereas in the case of mechanism II the positioning of the sulfur is not affected by the size of **R**. When modeled into the crystal structure [7, 9, 10] in this position there was enough space for the ethyl group. Therefore, mechanism I can easily explain that MCR is less efficient in ethyl-coenzyme M reduction than in methyl-coenzyme M reduction whereas mechanism II cannot. This interpretation is naturally based on the assumption, that the first step in the catalytic cycle is rate determining which is supported by the calculated energy profiles [22, 23].

MCR has been reported to catalyze the reduction of methyl-selenocoenzyme M (K_M = 0.3 mM; *V*max = 35 mU/mg), difluoromethyl-coenzyme M (K_M = 2.5 mM; *V*max = 20 mU/mg) and 3-(methylthio)propionate (K_M = 1.3 mM; *V*max = 1.3 mU/mg)[47]. As seen from the extremely low *V*max, these results have been obtained with cell extracts containing mainly inactive MCR, which was slowly reactivated under the assay conditions. The data are mentioned here only because they qualitatively show that these substrate analogues can be used as alternative substrates. Interestingly, difluoromethyl-coenzyme M was found to inactivate the enzyme at higher concentrations and was thus not only an alternative substrate but also an irreversible inhibitor [47]. It could thus be that MCR also catalyzes the reduction of trifluoromethyl-coenzyme M but is inactivated by the substrate analogue so rapidly that the reduction is overlooked.

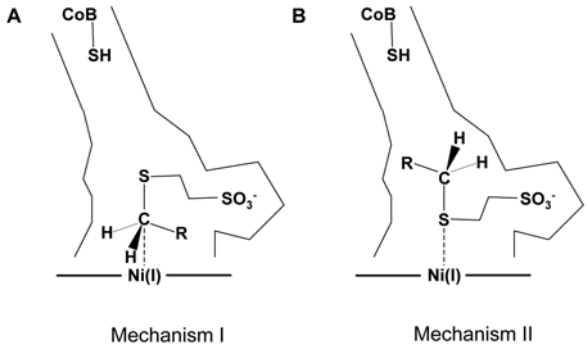

Fig. 8 Optimal position of methyl-coenzyme M in the active side of MCR assuming (**A**) catalytic mechanism I [9, 10] and (**B**) catalytic mechanism II [21-23]. The long aliphatic arm of coenzyme B can reach into the channel to the extent where its terminal thiol group is still at a distance of 8 Å to the Ni [7].

Reversible inhibitors

Allyl-coenzyme M was found to be a reversibly inhibitor of MCR (apparent K_i = 0.2 mM) and not a substrate: The previously reported formation in very low amounts of a gaseous product in cell extracts [52] can be explained by chemical reduction (see results) since the extracts contain cobalamins. The finding that allyl-coenzyme M is not reduced to propene is in favour of catalytic mechanism I, which predicts that allyl-coenzyme M reduction should be sterically hindered (**R** too bulky; see Fig. 8A). In case of mechanism II allyl-coenzyme M should have been reduced to propene or inactivated the enzyme due to the facile generation of the allyl radical. The same arguments also hold true for the finding that propyl-coenzyme M was not a substrate but a reversible inhibitor.

2-(Methoxy)ethanesulfonate has been reported to be an inhibitor of MCR (apparent K_i = 8.3 mM) [47]. The reason, why this analogue is not reduced to methane, is probably an energetic rather than a steric one: The C-O bond is much stronger than the C-S bond. This makes the first step more difficult in both discussed catalytic mechanisms.

Irreversible inhibitors of the 2-bromoethanesulfonate type

2-Bromoethanesulfonate is a well-known inhibitor of MCR and of methanogenesis [34]. In the results section it was shown that this inhibitor ($[I]_{0.5V}$ = 2 µM) quenched the MCR-red1 signal of active MCR already at very low concentration. The results indicate that the Ni(I) in the active site of MCR-red1 was oxidized to Ni(II) by 2-bromoethanesulfonate.

In solution, 2-bromoethanesulfonate has been shown to react with free Ni(I)F_{430} to bromide, ethene and sulfite [53]:

$2\ Ni(I)F_{430} + Br\text{-}CH_2CH_2SO_3^{1-} = 2\ Ni(II)F_{430} + Br^- + CH_2{=}CH_2 + SO_3^{2-}$

Probably the following reaction sequence takes place:

$Ni(I)F_{430} + Br\text{-}CH_2CH_2SO_3^{1-} = Ni(II)F_{430} + Br^- + \bullet CH_2CH_2SO_3^{1-}$

$\bullet CH_2CH_2SO_3^{1-} = CH_2{=}CH_2 + \bullet SO_3^{1-}$

$Ni(I)F_{430} + \bullet SO_3^{1-} = Ni(II)F_{430} + SO_3^{2-}$

An analogous fragmentation giving ethene was also observed as a side reaction when $Ni(I)F_{430}$ pentamethyl ester was reacted with the sulfonium ion *S*-methyl methyl-coenzyme M (Shu-Kun Lin, Ph.D. Thesis ETHZ 1992).

Reaction of F_{430} in the active site of MCR with 2-bromoethanesulfonate cannot proceed via the same sequence since per active site only one $Ni(I)F_{430}$ is present. Namely the last step in which the sulfur trioxide anion radical is reduced must be different. The sulfur trioxide anion radical is a strong oxidant that can probably generate other radicals within the active site. Indeed, when MCR-red1 was oxidized by 2-bromoethanesulfonate in the presence of coenzyme B, a radical signal was induced. Its hyperfine structure was characteristic of the electron spin being coupled to the nuclear spin of one hydrogen atom. In D_2O the hyperfine splitting remained, indicating that the hydrogen did not exchange with protons of water. When the enzyme was exposed to O_2 the split signal was replaced by a new signal without resolved hyperfine structure. Within the active site there is a thioglycine [7, 54] and two tyrosine residues [9, 10] that could be oxidized by the sulfur trioxide anion radical to a thioglycyl radical or a tyrosyl radical, respectively [55]. The split EPR signal is most similar to that reported for the glycyl radical in proteins [56, 57]. More detailed studies are needed to make an assignment.

Interestingly, also 3-bromopropionate, cyano-coenzyme M, seleno-coenzyme M and trifluoromethyl-coenzyme quenched the red1 signal and induced the split radical EPR signal when coenzyme B was present indicating that they in principle all reacted like 2-bromoethanesulfonate.

Quenching of the red1 signal of active MCR by 2-bromoethanesulfonate was more than ten fold enhanced in the presence of coenzyme B. This effect was most pronounced in the case of trifluoromethyl-coenzyme M, which quenched the EPR signal noticeably only in the presence of coenzyme B (Fig. 3). The coenzyme B dependence is taken as further evidence that coenzyme B has to bind to MCR before the nickel in MCR-red1 becomes reactive enough to react with methyl-coenzyme M or its substrate analogues.

2-Chloroethanesulfonate (apparent K_i = 70 μM) [34] and 2-azidoethanesulfonate (apparent K_i = 1 μM) [49] have been reported to be inhibitors of MCR. From their structure they are predicted to belong to the group of irreversible MCR inhibitors headed by 2-bromoethanesulfonate. Bromomethanesulfonate (apparent K_i = 1.5 μM) [58] and chloromethanesulfonate ($[I]_{0.5V}$ = 0.25 mM) [49] are also predicted to quench the red1 signal of active MCR but their reduction products will be different from those generated by 2-bromoethanesulfonate reduction.

Irreversible inhibitors of the 3-bromopropanesulfonate type

3-Bromopropanesulfonate is the MCR inhibitor with the by far lowest $[I]_{0.5V}$ of < 0.1 μM. When this compound reacts with MCR-red1 the enzyme is almost immediately inactivated and its EPR signal converted to the Ni based EPR signal MCR-BPS (Fig. 6A) similar in line shape to that of the MCR-ox signals (Fig. 7). The induction of the signal was not dependent on the presence of coenzyme B. In its presence almost the same signal was induced differing, however, only very slightly in the *g* values. The MCR-BPS signal was quenched when the inactive enzyme was exposed to air but it was stable when 10 mM 2-bromoethanesulfonate was added, which is quite remarkable considering that 25 μM 2-bromoethanesulfonate are sufficient to very rapidly quench the MCR-red1 signal. Since the stable MCR-BPS signal was induced in the absence of coenzyme B it cannot be argued that the entrance to the active site was blocked by coenzyme B and thus the active site was not accessible to the 2-bromoethanesulfonate. The results thus indicate that the EPR signal of MCR-BPS must be derived from Ni that can no longer be oxidized by 2-bromoethanesulfonate. This theoretically could be a Ni(III) or a high spin Ni(II) axially coordinated to a radical [59], which are both resonating structures. Four-coordinated or axially weakly six-coordinated Ni(III) is most certainly excluded since the EPR signal of MCR-BPS by no means resembles that of $Ni(III)F_{430}$ [60].

High spin $Ni(II)F_{430}$ axially coordinated to a radical as shown in Fig. 9 is predicted to exhibit an EPR signal that shows hyperfine splitting due to the coupling with the four nitrogens of the tetrapyrrolic ring system. Probably due to line broadening the expected hyperfine splitting is not apparent (Fig. 6). The hyperfine splitting can, however, readily be seen in the MCR-ox signals [26] which are thought to be derived from a high spin Ni(II) axially coordinated to a thiyl radical [61]. It is therefore proposed that MCR-BPS is generated from MCR-red1 as shown in Fig. 9. Consistent with this interpretation is the finding that 3-iodopropanesulfonate and 4-bromobutyrate also induced the MCR-BPS signal. The three compounds have in common that the radical formed by reduction cannot decompose in the manner described for 2-bromoethanesulfonate. 3-Azidopropanesulfonate ($[I]_{0.5V}$ = 40 μM) and 4-bromobutanesulfonate ($[I]_{0.5V}$ = 6 μM), which have been reported to be strong inhibitors of MCR [49], are predicted to react similarly to 3-bromopropanesulfonate.

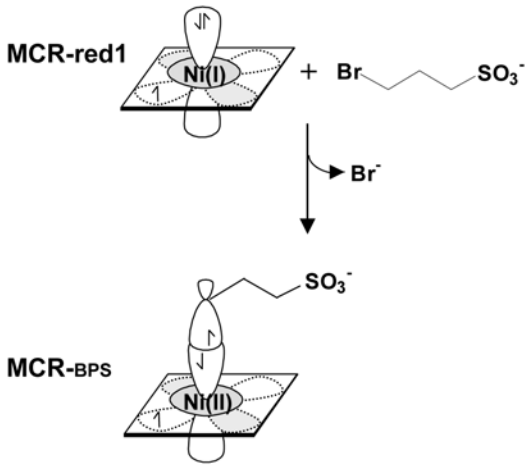

Fig. 9 Proposed mechanism of MCR-BPS formation from MCR-red1 and 3-bromopropanesulfonate (BPS). It is assumed that a high spin Ni(II) with an axial alkyl radical as ligand is formed as indicated by the Ni based EPR signal. It is a resonating structure of an alkyl-Ni(III).

When MCR-BPS formed in the presence of coenzyme B was exposed to O_2, a radical signal was induced, which differed from that induced by 2-bromoethanesulfonate in the presence of coenzyme B. The O_2 induced signal had some structure, which has to be analyzed in detail by high field EPR and ENDOR spectroscopy before an interpretation is possible.

Conclusion

Most of the results are consistent with catalytic mechanism I, in which the first step in the catalytic cycle is a nucleophilic substitution yielding methyl-Ni(III). The low catalytic efficiency of ethyl-coenzyme M reduction, the inertness of allyl-coenzyme M as a substrate and the observed inversion of stereoconfiguration are much less easy to explain with the alternative mechanism II, in which methyl-coenzyme M is reduced to a free methyl radical as first step in the catalytic cycle. But none of the findings completely exclude mechanism II. The finding that the oxidation of Ni(I) to Ni(II) in the active site of MCR-red1 by 2-bromoethanesulfonate is dependent on coenzyme B shows that, upon coenzyme B binding, the reactivity of the Ni(I) species is increased. This had previously already become evident from the finding that the thiol group of coenzyme M interacts with Ni(I) of MCR-red1 only in the presence of coenzyme B [14]. Because the structural consequences of coenzyme B binding, which lead to the enhanced reactivity, are still unknown, they can not be taken into consideration in density functional calculations which, so far, constitute the main argument in support of mechanism II [22-23]. The formation of MCR-BPS from MCR-red1 and 3-bromopropanesulfonate was interpreted by us to proceed in a reaction yielding an alkylated Ni, most probably a high spin Ni(II) with the alkyl radical as axial ligand (Fig. 9). The reaction can be formulated as nucleophilic substitution or as oxidative addition and could serve as model reaction for the first step in methyl-coenzyme M reduction.

Acknowledgements This work was supported by the Max Planck Society, the Deutsche Forschungsgemeinschaft, the Fonds der Chemischen Industrie and by the Swiss National Science Foundation. We thank Reinhard Böcher for technical assistance. Meike Goenrich is grateful to the Claussen-Simon-Foundation for a fellowship

References

1. Wolfe RS (2004) ASM News 70:15-18
2. Thauer RK (1998) Microbiology 144:2377-2406
3. Goubeaud M, Schreiner G, Thauer RK (1997) Eur J Biochem 243:110-114
4. Becker DF, Ragsdale SW (1998) Biochemistry 37:2639-2647
5. Mahlert F, Grabarse W, Kahnt J, Thauer RK, Duin EC (2002a) J Biol Inorg Chem 7:101-112
6. Krüger M, Meyerdierks A, Glockner FO, Amann R, Widdel F, Kube M, Reinhardt R, Kahnt J, Bocher R, Thauer RK, Shima S (2003) Nature 426:878-881
7. Ermler U, Grabarse W, Shima S, Goubeaud M, Thauer RK (1997) Science 278:1457-1462
8. Grabarse W, Mahlert F, Shima S, Thauer RK, Ermler U (2000) J Mol Biol 303:329-344
9. Grabarse W, Mahlert F, Duin EC, Goubeaud M, Shima S, Thauer RK, Lamzin V, Ermler U (2001a) J Mol Biol 309:315-330
10. Grabarse W, Shima S, Mahlert F, Duin EC, Thauer RK, Ermler U (2001b) Methyl-coenzyme M reductase. In: Messerschmidt A, Huber R, Poulos T, Wieghardt K (eds) Handbook of Metalloproteins. John Wiley & Sons, Chichester, pp 897-914
11. Jaun B, Pfaltz A (1986) J Chem Soc, Chem Commun:1327-1329
12. Rospert S, Böcher R, Albracht SPJ, Thauer RK (1991) FEBS Lett 291:371-375
13. Holliger C, Pierik AJ, Reijerse EJ, Hagen WR (1993) J Am Chem Soc 115:5651-5656
14. Finazzo C, Harmer J, Bauer C, Jaun B, Duin EC, Mahlert F, Goenrich M, Thauer RK, Van Doorslaer S, Schweiger A (2003a) J Am Chem Soc 125:4988-4989
15. Finazzo C, Harmer J, Jaun B, Duin EC, Mahlert F, Thauer RK, Van Doorslaer S, Schweiger A (2003b) J Biol Inorg Chem 8:586-593
16. Horng YC, Becker DF, Ragsdale SW (2001) Biochemistry 40:12875-12885
17. Jaun B (1993) Methane formation by methanogenic bacteria: redox chemistry of coenzyme F430. In: Sigel H, Sigel A (eds) Metal Ions in Biological Systems. Marcel Dekker, New York, pp 287-337
18. Lin S-K, Jaun B (1992) Helv Chim Acta 75:1478-1490
19. Signor L, Knuppe C, Hug R, Schweizer B, Pfaltz A, Jaun B (2000) Chem Eur J 6:3508-3516
20. Tada M, Masuzawa Y (1997) Chem Commun 22:2161-2162

21. Ghosh A, Wondimagegn T, Ryeng H (2001) Curr Opin Chem Biol 5:744-750
22. Pelmenschikov V, Blomberg MR, Siegbahn PE, Crabtree RH (2002) J Am Chem Soc 124:4039-4049
23. Pelmenschikov V, Siegbahn PE (2003) J Biol Inorg Chem 8:653-662
24. Ahn Y, Krzycki JA, Floss HG (1991) J Am Chem Soc 113:4700-4701
25. Lin S-K, Jaun B (1991) Helv Chim Acta 74:1725-1738
26. Mahlert F, Bauer C, Jaun B, Thauer RK, Duin EC (2002b) J Biol Inorg Chem 7:500-513
27. Telser J, Horng YC, Becker DF, Hoffman BM, Ragsdale SW (2000) J Am Chem Soc 122:182-183
28. Telser J, Davydov R, Horng YC, Ragsdale SW, Hoffman BM (2001) J Am Chem Soc 123:5853-5860
29. Tang Q, Carrington PE, Horng YC, Maroney MJ, Ragsdale SW, Bocian DF (2002) J Am Chem Soc 124:13242-13256
30. Singh K, Horng YC, Ragsdale SW (2003) J Am Chem Soc 125:2436-2443
31. Piskorski R, Jaun B (2003) J Am Chem Soc 125:13120-13125
32. Craft JL, Horng YC, Ragsdale SW, Brunold TC (2004) J Biol Inorg Chem 9:77-89
33. Wasserfallen A, Nölling J, Pfister P, Reeve J, de Macario EC (2000) International Journal of Systematic & Evolutionary Microbiology 50:43-53
34. Gunsalus RP, Romesser JA, Wolfe RS (1978) Biochemistry 17:2374-2377
35. Kobelt A, Pfaltz A, Ankel-Fuchs D, Thauer RK (1987) FEBS Lett 214:265-268
36. Ellermann J, Hedderich R, Böcher R, Thauer RK (1988) Eur J Biochem 172:669-677
37. Rospert S, Voges M, Berkessel A, Albracht SPJ, Thauer RK (1992) Eur J Biochem 210:101-107
38. Rospert S, Linder D, Ellermann J, Thauer RK (1990) Eur J Biochem 194:871-877
39. Bonacker LG, Baudner S, Mörschel E, Böcher R, Thauer RK (1993) Eur J Biochem 217:587-595
40. Bradford MM (1976) Anal Biochem 72:248-254
41. Beinert H, Albracht SPJ (1982) Biochimica et Biophysica Acta 683:245-277
42. Schönheit P, Moll J, Thauer RK (1980) Arch Microbiol 127:59-65.
43. Bonacker LG, Baudner S, Thauer RK (1992) Eur J Biochem 206:87-92
44. Reeve JN, Nölling J, Morgan RM, Smith DR (1997) J Bacteriol 179:5975-5986
45. Hedderich R, Thauer RK (1988) FEBS Lett 234:223-227
46. Gunsalus RP, Wolfe RS (1978) FEMS Lett 3:191-193
47. Wackett LP, Honek JF, Begley TP, Wallace V, Orme-Johnson WH, Walsh CT (1987) Biochemistry 26:6012-6018
48. Belay N, Daniels L (1988) A v Leeuwenhoek 54:113-125
49. Ellermann J, Rospert S, Thauer RK, Bokranz M, Klein A, Voges M, Berkessel A (1989) Eur J Biochem 184:63-68
50. Albracht SPJ, Ankel-Fuchs D, van der Zwaan JW, Fontijn RD, Thauer RK (1986) Biochim Biophys Acta 870:50-57
51. Albracht SPJ, Ankel-Fuchs D, Böcher R, Ellermann J, Moll J, van der Zwaan JW, Thauer RK (1988) Biochim Biophys Acta 955:86-102
52. Wackett LP, Honek JF, Begley TP, Shames SL, Niederhoffer EC, Hausinger RP, Orme-Johnson WH, Walsh C (1988) Methyl-S-coenzyme-M reductase: A nickel-dependent enzyme catalyzing the terminal redox step in methane biogenesis. In: Lancaster J, JR (ed) The Bioinorganic Chemistry of Nickel. VCH Publishers Inc., Weinheim, pp 249-274
53. Holliger C, Kengen SW, Schraa G, Stams AJ, Zehnder AJ (1992) J Bacteriol 174:4435-4443
54. Selmer T, Kahnt J, Goubeaud M, Shima S, Grabarse W, Ermler U, Thauer RK (2000) J Biol Chem 275:3755-3760
55. Stubbe JA, van der Donk WA (1998) Chem Rev 98:705-762
56. Wagner AF, Frey M, Neugebauer FA, Schafer W, Knappe J (1992) Proc Natl Acad Sci U S A 89:996-1000
57. Knappe J, Wagner AF (2001) Adv Protein Chem 58:277-315
58. Olson KD, Chmurkowska-Cichowlas L, McMahon CW, Wolfe RS (1992) J Bacteriol 174:1007-1012
59. Wondimagegn T, Ghosh A (2001) J Am Chem Soc 123:1543-1544
60. Jaun B (1990) Helv Chim Acta 73:2209-2217
61. Duin EC, Signor L, Piskorski R, Mahlert F, Clay MD, Goenrich M, Thauer RK, Jaun B, Johnson MK (2004) J Biol Inorg Chem 9:563-576

J Biol Inorg Chem (2004), submitted for publication on 01 september 2004

ORIGINAL ARTICEL

Meike Goenrich · Evert C. Duin
Felix Mahlert · Rudolf K. Thauer

Temperature dependence of methyl-coenzyme M reductase (MCR) activity and of the formation of the MCR-red2 state induced by coenzyme B

Abstract Methyl-coenzyme M reductase (MCR) catalyses the formation of methane from methyl-coenzyme M (CH_3-S-CoM) and coenzyme B (HS-CoB) in methanogenic archaea. The enzyme has an $\alpha_2\beta_2\gamma_2$ subunit structure forming two structurally interlinked active sites each with a molecule F_{430} as prosthetic group. The nickel porphinoid must be in the Ni(I) oxidation state for the enzyme to be active. The active enzyme exhibits an axial Ni(I) based EPR signal and a UV-visible spectrum with an absorption maximum at 385 nm. This state is called the MCR-red1 state. In the presence of coenzyme M (HS-CoM) and coenzyme B the MCR-red1 state is in part converted reversibly into the MCR-red2 state, which shows a rhombic Ni(I) based EPR signal and a UV-visible spectrum with an absorption maximum at 420 nm. We report here for MCR from *Methanothermobacter marburgensis* that the MCR-red2 state is also induced by several coenzyme B analogues and that the degree of induction by coenzyme B is temperature dependent. When the temperature was lowered below 20°C the percentage of MCR in the red2 state decreased and that in the red1 state increased. These changes with temperature were fully reversible. It was found that at most 50% of the enzyme was converted to the MCR-red2 state under all experimental conditions. These findings indicate that in the presence of both coenzyme M and coenzyme B only one of the two active sites of MCR can be in the red2 state (half-of-the-sites reactivity). Based on this interpretation a two-stroke engine mechanism for MCR is proposed.

Keywords Methyl-coenzyme M reductase · Nickel enzymes · Factor 430 · EPR spectroscopy · Half-of-the-sites reactivity · Mechanism of methane formation · Methanogenic archaea

Abbreviations MCR: methyl-coenzyme M reductase · CH_3-S-CoM: methyl-coenzyme M · HS-CoM: coenzyme M · HS-CoB: coenzyme B · MCR-red1: active MCR exhibiting the EPR signals red1a, red1c or red1m · MCR-red1c: MCR-red1 in the presence of 10 mM coenzyme M · MCR-red2: MCR exhibiting the EPR red2 signal · MCR-red1/2: MCR exhibiting both the EPR red1 and red2 signal · MCR-ox: MCR exhibiting the EPR signals ox1, ox2 or ox3

INTRODUCTION

Globally approximately 1 billion tons of methane are generated by the metabolic activity of methanogenic archaea in anoxic environments such as fresh water sediments, swamps, the hindgut of termites and the rumen of sheep and cows [1, 2]. In all methanogens methane is formed from methyl-coenzyme M (CH_3-S-CoM) and coenzyme B (HS-CoB):

CH_3-S-CoM + HS-CoB = CH_4 + CoM-S-S-CoB
$\Delta G^{o'}$ = -30 kJ/mol

($\Delta G^{o'}$ was calculated from ΔGf^o = -112.5 kJ/mol for methanol reduction with H_2 to methane and water [3], from $\Delta G^{o'}$ = -27.5 kJ/mol for methyl-coenzyme M formation from methanol and coenzyme M [4] and $E^{o'}$ = -140 mV for the CoM-S-S-CoB/HS-CoM + HS-CoB couple [5]. In previous calculations [1] $E^{o'}$ was assumed to be –200 mV). The reverse reaction is most probably involved in the anaerobic oxidation of methane [6, 7].

M. Goenrich · F. Mahlert · R. K. Thauer (✉)
Max-Planck-Institut für terrestrische Mikrobiologie
and Laboratorium für Mikrobiologie, Fachbereich Biologie,
Philipps-Universität, Karl-von-Frisch-Strasse,
35043 Marburg, Germany
E-mail: thauer@staff.uni-marburg.de
Fax: +49 6421178109

E. C. Duin
Department of Chemistry and Biochemistry,
Auburn University, AL 36849, USA

Methane formation is catalysed by methyl-coenzyme M reductase (MCR). The 300 kDa enzyme is composed of three different subunits of molecular mass 66 kDa (α subunit), 48 kDa (β subunit) and 37 kDa (γ subunit) and each subunit is present twice (values given are for MCR I from *Methanothermobacter marburgensis*). Per mol the enzyme contains 2 mol of the nickel porphinoid F_{430} tightly but not covalently bound. The prosthetic group must be in the Ni(I) oxidation state for the enzyme to be active. The redox potential $E^{o'}$ of the $F_{430}Ni(II)/F_{430}Ni(I)$ couple has been determined to be between -600 and -700 mV [8]. Due to the negative redox potential MCR is a very labile enzyme rapidly inactivated in the presence of trace amounts of O_2 or of other electron acceptors [1].

The crystal structure of inactive MCR from *M. marburgensis* has been determined to 1.16 Å resolution [9-12]. The structure revealed the presence of two active sites with $F_{430}Ni(II)$ deeply buried within the protein and accessible from the outside only via a long narrow channel. Methyl-coenzyme M can be positioned in the cavity above F_{430} such that either its methyl group or the thioether sulfur interact with the Ni(I). Methyl-coenzyme M must enter the channel before coenzyme B because after coenzyme B binding the substrate channel is completely locked. Coenzyme B binds in a manner that its thioheptanoyl group points towards F_{430} and the phosphate moiety towards the entrance of the channel. The sulfur of coenzyme B gets positioned above the Ni(I) of F_{430} in a distance of 8 Å, which is too far for the thiol group to directly interact with the Ni(I). The channel and the coenzyme binding sites are formed by residues of subunits α´, α, β and γ and equivalently α, α´, β´ and γ´. Whereas the porphinoid ligand system of F_{430} is thus tightly attached to the one α subunit, the distal axial ligand to nickel is contributed by a glutamine residue of the second α' subunit indicating that the two active sites are structurally and functionally interlinked. A conformational change in the one active sites can be directly transferred via the α subunits to the other site. The α subunit contains five modified amino acids with still unknown function [13]. One of them is a highly conserved thioglycine forming a thiopeptide bond, which is susceptible to reduction induced trans-cis isomerisation and which could therefore play a key role in coupling of the two active sites [12].

Active MCR has a greenish colour with an absorbance maximum at 385 nm [14-16]. It exhibits a Ni(I) based axial EPR signal designated MCR-red1 (g_z = 2.25; g_y = 2.07; g_x = 2.06). Double integration of the signal of the fully active enzyme revealed that both active sites contain F_{430} in the reduced form, the spin concentration per Ni being approximately 0.9. The red1 signal shows a superhyperfine splitting due to the interaction of the electron of Ni(I) with the nuclear spin of the four nitrogens of the tetrapyrrolic ring system. The superhyperfine splitting is clearly resolved when the active enzyme is in the absence or presence of its substrates. It is much less resolved when the enzyme is in the presence of coenzyme M (MCR-red1c) [14, 16], which inhibits MCR competitively to methyl-coenzyme M [14, 16, 17].

When MCR-red1c is supplemented with coenzyme B a novel Ni(I) based rhombic EPR signal designated MCR-red2 (g_z = 2.29; g_y = 2.24; g_x = 2.18) is induced at the expense of the red1 signal. MCR with fully induced red2 signal shows the red1 and red2 signal at almost equal intensity each with a spin concentration per Ni of approximately 0.4 [16]. Concomitantly with the change in the EPR spectrum the absorption maximum at 385 nm decreased and an absorption at 420 nm increased [14, 16]. In the presence of coenzyme M and coenzyme B MCR thus appears to be present for 50% in a MCR-red1 state and for 50% in the MCR-red2 state [14, 16].

The conversion of the MCR-red1 state into the MCR-red2 state upon addition of coenzyme B occurs only in the presence of coenzyme M and is associated with the reversible coordination of the thiol group of coenzyme M to the active site Ni(I) as revealed by EPR and ENDOR spectroscopic data with unlabelled and ^{33}S labelled coenzyme M [18, 19]. Apparently the addition of coenzyme B induces a conformational change in MCR-red1c bringing the thiol group of coenzyme M into binding distance of the Ni(I). Such a conformational change is probably also required in the reaction of methyl-coenzyme M with the Ni(I), which has been proposed to be the first step in the catalytic cycle of methyl-coenzyme M reduction to methane in all but one discussed mechanism [17, 20-25]. The finding that in the presence of methyl-coenzyme M the addition of coenzyme B to MCR-red1 does not induce a change in the UV-visible and EPR spectrum [16] can be explained assuming that the coenzyme B triggered conformational change is the rate-limiting step in methane formation from methyl-coenzyme M.

Most of the biochemical properties reported for MCR in the literature were obtained for MCR isoenzyme I from *M. marburgensis,* which contains two MCR isoenzymes [26-28] and has a growth temperature optimum of 65°C. The following study was therefore also performed with purified MCR I from the hydrogenotrophic archaeon. We report here that the conformational change induced in MCR by coenzyme B in the presence of coenzyme M becomes thermodynamically unfavourable at temperatures below 20°C and that this correlates with enzyme activity. We further provide evidence that the conformational change induced by coenzyme B is restricted at the time to only one of the two active sites of MCR.

Material and Methods

Methanothermobacter marburgensis (*Methanobacterium thermoautotrophicum,* strain Marburg [29]) is the strain deposited under DSM 2133 in the Deutsche Sammlung von Mikroorganismen und Zellkulturen (Braunschweig).

Coenzyme M (2-mercaptoethanesulfonate) was obtained from Merck (Darmstadt); methyl-coenzyme M was synthesized from coenzyme M by methylation with methyl iodide (Fluka) [16, 30]. Coenzyme B (*N*-7-mercaptoheptanoylthreonine phosphate) was prepared from the symmetric disulfide CoB-S-S-CoB by reduction with $NaBH_4$ [31, 32]. *N*-6-mercaptohexanoylthreonine phosphate (HS-CoB_6) and *N*-8-mercaptooctanooylthreonine phosphate (HS-CoB_8) were synthesized and purified as previously described [32, 33].

Purification of active MCR

M. marburgensis was grown at 65°C in a 13 L glass fermenter (New Brunswick) containing 10 L mineral medium stirred at 1200 rpm and gassed with 80% H_2/20% CO_2/0.1% H_2S at a rate of 1200 mL/min [16]. When an ΔOD_{578} of 4.5 was reached, the gas supply was switched to 100% H_2 for 30 min to induce the EPR signals MCR-red1 and red2 in the cells. After 30 min the cells were cooled to 10°C within 10 min under continuous gassing and harvested anaerobically by centrifugation using a flow-through centrifuge (Hettich, centrifuge 17 RS). Approximately 70 g of wet cells were obtained. From these cells only the MCR isoenzyme I was purified [26, 28]. All steps of the purification were performed in the presence of 10 mM coenzyme M and in an anaerobic chamber (Coy Instruments) filled with 95% N_2/5% H_2 as described previously [16]. During purification the enzyme lost its MCR-red2 signal due to the removal of coenzyme B. In one purification generally 150 mg active MCR in the red1c state (in 10 mL) were obtained. The spin concentration per mol F_{430} was approximately 0.9 per mol F_{430}.

The protein concentration was determined by using the method of Bradford [34] with bovine serum albumin (Serva) as standard or by measuring the absorbance difference of oxidized enzyme (MCR-silent) at 420 nm using an ε = 44,000 $M^{-1}cm^{-1}$ for a molecular mass of 280,000 Da. Both methods yielded almost the same results.

MCR activity determination

Methyl-coenzyme M reductase activity was determined by following methane formation at temperatures between 0°C and 75°C gas-chromatographically. The assays were performed in 8 mL serum bottles containing 0.4 mL assay solution and closed with a rubber stopper. The assay solution was composed of 50 mM Tris/HCl pH 7.6, 10 mM methyl-coenzyme M, 0.5 mM CoB-S-S-CoB, 10 mM Ti(III)citrate, 0.3 mM hydroxycobalamin and 20 – 200 µg of MCR. The gas phase was in both assays 95% N_2/5% H_2. The reaction was started by the addition of MCR. At intervals of 2 min, 0.2 mL gas samples were withdrawn and analyzed for methane by gas-chromatography [15, 28].

EPR spectroscopy

Samples (0.35 mL) were analyzed for EPR spectra at 77 K in 0.3 cm (inner diameter) quartz tubes with 95% N_2/5% H_2 as gas phase and closed with a closed off rubber tube. For room temperature EPR measurements, samples were analyzed in quartz flat cell tubes with 95% N_2/5% H_2 as gas phase and closed with parafilm. The samples contained at least 2.2 – 31 mg MCR (7.9 – 113 nmol) in 10 Tris/HCl pH 7.6. EPR spectra at X-band (9.4 GHz) were obtained with a Bruker EMX-6/1 EPR spectrometer composed of the EMX 1/3 console, ER 041 X6 bridge with built-in ER-0410-116 microwave frequency counter, ER-070 magnet and ER-4102st standard universal rectangular cavity. All spectra were recorded with a field modulation frequency of 100 kHz. Cooling of the sample was performed either with an Oxford Instruments ESR 900 cryostat with an ITC4 temperature controller or with liquid nitrogen in a finger dewar at 77 K.

EPR spin quantitations were carried out under non-saturating conditions using 10 mM copper perchlorate as the standard (10 mM $CuSO_4$; 2 M $NaClO_4$; 10 mM HCl). All signal intensities are expressed as spin per mol F_{430}.

Results

MCR I was purified from *Methanothermobacter marburgensis* grown at 65°C on 80%H_2/20%CO_2 and, before harvest, gassed for 30 min with 100%H_2 to induce the MCR-red states [16]. All buffers used during the

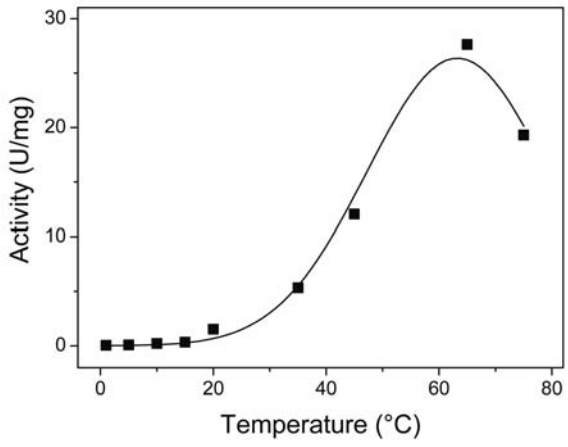

Fig. 1 Temperature dependence of methane formation from methyl-coenzyme M and coenzyme B as catalysed by MCR from *Methanothermobacter marburgensis*. The 0.4-mL assay mixture contained 50 mM Tris/HCl pH 7.6, 1 mM coenzyme B, 10 mM methyl-coenzyme M, 10 mM Ti(III)citrate, 0.3 mM hydroxycobalamin and purified MCR-red1c: 200 µg at temperatures between 0°C and 15°C and 20 µg at temperatures above 15°C. The specific activity was approximately 50 mU/mg at 1°C and 220 mU/mg at 10°C.

Tab. 1 Effect of coenzyme B and coenzyme B analogues on the activity and EPR spectroscopic properties of active methyl-coenzyme M reductase (MCR) from *Methanothermobacter marburgensis*.

		Kinetic properties	EPR signal	
			MCR-red1c + HS-CoB or one of its analogues	After oxidation with O_2
Substrate		**app. K_M (mM)**		
N-7-mercaptoheptanoylthreonine phosphate (HS-CoB)	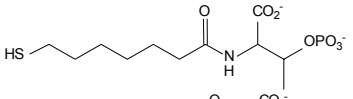	0.2 (30U/mg) [a]	MCR-red1/2 (0.6/0.3)[b]	MCR-ox3 (0.45)[b]
N-6-mercaptohexanoylthreonine phosphate (HS-CoB_6) [27, 31]	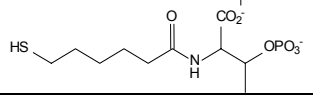	n.d. (0.1U/mg)[a]	MCR-red1/2 (0.8/0.1)[b]	MCR-ox3 (0.1)[b]
Inhibitors		**app. K_i (µM)**		
N-6-mercaptohexanoylthreonine phosphate (HS-CoB_6) [27, 31]		0.1		
N-7-(methylthio)heptanoylthreonine phosphate (CH_3-S-CoB) [14, 42]	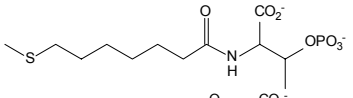	6	MCR-red1/2 (0.6/0.3)[b]	No signal
N-8-mercaptooctanoylthreonine phosphate (HS-CoB_8) [27, 43]	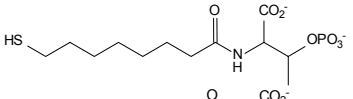	15	MCR-red1c (0.9)[b]	No signal
N-nonanoylthreonine phosphate (CH_3-CH_2-CoB) [14]]	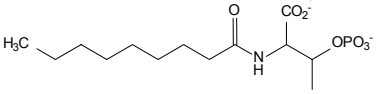	n.d.	MCR-red1c (0.9)[b]	No signal
N-6-(methylthio)hexanoylthreonine phosphate (CH_3-S-CoB_6) [43]	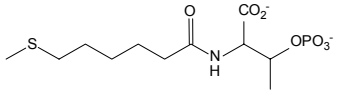	9	n.d.	n.d.
N-8-(methylthio)octanoylthreonine phosphate (CH_3-S-CoB_8) [43]	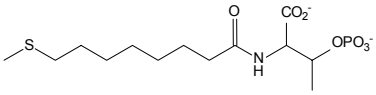	No inhibition (1mM)	n.d.	n.d.

[a]apparent V_{max}; [b]spin concentration per mol F_{430}; n.d.= not determined

anaerobic purification contained 10 mM coenzyme M. The purified enzyme generally showed the UV-visible spectrum (see Fig. 3) and EPR signal (see Fig. 4A1) characteristic for MCR-red1c [16]. The spin concentration was generally near 0.9 per mol F_{430}. With these preparations we investigated the induction of the MCR-red2 state by coenzyme B and by coenzyme B analogues. During these studies we found that the induction is temperature dependent below 20°C and that MCR-red1 rather than MCR-red2 shows a room temperature EPR signal. The temperature dependence of MCR-red1 activity is given in Figure 1. Purified MCR-red1c from *M. marburgensis* had a specific activity of approximately 0.1 units per mg at 0°C and one of approximately 30 units per mg at 65°C, the temperature activity optimum of this not increase significantly when the coenzyme B concentration (5 mM) and/or the coenzyme M concentration (10 mM) in the enzyme solution were enzyme (Fig. 1). From 0°C to 65°C the Q_{10} ($V_{T+10°C}$/ V_T) continuously decreased from approximately 4 between 0°C and 10°C to below 2 between 55°C and 65°C.

Induction of the MCR-red2 state by coenzyme B and coenzyme B analogues

When MCR-red1c solutions at room temperature (spin concentration of 0.9 per mol Ni) were supplemented with coenzyme B at 5 mM concentration approximately 35% of MCR-red1 was converted into the MCR-red2 state and 65% remained in the MCR-red1 state as indicated by the EPR spectrum measured at 77 K (Table 1). The spin concentration of the red2 signal was 0.3 in the shown experiment but as high as 0.4 in some experiments. It did increased. The MCR-red2 state was not induced when coenzyme M was omitted or substituted by methyl-coenzyme M (not shown).

The coenzyme B induced MCR-red2 signal was converted into the MCR-ox3 signal (g_z = 2.22; g_y = 2.14; g_x = 2.13) and the MCR-red1 signal disappeared upon exposure of the enzyme to air. The spin concentration of the ox3 signal was 0.45 per mol F_{430} (Table 1) and thus close to the spin concentration of the red2 signal, which was 0.3 per mol F_{430}. The conversion of the red2 signal into the ox3 signal upon exposure of active MCR to air is a means to probe for the MCR-red2 state [35].

The coenzyme B analogue *N*-6-mercaptohexanoylthreonine phosphate (HS-CoB_6) has been reported to be both a substrate and an inhibitor of coenzyme B (for structures see Table 1) [23, 32]. With HS-CoB_6 as substrate, MCR has less than 1% of the activity shown with HS-CoB (see also [23]). We therefore tested whether this compound could also induce the MCR-red2 state, which was found to be the case (not shown). However, even at relatively high concentrations of HS-CoB_6 (5mM) only approximately 10% of the MCR-red1 state was converted to the MCR-red2 state, which was reflected in the low intensity of the ox3 signal exhibited by the enzyme after exposure to air (Table 1).

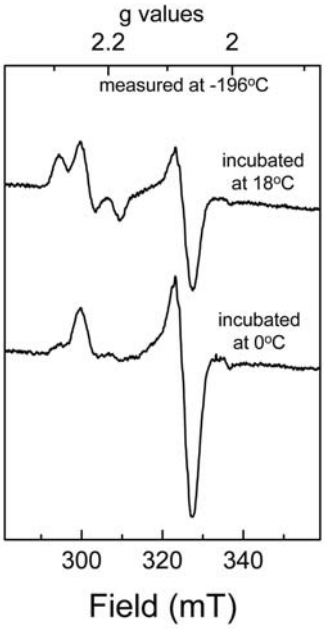

Fig. 2 EPR spectra at –196°C (77 K) of methyl-coenzyme M reductase in the MCR-red1/2 state prepared at 18°C (291 K) and at 0°C (273 K). MCR-red1/2 = active MCR in the presence of 10 mM coenzyme M and 5 mM coenzyme B exhibiting the axial MCR-red1 signal (g_z = 2.25; g_y = 2.07; g_x = 2.06) and the rhombic MCR-red2 signal (g_z = 2.29; g_y = 2.24; g_x = 2.18). The sample at 18°C and that at 0°C were frozen by immersion of the EPR tubes in liquid nitrogen. The concentration of purified enzyme in both samples was 2.2 mg (7.9 nmol) in 0.35 mL 10 mM Tris/HCl pH 7.6. The spin concentration in the samples was approximately 0.9 per mol F_{430}. Spectra were recorded under the following conditions: microwave frequency, 9439 MHz; microwave power incident to the cavity, 2.01 mW; temperature, -196°C (77 K); modulation amplitude, 0.6 mT.

Of interest is that CH_3-S-CoB can also induce the MCR-red2 state although this coenzyme B analogue is not a substrate and that HS-CoB_8 and CH_3-CH_2-CoB cannot induce the MCR-red2 state although these compounds are potent inhibitors (Table 1) [35]. The finding that the red2 signal exhibited by active MCR in the presence of coenzyme M and methyl-coenzyme B was quenched by O_2 rather than converted to the ox3 signal (Table 1) indicates that for the formation of the ox3 signal the free thiol group of coenzyme B is required.

Temperature dependent equilibrium between the MCR-red1 and MCR-red2 states

Fig. 2 shows the EPR spectrum measured at –196°C (77 K) of MCR-red1c to which at room temperature (18°C, 291 K) coenzyme B had been added. Double integration revealed the presence of 40% MCR-red2 and 60% MCR-red1. When instead the temperature of the sample was lowered to 0°C (273 K) before the sample was frozen, the percentage of MCR-red2 in the frozen EPR sample decreased to near 10% and that of MCR-red1 increased to 90% (Fig. 2). This temperature dependent change was also seen in the UV-visible spectrum (Fig. 3). At 0°C the spectrum was very similar to that of MCR-red1c in the absence of coenzyme B (Fig. 3, dashed line). Upon increase of the temperature to 25°C the absorption at 385 nm, reflecting the concentration of MCR-red1, decreased. These changes were reversible. Apparently under the experimental conditions the MCR-red1 and MCR-red2 states were in a temperature dependent equilibrium. As

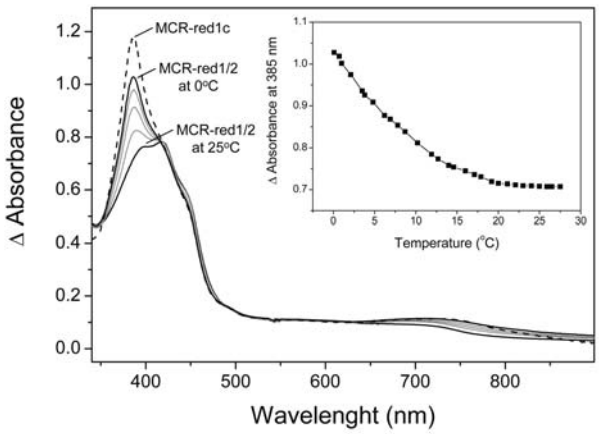

Fig. 3 UV-visible spectra of methyl-coenzyme M reductase in the MCR-red1/2 state at temperatures between 25°C and 0°C. For comparison the spectrum of MCR in the red1c state at room temperature is given (---). MCR-red1/2 = active MCR in the presence of 10 mM coenzyme M and 5 mM coenzyme B. MCR-red1c = active MCR in the presence of 10 mM coenzyme M. The inset shows a plot of the absorbance changes at 385 nm versus the temperature. The concentration of purified enzyme was 1.4 mg (5.1 nmol) in 1 mL 10 mM Tris/HCl pH 7.6. The spectra were not corrected for the 10% inactive MCR present in the samples.

indicated from the plot of the absorbance at 385 nm versus the temperature, maximal conversion of the MCR-red1 state into the MCR-red2 state was reached at 20°C (Inset of Fig. 3). Above this temperature the percentage of conversion remained constant.

The lowest temperature investigated was 0°C at which approximately 10% of the MCR was present in the red2 state. At temperatures below 0°C the samples froze. When the samples were supplemented with ethylene glycol (10%) to prevent freezing maximal conversion of the MCR-red1 state into the MCR-red2 state was already reached at about 5°C (not shown) indicating that in the presence of ethylene glycol the enzyme stayed flexible to lower temperatures.

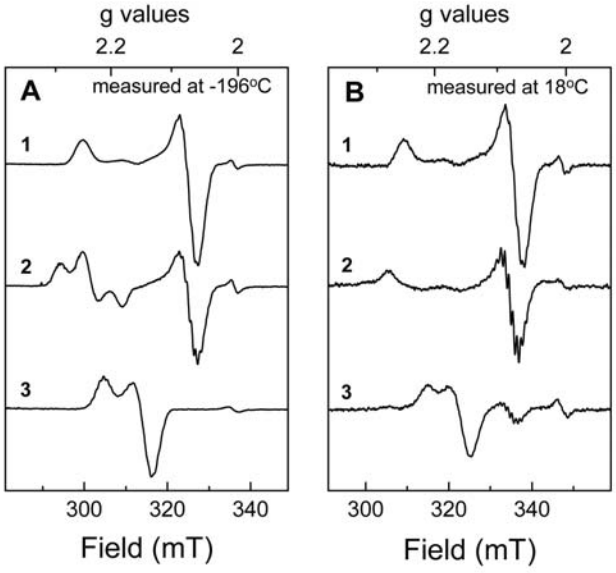

Fig. 4 EPR spectra of methyl-coenzyme M reductase measured (**A**) at –196°C (77 K) and (**B**) at room temperature (18°C, 291 K). (1) MCR-red1c = active methyl-coenzyme M reductase in the presence of 10 mM coenzyme M; (2) MCR-red1/2 = samples as in 1 but supplemented with 5 mM coenzyme B. (3) MCR-ox3 = samples as in 2 but after exposure to air. Before measurement all samples were at room temperature. For measurement of the EPR spectra at -196°C the samples were frozen in liquid nitrogen (**A**) and for the measurements at 18°C the samples were left at room temperature (**B**). The concentration of purified enzyme in samples **A** was 8.9 mg (32 nmol) and in samples **B** 31 mg (113 nmol) in 0.35 mL 10 mM Tris/HCl pH 7.6. Spectra were recorded under the following conditions: microwave frequency, (**A**) 9434 MHz, (**B**) 9746 MHz; microwave power incident to the cavity, (**A**) 2.00 mW, (**B**) 6.35 mW; temperature, (**A**) –196°C (77 K), (**B**) 18°C (291 K); modulation amplitude, 0.6 mT.

The double integral of the EPR signals **A**1 and **A**2 were almost identical and that of the signal **A**3 was 50% of that of **A**1 and **A**2. The double integral of the signal **B**2 was 56% of that of **B**1 and that of **B**3 was 45% of that of **B**1. When corrected for the different protein concentrations signal **B**1 had 3.3%, signal **B**2 had 1.8% and signal **B**3 had 3.1% of the intensity of the signals **A**1, **A**2 and **A**3, respectively.

Room temperature EPR spectra of the MCR-red1 and MCR-red2 states

The finding that the MCR-red2 state is converted into the MCR-red1 state when the temperature is lowered below 20°C raised the question whether the concentration of the MCR-red2 state determined by EPR spectroscopy in the experiments reported above were underestimated. The EPR spectra were routinely measured at –196°C (77 K) after freezing of the sample at room temperature in liquid nitrogen. It is therefore conceivable that during freezing some of the MCR-red2 state was always converted to the MCR-red1 state. If so then at room temperature the percentage of MCR in the red2 state could be as high as 100% rather than 30-50% as reported above.

We therefore tested what happens, when the EPR tubes with the samples are frozen in liquid nitrogen/ethanol mixtures, in which cooling of the samples is much more rapid than in liquid nitrogen alone. Even under these conditions only maximally 50% of the active enzyme was observed to be in the MCR-red2 state (not shown).

Another indication that maximally 50% of active MRC can be converted into the red2 state also comes from room temperature EPR measurements (Fig. 4B). For MCR-red1c the EPR spectrum measured at –196°C (77 K) (Fig. 4A1) and 18°C (291 K) (Fig. 4B1) were almost identical in line shape. The signal at 18°C had, however, only 3.3% of the intensity of that at –196°C. For MCR-red1c supplemented with coenzyme B the EPR spectra measured at –196°C (Fig. 4A2) and 18°C (Fig. 4B2) were different. The spectrum at 18°C lacked the red2 signal and the red1 signal had only 1.8% of the intensity of that at –196°C. Comparison of the EPR spectra determined at room temperature revealed that the red1 signal exhibited by MCR-red1c (Fig. 4B1) had almost twice the intensity of the red1 signal shown by the enzyme in the presence of coenzyme B (Fig. 4B2). This was reproducible. Because of the low EPR signal intensities at room temperature the differences in red1 signal intensities can be taken only as supporting rather than proving that in the presence of coenzyme B only 50 % of the enzyme are converted into the MCR-red2 state.

To understand why the red1 signal rather than the red2 signal is visible at room temperature, the temperature dependence of the red1 and red2 signal intensities of MCR in the frozen state was determined (Fig. 5). It was found that the intensity of the MCR-red2 signal started to decrease at much lower temperatures (125 K) than the intensity of the red1 signal (175 K). For experimental reasons the temperature dependence could not be determined down to 273 K (0°C). From the slopes of signal intensity decrease it can be estimated, however, that at 0°C the intensity of the red2 signal should already be too low to be detectable.

As a control the samples at room temperature were exposed to air and then their EPR spectrum was measured at –196°C (Fig. 4A3) and 18°C (Fig. 4B3). At both

temperatures the ox3 signal was seen. At 18°C the intensity of the ox3 signal was 3.1% of that at –196°C. Apparently only the red2 signal does not show up at room temperature.

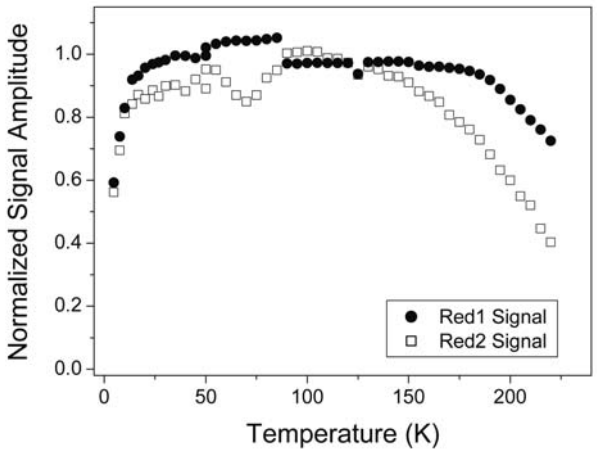

Fig. 5 Intensities of the EPR signals of MCR-red1/2 measured at different temperatures. (●) Red1 signal; (□) red2 signal. Active MCR in the presence of 10 mM coenzyme M was supplemented at room temperature with 5 mM coenzyme B to induce the MCR-red1/2 state and subsequently frozen in liquid nitrogen. In the measurement, the temperature of the frozen sample was varied from 4.5 to 220 K via an Oxford Instruments ESR 900 cryostat with an ITC4 temperature controller. The normalized signal amplitudes of the red1 and red2 signals were determined by measuring the height of the $g_{x,y}$ = 2.066 peak for the red1 component and of the g_z = 2.288 peak for the red2 component at different temperatures. These amplitudes where normalized for power (non-saturating), gain, and temperature, and plotted against the temperature. The concentration of purified enzyme was 30 mg (108 nmol) in 0.35 mL 50 mM Tris/HCl pH 7.6. EPR conditions: microwave frequency, 9458 MHz; microwave power, 2.01 µW (from 4.5-50 K) or 0.201 mW (from 50-220 K).

Discussion

Principally finding 50% of MCR in the red2 state and 50% of MCR in the red1 state can have two explanations: (i) 50% of all MCR molecules are in a form in which both active sites are in the red1 state (MCR-red1/1) and 50% in which both active sites are in the red2 state (MCR-red2/2); and (ii) in all MCR molecules of the two active sites only one is in the red1 state and the other in the red2 state (MCR-red1/2). The finding that the relative proportion of the two states varied below 20°C but was constant at 50% above 20°C can best be explained assuming that at 20°C and above this temperature all the MCR molecules were in a red1/2 state (reaction 1).

(1) MCR-red1/1 + HS-CoM + HS-CoB ⇆ MCR-red1/2

The results thus indicate that in the presence of coenzyme M and coenzyme B the two active sites in one MCR molecule are in two different states suggesting that active MCR shows "half- of-the-sites reactivity" [36]. Half-of-the-sites reactivity has been reported for many multimeric enzymes examples being CTP synthase, phosphoribosylpyrophosphate aminotransferase and glutamine synthase [37], the pyruvate dehydrogenase complex [38] and aldehyde dehydrogenase [39, 40].

Interestingly, the red1 states in MCR-red1/1 and MCR-red1/2 appear not to be identical, as to be expected from a half-of-the-sites reactivity mechanism in which the binding of substrates in the one active site affects the reactivity in the second active site. Thus the g-values of the red1 signal exhibited by MCR-red1/2 (g_z = 2.27; g_y = 2.08; g_x = 2.07) and by MCR-red1/1 (g_z = 2.25; g_y = 2.07; g_x = 2.06) are slightly but significantly different. In addition MCD measurements show that the 800 nm band characteristic for the MCR-red1/1 spectrum is absent or much less intense in the MCR-red1/2 spectrum [14]. Also the reactivity of MCR-red1/1 and of MCR-red1/2 towards oxidants is different. Whereas MCR-red1/1 is rendered completely ERR silent in the presence of polysulfide, sulfite and O_2 , the EPR signal of the enzyme in the red1/2 state is converted to the EPR signals ox1 by polysulfide, to ox2 by sulfite and to ox3 by O_2 [35] (for mechanism see [14, 41, 42]). The spin concentration per mol F_{430} of the ox signals of the inactive MCR-ox states are generally higher than 0.5 per mol F_{430}, in some cases as high as 0.8 [15, 35, 43] indicating that both the red1 and the red2 signals of MCR-red1/2 are converted to an ox form as exemplified for ox1 formation in reaction 2.

(2) MCR-red1/2 + polysulfide → MCR-ox1/1

However, hundred percent conversion of MCR into the ox states has never been observed which can be explained taken into account that that MCR-red1/2 is in equilibrium with MCR-red1/1 (reaction 1) and that the MCR-red1/1 state is rendered EPR silent in the presence of oxidants (reaction 3).

(3) MCR-red1/1 + polysulfide → MCR-silent

The reduction of methyl-coenzyme M with coenzyme B catalysed by MCR takes place in a hydrophobic pocket from which water is excluded [9, 12]. The two substrates thus have to be stripped of water when entering the active site and after reacting the product CoM-S-S-CoB has to be expelled into the water phase. The latter is most probably achieved by a conformational change of the enzyme, which is driven by one of the exergonic steps in the catalytic cycle [24, 25]. This conformational change could be restricted to the active site, in which the exergonic step occurs, or could be extended to the second active site. The finding of half-of-the-sites reactivity for MCR is in favour of the extension to the second site. We therefore propose that MCR operates similarly to a two-stroke engine as outlined in the cartoon shown in Fig. 6. The intertwined hexameric structure of MCR is optimally

suited for such a mechanism. Two-stroke mechanisms have been postulated previously for the chaperone system GroEL/GroES [44] and for the 20S proteasome [45].

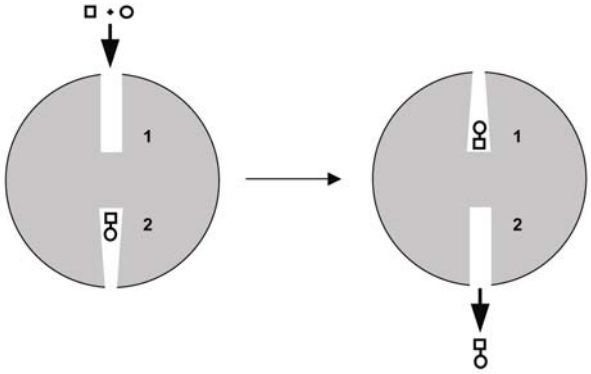

Fig. 6 Cartoon of the two-stroke engine mechanism proposed for methyl-coenzyme M reductase. The scheme shows a MCR molecule containing the two active sites (1) and (2). The binding of methyl-coenzyme M (□) and coenzyme B (○) to one active site induces a conformational change, which is required to expel the product heterodisulfide (○-□) from the second site into the water phase.

How could one obtain experimental evidence for the proposed two-stroke catalytic mechanism of MCR? One would have to show in stopped-flow experiments that intermediates in the catalytic cycle oscillate in their concentrations with a frequency twice that of the turnover number of the enzyme. Attempts to identify intermediates have failed until now. An explanation for this could be that under the experimental conditions employed (65°C and HS-CoB as substrate) the rate-limiting step in methane formation is the conformational change associated with ternary complex formation from MCR, methyl-coenzyme M and coenzyme B as outlined in the "Introduction". Our results reported here on the temperature dependence of MCR and on the induction of the MCR-red2 state by HS-CoB_6, with which MCR shows less than 1% of the activity observed with HS-CoB, may help in the future to find conditions where intermediates in the catalytic cycle of MCR can be observed.

Acknowledgements This work was supported by the Max Planck Society, the Deutsche Forschungsgemeinschaft, the Fonds der Chemischen Industrie and by a fellowship from the Claussen-Simon-Stiftung (M.G.). We thank Antonio Pierik for his help in measuring the room temperature EPR spectra.

References

1. Thauer RK (1998) Microbiology 144:2377-2406
2. Wolfe RS (2004) ASM News 70:15-18
3. Thauer RK, Jungermann K, Decker K (1977) Bact Rev 41:100-180
4. Sauer K, Thauer RK (1997) Eur J Biochem 249:280-285
5. Tietze M, Beuchle A, Lamla I, Orth N, Dehler M, Greiner G, Beifuss U (2003) Chembiochem 4:333-335
6. Hallam SJ, Girguis PR, Preston CM, Richardson PM, DeLong EF (2003) Appl Environ Microbiol 69:5483-5491
7. Krüger M, Meyerdierks A, Glockner FO, Amann R, Widdel F, Kube M, Reinhardt R, Kahnt J, Bocher R, Thauer RK, Shima S (2003) Nature 426:878-881
8. Piskorski R, Jaun B (2003) J Am Chem Soc 125:13120-13125
9. Ermler U, Grabarse W, Shima S, Goubeaud M, Thauer RK (1997) Science 278:1457-1462
10. Grabarse W, Mahlert F, Shima S, Thauer RK, Ermler U (2000) J Mol Biol 303:329-344
11. Grabarse W, Mahlert F, Duin EC, Goubeaud M, Shima S, Thauer RK, Lamzin V, Ermler U (2001a) J Mol Biol 309:315-330
12. Grabarse W, Shima S, Mahlert F, Duin EC, Thauer RK, Ermler U (2001b) Methyl-coenzyme M reductase. John Wiley & Sons, Chichester
13. Selmer T, Kahnt J, Goubeaud M, Shima S, Grabarse W, Ermler U, Thauer RK (2000) Journal of Biological Chemistry 275:3755-3760
14. Duin EC, Signor L, Piskorski R, Mahlert F, Clay MD, Goenrich M, Thauer RK, Jaun B, Johnson MK (2004) J Biol Inorg Chem 9:563-576
15. Goubeaud M, Schreiner G, Thauer RK (1997) Eur J Biochem 243:110-114
16. Mahlert F, Grabarse W, Kahnt J, Thauer RK, Duin EC (2002a) J Biol Inorg Chem 7:101-112
17. Goenrich M, Mahlert F, Duin EC, Bauer C, Jaun B, Thauer R. K (2004) J Biol Inorg Chem in press
18. Finazzo C, Harmer J, Bauer C, Jaun B, Duin EC, Mahlert F, Goenrich M, Thauer RK, Van Doorslaer S, Schweiger A (2003a) J Am Chem Soc 125:4988-4989
19. Finazzo C, Harmer J, Jaun B, Duin EC, Mahlert F, Thauer RK, Van Doorslaer S, Schweiger A (2003b) J Biol Inorg Chem 8:586-593
20. Jaun B (1990) Helv Chim Acta 73:2209-2217
21. Berkessel A (1991) Bioorg Chem 19:101-115
22. Signor L, Knuppe C, Hug R, Schweizer B, Pfaltz A, Jaun B (2000) Chem Eur J 6:3508-3516
23. Horng YC, Becker DF, Ragsdale SW (2001) Biochemistry 40:12875-12885
24. Pelmenschikov V, Blomberg MR, Siegbahn PE, Crabtree RH (2002) J Am Chem Soc 124:4039-4049
25. Pelmenschikov V, Siegbahn PE (2003) J Biol Inorg Chem 8:653-662
26. Rospert S, Linder D, Ellermann J, Thauer RK (1990) Eur J Biochem 194:871-877
27. Bonacker LG, Baudner S, Thauer RK (1992) Eur J Biochem 206:87-92
28. Bonacker LG, Baudner S, Mörschel E, Böcher R, Thauer RK (1993) Eur J Biochem 217:587-595
29. Wasserfallen A, Nolling J, Pfister P, Reeve J, Conway de Macario E (2000) International Journal of Systematic and Evolutionary Microbiology 50 Pt 1:43-53
30. Gunsalus RP, Romesser JA, Wolfe RS (1978) Biochemistry 17:2374-2377
31. Kobelt A, Pfaltz A, Ankel-Fuchs D, Thauer RK (1987) FEBS Lett 214:265-268
32. Ellermann J, Hedderich R, Böcher R, Thauer RK (1988) Eur J Biochem 172:669-677
33. Olson KD, McMahon CW, Wolfe RS (1991) Proc Natl Acad Sci U S A 88:4099-4103

34. Bradford MM (1976) Anal Biochem 72:248-254
35. Mahlert F, Bauer C, Jaun B, Thauer RK, Duin EC (2002b) J Biol Inorg Chem 7:500-513
36. Levitski A, Stallcup W, Koshland DE (1971) Biochemistry 10:3371
37. Walsh C (1979) Enzymatic reaction mechanisms. In: Bartlett AC, McCombs LW (eds) Enzymatic reaction mechanisms. W. H. Freeman and Company, San Francisco
38. Khailova LS, Korochkina LG (1985) Biochem Int 11:509-516
39. Zhou J, Weiner H (2000) Biochemistry 39:12019-12024
40. Weiner H, Wei B, Zhou J (2001) Chem Biol Interact 130-132:47-56
41. Craft JL, Horng YC, Ragsdale SW, Brunold TC (2004) J Biol Inorg Chem 9:77-89
42. Craft JL, Horng YC, Ragsdale SW, Brunold TC (2004) J Am Chem Soc 126:4068-4069
43. Duin EC, Cosper NJ, Mahlert F, Thauer RK, Scott RA (2003) J Biol Inorg Chem 8:141-148
44. Lorimer G (1997) Nature 388:720-721, 723
45. Hutschenreiter S, Tinazli A, Model K, Tampe R (2004) EMBO J 23:2488-2497
46. Ellermann J, Kobelt A, Pfaltz A, Thauer RK (1987) FEBS Lett 220:358-362
47. Olson KD, Chmurkowska-Cichowlas L, McMahon CW, Wolfe RS (1992) J Bacteriol 174:1007-1012

J|A|C|S COMMUNICATIONS

Published on Web 04/05/2003

Coenzyme B Induced Coordination of Coenzyme M via Its Thiol Group to Ni(I) of F_{430} in Active Methyl-Coenzyme M Reductase

Cinzia Finazzo,† Jeffrey Harmer,† Carsten Bauer,‡ Bernhard Jaun,‡ Evert C. Duin,§,|| Felix Mahlert,§ Meike Goenrich,§ Rudolf K. Thauer,§ Sabine Van Doorslaer,†,⊥ and Arthur Schweiger*,†

Physical Chemistry and Organic Chemistry, ETH Zurich, CH-8093 Zurich, Switzerland, and Max-Planck-Institut für terrestrische Mikrobiologie, D-35043 Marburg, Germany

Received January 31, 2003; E-mail: schweiger@esr.phys.chem.ethz.ch

Methane is formed in methanogenic archaea by the reduction of methyl-coenzyme M ($CH_3-S-CoM$) with coenzyme B ($HS-CoB$) to CH_4 and the heterodisulfide $CoM-S-S-CoB$.[1] This reaction is catalyzed by methyl-coenzyme M reductase (MCR), which is composed of three different subunits in an $\alpha_2\beta_2\gamma_2$ arrangement and which contains tightly bound 2 mol of the nickel porphinoid F_{430}. Crystal structures of the 300 kDa enzyme with and without coenzymes or product bound have been resolved to 1.16 Å.[2] They were, however, only obtained for the enzyme in the inactive Ni(II) state. For the enzyme to be active, the prosthetic group has to be in the Ni(I) oxidation state,[3−5] which is rapidly lost by autoxidation of the Ni(I).[6] Therefore, it has not been known until now how within the active enzyme the active site Ni(I) interacts with the substrates.

Active MCR exhibits an axial EPR signal MCR_{red1} derived from Ni(I) which does not change significantly when $CH_3-S-CoM$ alone or together with $HS-CoB$ are added to the active enzyme, showing that although an enzyme−substrate−complex is formed, there is no detectable direct interaction of the substrates with the Ni(I) of the prosthetic group.[7] The XAS data of the active enzyme are also the same in the absence and presence of the substrates.[8]

The reduction of $CH_3-S-CoM$ catalyzed by MCR is inhibited by coenzyme M ($HS-CoM$), inhibition being reversible and competitive to $CH_3-S-CoM$. In the presence of only $HS-CoM$, the enzyme shows the axial MCR_{red1} EPR signal. In the presence of both $HS-CoM$ and $HS-CoB$, however, the axial signal is partially converted into the highly rhombic EPR signal MCR_{red2}.[7] On the basis of ^1H and ^{14}N data obtained from electron nuclear double resonance (ENDOR) and hyperfine sublevel correlation spectroscopy (HYSCORE) measurements, it was proposed that in the MCR_{red2} state $HS-CoM$ is axially coordinated to Ni(I).[9] Here we report experiments with ^{33}S-labeled $HS-CoM$, proving that the thiol group of $HS-CoM$ coordinates to the Ni(I) ion of F_{430}.

[2-^{33}S]-coenzyme M (**4**) (Scheme 1) was synthesized in a one-pot procedure starting from elemental sulfur ($[^{33}S_8]$-S_8)[10] and potassium cyanide[11] according to Scheme 1.[12]

Figure 1 shows the X-band EPR spectra of $MCR_{red2}-HS-CoM$ (^{32}S (99.25%) with nuclear spin $I = 0$, ^{33}S (0.75%) with $I = 3/2$) and $MCR_{red2}-H^{33}S-CoM$. For a better comparison, the signals of MCR_{red1} were subtracted from the red1/red2 mixture normally shown by these preparations. The EPR spectrum of ^{33}S-labeled MCR_{red2} shows a pronounced line broadening at the high-field feature corresponding to the g_3 principal value. This is a strong indication for the presence of a large ^{33}S hyperfine coupling along this principal axis direction. No significant broadenings are observed

Scheme 1. Synthesis of [2-^{33}S]-Coenzyme M[a]

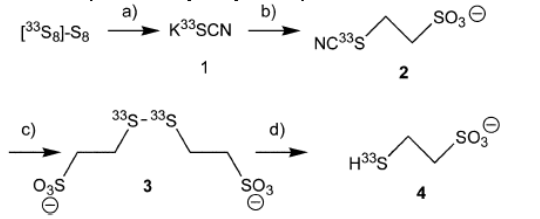

[a] Conditions: (a) N_2, KCN, EtOH, 4 h, reflux. (b) N_2, $BrCH_2CH_2SO_3Na$, DMF, 4 h, 120 °C. (c) (1) N_2, K_2CO_3, H_2O, 1 h, 60 °C; (2) H^+, NH_3. (d) N_2, DTT, H_2O, 30 min. Overall yield from $[^{33}S_8]$-S_8, 87% (NMR); after final purification for MCR-assay, 44%.

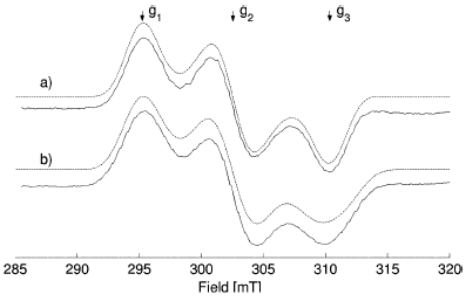

Figure 1. X-band EPR spectra of MCR in the MCR_{red2} state (coenzyme M inhibited enzyme in the presence in coenzyme B). (a) With $HS-CoM$. (b) With $H^{33}S-CoM$. Solid lines: experimental spectra after subtraction of MCR_{red1} signals. Dashed lines: simulations, spectrum b used the same spin Hamiltonian parameters as in (a) but with the addition of a ^{33}S hyperfine interaction, $|A_{1,2}| = 20$ MHz, $|A_3| = 35$ MHz. Experimental conditions: 77 K, modulation amplitude 0.6 mT, microwave frequency 9.45 GHz (Supporting Information contains further details).

at g_1 and g_2. From spectral simulations, the ^{33}S hyperfine coupling along g_3 is estimated to be roughly $|A_3| = 35$ MHz, with upper limits along g_1 and g_2 of $|A_{1,2}| = 25$ MHz.

In contrast to MCR_{red2}, when either the ox1 or the red1 form of MCR is incubated in the presence of $H^{33}S-CoM$, no significant line broadenings are observed in the EPR spectra. This shows that any interaction with ^{33}S in these two forms is small (as compared to the EPR spectral resolution).

A clear-cut proof of the coordination of $HS-CoM$ to Ni(I) is obtained from HYSCORE spectra measured at Q-band[13] at the low-field end (g_1 value) of the EPR spectrum. Figure 2a and 2b shows the single-crystal-like HYSCORE spectra of $MCR_{red2}-HS-CoM$ and $MCR_{red2}-H^{33}S-CoM$ at g_1 which are free of contributions from other paramagnetic species of MCR. The additional peaks observed in Figure 2b originate from ^{33}S interactions (labeled in Figure 2b). The two cross-peaks in the (− +)-quadrant at (−10.8, 31.8) MHz and (−31.8, 10.8) MHz are assigned to triple-quantum transitions

† Physical Chemistry, ETH Zurich.
‡ Organic Chemistry, ETH Zurich.
§ Max-Planck-Institut.
|| Current address: Department of Chemistry, Auburn University, AL 36849-5312.
⊥ Current address: Spectroscopy in Biophysics and Catalysis (SIBAC Laboratory), University of Antwerp, 2610 Wilrijk, Belgium.

10.1021/ja0344314 CCC: $25.00

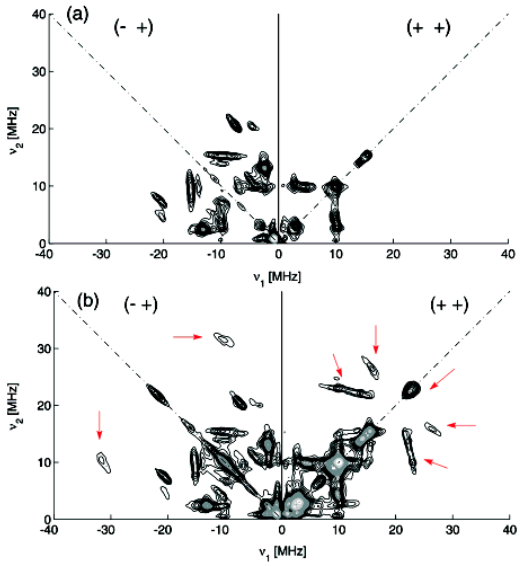

Figure 2. Q-band HYSCORE spectra recorded at 25 K of MCR in the MCR_{red2} state; observer position at g_1. (a) With HS−CoM. (b) With $H^{33}S$−CoM. The arrows identify peaks that originate from ^{33}S interactions. The Supporting Information contains further details.

with $\Delta m_I = 3$. For a simplified system with an isotropic g tensor and an axial hyperfine tensor, the two triple-quantum frequencies can be written to first order as

$$\nu_{TQ}^{(+/-)} = 3\left[\left(\pm\frac{A_\perp}{2} + \nu_I\right)^2 \sin^2\beta + \left(\pm\frac{A_{||}}{2} + \nu_I\right)^2 \cos^2\beta\right]^{1/2}$$

with the hyperfine principal values $A_\perp$ and $A_{||}$, the nuclear Zeeman frequency ν_I, and the angle β between the $A_{||}$ principal axis and the static magnetic field vector $\mathbf{B}_0$. For a nuclear quadrupole interaction that is small as compared to the hyperfine interaction, these frequencies are to first-order independent of the nuclear quadrupole interaction and differ by $6\nu_I$ for $\beta = 0, 90°$. In Figure 2b, the observed splitting of 20.9 MHz is slightly smaller than $6\nu_I = 21.7$ MHz, indicating that the orientations selected in this experiment are close to the principal axis of $A_\perp$. The ^{33}S hyperfine coupling A along g_1 can easily be estimated from the equation

$$\nu_{TQ}^{(+)^2} - \nu_{TQ}^{(-)^2} = 18\nu_I(a_{iso} + T(3\cos^2\beta - 1)) = 18\nu_I A$$

where a_{iso} is the isotropic hyperfine coupling, and T is the dipolar coupling.[14] Along g_1, we then find $|A| = 13.8$ MHz, and for the principal value $|A_\perp|$ we estimate a coupling of about 15 MHz.

Several additional peaks are observed in the (+ +)-quadrant of Figure 2b. The strong diagonal peak at 23 MHz is most probably a sulfur double-quantum transition ($\Delta m_I = 2$), and the cross-peaks represent correlations between sulfur transitions and/or nitrogen−sulfur combination transitions. An unequivocal assignment of all of the new peaks observed in the ^{33}S sample is difficult because the HYSCORE spectrum could only be observed along g_1. This is because the large anisotropy of the ^{33}S hyperfine coupling broadens the peaks beyond detection as soon as the B_0 observer field in the HYSCORE experiments is shifted to higher values.

The combination of EPR and HYSCORE data proves that, in the MCR_{red2} state, HS−CoM is directly coordinated to the Ni(I) ion. An estimate of the spin density on ^{33}S can be obtained from the hyperfine tensor and by considering the relative signs of the principal values. Assuming three positive principal values [$(A_1, A_2, A_3) = (15, 15, 35)$ MHz] yields an isotropic part of $a_{iso} = 21.7$ MHz and a dipole part of (−6.7, −6.7, 13.4) MHz. For a hyperfine tensor [$(A_1, A_2, A_3) = (-15, -15, 35)$ MHz], the isotropic part is $a_{iso} = 1.7$ MHz, and the dipole part is (−16.7, −16.7, 33.4) MHz. In the first case, a spin density of 0.6% in the s-orbital is estimated from the isotropic part, and a spin density of 7% in a 3p-orbital is estimated from the dipolar part.[15] For the second case, the corresponding values are 0.05% (s-orbital) and 17% (3p-orbital). In either case, the large spin density on the sulfur ligand is further proof that the ground state of MCR_{red2} has a relatively high percentage of d_{z^2} character, and the large hyperfine coupling A_3 corroborates the proposal that the g_3 principal axis is perpendicular to the macrocycle.[9]

On the basis of the finding that the HS−CoM interaction is dependent on the presence of HS−CoB in MCR_{red2}, we propose that HS−CoB is not only required as a second substrate,[16] but also to induce a change forcing the real substrate, CH_3−S−CoM, and Ni(I) of the prosthetic group to interact in the active enzyme MCR_{red1}.

Acknowledgment. This work was supported by the Swiss National Science Foundation, by the Max Planck Society, and by the Fonds der Chemischen Industrie.

Supporting Information Available: Analytical data of [2-^{33}S]-coenzyme M (4, NH_4^+-form) and experimental procedures (PDF). This material is available free of charge via the Internet at http://pubs.acs.org.

References

(1) Thauer, R. K. *Microbiology* **1998**, *144*, 2377−2406.
(2) Grabarse, W.; Mahlert, F.; Duin, E. C.; Goubeaud, M.; Shima, S.; Thauer, R. K.; Lamzin, V.; Ermler, U. *J. Mol. Biol.* **2001**, *309*, 315−330.
(3) Goubeaud, M.; Schreiner, G.; Thauer, R. K. *Eur. J. Biochem.* **1997**, *243*, 110−114.
(4) Telser, J.; Davydov, R.; Horng, Y. C.; Ragsdale, S. W.; Hoffman, B. M. *J. Am. Chem. Soc.* **2001**, *123*, 5853−5860.
(5) Tang, Q.; Carrington, P. E.; Horng, Y. C.; Maroney, M. J.; Ragsdale, S. W.; Bocian, D. F. *J. Am. Chem. Soc.* **2002**, *124*, 13242−13256.
(6) Mahlert, F.; Bauer, C.; Jaun, B.; Thauer, R. K.; Duin, E. C. *J. Biol. Inorg. Chem.* **2002**, *7*, 500−513.
(7) Mahlert, F.; Grabarse, W.; Kahnt, J.; Thauer, R. K.; Duin, E. C. *J. Biol. Inorg. Chem.* **2002**, *7*, 101−112. Erratum: *J. Biol. Inorg. Chem.* **2002**, *7*, 351.
(8) Duin, E. C.; Cosper, N. J.; Mahlert, F.; Thauer, R. K.; Scott, R. A. *J. Biol. Inorg. Chem.* **2002**, *8*, 141−148.
(9) Finazzo, C.; Harmer, J.; Jaun, B.; Duin, E. C.; Mahlert, F.; Thauer, R. K.; Van Doorslaer, S.; Schweiger, A. *J. Biol. Inorg. Chem.*, in press.
(10) [$^{33}S_8$]-S_8 was purchased from Campro Scientific, Berlin, Germany. The analysis of (isotopic) purity of [$^{33}S_8$]-S_8 was established by the Kurchatov Institute, Moscow, Russia (isotopic purity: 99.79%; purity: > 99.95%).
(11) Castiglioni, A. *Gazz. Chim. Ital.* **1933**, *63*, 171.
(12) During development of the procedure with natural abundance sulfur, each intermediate was isolated and characterized. The product was converted to the ammonium salt by ion exchange with Amberlite, and inorganic salts (NH_4Br) were removed by precipitation of **4** with diethyl ether from a concentrated solution in methanol. The sample used for the experiments with the enzyme was recrystallized from methanol/2-propanol to remove a small inorganic impurity that quenched the MCR_{red2} signal. The details of the development of the synthesis and the analytical data for all intermediates will be published elsewhere.
(13) Gromov, I.; Shane, J.; Forrer, J.; Rakhmatoullin, R.; Rozentzwaig, Yu.; Schweiger, A. *J. Magn. Reson.* **2001**, *149*, 196−203.
(14) Schweiger, A.; Jeschke, G. *Principles of Pulse Electron Paramagnetic Resonance*; Oxford University Press: New York, 2001.
(15) Morton, J. R.; Preston, K. F. *J. Magn. Reson.* **1978**, *30*, 577−582.
(16) Horng, Y. C.; Becker, D. F.; Ragsdale, S. W. *Biochemistry* **2001**, *40*, 12875−12885.

JA0344314

J Biol Inorg Chem (2004) 9: 563–576
DOI 10.1007/s00775-004-0549-9

ORIGINAL ARTICLE

**Evert C. Duin · Luca Signor · Rafal Piskorski
Felix Mahlert · Michael D. Clay · Meike Goenrich
Rudolf K. Thauer · Bernhard Jaun · Michael K. Johnson**

Spectroscopic investigation of the nickel-containing porphinoid cofactor F_{430}. Comparison of the free cofactor in the +1, +2 and +3 oxidation states with the cofactor bound to methyl-coenzyme M reductase in the silent, red and ox forms

Received: 18 December 2003 / Accepted: 14 April 2004 / Published online: 25 May 2004

Abstract Methyl-coenzyme M reductase (MCR) catalyzes the methane-forming step in methanogenic archaea. It contains the nickel porphinoid F_{430}, a prosthetic group that has been proposed to be directly involved in the catalytic cycle by the direct binding and subsequent reduction of the substrate methyl-coenzyme M. The active enzyme (MCRred1) can be generated in vivo and in vitro by reduction from MCRox1, which is an inactive form of the enzyme. Both the MCRred1 and MCRox1 forms have been proposed to contain F_{430} in the Ni(I) oxidation state on the basis of EPR and ENDOR data. In order to further address the oxidation state of the Ni center in F_{430}, variable-temperature, variable-field magnetic circular dichroism (VTVH MCD), coupled with parallel absorption and EPR studies, have been used to compare the electronic and magnetic properties of MCRred1, MCRox1, and various EPR silent forms of MCR, with those of the isolated penta-methylated cofactor (F_{430}M) in the +1, +2 and +3 oxidation states. The results confirm Ni(I) assignments for MCRred1 and MCRred2 forms of MCR and reveal charge transfer transitions involving the Ni d orbitals and the macrocycle π orbitals that are unique to Ni(I) forms of F_{430}. Ligand field transitions associated with $S = 1$ Ni(II) centers are assigned in the near-IR MCD spectra of MCRox1-silent and MCR-silent, and the splitting in the lowest energy d d transition is shown to correlate qualitatively with assessments of the zero-field splitting parameters determined by analysis of VTVH MCD saturation magnetization data. The MCD studies also support rationalization of MCRox1 as a tetragonally compressed Ni(III) center with an axial thiolate ligand or a coupled Ni(II)-thiyl radical species, with the reality probably lying between these two extremes. The reinterpretation of MCRox1 as a formal Ni(III) species rather than an Ni(I) species obviates the need to invoke a two-electron reduction of the F_{430} macrocyclic ligand on reductive activation of MCRox1 to yield MCRred1.

Keywords Methyl-coenzyme M reductase · Nickel enzymes · Factor 430 · Methanogenic archaea · Magnetic circular dichroism spectroscopy

Abbreviations F_{430}: cofactor 430 · F_{430}M: penta-methylated form of cofactor 430 · Ni(I)F_{430}M: F_{430}M with the nickel atom in the +1 oxidation state · Ni(II)F_{430}M: F_{430}M with the nickel atom in the +2 oxidation state · Ni(III)F_{430}M: F_{430}M with the nickel atom in the +3 oxidation state · MCR: methyl-coenzyme M reductase · MCRox1: MCR exhibiting the MCR-ox1 EPR signal · MCRox1-silent: EPR silent form of MCR obtained from the MCRox1 form · MCRred1: MCR exhibiting the EPR signals red1c and/or red1m · MCRred1c: MCRred1 in the presence of coenzyme M · MCRred1m: MCRred1 in the presence of methyl-coenzyme M · MCRred2: MCR exhibiting both the red1 and red2 EPR signals · MCRred1-silent:

Electronic Supplementary Material Supplementary material is available in the online version of this article at http://dx.doi.org/10.1007/s00775-004-0549-9

E. C. Duin (✉)
Department of Chemistry and Biochemistry,
Auburn University, Auburn, AL 36849, USA
E-mail: duinedu@auburn.edu
Fax: +1-334-8446959

L. Signor · R. Piskorski · B. Jaun
Laboratorium für Organische Chemie,
ETH Zürich, 8093 Zürich, Switzerland

F. Mahlert · M. Goenrich · R. K. Thauer
Max-Planck-Institut für terrestrische Mikrobiologie
and Laboratorium für Mikrobiologie, Fachbereich Biologie,
Philipps-Universität, Karl-von-Frisch-Strasse,
35043 Marburg, Germany

M. D. Clay · M. K. Johnson
Department of Chemistry and Center for Metalloenzyme Studies,
University of Georgia, Athens, GA 30602, USA

EPR silent form of MCR obtained from the MCRred1 form · MCRsilent: EPR silent form of MCR

Introduction

Methanogenic archaea can use different substrates to produce CH_4, the end product of their energy metabolism [1]. Methyl-coenzyme M (CH_3-S-CoM; Fig. 1) is common to all pathways irrespective of the original substrate. Methyl-coenzyme M reductase (MCR) catalyzes the reduction of methyl-coenzyme M with coenzyme B (HS-CoB; Fig. 1) to CH_4 and the mixed disulfide of coenzyme M (HS-CoM; Fig. 1) and coenzyme B:

$$CH_3\text{-}S\text{-}CoM + HS\text{-}CoB + CH_4 + CoM\text{-}S\text{-}S\text{-}CoB$$

At the heart of this process is the nickel-containing tetrapyrrole factor 430 (F_{430}; Fig. 1). This tetrapyrrole has a unique structure [2, 3]. The π-chromophore extends only over three of the four nitrogens, making F_{430} the most extensively reduced tetrapyrrole found in nature. Two additional rings are found in F_{430}, a lactam ring fused to ring B and a six-membered carbocycle formed through intramolecular acylation of C_{15} by the propionic acid side chain at ring D. F_{430} was named after its characteristic absorption spectrum in the Ni(II)F_{430} state, which exhibits a broad intense band at 430 nm. This band consists of several unresolved bands that are better resolved in variable-temperature, variable-field magnetic circular dichroism (VTVH MCD) spectra [4, 5].

Native, as-isolated, F_{430} is thermally unstable to epimerization of the acid side chains at β-carbon positions 12 and 13 of pyrrole ring C to form the 13-monoepimer and ultimately the 12,13-diepimer [6]. It is also oxidatively unstable, being slowly oxidized in air to 12,13-didehydro-F_{430}, which is termed F_{560} because it exhibits an absorption maximum at 560 nm [6]. F_{430} is present in cells in the pentacid form (Fig. 1, R = H). Depending on the temperature, the divalent nickel ion in native F_{430} can be found in two forms in aqueous solutions, a tetragonally coordinated paramagnetic ($S = 1$) form with two water molecules as the axial ligands or a four-coordinated diamagnetic ($S = 0$) form [4, 7]. F_{430} has also been prepared as a pentamethyl ester [2] and a pentamide [8]. For the present study, F_{430} in the pentamethyl ester form (F_{430}M; Fig. 1, R = CH_3) was used due to its solubility in non-coordinating organic solvents, which prevents epimerization and facilitates control over the axial coordination. In the absence of coordinating ligands, the Ni centers in both Ni(I)F_{430}M and Ni(II)F_{430}M are four-coordinate [9]. In the presence of coordinating ligands, both five- and six-coordinated Ni(II)F_{430}M can be formed depending on the nature and concentration of ligand. In contrast, the Ni(III)F_{430}M form could only be prepared as a six-coordinated form with two molecules of the solvent as the axial ligands [9, 10].

The recent development of methods to obtain highly active preparations [11, 12, 13] has stimulated renewed interest in understanding structure/function relationships in MCR, for recent reviews see [1, 14, 15]. All relevant states are now under investigation or have been characterized with a combination of crystallography [16, 17, 18, 19] and spectroscopic approaches involving X-ray absorption spectroscopy (XAS) [20, 21], resonance Raman (RR) spectroscopy [21], EPR spectroscopy [12, 13, 22], and electron nuclear double resonance (ENDOR) spectroscopy [23, 24, 25].

MCR in the red1 form ($g = 2.25$, 2.07, and 2.06) is the active form of the protein and has the nickel in the +1 oxidation state with the unpaired electron in d_{x2-y2}[11, 26]. Active MCR is very unstable, but can be stabilized by the presence of methyl-coenzyme M or the substrate analog coenzyme M. These compounds have an effect on the spectroscopic properties of MCR and it is possible to distinguish between the MCRred1m form (m for *m*ethyl-coenzyme M) and the MCRred1c form (c for coenzyme M) [13]. In addition to spectroscopic differences, these two forms also behave different chemically. Upon addition of coenzyme B to MCR in the red1c form, a new EPR signal, MCRred2 ($g = 2.29$, 2.24, and 2.18) is induced [13]. In contrast, the red2 signal was not induced

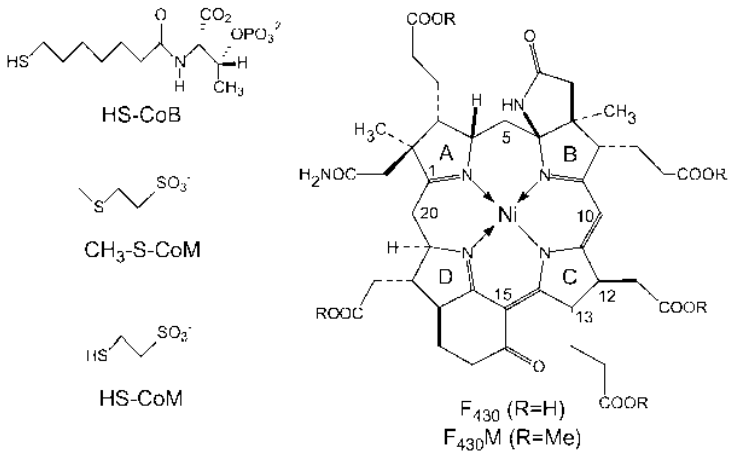

Fig. 1 Structures of coenzyme B (*HS-CoB, N*-7-mercapto-heptanoyl-*O*-phospho-L-threonine), methyl-coenzyme M (*CH_3-S-CoM*, 2-(methyl-thio)ethanesulfonate), coenzyme M (*HS-CoM*, 2-mercaptoethanesulfonate) and factor 430 (*F_{430}*)

when coenzyme B was added to MCR in the red1m form [13]. The red2 form has nickel in the +1 oxidation state and is inactive [13], but can be converted back to the active MCRred1 form by removal of coenzyme M and/or coenzyme B. MCRred2 is converted into the MCRox1 form ($g = 2.23$, 2.17, and 2.15) by addition of polysulfide [12]. The MCRox1 form is also inactive but can be converted back into the active MCRred1 form by incubation with titanium(III) citrate [11], a compound that can reduce free Ni(II)F_{430} to Ni(I)F_{430}.

Since titanium(III) citrate was absolutely necessary for the activation of MCRox1, the activation was assumed to be a reductive process. If the nickel in the MCRox1 form is Ni(III), reduction would involve a two-electron process leading to the +1 oxidation state. However, based on the EPR and ENDOR spectra [22, 23], it was proposed that in the MCRox1 form the nickel is already in the +1 oxidation state. Consequently, the electrons needed to activate MCRox1 must be used to reduce something other than the nickel, and on the basis of RR experiments and redox titrations with titanium(III) citrate, it was proposed that activation involves reduction of a double bond in the macrocycle ring [21]. However, this hypothesis is not consistent with the recent direct determination of the number of electrons needed to reduce Ni(II)F_{430} to the species exhibiting the MCR-red1-type spectra [27]. In addition, XAS studies revealed that the energy of the nickel K-edge in the MCRox1 sample was close to that observed for EPR-silent MCR forms with the nickel in the +2 oxidation state [20]. Therefore, we considered the possibility that the MCRox1 state corresponds to high spin Ni(II) ($S = 1$) coupled to a thiyl radical on the axial sulfur ligand [20].

In this study, we report a detailed comparison of the electronic and magnetic properties of the MCRred, MCRox and various EPR silent forms of MCR with those exhibited by free F_{430}M with the nickel in the +1, +2 and +3 oxidation state, using VTVH MCD spectroscopy coupled with parallel absorption and EPR data. The results confirm Ni(I) assignments for MCR-red1 and MCRred2, facilitate comparison of the ground- and excited-state properties of EPR-silent Ni(II) forms of MCR and F_{430}M, and support the characterization of MCRox1 as a tetragonally compressed Ni(III) species or a coupled Ni(II)-thiyl radical species rather than a Ni(I) species.

Materials and methods

Methanothermobacter marburgensis(formerly *Methanobacterium thermoautotrophicum,* strain Marburg [28]) is the strain deposited under DSM 2133 in the *Deutsche Sammlung von Mikroorganismen und Zellkulturen* (Braunschweig). Coenzyme B (*N*-7-mercaptoheptanoyl-*O*-phospho-L-threonine) and methyl-coenzyme M (2-(methylthio)ethanesulfonate) were prepared as previously described [13, 29, 30]. Coenzyme M (2-mercaptoethanesulfonate) was obtained from Merck (Darmstadt). All gases and gas mixtures were obtained from Messer Griesheim (Siegen), and ethylene glycol was obtained from Merck.

Purification of MCR in the silent, red1c, or ox1 states

M. marburgensis was grown at 65 °C in a 13-l glass fermenter (New Brunswick) containing 10 l of growth medium. The mineral-salt medium [31] contained 65 mM KH_2PO_4, 50 mM NH_4Cl, 30 mM Na_2CO_3, 0.5 mM nitrilotriacetic acid, 2 mM $MgCl_2$, 50 μM $FeCl_2$, 1 μM $CoCl_2$, 1 μM Na_2MoO_4, 5 μM $NiCl_2$, and 20 μM resazurin. It was made anaerobic at 65 °C by sparging with 80% H_2/20% CO_2/0.1% H_2S at a rate of 1,200 ml/min. After 1 h of equilibration, the medium was inoculated with 150 200 ml of fresh culture. At a ΔOD_{578} of 4.5, the cells were harvested. To obtain MCR in the MCRsilent state no special treatment before harvesting is necessary. The gas supply was switched to 100% H_2 for a period of 30 min before harvesting to induce the MCRred1 and MCRred2 forms in the cells, or to 80% N_2/20% CO_2 to induce the MCRox1 form. After 30-min incubation, the cells were cooled over a 10-min period to 10 °C under continuous gas flow and were then harvested anaerobically by centrifugation using a flow-through centrifuge (Hettich, contifuge 17 RS). Approximately 50 g of wet cells was obtained. The purification of MCR isoenzyme I [32, 33, 34] in the MCRsilent state was done under aerobic conditions. To obtain the MCR isoenzyme in the MCRred1c or MCRox1 state, the purification was performed in an anaerobic chamber (Coy Instruments) filled with 95% N_2/5% H_2, as described previously [13].

MCRsilent was purified from 80% H_2/20% CO_2 gassed cells without extra addition of any of the coenzymes to the buffers, typically yielding 150 mg of MCRsilent (in 120 ml). MCRred1 was purified from 100% H_2 gassed cells in the presence of coenzyme M [13]. The MCRred2 signal was lost during purification due to removal of coenzyme B. This method generally yielded 150 mg MCRred1c (in 120 ml) with 0.5 0.9 spins per nickel. The specific activity of the purified enzyme was 10 30 U per mg protein calculated for one spin per mol F_{430} [13]. Methyl-coenzyme M reductase activity was determined as previously described [13]. MCRox1 was purified from 80%N_2/20% CO_2 gassed cells with methyl-coenzyme M present in all steps. The method generally yielded approximately 150 mg MCRox1 (in 120 ml) with 0.5 0.8 spins per nickel [13].

Preparation of MCRox1-silent, MCRred1-silent, MCRred2, and MCRred1m

MCRred1-silent was made from MCRred1c by exposure of this form to air. Ni(I) was immediately oxidized to Ni(II). The conversion of MCRox1 into MCRox1-silent occurs slowly in samples kept under

aerobic conditions at room temperature. It generally takes a couple of days for a full conversion, but in some samples there is still MCRox1 left after several weeks of incubation. The MCRred2 state is formed from the MCRred1c state in the presence of 10 mM coenzyme M by the addition of 4 mM coenzyme B to the sample. Although we obtained a sample that shows a mixture of MCRred1 and MCRred2 signals in EPR spectroscopy [13], we still designated this preparation the MCRred2 form since the "leftover" red1 signal shows a different behavior in EPR than the original red1c signal (see text for more details). To obtain the MCRred1m form, MCR in the red1c form was concentrated 80-fold by centrifugation in an Amicon cell with a 100-kDa cut-off (Millipore, Bedford MA) and then diluted 10-fold. The solution was adjusted to a final concentration of 10 mM methyl-coenzyme M.

Purification of Ni(II)F_{430}M and preparation of Ni(I)F_{430}M, Ni(II)F_{430}M dithiophenolate, and Ni(III)F_{430}M

Ni(II)F_{430}M

Ni(II)F_{430} pentamethyl ester (Ni(II)F_{430}M) was prepared as described earlier [2]. Traces of halogenated solvents and of water were eliminated by threefold precipitation of Ni(II)F_{430}M from dry THF with dry toluene. The sample was then dried under HV overnight just before use.

Solvent purification. 2-Methyl-tetrahydrofuran was distilled three times from potassium metal; toluene was distilled from sodium metal; propionitrile (FLUKA, purum) was stored over Na_2SO_4 for 48 h, filtered, refluxed with P_2O_5under N_2 for 2 h, distilled, and redistilled over a large refractory column with a reflux ratio of 10:1 taking the middle 30%.

Ni(II)F_{430}M dithiophenolate

In a glass reactor with two side arms and an attached MCD cell (see Fig. S1 in Electronic Supplementary Material), solutions of tetrabutylammonium thiophenolate in dichloromethane/toluene 1:1 (v/v) and of Ni(II)F_{430}M in the same solvent mixture were placed into the two side arms and degassed by three freeze thaw cycles on the vacuum line. The apparatus was sealed at 10^{-6} mbar. Then the two solutions were allowed to mix and an aliquot was transferred into the MCD cell, which was frozen in liquid N_2 and sealed off.

The amount of Ni(II) present was calculated from the intensity of the 439-nm band ($\epsilon = 19{,}900\ M^{-1}\ cm^{-1}$) in the absorption spectrum [2]. The final concentrations were 0.6 mM Ni(II)F_{430}M and 60 mM tetrabutylammonium thiophenolate.

Ni(I)F_{430}M

A thoroughly degassed solution of Ni(II)F_{430}M (0.56 mM) in dry 2-methyl-THF was brought into contact with ca. 200 µl of sodium amalgam (0.02% (w/w)) within a vacuum-sealed glass ampoule at RT (see Fig. S1 in Electronic SupplEmentary Material).

The progress of the reaction was monitored by absorption spectroscopy after regular contact intervals. For this purpose, the solution was allowed to flow into an attached MCD cell thus interrupting the contact with the amalgam. When the reduction was complete, the solution was divided in two aliquots: one was transferred to an attached EPR tube, the other to the attached MCD cell. With all side arms frozen in liquid N_2, the MCD cell and the EPR tube were sealed off and stored in liquid N_2.

The amount of Ni(I) present was calculated from the intensity of the 380 nm band ($\epsilon = 29{,}600\ M^{-1}\ cm^{-1}$) in the absorption spectrum [35].

Ni(III)F_{430}M

The samples of Ni(III)F_{430}M were prepared by bulk electrolysis of Ni(II)F_{430}M in the glass-forming electrolyte propionitrile-toluene 1:1 (v/v) 0.1 M $TBABF_4$.

Electrolyte solution. The required amount of tetrabutylammonium tetrafluoroborate ($Bu_4{}^+NBF_4{}^-$) was dried under HV overnight, flushed with Ar and dissolved in propionitrile/toluene 1:1 (v/v) to give a 0.1 M stock solution. The electrolyte solution was filtered over freshly activated neutral alumina and handled with gastight syringes under Ar thereafter.

Bulk electrolysis in high-vacuum cell. (See Fig. S2 in Electronic Supplementary Material). The cell consisted of three compartments separated by fritted glass disks. The sample compartment contained the working electrode (cylindrical platinum grid), the quasi-reference electrode (Ag/AgCl in a Luggin capillary), and a small-area platinum electrode for analytical cyclic voltammetry. The central compartment and the counterelectrode (rolled platinum grid) compartments were filled with electrolyte solution (bridge). Electrolysis was performed under HV (partial pressure of the solvent). The EPR tube and MCD cell (fixed together in a y shape) were attached to the working electrode compartment. Ni(II)F_{430}M (1 µmol), dissolved in a small volume of dry THF/toluene (5:1) (v/v), was introduced into the working electrode compartment, the solvent was evaporated, and the cell was evacuated under HV overnight. The vacuum was broken with N_2 and the cell was filled with the electrolyte solution which was then thoroughly degassed through four freeze pump thaw cycles. Under vacuum (partial pressure of the solvent), the solution was allowed to flow into each one of the three cell compartments (1.5 ml in the working electrode

compartment), and after Ni(II)F_{430}M had dissolved, electrolysis was started. When electrolysis was complete, aliquots of the Ni(III)F_{430}M solution were transferred into the EPR tube and MCD cell, which were successively sealed under vacuum while the solutions in the EPR tube, the MCD cuvette, and the electrolysis cell were all kept frozen in liquid N_2.

The amount of Ni(III) present was estimated from comparison with absorption spectra obtained by spectroelectrochemistry [9, 10].

Preparation of MCR samples for spectroscopic investigations

For the spectroscopic measurements, the different MCR samples were concentrated by ultrafiltration in an Amicon cell with a membrane with a 100-kDa cut-off (Millipore, Bedford, MA). The final concentration of the sample was chosen so that after addition of 60% ethylene glycol, the absorption of the most intense bands in a 1-mm quartz cuvette would have an OD~1. After measuring the absorption spectra, the samples were frozen in parallel in MCD cuvettes and EPR tubes. The ratio of the different forms present in the respective samples was determined by double integration of the EPR signals versus a copper perchlorate standard of known concentration, and this value was compared to the protein concentration. The protein concentration was determined either by the method of Bradford [36], with bovine serum albumin (Serva) as standard, or by measuring the absorbance of oxidized enzyme (MCR-silent) at 420 nm using an $\epsilon = 44{,}000\ M^{-1}\ cm^{-1}$ and a molecular mass of 280,000 Da [30]. Both methods yielded essentially the same results.

The F_{430}M samples were prepared by Dr. Jaun's group in Switzerland and were frozen and stored in liquid nitrogen for transport to the USA. The Ni(I)F_{430}M and Ni(II)F_{430} M samples were thawed, and the absorption spectra were checked before the samples were inserted into the MCD magnet. The Ni(III)F_{430}M sample was transferred frozen onto the cold sample probe that was inserted into the MCD magnet. The absorption spectrum at room temperature was checked after the MCD measurements.

Spectroscopic measurements

VTMCD spectroscopic measurements were performed using an Oxford Instruments Spectromag 4000 split-coil superconducting magnet mated to either a Jasco J715 or a Jasco J730 spectropolarimeter. The experimental protocols used in variable-temperature MCD studies for accurate sample temperature and magnetic field measurements, anaerobic sample handling, and assessment of residual strain in frozen samples have been described elsewhere [37, 38]. MCD intensity is expressed as $\Delta\epsilon$ (ϵ_{LCP} ϵ_{RCP}), where ϵ_{LCP} and ϵ_{RCP} are the molar extinction coefficients for the absorption of left and right circularly polarized light, respectively, and is corrected for contributions from natural circular dichroism. The MCD spectra were measured at 1.7, 4.2, and 10 K with an applied field of 6 T in the wavelength region from 200 1400 nm. For paramagnetic chromophores, the spectra are temperature-dependent, with intensity increasing with decreasing temperature, and for diamagnetic chromophores, the spectra are temperature-independent. VTVH MCD magnetization data were collected by monitoring MCD intensity at a fixed temperature as a function of the applied magnetic field. The data were corrected for temperature-independent contributions by extrapolating plots of MCD intensity versus inverse temperature to infinite temperature and subtracting a proportional correction at each field. Data are plotted as percent magnetization against $\beta B/2k\ T$, where percent magnetization is the percentage of the MCD intensity relative to saturation at the maximum magnetic field used (6.0 T), β is the Bohr magneton, B is the magnetic field strength, k is the Boltzmann constant, and T is the absolute temperature. For Ni(I) and Ni(III) $S = 1/2$ ground states, MCD magnetization data were simulated using EPR derived g values [39]. For high-spin Ni(II) $S = 1$ ground states, VHVT MCD magnetization data were analyzed according to the protocols developed by Neese and Solomon [40].

EPR spectra at X-band (9 GHz) were obtained with a Bruker EMX spectrometer. All spectra were recorded with a field modulation frequency of 100 kHz. Cooling of the sample was either performed with an Oxford Instruments ESR 900 cryostat with an ITC4 temperature controller or with liquid nitrogen in a finger Dewar at 77 K. Samples were analyzed by EPR spectroscopy in 0.3-cm (inner diameter) quartz tubes. The anaerobic samples had 95% N_2/5% H_2 gas in the headspace and were closed with a closed-off rubber tube. Spin quantitations were carried out under non-saturating conditions using 10 mM copper perchlorate as the standard (10 mM $CuSO_4$, 2 M $NaClO_4$, 10 mM HCl). The programs of S.P.J. Albracht were used for computer simulations of the EPR signals [41].

Results and discussion

A summary of the currently available data concerning the geometry and coordination around the nickel in F_{430}M and the different MCR forms is shown in Fig. 2. Five ligands are present in all MCR forms, the four equatorial nitrogen ligands from F_{430} and the distal axial oxygen ligand (pointing away from the active-site channel) from the side chain of a glutamine residue. The structures of the three EPR-silent MCR forms, MCR-silent, MCRox1-silent and MCRred1-silent, have been determined by crystallography [16, 18]. The names of the different forms reflect the way these forms are produced (see Materials and methods). All EPR-silent forms have the nickel in the +2 oxidation state. The proximal axial

568

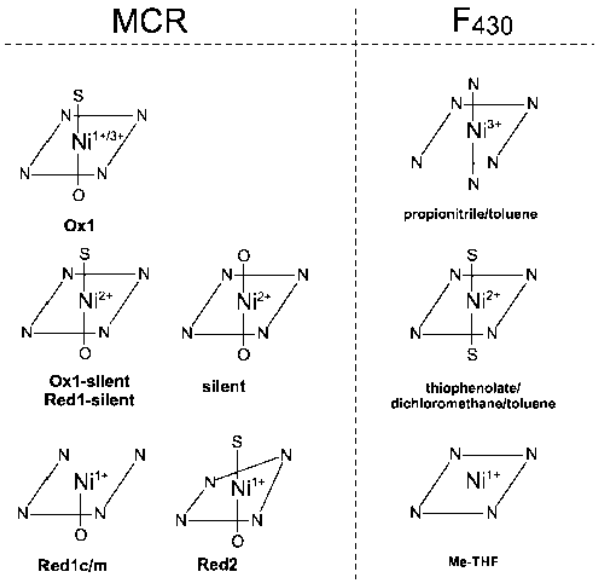

Fig. 2 Representations of the coordination and geometry around the nickel ion in several forms of methyl-coenzyme M reductase (*MCR*) and factor 430 (F_{430}). *Me-THF* 2-methyl-tetrahydrofuran

ligand in MCRsilent is the oxygen from the sulfonate group of the CoM-S-S-CoB heterodisulfide. For MCRox1-silent, the proximal axial ligand is the sulfur from the thiol (or thiolate) group of coenzyme M that is present in the active-site channel. For MCRred1-silent, the occupancy of the proximal axial position is dependent on the method of preparation [14, 18]. In this report, the MCRred1-silent form was made from MCRred1c. Due to the presence of 10 mM coenzyme M in the buffer, this leads to a silent preparation with 100% occupancy of the proximal axial position. The MCRox1 form has the same coordination as the MCRox1-silent form, as deduced from γ-irradiation and XAS measurements [20, 21, 22]. There is a discrepancy in the literature concerning the nickel coordination in the red1 forms [20, 21]. Our XAS studies on samples with up to 90% red1 present, clearly indicated that both the red1m and red1c forms have five-coordinated nickel. ENDOR spectroscopy and hyperfine sublevel correlation (HYSCORE) studies showed that the MCRred2 form is six-coordinate with the proximal axial position being the sulfur from the thiol (or thiolate) group of coenzyme M [24, 25]. With both MCRox1 and MCRred2 having similar coordination around the nickel, the spectroscopic differences (see below also) are attributed to the fact that the MCRred2 form is at least one electron more reduced and the macrocycle in the MCRred2 form is probably significantly distorted, either electronically or geometrically.

Ni(II)F_{430}M can be prepared in an $S=0$ four-coordinated or $S=1$ five- or six-coordinated states. Only the $S=1$ states give rise to temperature-dependent MCD bands. The solvent used for preparing MCD samples of Ni(II), dichloromethane/toluene, does not coordinate the nickel, but it was possible to generate a six-coordinated Ni(II) form with two axial sulfur ligands by adding a large excess of thiophenolate. The Ni(I)F_{430}M form was prepared in 2-methyl-tetrahydrofuran (Me-THF) which resulted in a four-coordinated nickel center [35]. It turned out to be very difficult to prepare samples of Ni(III)F_{430}M for VTVH MCD measurements. To conduct VTVH MCD measurements, the organic solvent mixture must form a glass on freezing in liquid He. However, none of the usual glassing agents could be used, because their hydroxyl or ether groups would immediately react with the Ni(III), which is a very strong oxidant. Therefore, Ni(III)F_{430}M was prepared in toluene/propionitrile which allows reversible electrolytic oxidation to Ni(III)F_{430}M and at the same time forms a glass on freezing with enough clarity to perform the MCD measurements. EPR studies (see below also) have shown that the nickel in this form is six-coordinate with the two axial positions occupied by the nitrogen atoms of two acetonitrile molecules [10].

EPR spectra

EPR spectra of the EPR-active forms of MCR and F_{430}M that were used for VTVH MCD investigations are shown in Fig. 3, and the principal g values, line widths, and ^{14}N coupling constants based on spectral simulations are given in Table 1. MCRsilent, MCRox1-silent, and MCRred1-silent samples were completely devoid of EPR signals. Spin quantitation of the $S=1/2$ resonances shown in Fig. 3 indicates that each of the samples used in the MCD investigations is likely to be a mixture of at least two species. The MCRox1 resonance ($g=2.23, 2.17, 2.15$) accounted for 0.66 spins/Ni, indicating that 34% of the sample is in the MCRox1-silent form. The MCRred1c and MCRred1m resonances ($g=2.25, 2.07, 2.06$) accounted for 0.74 spins/Ni and 0.54 spins/Ni, respectively, indicating that 26 and 46% of the samples, respectively, are in the MCRred1-silent form. The MCRred2 sample is a mixture of a red1-type resonance ($g=2.27, 2.08, 2.07$) and red2 resonance ($g=2.29, 2.24, 2.18$). Spin concentrations were determined by simulating spectra as the sum of two resonances and quantifying each component separately. The MCRred2 sample shown in Fig. 3 comprises a red2 resonance accounting for 0.36 spins/Ni and a red1 resonance accounting for 0.55 spins/Ni, indicating that 9% of the sample is in the MCRred1-silent form. The MCR samples were prepared in the presence of 60% (v/v) ethylene glycol, in order to obtain a glass on freezing for parallel VTVH MCD studies. The spectra are generally in good agreement with published data [12, 13]. The presence of glassing agents like glycerol and (poly)ethylene glycol can perturb EPR signals, with the most common effect being narrower line widths due to decreased heterogeneity in the frozen solution. Such an effect is detectable on the

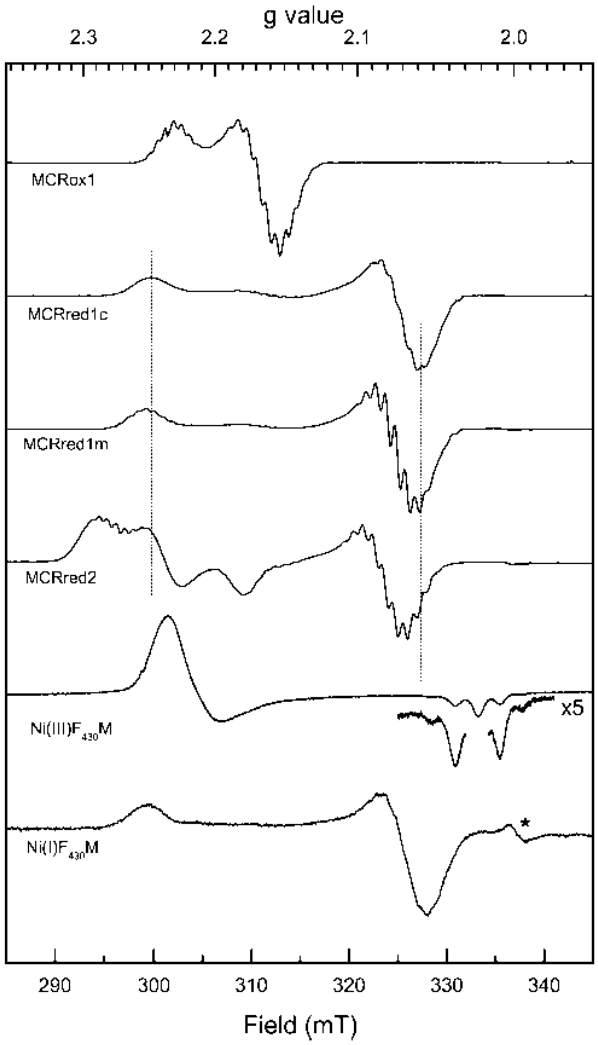

Fig. 3 EPR spectra of different forms of methyl-coenzyme M reductase (*MCR*) and F_{430} pentamethyl ester (*$F_{430}M$*). All MCR samples were prepared in 50 mM TrisHCl, pH 7.6 and 60% ethylene glycol. The MCRox1-silent, *MCRox1*, and *MCRred1m* samples also contained 10 mM methyl-coenzyme M. The *MCRred1c* sample contained 10 mM coenzyme M. The *MCRred2* sample contained 10 mM coenzyme M and 4 mM coenzyme B. The concentrations of the MCR samples were in the range 0.4–0.5 mM (1.4–1.8 mg/ml). *Vertical dashed lines* indicate the shift in *g*values for the signals in the *MCRred2* sample in comparison to the signals in the *MCRred1c* and *MCRred1m* samples. *Ni(III)$F_{430}M$*(2.4 mM, ca. 60% in the Ni(III) form) was prepared in propionitrile-toluene 1:1 (v/v) and 0.1 M tetrabutylammonium fluoroborate. *Ni(II)$F_{430}M$*(0.6 mM) was prepared in dichloromethane/toluene 1:1 (v/v) and 60 mM tetrabutylammonium thiophenolate. *Ni(I)$F_{430}M$*(0.56 mM) was prepared in 2-methyl-THF. The *asterisk* indicates the presence of a small radical impurity with $g = 2.002$ due to a π-radical of $F_{560}M$ reduced by one electron. EPR conditions: microwave frequency, 9.430 GHz; microwave power, 2.01 mW; temperature, 77 K; modulation amplitude, 0.6 mT

red1m signal. In aqueous solutions only $g_\perp$shows resolved hyperfine structure. In the presence of ethylene glycol, this can also be detected on $g_{||}$ due to a narrower line width. A different ethylene glycol-induced effect is detectable in the spectrum of the MCRred2 sample. Here a mixture of the red1 and red2 signals is observed, but both the $g_{||}$ and $g_\perp$ components of the red1 signal are shifted to lower field. The shift is indicated by the vertical dashed lines in Fig. 3 and documented in terms of *g* values in Table 1. Since this was not detected for the red1c and red1m EPR signals, this suggests that the red1 signal in the red2 sample is not the same as the original MCRred1c signal.

The EPR signals shown in Fig. 3are interpreted as follows. MCRox1, MCRred1c and MCRred1m all exhibit $S = 1/2$ resonances with an axial line shape; $g_{||} > g_\perp$, which, coupled with the superhyperfine structure due to the nuclear spin ($I = 1$) of the four nitrogen ligands from F_{430}, indicates that the unpaired electron is in the d_{x2-y2} orbital which lies in the plane of the macrocycle. The Ni(I)F_{430}M resonance is very similar to the red1-type resonances, although the macrocycle ^{14}N hyperfine is not well resolved. For these red1-type species, the ground-state properties are readily rationalized in terms of a d^9,$S = 1/2$ Ni(I) species [42, 43].

The observed *g* values and anisotropy of the ox1 resonance are entirely consistent with a tetragonally compressed d^7, $S = 1/2$ Ni(III) species. However, it is difficult to envisage a tetragonally compressed geometry with S and O axial ligands [22, 23, 44]. Alternatively, the ox1 resonance can be rationalized in terms of a d^9, $S = 1/2$ Ni(I) species [42, 43], with an admixed ground state involving a significant d_{z2} contribution as a result of an axial thiol ligand, being invoked to explain the increase in $g_\perp$ compared to red1-type species. However, this explanation is inconsistent with red1-type species being more reduced than ox1, since it has recently been shown that formation of red1 does not involve reduction of macrocycle [27]. A third possibility is that ox1 resonance corresponds to a d^8, $S = 1$ Ni(II) species antiferromagnetically coupled to an axial thiyl radical [20]. However, it is unclear how such a coupled system could result in a $S = 1/2$ ground state with the observed *g*-value anisotropy and N-coupling constants indicative of an unpaired electron in d_{x2-y2}. Hence, one of the primary objectives of the VTVH MCD studies was to discriminate between Ni(III), Ni(I), and Ni(II)/thiyl radical possibilities for the MCRox1 species.

Although there is convincing evidence that the MCRred2 resonance corresponds to a Ni(I) species [13], the *g*values ($g = 2.29$, 2.24, and 2.18) are not characteristic of a d^9,$S = 1/2$ Ni(I) species with the unpaired electron in d_{x2-y2}. Rather the recent ^{14}N- and ^{1}H- ENDOR data [24] coupled with the direct evidence of axial S coordination provided by EPR and HYSCORE data for samples prepared using $H^{33}S$-CoM [25] suggest that the anomalous *g* values are a consequence of an admixed ground state with a relatively high percentage of d_{z2} character.

Ni(III)F_{430}M exhibits an axial $S = 1/2$ resonance with $g_\perp > g_{||}$. Coupled with the absence of resolved ^{14}N

570

Table 1 Parameters used to simulate the Ni-based EPR signals of methyl-coenzyme M reductase (*MCR*). For sample conditions see Fig. 3. The *g* values for F_{430} pentamethyl ester ($F_{430}M$) are included for comparison

EPR signal	*g* values			Line width (mT)			^{14}N interaction (mT)		
	g_z	g_y	g_x	w_z	w_y	w_x	A_z	A_y	A_x
MCRox1	2.2310	2.1667	2.1532	0.65	0.72	0.72	0.78	0.95	0.95
MCRred1c	2.2500	2.0710	2.0605	0.90	0.80	0.90	0.88	0.99	0.99
MCRred1m	2.2515	2.0730	2.0635	0.70	0.60	0.80	0.88	0.99	0.99
MCRred1[a]	2.2745	2.0820	2.0680	0.60	0.65	0.75	0.84	0.99	0.99
MCRred2[b]	2.2940	2.2385	2.1790	2.80	2.65	2.50	–	–	–
Ni(III)F_{430}M	2.020	2.211	2.211						
Ni(I)F_{430}M	2.250	2.074	2.065						

[a]Red1 EPR signal present in the MCRred2 sample showing a mixture of red2 and red1 signals
[b]No resolved hyperfine was detected for MCRred2

hyperfine from the macrocycle and the resolved ^{14}N hyperfine from the two equivalent propionitrile axial ligands on $g_{||}$, the EPR signal is readily interpreted in terms of a tetragonally elongated octahedral low-spin d^7 system with the unpaired electron in d_{z^2} which is oriented perpendicular to the plane of the macrocycle [42, 43].

Absorption spectra

Room-temperature absorption spectra in the 200 800 nm region for each of the different forms of MCR and F_{430}M investigated in this work are shown in Figs. S3 and S4 (Electronic Supplementary Material), respectively. The spectra are similar in that each shows a set of relatively intense bands in the 350 500 nm region corresponding to $\pi \rightarrow \pi^*$ transitions associated with the unsaturated part of the corphin ring of F_{430}. In addition, MCRred1c, MCRred1m, MCRred2, and Ni(I)F_{430}M, which all contain Ni(I) centers, exhibit weaker bands in the 500 800 nm region. The absorption spectra of the MCRox1-silent and MCRox1 are quite similar with broad absorption bands centered at 423 and 415 nm, respectively. The MCRox1 sample also shows a weak band at around 650 nm. In accord with the EPR spin quantitations, the shoulders in the 400 450 nm region in the red1 spectra are consistent with contributions from MCRred1-silent species, with absorption properties analogous to those of MCRox1-silent. The absorption spectrum of MCRred2 is dominated by a broad band centered at 416 nm with shoulders at ~390 and ~450 nm. Our sample of Ni(III)F_{430}M showed two bands, one band at 361 nm due to the Ni(III) form and one band at 438 nm due to the Ni(II) form. Comparison with absorption spectra obtained by spectroelectrochemistry indicates that only ca. 60% of the nickel was present in the +3 oxidation state in this Ni(III)F_{430}M sample [9, 10]. The Ni(II) species in the Ni(III)F_{430}M sample is likely to be in the $S = 0$ state since propionitrile only coordinates to the Ni(III) form (see below). The absorption spectrum of Ni(I)F_{430}M, which comprises an intense band at 383 nm and a weaker band centered at 759 nm, confirms the interpretation of the MCRred1 absorption spectra discussed above and indicates that a weak band centered in the 700 800 nm region is a characteristic feature of red1-type species. The Ni(I)F_{430}M sample was >90% Ni(I); the Ni(II)F_{430}M dithiophenolate was homogeneous based on the absorption spectrum and exclusively Ni(II) based on the absence of EPR signals.

VTVH MCD studies

Variable-temperature MCD spectra in the 200 1400 nm region for each of the different forms of MCR and F_{430}M that were investigated in this work are shown in Figs. 4 and 5, respectively. Panel A in both figures shows the MCD spectra recorded at 1.7, 4.2, and 10.1 K with an applied field of 6 T, and panel B shows VTVH MCD saturation magnetization data at selected wavelengths. In terms of excited-state electronic properties, the MCD spectra shown in Figs. 4 and 5 can be broadly classified into three groups.

The first group comprises MCRox1-silent, MCRox1, and Ni(II)F_{430}M. All three exhibit intense temperature-dependent MCD bands in the macrocycle $\pi \rightarrow \pi^*$ region (300 500 nm) comprising a positive band between 400 and 450 nm and two negative bands between 350 and 400 nm. In addition, the MCRox1-silent and MCRox1 samples show weak temperature-dependent bands in the 700 1400 nm region that are attributed to Ni d d transitions. No significant bands were observed in this region for Ni(II)F_{430}M. MCD studies on aqueous bis-aquo, bis-imidazole, and bis-cyano forms of F_{430} showed the presence of weak d d bands in this area for all three forms [45]. Based on the binding constants and concentration of thiophenolate, most of the Ni(II)F_{430}M should be six-coordinated. The cumulative constants for formation of five- and six-coordinated tetraethylammonium thiophenolate complexes of F_{430}M in dry CH_2Cl_2 are: $\log \beta_1 = 3.16 \pm 0.2$ and $\log \beta_2 = 4.31 \pm 0.2$ [46]. We do not have a good explanation for the absence or weakness of the near-IR Ni(II) d d bands in the bis-thiophenolate complex. The spectra of all three species in the first group are very similar to those previously reported for the MCR-silent Ni(II) species in the $\pi \rightarrow \pi^*$ region [4,

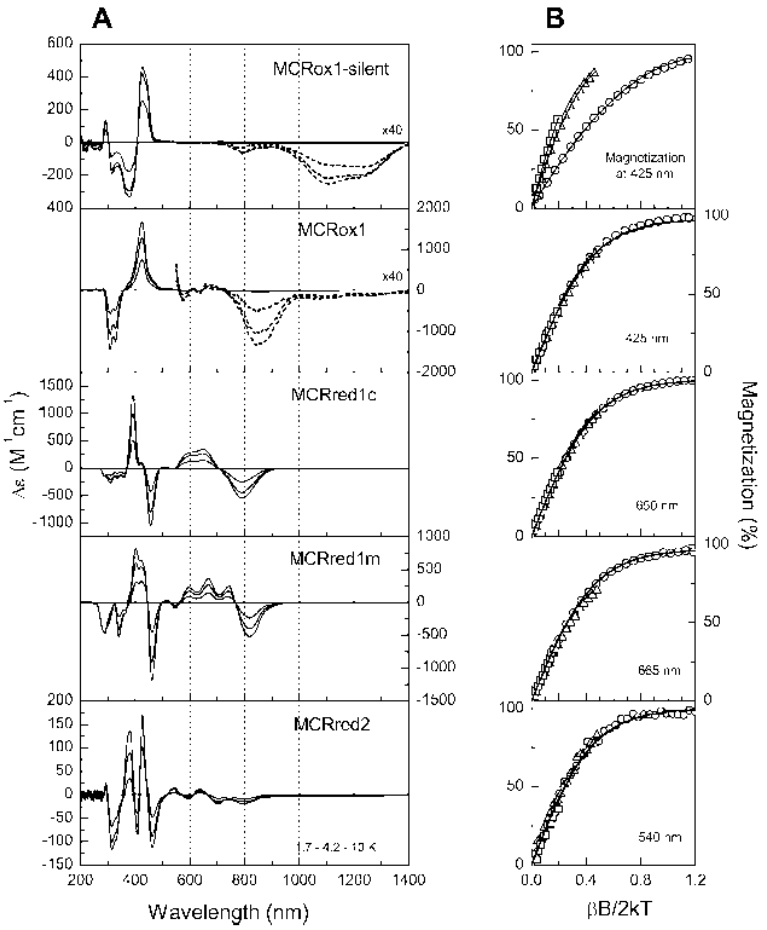

Fig. 4 Magnetic circular dichroism spectra (**A**) and saturation magnetization data (**B**) for different forms of methyl-coenzyme M reductase (*MCR*). For sample conditions see Fig. 3. Optical path length $l = 0.1$ cm.**A** MCD spectra at 1.7, 4.2, and 10 K with an applied field of 6 T. MCD intensity increases with decreasing temperature. The *dashed lines* are spectra multiplied by a factor of 40. **B** VHVT MCD saturation magnetization data collected at selected wavelengths at fixed temperatures of 1.7 (*circles*), 4.2 (*triangles*), and 10 K (*squares*), with magnetic fields between 0–6 T. *Solid lines* are fits or simulations of the magnetization data using the following parameters: *MCRox1-silent*, $S = 1$, $g_0 = 2.2$ (fixed isotropic real g value), $D = +10.0$ cm^{-1}, $E/D = 0.33$, 99% z-polarized; *MCRox1*, $S = 1/2$, $g_{\|} = 2.231$, $g_{\perp} = 2.160$; *MCRred1c*, $S = 1/2$, $g_{\|} = 2.250$, $g_{\perp} = 2.066$; *MCRred1m*, $S = 1/2$, $g_{\|} = 2.252$, $g_{\perp} = 2.068$; *MCRred2*, $S = 1/2$, $g_{\|} = 2.294$, $g_{\perp} = 2.220$

5]. This is illustrated in Fig. 6, which compares the room-temperature absorption and 1.7 K MCD spectra of MCRox1-silent and MCR-silent. The minor differences in both the $\pi \rightarrow \pi^*$ bands in the UV-visible region and the d d bands in the near-IR region (790, 1110, and 1260 nm for MCRox1-silent compared to 760, 1090, and 1260 nm for MCR-silent) are attributed, at least in part, to the difference in axial coordination, i.e., the oxygen from the sulfonate group of the CoM-S-S-CoB heterodisulfide in MCR-silent is replaced by sulfur from the thiol group of coenzyme M in MCRox1-silent [16]. Relatively small changes in the d d bands were expected, because sulfur and oxygen ligands generally have similar ligand field strengths.

The negative MCD bands centered near 800, 1,100, and 1,250 nm in MCRox1-silent and MCR-silent are assigned to components of the $^3A_{2g} \rightarrow {}^3T_{2g}$lowest energy spin-allowed d d transition of a Ni(II) center under idealized O_h symmetry (see Fig. 7). Assignment of these near-IR bands as d d transitions is based on extensive near-IR MCD studies of MCR-silent and the aqueous bis-aquo, bis-imidazole, and bis-cyano forms of F_{430} and the close correlation between the splitting of the lowest energy d d band and the magnitude of the axial ground-state zero-field splitting for the $S = 1$ ground state as deduced by SQUID saturation magnetization measurements [45].

The ground-state zero-field splitting is a consequence of mixing of the lowest energy d d excited state into the ground state via second-order spin-orbit coupling. If the deviation of the ligand field from idealized octahedral symmetry is small, perturbation theory can be used to assess the axial zero-field splitting parameter (D) based on estimates of the energies and energy separation between the $^3B_{1g} \rightarrow {}^3B_{2g}$ and the rhombically split

572

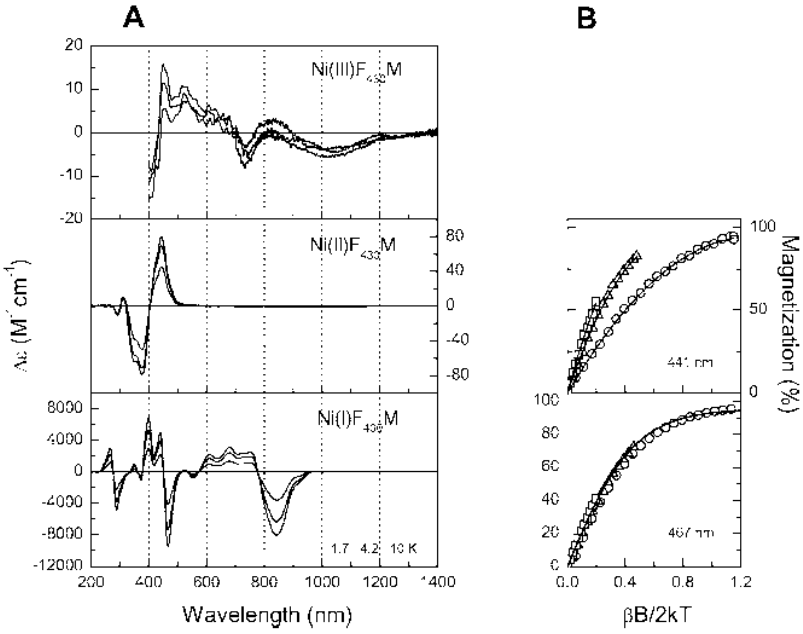

Fig. 5 Magnetic circular dichroism spectra (**A**) and saturation magnetization data (**B**) for different forms of F_{430} pentamethyl ester ($F_{430}M$). For sample conditions see Fig. 3. Optical path length: $l = 0.1$ cm. **A** MCD spectra at 1.7, 4.2, and 10 K, with an applied field of 6 T. **B** VHVT MCD saturation magnetization data collected at selected wavelengths at 1.7 (*circles*), 4.2 (*triangles*), and 10 K (*squares*), with magnetic fields between 0–6 T. *Solid lines* are fits or simulations of the magnetization data using the following parameters: *Ni(II)F*$_{430}$*M*, $S = 1$, $g_0 = 2.2$ (fixed isotropic real g value), $D = +10.0$ cm^{-1}, $E/D = 0.33$; 99% z-polarized; *Ni(I)F*$_{430}$*M*: $S = 1/2$, $g_{\|} = 2.250$, $g_{\perp} = 2.070$

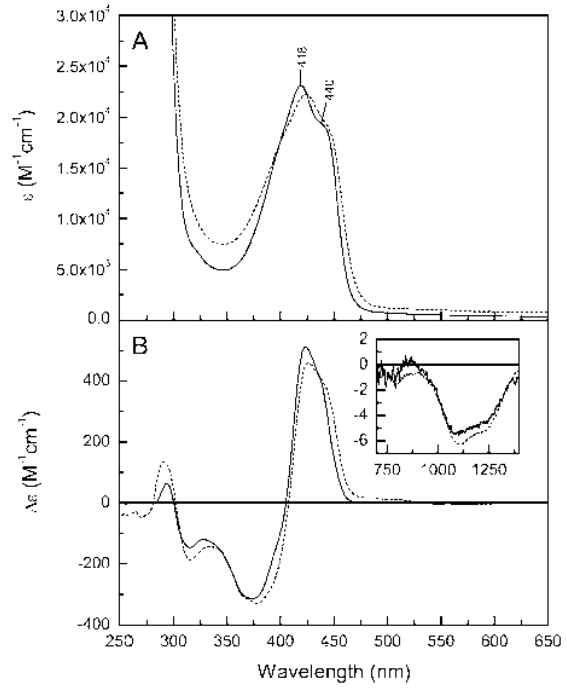

Fig. 6 Absorption spectra (**A**) and magnetic circular dichroism spectra (**B**) of methyl-coenzyme M reductase (MCR) in the MCRsilent (*solid line*) and MCRox1-silent (*dotted line*) forms. The MCR samples were prepared in 50 mM TrisHCl, pH 7.6, and 60% ethylene glycol; the MCRox1-silent sample contained 10 mM methyl-coenzyme M. The absorption spectra were recorded at room temperature and the MCD spectra were recorded at 1.7 K with an applied field of 6 T. The sample concentrations of the MCR samples were 0.4–0.5 mM (1.4–1.8 mg/ml). Optical path length: $l = 0.1$ cm. The *insert* shows an overlay of the 1.7 K MCD spectra in the 700–1,400 nm region

$^3B_{1g} \rightarrow {}^3E_g$ components of the lowest energy d d transition under idealized D_{4h} symmetry (Fig. 7), and the one-electron spin-orbital coupling constant [47]:

$$D = -\zeta^2[E(^3E_g) - E(^3B_{2g})]/[E(^3E_g) \times E(^3B_{2g})] \qquad (1)$$

This procedure assumes isotropic spin-orbit coupling and hence neglects anisotropy in covalent interactions. However, the use of this simplistic formalism is justified by the good agreement between the values of D assessed using Eq. (1) and those determined via analysis of SQUID saturation magnetization studies [45]. For example, for the aqueous bis-aquo, bis-imidazole, and bis-cyano forms of F_{430}, D was estimated to be 10.5, 3.2, and 2.4 cm^{-1}, respectively, using Eq. (1) with $\zeta = 500$ cm^{-1}, compared to D of 9.8 ± 0.5, 3.4 ± 0.2, and 2.0 ± 0.3 cm^{-1}, using SQUID saturation magnetization data [45]. The splitting of the lowest energy d d band indicates that aqueous F_{430} has a tetragonally distorted octahedral Ni(II) center and the positive sign for D indicates a tetragonal elongation even for the bis-cyano derivative.

The signs and relative intensities of the near-IR d d bands for MCRox1-silent and MCRox1 are quite different to those observed in aqueous F_{430} samples [45]. All three transitions exhibit negative MCD bands and the two lowest energy bands are most intense in MCRox1-silent and MCRox1, whereas the lowest energy transition to the ^3E_g excited state has a weak derivative-shaped MCD band, and the higher energy transition to the $^3B_{2g}$ excited state has a more intense negative MCD band. This suggests significant differences in the Ni(II) ligand field for F_{430} bound in MCR compared to aqueous F_{430}, and results in ambiguity concerning the sign of D, since it is unclear which pair of

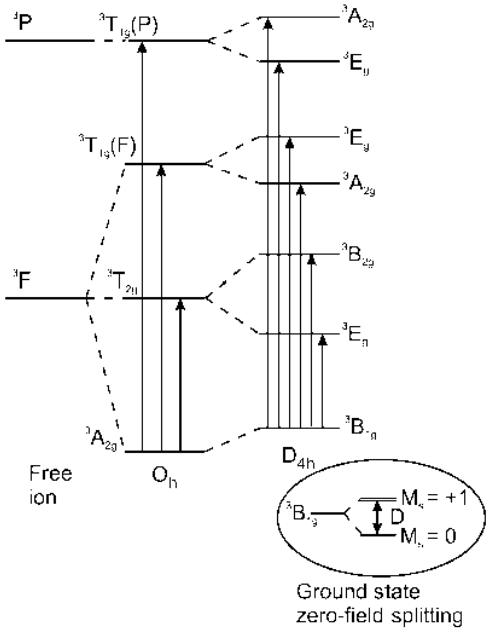

Fig. 7 Energy-level diagram for the spin-allowed d–d bands of Ni(II) under O_h and D_{4h} symmetry. *Inset* shows the ground-state zero-field splitting. The indicated energy ordering is for a tetragonal elongation

transitions should be assigned to the components of the $^3B_{1g}. \rightarrow {}^3E_g$ transition. For example, in MCRox1, if the bands at 1110 and 1260 nm are assigned to the components of the $^3B_{1g}. \rightarrow {}^3E_g$ transition, Eq. (1) predicts $D = +9.7$ cm^{-1}($\zeta = 500$ cm^{-1}), whereas if the bands at 790 and 1110 nm are assigned to the components of the $^3B_{1g}. \rightarrow {}^3E_g$ transition, Eq. (1) predicts $D = 8.3$ cm^{-1} ($\zeta = 500$ cm^{-1}). SQUID saturation magnetization for MCD-silent indicated that ambiguity results from a rhombic ground state, since optimal fits were obtained with $|D| = 9.0 \pm 0.5$ cm^{-1}with $E/D = 0.33$ [45].

In the rhombic limit ($E/D = 0.33$), EPR and SQUID saturation magnetization measurements cannot distinguish between $D > 0$ and $D < 0$. However, VHVT MCD measurements for discrete transitions can discriminate between these two possibilities provided information on the transition polarization is available [40]. To this end, VHVT MCD data for MCRox1-silent were collected and analyzed using the protocol developed by Neese and Solomon [40] for the $\pi \rightarrow \pi^*$ transition at 425 nm (Fig. 4). Recent DFT calculations indicate that this transition is polarized along a unique axis in the plane of the ligand macrocycle [48]. Significantly, fits could not be obtained for a near-axial system with $D \sim +10$ cm^{-1} for *x*-, *y*- or *xy*-polarized transitions the situation expected for a transition polarized in the plane of the macrocycle for a tetragonally elongated octahedral Ni(II) center with the zero-field splitting axis along elongation (*z*) axis. Optimal fits were obtained for $|D| = 10 \pm 1$ cm^{-1} and $|E/D| = 0.33$, with the sign of D and E depending on the transition polarization as defined by the zero-field splitting axis system. For example, equally good fits were obtained for a *z*-polarized transition with $D = +10 \pm 1$ cm^{-1} and $E/D = +0.33$ ($D > 0$ and $E > 0$), a *y*-polarized transition with $D = 10 \pm 1$ cm^{-1} and $E/D = +0.33$ ($D < 0$ and $E < 0$), and an *x*-polarized transition with $D = 10 \pm 1$ cm^{-1} and $E/D = 0.33$ ($D < 0$ and $E > 0$). These results dictate that the weakest ligand-field axis corresponds to the axis of the transition polarization, since only the *z*-polarized fit results in a positive value of D. Hence, we conclude that the axis perpendicular to the plane of the macrocycle is not the weakest ligand-field axis for the enzyme-bound Ni(II) F_{430}cofactor. Similar VHVT MCD saturation magnetization data and analyses were obtained for the six-coordinated Ni(II)F_{430}M with thiophenolate axial ligands in 1:1 dichloromethane/toluene, see Fig. 5.

After correction for a minor contribution from MCRox1-silent (34% based on the MCRox1 $S = 1/2$ spin quantitation), the VTVH MCD saturation magnetization data for MCRox1 at 425 nm were not nested and were readily fit to an *xy*-polarized transition from an $S = 1/2$ ground state with the EPR-determined *g* values (see Fig. 4). In addition to the difference in ground-state spin, the MCD spectra also show that MCRox1 and MCRox1-silent differ in terms of the energies and multiplicity of d d transitions in the 700 1,400 nm region (see Fig. 4). The weak negative bands at 1,100 and 1,250 nm in the spectra of MCRox1 are attributed to contributions from MCRox1-silent. Hence, the broad negative band centered at 850 nm is the only feature that can be attributed to a d d band in MCRox1. As MCRox1 and MCRox1-silent have similar coordination environments (Fig. 2), this argues strongly against a Ni(I) assignment for MCRox1. A tetragonally elongated octahedral Ni(I) species would be expected to exhibit split d d bands to lower energy than the d d bands for equivalent Ni(II) center. Moreover, MCRox1 does not exhibit the intense charge transfer transitions in the 500 900 nm region that appear to be a unifying feature of the MCD spectra of Ni(I) forms of MCR and F_{430} (see below).

The MCD data for MCRox1 can, however, be interpreted in terms of a coupled Ni(II)/thiyl radical or a tetragonally compressed octahedral Ni(III) description. The similarity in the MCD spectra in the $\pi \rightarrow \pi^*$ region between MCRox1 and MCRox1-silent and the observation of a d d band at 850 nm (see Fig. 4) are both consistent with a coupled Ni(II)/thiyl radical description for MCRox1. Antiferromagnetic coupling between the $S = 1/2$ thiyl radical and the $S = 1$ Ni(II) center would result in an $S = 1/2$ ground state and a low-lying $S = 3/2$ excited state that would probably not be significantly populated at the temperatures used in the VHVT MCD saturation magnetization study. The unpaired electron in $S = 1/2$ ground state of the coupled system would need to be a molecular orbital in the *xy*-plane in order to explain the similarity in the N-coupling constants for ox1- and red1-type species [22, 23]. Alternatively, the

band at 850 nm is also entirely consistent with the energy expected for a component of the lowest energy d d band of a tetragonally compressed Ni(III) species. The argument against a tetragonally compressed octahedral Ni(III) formulation of MCRox1 has centered around the difficulty of obtaining a tetragonally compressed octahedral geometry with weak-field (S and O) axial ligands. However, the VHVT MCD saturation magnetization results for MCRox1-silent, which indicate that the axial ligands do not constitute the weak-field axis in MCRox1-silent, suggest that the protein environment of the macrocycle may play a role in attenuating and preventing a significant increase in the equatorial ligand field as the Ni oxidation state increases. The increase in axial ligand field strength with increasing Ni oxidation state would then account for the transition from tetragonally elongated to tetragonally compressed octahedral geometry on progressing from Ni(I) MCRred1 and MCRred2, to Ni(II) MCRox1-silent and to Ni(III) MCRox1. Calculations will be required to distinguish between Ni(III) and coupled Ni(II)/thiyl possibilities for MCRox1.

The second group of MCD spectra comprises MCRred1c, MCRred1m, MCRred2, and Ni(I)F_{430}M samples (see Figs. 4 and 5). In the $\pi \rightarrow \pi^*$ region, this group exhibits a set of one or two positive bands centered at around 400 nm and a negative band centered near 450 nm, i.e., opposite signs for the MCD bands compared to the group of Ni(II) cofactors discussed above. In addition, they show a set of intense positive and negative bands in the 500 700 nm region that appear to be unique to forms of MCR and F_{430} containing cofactors with Ni in the +1 oxidation state. On the basis of the large $|\Delta\epsilon|/\epsilon$ ratios compared to the macrocycle $\pi \rightarrow \pi^*$ transitions, these bands are attributed to charge transfer transitions involving the Ni(I) d orbitals and the π orbitals of the macrocyclic ligand. In accord with this conclusion, DFT calculations published while this manuscript was in review, have assigned these bands to Ni d to macrocycle π^* charge transfer transitions [48]. The appearance of these bands in the visible region is a direct consequence of the increase in the energy of the Ni 3d orbitals on reduction to Ni(I) and hence appears to be a unique attribute of Ni(I) forms of F_{430}. Ni(I) d-d transitions are expected at wavelengths above 1400 nm and outside the region investigated in the work. This shift occurs for example in Ni(I) and Ni(II) complexes of a series of tetraaza macrocycles, for which the Ni(I) d d transition is shifted to lower energy by ~4000 cm^{-1} compared to the lowest energy Ni(II) d d band [49]. VTVH MCD studies in the 1400 2000 nm region using D_2O buffer solutions are planned to facilitate observation of Ni(I) d d bands.

VTVH MCD saturation data for MCRred1c, MCRred1m, and MCRred2 using bands in the 500 700 nm region (Fig. 4), and for Ni(I)F_{430}(M) at 467 nm (Fig. 5) indicate $S = 1/2$ ground states, and the data are fit to a good approximation by the EPR-determined g values. In accord with the EPR spin quantitations, the combination of anomalous temperature-dependent behavior coupled with nested magnetization data for bands in the $\pi \rightarrow \pi^*$ region indicated varying contributions from Ni(II)MCRred1-silent forms in the MCD spectra of MCRred1c, MCRred1m, and MCRred2 (see Fig. 4). The ability to detect MCD bands from the Ni(II)MCRred1-silent form in these samples is dependent on the $S = 1/2$ spin quantitation and intensity of the MCD bands due to the red1 or red2 species. Hence the presence of the Ni(II)MCRred1-silent form is not detectable in MCRred1c and Ni(II)F_{430}M, is detected as a shoulder in MCRred1m, and is detected as a separate band centered at 425 nm in MCRred2. In the case of the MCRred2 sample, this was concluded from studying several samples that contained different ratios of MCRred2 and MCRred1-silent. Unfortunately, the mixture of three paramagnetic species in MCRred2 samples makes it very difficult to assess differences in the MCD spectra corresponding to the $S = 1/2$ MCRred2 and MCRred1-type species.

The third group comprises only Ni(III)F_{430}M which showed MCD bands with very weak intensity even at 1.7 K. Consequently a very concentrated sample was prepared (2.4 mM), but the poor quality of the glass coupled with the high absorption of the chromophore between 200 and 400 nm only permitted spectra to be recorded in the 400 1,400 nm region (Fig. 5). A temperature-dependent band at 450 nm is tentatively attributed to the $S = 1/2$ Ni(III)F_{430}M. However, this could not be confirmed via VTVH MCD saturation studies, because the data were too noisy for meaningful interpretation. In addition, two temperature-independent negative bands are observed at 740 and 1,050 nm that are tentatively attributed to d d bands of square planar, $S = 0$ Ni(II)F_{430}M. Similar bands were observed for Ni(II)F_{430}M in Me-THF in the absence of exogenous axial ligands (not shown). MCD samples with a lower concentration of Ni(III)F_{430}M did not show any major additional bands in the 200 400 nm region (not shown). The weakness of the temperature-dependent MCD bands associated with Ni(III)F_{430}M is surprising in light of the intensity of the temperature-dependent MCD bands from Ni(I)F_{430}M and Ni(II)F_{430}M. However, we cannot rule out the possibility that this is a consequence of reduction of Ni(III)F_{430}M during sample handling, rather than an intrinsic electronic property of a Ni(III) form of F_{430} with the unpaired electron in d_{z^2}. Ni(III)F_{430}M is a very strong oxidant with a redox potential of ca. +1.5 V vs. NHE [10]. Consequently, extreme care was taken with sample handling. The samples were frozen in absorption cuvettes immediately after preparation; and following storage in liquid nitrogen, the frozen samples were transferred directly onto a precooled MCD probe without thawing. However, it is premature at this stage to suggest possible electronic rationalizations for the weak temperature-dependent MCD intensity observed for Ni(III)F_{430}M.

Conclusions

VTVH MCD spectroscopy, in combination with parallel absorption and EPR studies, has proven effective for characterizing the electronic and magnetic properties of the F_{430} cofactor in various forms of MCR and as purified in organic solvents. The results confirm Ni(I) assignments for MCRred1 and MCRred2 forms of MCR and show that Ni(I)F_{430}M closely approximates red1 forms of MCR in terms of both ground- and excited-state electronic properties. MCD studies also reveal Ni d to macrocycle π^* charge-transfer transitions in the 500 700 nm region that appear to be uniquely characteristic of Ni(I) forms of F_{430}. The $S = 1$ Ni(II) forms of F_{430} in MCRox1-silent, MCR-silent, and bis-thiophenolate Ni(II)F_{430}M all exhibit similar MCD spectra in the $\pi \rightarrow \pi^*$ region. Moreover, ligand field transitions associated with distorted octahedral $S = 1$ Ni(II) centers are assigned in the near-IR MCD spectra of MCRox1-silent and MCR-silent. Assessments of the ground-state zero-field splitting within the $S = 1$ ground state based on the splitting in the lowest energy d d transition and analysis of VTVH MCD saturation are shown to be in good agreement, and both indicate rhombically distorted octahedral coordination. As expected based on the crystallographic data [16], the ligand field shows only minor perturbation when the oxygen from the sulfonate group of the CoM-S-S-CoB heterodisulfide in MCR-silent is replaced as an axial ligand by sulfur from the thiol group of coenzyme M in MCRox1-silent.

The most important contribution of the MCD results lies in addressing the ongoing controversy concerning the nature of the MCRox1 species. EPR, ENDOR, and resonance Raman data, coupled with the ability to generate MCRox1 from the Ni(II) MCRox1-silent form via γ-irradiation at low temperatures, have all been interpreted in terms of a Ni(I) species [21, 22, 23]. However, the MCD data in both the $\pi \rightarrow \pi^*$ and d d regions do not support a Ni(I) formulation. Rather the data are interpreted in terms of either a tetragonally compressed Ni(III) species or a coupled Ni(II)-thiyl radical species. The latter conclusion is most consistent with UV-visible absorption and XAS data [20], and can provide a viable alternative rationalization of the EPR and ENDOR data provided the unpaired electron in the $S = 1/2$ ground state is predominantly in the equatorial plane. Moreover, these interpretations of the origin of MCRox1 obviate the need to invoke reductive activation of the macrocycle [21], since the Ni center is formally in the +3 oxidation state under both scenarios. The ability to generate MCRox1 from the Ni(II) MCRox1-silent form via γ-irradiation at low temperatures could be rationalized in terms of the known ability of this procedure to generate intense radical signals in protein samples. From crystallization studies, it is known that there is a water molecule present in the MCRox1-silent form close to the Ni(II)-thiolate group that could trigger cryooxidation of the thiolate ligand or Ni(II) center in the MCRox1 form [16]. This would be, to our knowledge, the first example where the "cryoreduction" procedure might have resulted in formal oxidation of a metal center. DFT calculations are planned to assess if MCRox1 is best considered as a tetragonally compressed Ni(III) species with an axial thiolate ligand or a coupled Ni(II)-thiyl radical species, but the reality is likely to lie between these two extremes.

Acknowledgements This work was supported by the Max-Planck-Gesellschaft (R.K.T), by the Fonds der Chemischen Industrie (R.K.T.), and by grants from the National Institutes of Health (GM60329 and GM62542 to M.K.J.), the National Science Foundation (MCB98008857 to M.K.J) and the Swiss National Science Foundation (20-66773 to L.S, R.P, B.J). M.G is a recipient of a scholarship of the Claussen-Simon-Stiftung. We thank Dr. Richard C. Conover for help in fitting the VHVT MCD saturation magnetization data and the reviewers for many insightful comments and suggestions.

References

1. Thauer RK (1998) Microbiology 144:2377–2406
2. Pfaltz A, Jaun B, Fässler A, Eschenmoser A, Jaenchen R, Gilles HH, Diekert G, Thauer RK (1982) Helv Chim Acta 65:828–865
3. Färber G, Keller W, Kratky C, Jaun B, Pfaltz A, Spinner C, Kobelt A, Eschenmoser A (1991) Helv Chim Acta 74:697–716
4. Hamilton CL, Scott RA, Johnson MK (1989) J Biol Chem 264:11605–11613
5. Cheesman MR, Ankel-Fuchs D, Thauer RK, Thompson AJ (1989) Biochem J 260:613–616
6. Pfaltz A, Livingston DA, Jaun B, Diekert G, Thauer RK, Eschenmoser A (1985) Helv Chim Acta 68:1338–1358
7. Shiemke AK, Shelnutt JA, Scott RA (1989) J Biol Chem 264:11236–11245
8. Hamilton CL, Ma L, Renner MW, Scott RA (1991) Biochim Biophys Acta 1074:312–319
9. Jaun B (1993) In: Sigel H, Sigel A (eds) Metal ions in biological systems. Marcel Dekker, New York, pp 287–337
10. Jaun B (1990) Helv Chim Acta 73:2209–2217
11. Goubeaud M, Schreiner G, Thauer RK (1997) Eur J Biochem 243:110–114
12. Mahlert F, Bauer C, Jaun B, Thauer RK, Duin EC (2002) J Biol Inorg Chem 7:500–513
13. Mahlert F, Grabarse W, Kahnt J, Thauer RK, Duin EC (2002) J Biol Inorg Chem 7:101–112 and 7:151
14. Duin EC (2004) In: Warren MJ, Smith A (eds) Tetrapyrroles: their birth, life and death. Landes Bioscience, Georgetown (in press)
15. Ragsdale SW (2003) In: Kadish KM, Smith KM, Guilard R (eds) Porphyrin handbook. Elsevier, San Diego, pp 205–228
16. Ermler U, Grabarse W, Shima S, Goubeaud M, Thauer RK (1997) Science 278:1457–1462
17. Grabarse W, Mahlert F, Shima S, Thauer RK, Ermler U (2000) J Mol Biol 303:329–344
18. Grabarse W, Mahlert F, Duin EC, Goubeaud M, Shima S, Thauer RK, Lamzin V, Ermler U (2001) J Mol Biol 309:315–330
19. Grabarse W, Shima S, Mahlert F, Duin EC, Thauer RK, Ermler U (2001) In: Messerschmidt A, Huber R, Poulos T, Wieghardt K (eds) Handbook of metalloproteins. Wiley, Chichester, pp 897–914
20. Duin EC, Cosper NJ, Mahlert F, Thauer RK, Scott RA (2003) J Biol Inorg Chem 8:141–148
21. Tang Q, Carrington PE, Horng YC, Maroney MJ, Ragsdale SW, Bocian DF (2002) J Am Chem Soc 124:13242–13256

22. Telser J, Davydov R, Horng Y-C, Ragsdale SW, Hoffman BM (2001) J Am Chem Soc 123:5853–5860
23. Telser J, Horng Y-C, Becker DF, Hoffman BM, Ragsdale SW (2000) J Am Chem Soc 122:182–183
24. Finazzo C, Harmer J, Jaun B, Duin EC, Mahlert F, Thauer RK, Van Doorslaer S, Schweiger A (2003) J Biol Inorg Chem 8:586–593
25. Finazzo C, Harmer J, Bauer C, Jaun B, Duin EC, Mahlert F, Goenrich M, Thauer RK, Van Doorslaer S, Schweiger A (2003) J Am Chem Soc 125:4988–4989
26. Rospert S, Böcher R, Albracht SPJ, Thauer RK (1991) FEBS Lett 291:371–375
27. Piskorski R, Jaun B (2003) J Am Chem Soc 125:13120–13125
28. Wasserfallen A, Nölling J, Pfister P, Reeve J, de Macario EC (2000) Int J Syst Evol Microbiol 50:43–53
29. Kobelt A, Pfaltz A, Ankel-Fuchs D, Thauer RK (1987) FEBS Lett 214:265–268
30. Ellermann J, Hedderich R, Böcher R, Thauer RK (1988) Eur J Biochem 172:669–677
31. Schönheit P, Moll J, Thauer RK (1980) Arch Microbiol 127:59–65
32. Rospert S, Linder D, Ellermann J, Thauer RK (1990) Eur J Biochem 194:871–877
33. Bonacker LG, Baudner S, Thauer RK (1992) Eur J Biochem 206:87–92
34. Bonacker LG, Baudner S, Mörschel E, Böcher R, Thauer RK (1993) Eur J Biochem 217:587–595
35. Jaun B, Pfaltz A (1986) J Chem Soc Chem Commun 1327–1329
36. Bradford MM (1976) Anal Biochem 72:248–254
37. Johnson MK (1988) In: Que L Jr (ed) Metal clusters in proteins. American Chemical Society, Washington, DC, pp 326–342
38. Thomson AJ, Cheesman MR, George SJ (1993) Methods Enzymol 226:199–232
39. Johnson MK (2000) In: Que L Jr (ed) Physical methods in bioinorganic chemistry. University Science Books, Sausalito, pp 233–285
40. Neese F, Solomon EI (1999) Inorg Chem 38:1847–1865
41. Beinert H, Albracht SPJ (1982) Biochim Biophys Acta 683:245–277
42. Margerum DW, Anliker SL (1988) In: Lancaster JR Jr (ed) The bioinorganic chemistry of nickel. VCH Verlagsgesellschaft, Weinheim, Germany, pp 29–51
43. Salerno JC (1988) In: Lancaster JR Jr (ed) The bioinorganic chemistry of nickel. VCH Verlagsgesellschaft, Weinheim, Germany, pp 53–71
44. Renner MW, Fajer J (2001) J Biol Inorg Chem 6:823–830 and (2002) 7:352
45. Ma L (1993) PhD Thesis, University of Georgia, Athens, GA, USA
46. Knuppe K (1997) PhD Thesis, ETH Zürich, Switzerland
47. Busch DH (1966) Helv Chim Acta 174–182
48. Craft JL, Horng Y-C, Ragsdale SW, Brunold TC (2004) J Biol Inorg Chem 9:77–89
49. Suh MP, Kim HK, Kim MJ, Oh KY (1992) Inorg Chem 31:3620–3625

V Diskussion

Eine wichtige Voraussetzung für die umfangreiche Untersuchung eines Enzyms und dessen Katalysemechanismus ist die Verfügbarkeit von ausreichenden Mengen an aktiven und gereinigtem Enzym. Da Methyl-Coenzym M Reduktase (MCR) in den Zellen von *Methanothermobacter marburgensis* ca. 10% des gesamten löslichen Zellproteins ausmacht (Albracht et al. 1988), war die Menge im Falle dieses Enzyms nie ein Problem. Lange Zeit war es jedoch nicht möglich, aktive MCR zu erhalten. So betrug die Aktivität des gereinigten Enzyms Mitte der 80er Jahre nur ca. 0.1 U mg^{-1} (Ankel-Fuchs and Thauer 1986; Hartzell and Wolfe 1986). Aus der Methanbildungsrate einer wachsenden Kultur und dem Anteil von MCR am Gesamtprotein konnte allerdings eine Maximalaktivität von MCR auf 50-100 U mg^{-1} errechnet werden (Albracht et al. 1986; Ankel-Fuchs and Thauer 1986). Durch *in vivo*-Reduktion von *M. marburgensis*-Kulturen vor der Ernte mit molekularem Wasserstoff gelang es schließlich, MCR in die aktive Form zu überführen und mit einer Aktivität von 20 U mg^{-1} anzureichern. Allerdings war es nicht möglich, die beiden Isoenzyme von MCR ohne erheblichen Verlust an Aktivität und somit auch an EPR-Signal voneinander zu trennen (Rospert et al. 1991; Bonacker et al. 1993). Einige Jahre später konnte enzymatisch aktives MCR-red1 erstmals *in vitro* induziert werden, indem enzymatisch inaktives MCR-ox1, gereinigt aus Zellen nach 80% N_2/20% CO_2-Begasung, zusammen mit Ti(III)Citrat und Methyl-Coenzym M (CH_3-S-CoM) bei alkalischem pH und 60°C inkubiert wurde. Korrigiert auf eine MCR-red1-Signalintensität von 1 Spin pro mol F_{430} zeigten solche Präparationen eine maximale Aktivität von 80-100 U mg^{-1} (Goubeaud et al. 1997). Schließlich wurde eine Methode entwickelt, die es erlaubte, durch *in vivo*-Begasung mit H_2 aktive MCR-red1 zu induzieren und mit hohen Spinkonzentrationen und Aktivitäten bis zur apparente Homogenität zu reinigen. Ausgehend von diesen Präparationen wurden zudem Bedingungen gefunden und beschrieben, unter denen die verschiedenen EPR-aktiven Zustände von MCR induziert werden können (Mahlert et al. 2002a; Mahlert et al. 2002b). Mit Ausnahme von MCR-red1 und MCR-BPS konnten alle EPR-Signale von MCR vormals nur *in vivo* induziert werden.

Erst diese Methode der Reinigung hochaktiver MCR ermöglichte die in dieser Arbeit beschriebenen Untersuchungen zum Einfluß einer großen Anzahl von Methyl-Coenzym M- und Coenzym B-Analoga auf die Aktivität des Enzyms und den Nickelzustand in F_{430}, sowie zur Koordinierung und Geometrie von Nickel in den verschiedenen MCR-Zuständen. Durch eine

zeitliche Straffung und Optimierung des Reinigungsprozesses konnten hochreine Enzymfraktionen mit einer Spinkonzentration von über 0,9 pro mol F_{430} präpariert werden, die zudem eine beträchtlich längere Halbwertszeit aufwiesen. Ein sehr starkes Ankonzentrieren des homogenen Enzyms am Ende der Reinigung scheint ebenfalls die Stabilität des Enzyms zu erhöhen (nicht gezeigt). Während in früheren Präparationen das Enzym im MCR-red1-Zustand lediglich eine Halbwertszeit von nur 4 Stunden besaß (Felix Mahlert und Evert Duin, persönliche Mitteilung), bleibt gereinigtes MCR-red1c während der Lagerung im Anaerobenzelt bei Raumtemperatur inzwischen bis zu 7 Tagen ohne den Verlust von Aktivität und Spinkonzentration stabil. Dies ermöglichte die Durchführung zeitlich umfangreicher Versuchsreihen innerhalb einer Enzympräparation. Ein direkter Vergleich der Daten wird somit besser gewährleistet. Die Ergebnisse der vorliegenden Arbeit sollen nun bezüglich ihrer Relevanz im Rahmen der aktuellen Diskussion um einen postulierten Katalysemechanismus von MCR diskutiert werden.

Bereits im Eingangskapitel wurden die beiden derzeit diskutierten Modelle zum Katalysemechanismus von MCR ausführlich vorgestellt (siehe EINLEITUNG). Mechanismus I postuliert im ersten Katalyseschritt einen nukleophilen Angriff des Ni(I) von F_{430} auf die Methylgruppe von Methyl-Coenzym M und daraus resultierend die Bildung einer Methyl-Ni(III)-Zwischenstufe (Ermler et al. 1997; Grabarse et al. 2001a; Grabarse et al. 2001b). In Mechanismus II wird dagegen ein Angriff von Ni(I) auf den Thioetherschwefel von Methyl-Coenzym M formuliert. Die hervorgerufene homolytische Spaltung der Schwefel-Kohlenstoff-Bindung generiert anschließend ein Methylradikal (Ghosh et al. 2001; Pelmenschikov et al. 2002; Pelmenschikov and Siegbahn 2003). Argumente, die für oder gegen den einen oder anderen Mechanismus sprechen, können beispielsweise aus Experimenten mit Substratanaloga gezogen werden. Tatsächlich scheinen die erzielten Ergebnisse durch Untersuchungen mit Methyl-Coenzym M-Analoga einen Reaktionsmechanismus nach dem Schema von Mechanismus I zu unterstützen:

(i) Eine Begründung liefert die Umkehr der Stereokonfiguration, wie sie bei der Reduktion des Substratanalogs Ethyl-Coenzym M zu Ethan beobachtet wurde (Ahn et al. 1991). Obwohl die Kenntnis darüber nicht aus der vorliegenden Arbeit stammt, so sollte dieser Aspekt jedoch der Vollständigkeit halber hier erwähnt werden. Im Falle von Mechanismus I würde die S_N2-Reaktion im ersten Katalyseschritt zu einer solchen Inversion führen (siehe bereits EINLEITUNG). Im Gegensatz dazu würde eine Inversion der Stereokonfiguration im Mechanismus

II eine Wasserstoffabstraktion durch das Methylradikal erfordern, bevor es Zeit hat, sich innerhalb des aktiven Zentrums zu drehen. Bei den Versuchen von Ahn et al. (1991) muß allerdings berücksichtigt werden, daß maximal nur etwa 50-60% des synthetisch hergestellten Ausgangsenantiomers in das andere Enantiomer umgewandelt wurden. Gründe hierfür könnten eine unzureichende optische Reinheit des synthetisierten und eingesetzten Ethyl-Coenzym M sein oder aber die sehr rauhen Bedingungen unter denen das entstandene Ethan zum Zwecke der anschließenden Analyse der Stereokonfiguration zu Essigsäure umgewandelt wurde. Nicht auszuschließen ist aber auch die Möglichkeit, daß durch die Enzymreaktion im zeitlichen Verlauf teilweise Racemate entstehen.

(ii) Ethyl-Coenzym M wird als Substrat von MCR mit einer deutlich geringeren Effizienz reduziert (<1%) im Vergleich zu Methyl-Coenzym M. Um diese Beobachtung in Bezug zu den beiden postulierten Katalysemechanismen zu setzen, muß der Blick ins aktive Zentrum des Enzyms gerichtet werden. Mechanismus I nimmt an, daß in einer nukleophilen Substitutionsreaktion am Methylkohlenstoff die Methylthioetherbindung heterolytisch gespalten wird. Für eine maximale Reaktivität muß somit die Methylgruppe von Methyl-Coenzym M direkt über dem Nickel positioniert sein. Dagegen wäre es in Mechanismus II der Thioetherschwefel, der axial über dem Nickel stehen muß, um so eine optimale Position für die postulierte homolytische Spaltung der Schwefel-Kohlenstoffbindung einzunehmen (Abb. 9A). Die Methylgruppe von Methyl-Coenzym M ist demnach in Richtung der Thiolgruppe von Coenzym B hin orientiert und nicht wie in Mechanismus I in Richtung des Ni(I). Wenn nun wie im Falle von Ethyl-Coenzym M sich anstelle eines der Wasserstoffatome in der Methylgruppe ein Methylrest befindet, so könnte in Mechanismus I der mit Ni(I) reagierende Kohlenstoff aufgrund sterischer Hinderung nicht mehr auf die selbe Weise positioniert werden wie im Falle von Methyl-Coenzym M. Dagegen wäre in Mechanismus II die Positionierung des Schwefels über dem Nickel davon unbeeinflußt (Abb. 9B). Basierend auf der Annahme, daß der erste Schritt des Katalysezyklus ratenbestimmend ist (Pelmenschikov et al. 2002; Pelmenschikov and Siegbahn 2003), kann also nur Mechanismus I die geringere Effizienz des Enzyms gegenüber Ethyl-Coenzym M erklären. Ähnlich sieht es auch aus im Falle von Allyl-Coenzym M und Propyl-Coenzym M. Die Untersuchungen in der vorliegenden Arbeit zeigten, daß es sich bei diesen beiden Substratanaloga um reversible Inhibitoren von MCR handelt. Beide Komponenten werden nicht durch das Enzym reduziert und haben aufgrund EPR-spektroskopischer Daten keinerlei Einfluß auf den Redoxzustand des Nickels von F_{430}. Nach Mechanismus II müßte beispielsweise Allyl-Coenzym M allerdings zu Propen reduziert oder das Enzym durch die

Bildung eines Allylradikals inaktiviert, d. h. in den Ni(II)-Zustand überführt werden. Das gleiche Argument gilt auch für Propyl-Coenzym M. Die früher beschriebene Bildung sehr kleiner Konzentrationen eines gasförmigen Produkts nach der Zugabe von Allyl-Coenzym M zu Zellextrakten von *Methanobacterium thermoautotrophicus* ΔH (Wackett et al. 1988) konnte als rein chemische Reduktion bedingt durch die Anwesenheit von Cobalaminen im Enzymassay identifiziert und somit als eine vom Enzym katalysierte Reaktion ausgeschlossen werden.

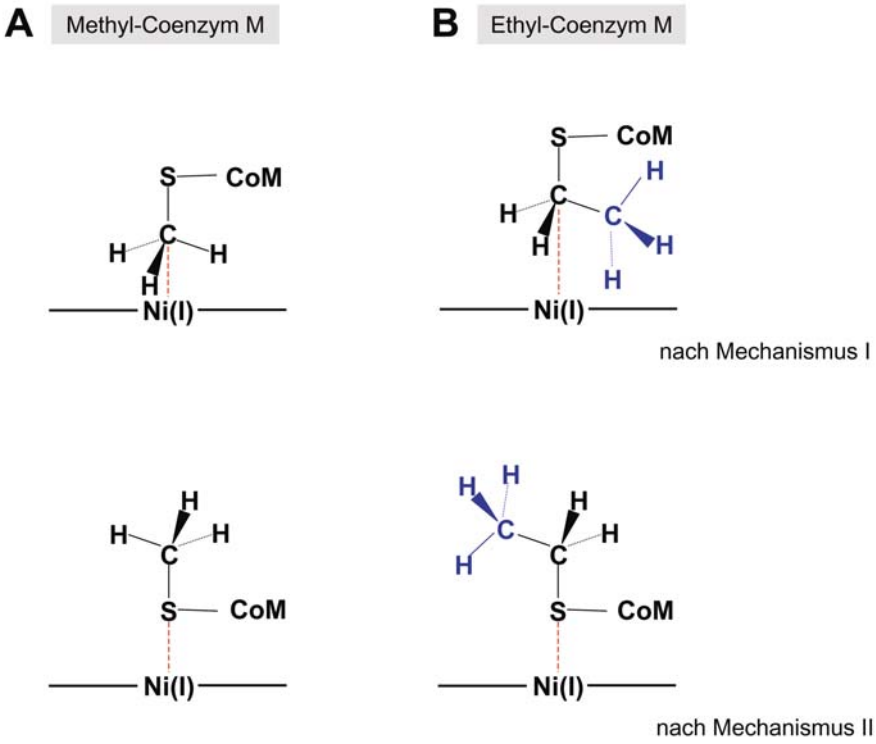

Abb. 9: Optimale Positionierung von Methyl-Coenzym M (A) und Ethyl-Coenzym M (B) im aktiven Zentrum von MCR nach Mechanismus I (Ermler et al. 1997; Grabarse et al. 2001a; Grabarse et al. 2001b) und nach Mechanismus II (Ghosh et al. 2001; Pelmenschikov et al. 2002; Pelmenschikov and Siegbahn 2003).

(iii) MCR besitzt zu 3-Bromopropansulfonat (BPS; $I_{0.5V}$ = 0.1 µM) eine etwa 20-fach höhere apparente Affinität als zu 2-Bromoethansulfonat (BES; $I_{0.5V}$ = 2 µM). Beide Substratanaloga inaktivieren MCR irreversibel durch die Oxidation von Ni(I). Damit einher geht möglicherweise eine reduktive Dehalogenierung wie sie bereits für 1,2-Dichlorethan gezeigt wurde (Holliger et al. 1992). Bei der Betrachtung beider Inhibitoren wird vor allem die strukturelle Ähnlichkeit zu Methyl-Coenzym M und dem Analog Coenzym M deutlich (Abb. 10). Im direkten Vergleich scheint es sich bei BPS eindeutig um ein Methyl-Coenzym M-Analog zu handeln, während BES eher ein Analog zu Coenzym M darstellt. Sowohl BPS als auch BES verfügen über eine Sulfonatgruppe, welche die Bindung über $Arg^{\gamma 120}$, $Tyr^{\alpha 444}$ und $His^{\beta 364}$ mit der Proteinmatrix der Bindungstasche für Methyl-Coenzym M ermöglicht. Die an Methyl-Coenzym

M angelehnte Geometrie von BPS, scheint für die Reaktion im Enzym insgesamt optimaler geeignet zu sein, als die von BES oder Coenzym M. Für eine vollständige Inaktivierung beider aktiven Zentren des aktiven Enzyms innerhalb weniger Sekunden durch BPS reichten bereits 1:1 stöchiometrische Mengen aus. BES benötigt dagegen für eine vollständige Inaktivierung von MCR im red1c-Zustand einen bis zu 25.000-fachen Überschuß gegenüber den zu inaktivierenden Reaktionszentren und eine Zeitspanne von etwa 20 min.

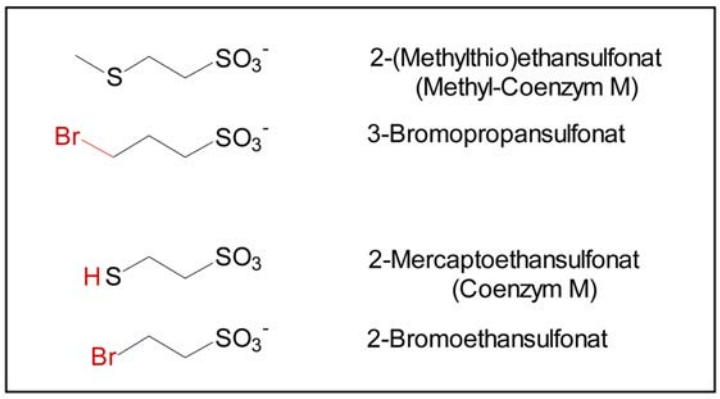

Abb. 10: Strukturen von Methyl-Coenzym M und dessen Analog 3-Bromopropansulfonat, sowie von Coenzym M und dessen Analog 2-Bromoethansulfonat. Von Methyl-Coenzym M abweichende Bereiche wurden mit Rot gekennzeichnet.

(iv) Das Methyl-Coenzym M-Analog 3-Bromopropansulfonat (BPS) induziert das MCR-BPS-Signal, welches als ein von einem Alkyl-Ni(III) stammenden Signal gedeutet werden kann. Versuche haben gezeigt, daß der enzymatisch inaktive MCR-BPS-Zustand labil gegenüber Sauerstoff ist, sich aber stabil gegenüber 10 mM 2-Bromoethansulfonat zeigt. Dabei reichen bemerkenswerterweise bereits 25 µM 2-Bromoethansulfonat aus, um innerhalb kurzer Zeit das MCR-red1-Signal komplett auszulöschen. Da die Stabilität des MCR-BPS-Signals gegenüber 2-Bromoethansulfonat in Abwesenheit von Coenzym B getestet wurde, entfällt das Argument Coenzym B könnte den Eingang zum aktiven Zentrum durch seine Bindung blockiert und somit das Vordringen von 2-Bromoethansulfonat verhindert haben. Demnach liegt das Nickelzentralatom von F_{430} in MCR-BPS in einem Zustand vor, in welchem es nicht weiter von 2-Bromoethansulfonat oxidiert werden kann. Theoretisch könnte dies ein Ni(III)-Zustand sein oder ein High Spin Ni(II), welches axial mit einem Radikal koordiniert ist (Wondimagegn and Ghosh 2001). Zudem kann eine Koordination von Brom zum Nickel ausgeschlossen werden, da Inhibierungen mit 3-Jodopropansulfonat ein identisches EPR-Spektrum liefern (siehe auch Rospert et al. 1992). Aufgrund des unterschiedlichen Kernspins von Brom (I = 3/2) und Jod (I = 5/2) hätte die Gegenwart von 3-Jodopropansulfonat im Falle einer engen räumlichen Nähe des Halogenatoms zum Nickel zu einer Verbreiterung des EPR-Signals geführt. Ein Vergleich der

EPR-Signale von freiem Ni(III)F_{430}M (Jaun 1990) zeigt keine Ähnlichkeit zu dem von MCR-BPS, womit ein tetrakoordinierter oder schwach axial hexakoordinierter Ni(III)-Zustand entgegen früherer Diskussionen (Rospert 1991) als Ursprung für dieses EPR-Signal ausgeschlossen werden kann. Bezogen auf die Linienform des MCR-BPS-Spektrums ist dieses vergleichbar mit denen der MCR-ox-Signale. VTVH-MCD-Daten scheinen dafür zu sprechen, daß exemplarisch das MCR-ox1-Signal auf einen Ni(II)-Zustand zurückzuführen ist, bei dem Ni(II) mit $S = 1$ antiferromagnetisch mit einem $S = 1/2$ Thiylradikal gekoppelt ist (Abb. 11). Um dabei die Superhyperfeinaufspaltung durch die Kopplung mit den vier Stickstoffatomen des Tetrapyrrolringsystems im ox1-Spektrum zu erklären, muß dabei das ungepaarte Elektron im xy-Orbital vorliegen (Duin et al. 2004). Ein Ni(II)/Radikal-Zustand wird analog zu MCR-ox1 ebenfalls für MCR-BPS angenommen. Allerdings zeigt MCR-BPS keine aufgelöste Superhyperfeinaufspaltung. Möglicherweise ist hier die Position des Nickels in bestimmten Grenzen variabel. Das damit verbundenen Auftreten von mehreren Werten für den *g*-Tensor würde so eine Vergrößerung der Linienbreite des MCR-BPS-Signals bewirken, wodurch die Kopplung mit den Stickstoffliganden praktisch überlagert wird. Ein solches Phänomen wurde bereits für MCR-red1c beobachtet (Mahlert et al. 2002a). Ob die Gründe für diesen Unterschied zu MCR-ox1 auf die unterschiedlichen radikalischen Liganden zurückzuführen ist, ist jedoch noch nicht geklärt. Im Allgemeinen wird durch die Bindung eines Liganden oder aber durch die Annahme einer einheitlichen Konformation eine höhere Auflösung der Hyperfeinaufspaltung erreicht. Ungeachtet dieser Unklarheit kann der Zustand des Nickels in MCR-BPS nach der Reaktion von MCR-red1 mit 3-Bromopropansulfonat unter einer reduktiven Dehalogenierung von BPS als High Spin Ni(II)F_{430} mit einem axialen Alkylradikalliganden beschrieben werden (Abb. 11).

Abb. 11: Koordinierung und Geometrie der Umgebung des Nickelatoms der prosthetischen Gruppe F_{430} in den MCR-Zuständen ox1 und BPS. In beiden Darstellungen wurde der untere axiale Sauerstoffligand von Glutamin$^{\alpha 147}$ vernachlässigt.

Formal stellt dies einen Alkyl-Ni(III)-Zustand dar, welcher für den Katalysemechanismus I propagiert wird. Die Reaktion, die zur Bildung des MCR-BPS-Zustandes führt, stellt somit entweder eine nukleophile Substitution oder eine oxidative Addition dar. Dadurch kann diese Reaktion durchaus als Modell für den ersten Schritt der Methyl-Coenzym M-Reduktion dienen.

Damit liefern einige der während der Doktorarbeit erzielten Ergebnisse Hinweise für einen Reaktionsmechanismus von MCR nach dem Prinzip von Mechanismus I. Allerdings muß festgehalten werden, daß keiner der Befunde Mechanismus II gänzlich ausschließt.

Hinsichtlich thermodynamischer Gesichtspunkte liefert Mechanismus I jedoch eine gravierende Schwierigkeit. Bei der Betrachtung der entsprechenden Redoxpotentiale fällt auf, daß das Methyl-Ni(III)-Intermediat ein viel zu geringes Oxidationsmittel darstellt, um wie vorgeschlagen ein Coenzym M-Thiylradikal zu generieren:

$Methyl\text{-}Ni(III)F_{430} \leftrightarrow Methyl\text{-}Ni(II)F_{430}$ $E_0' = >0$ mV (Jaun 1990)

$R\text{-}SH \leftrightarrow R\text{-}S\bullet + H\bullet$ $E_0' = +1{,}36$ V (Surhar et al. 1987; Lind et al. 1990)

Wesentlich attraktiver für einen solchen Oxidationsschritt erscheint $Ni(III)F_{430}$:

$Ni(III)F_{430} \leftrightarrow Ni(II)F_{430}$ $E_0' = +0{,}8$ V (Jaun 1990)

Aufgrund dieses Aspekts läßt sich der bisherige Mechanismus I (siehe Abb. 6; EINLEITUNG) in einen Mechanismus Ib umformulieren (Abb. 12): In einem Protonolyseschritt entsteht Methan hier bereits früher im Katalysezyklus aus Methyl-Ni(III) unter Bildung einer Ni(III)-Zwischenstufe. Anschließend wird Coenzym M-Thiolat zu Coenzym M-Thiylradikal oxidiert und damit einhergehend Ni(III) zu Ni(II) reduziert. Interessanterweise ergibt sich somit eine Situation, wie sie zur Zeit für den MCR-ox1-Zustand postuliert wird: Das Nickelzentralatom von F_{430} befindet sich im Ni(II)-Oxidationszustand und ist axial mit einem Thiylradikal ligiert (Duin et al. 2004). Tatsächlich ist MCR-ox1 jedoch enzymatisch inaktiv, womit eine katalytische Funktion im Reaktionsmechanismus auszuschließen ist. Zumindest kann eine physiologische Relevants postuliert werden, da dieser Zustand *in vivo* vorherrscht, wenn sich das Redoxpotential wachsender Kulturen bei einem Rückgang der H_2-Konzentration erhöht (Mahlert et al. 2002b). Desweiteren läßt sich MCR-ox1 *in vitro* sehr leicht reaktivieren (Goubeaud et al. 1997). MCR-ox1 stellt somit parallel zum Katalysezyklus einen „Reservezustand“ dar, in den das Enzym

beispielsweise übergeht, wenn die Zellen oxidativem Streß ausgesetzt sind. Möglicherweise unterscheidet sich der ox1-Zustand lediglich in konformellen Aspekten von einem Ni(II)/Thiylradikal-Intermediat im Reaktionsmechanismus (siehe unten).

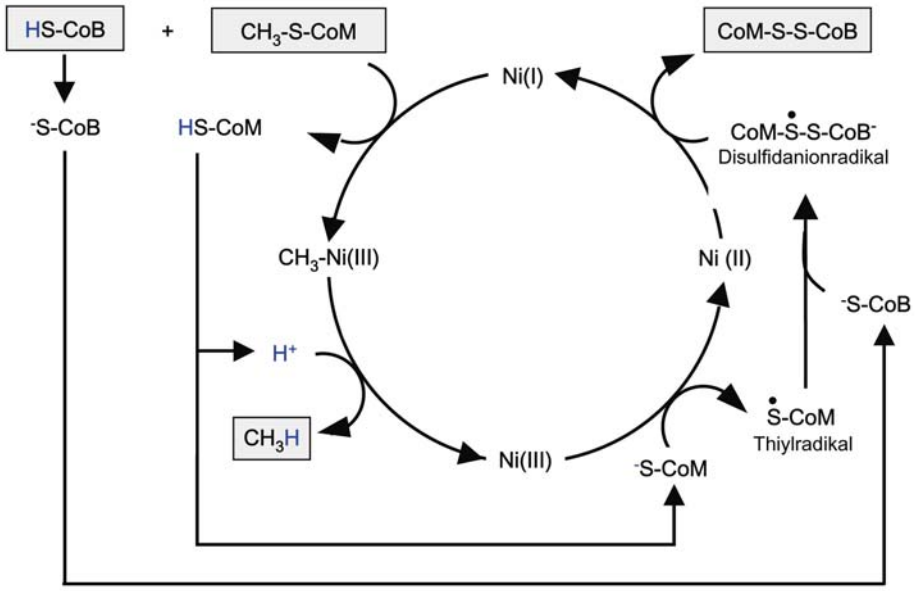

Abb. 12: Neuformulierter Mechanismus Ib der Methyl-Coenzym M Reduktase-Reaktion. Der Mechanismus basiert im wesentlichen auf Mechanismus I (Ermler et al. 1997; Grabarse et al. 2001a; Grabarse et al. 2001b) (siehe Abb. 6; EINLEITUNG).

Generell gilt für einen postulierten Enzymmechanismus, daß darin alle aktuellen und relevanten Forschungsergebnisse berücksichtigt werden müssen. So haben neuere Erkenntnisse über das Vorkommen von anaerober Methanoxidation (AMO) in marinen Sedimenten die Diskussion um die Reversibilität der Methanogenese im allgemeinen und der von MCR katalysierten Reaktion im speziellen aktuell aufkommen lassen. Vermittelt wird die anaerobe Methanoxidation durch mikrobielle Konsortien bestehend aus sulfatreduzierenden Bakterien und methanogenen Archaen (Boetius et al. 2000). *In vitro* Versuche konnten zeigen, daß in solchen marinen Sedimenten die Oxidation des Methans gekoppelt mit der Reduktion von Sulfat abläuft (Nauhaus et al. 2002). Aus mikrobiellen Matten, die aus anoxischen methanverbrauchenden Zonen des Schwarzen Meeres stammen, konnten bei der Suche nach AMO-assoziierten Zellkomponenten zwei Nickelhaltige Proteine im Verhältnis 1:4 isoliert werden (Krüger et al. 2003). Das dominante Nickel-Protein I zeigt die höchsten Sequenzhomologien zur MCR aus *Methanosarcinales* und zeichnet sich durch einen modifizierten Faktor F_{430} aus, dessen molekulare Masse mit 951,6 Da ca. 46 Da über der des bislang bekannten Faktors F_{430} aus MCR liegt. Der Ursprung dieser ungewöhnlichen Abweichung ist bislang noch unbekannt. Ebenso

unbekannt ist, ob diese Modifikation essentiell für eine mögliche reverse MCR-Reaktion sein könnte. Für die Reaktion zur Aktivierung von Methan am Beginn der sogenannten „Methanase“ (als eine Umkehr der Methanogenese) wurden bisher eine Umkehr der beiden bereits erwähnten und aktuell favorisierten MCR-Katalysemechanismen angenommen. Angelehnt an Mechanismus II (siehe Abb. 6; EINLEITUNG) könnte durch die Reduktion von Ni(I) zu Ni(II) ein Disulfidanionradikal generiert werden. Nach der Spaltung der Disulfidbindung führt die Wasserstoffabstraktion an Methan durch ein Coenzym B-Thiylradikal zur Bildung von Coenzym B und einem Methylradikal. Parallel dazu wird das Coenzym M-Thiolat and Nickel zu einem Ni(II)-Coenzym M-Thiolat-Komplex gebunden. Im letzten Schritt geht dann die Bildung von Methyl-Coenzym M mit der Rückreduktion des Nickels in den Ni(I)-Zustand einher. Eine weitere Möglichkeit bietet die Umkehr des neuformulierten Mechanismus Ib (siehe dazu Abb. 12): Die Aktivierung von Methan direkt durch das Nickelzentralatom von F_{430} geht dabei mit der Bildung eines Nickel-Methyl-Intermediats einher.

Für Mechanismus I wurden unter anderem ein Thiylradikal (von Coenzym M) und ein Disulfidanionradikal als Intermediate des katalytischen Zyklus formuliert (siehe EINLEITUNG). Dies erfolgte in Analogie zum katalytischen Mechanismus von Ribonukleotid-Reduktase (RNR) (Stubbe and van der Donk 1998; Kolberg et al. 2004) (Abb. 13). In einer ungewöhnlichen Reduktion katalysiert RNR die Umwandlung von Ribonukleotiden zu 2’-Desoxyribonukleotiden und spielt damit eine zentrale Rolle in der DNA-Biosynthese. Sowohl MCR als auch RNR katalysieren also im Prinzip die Reduktion eines Alkohols (in MCR ein methylierter Thio-Alkohol) zu einem Alkan unter Bildung eines Disulfids. In beiden Fällen folgt die Reaktion dabei einer oxidationsgetriebenen Reduktion: Zunächst wird ein Oxidationsmittel generiert, welches dazu dient, anschließend ein Thiylradikal herzustellen. Die Rolle des Oxidationsmittels übernimmt im MCR-Mechanismus I das alkylierte Nickel, während z. B. in RNR der Klasse I diese Rolle von einem Thyrosylradikal übernommen wird. Dieses entsteht ca. 35 Å entfernt vom aktiven Zentrum. Durch einen protonengekoppelten Elektrontransfer über eine Reihe von Wasserstoffgebundenen Aminosäureseitenketten löst dieses Radikal indirekt die Bildung eines Thiylradikals an einem Cystein im aktiven Zentrum aus (Nordlund et al. 1990; Nordlund et al. 1993; Uhlin and Eklund 1994; Ekberg et al. 1998; Stubbe et al. 2003). Im weiteren Verlauf des Katalysezyklus führen die Reaktionen des generierten Thiylradikals zur Entstehung eines Disulfidanionradikals (Ermler et al. 1997; Stubbe and van der Donk 1998; Grabarse et al. 2001a; Grabarse et al. 2001b; Kolberg et al. 2004). Als starkes Reduktionsmittel dient dieses in MCR zur Re-reduktion von Ni(II) zu Ni(I). In RNR trägt es zur Bildung eines Substratradikals bei,

welches nach einer Wasserstoffabstraktion schließlich als das Produkt 2'-Desoxyribonukleotid vorliegt.

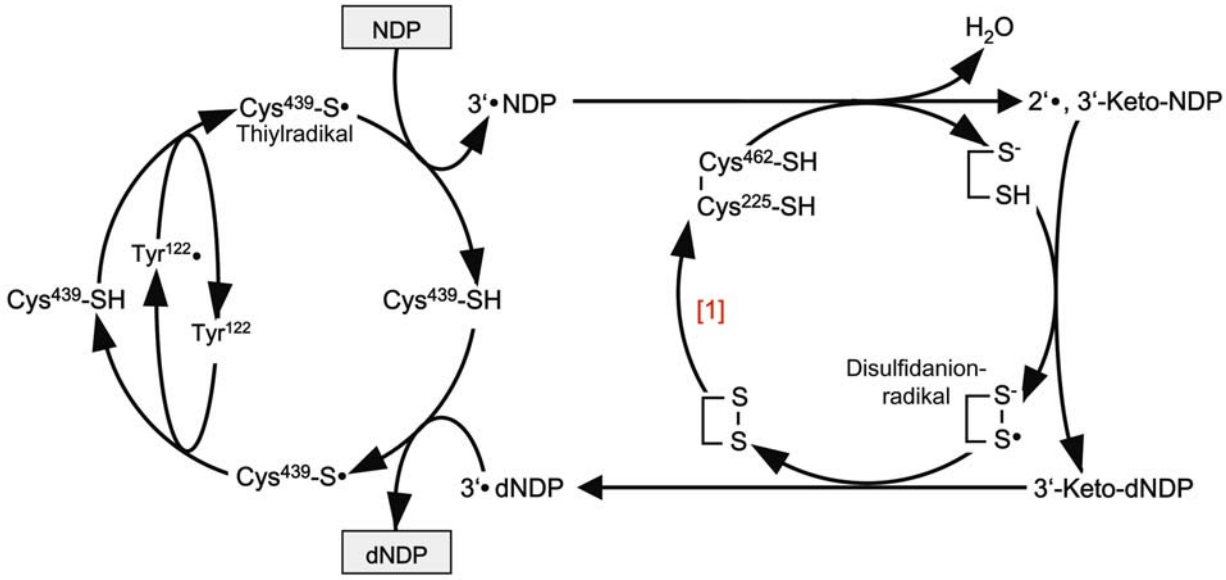

Abb. 13: Postulierter Reaktionsmechanismus der Reduktion von Ribonukleotiddiphosphat (NDP) zu 2'-Desoxyribonukleotiddiphosphat (dNDP) durch Klasse I Ribonukleotid-Reduktase (RNR) (Stubbe and van der Donk 1998; Kolberg et al. 2004). Klasse I RNR sind tetramere Enzyme ($\alpha_2\beta_2$). Das aktive Zentrum befindet sich dabei innerhalb des α_2-Homodimers (R1), das Tyrosylradikal Tyr^{122}• dagegen wird im β_2-Homodimer (R2) generiert. **[1]** Die Elektronen für diesen Reduktionsschritt werden über eine Redoxkette bestehend aus einem Cysteinpaar an der Oberfläche von R1 (Cys^{754} und Cys^{759}), Thioredoxin (oder Glutaredoxin) und dem NADPH-bindenden Flavoprotein Thioredoxin-Reduktase bereitgestellt (Holmgren 1988). Die Numerierung der Aminosäuren im Schema erfolgte nach den Sequenzdaten von *Escherichia coli*. Die Zahlen an den Intermediaten des Nukleotiddiphosphats (NDP/dNDP) geben die Position des Radikals bzw. der Ketogruppe am Ribosering wider.

In Diskussionen um ein Modell für den Katalysemechanismus von MCR taucht seit der Aufklärung der Proteinstruktur immer wieder die mögliche Beteiligung weiterer redoxaktiver Gruppen zusätzlich zu F_{430} auf (Ermler et al. 1997; Pelmenschikov et al. 2002). Geeignete Kandidaten scheinen die drei Aminosäuren $Tyrosin^{\beta 367}$, $Tyrosin^{\alpha 333}$ und $Thioglycin^{\alpha 445}$ zu sein, welche alle innerhalb des aktiven Zentrums lokalisiert und hochkonserviert sind (Ermler et al. 1997; Grabarse et al. 2000; Grabarse et al. 2001a; Grabarse et al. 2001b). Alle drei Aminosäuren ließen sich zu einem Radikal umwandeln. Bei $Tyrosin^{\beta 367}$ und $Tyrosin^{\alpha 333}$, die jeweils einen Abstand von 4,3 Å zum Nickel haben, würde es sich dabei um eine Ein-Elektronen-Oxidation (Stubbe and van der Donk 1998) und bei $Thioglycin^{\alpha 445}$, mit einem Abstand von 12 Å zum Nickel, um eine Ein-Elektronen-Reduktion handeln (Kandror et al. 1984). Die Reduktion von Thioglycin zum Thiokethylradikal könnte im katalytischen Zyklus als Elektronenüberträger bei

der Re-Reduktion von Ni(II)- zu Ni(I)F_{430} durch das Disulfidanionradikal fungieren (Grabarse et al. 2001a). Für das aufgrund seines negativen Redoxpotentials (zwischen –0,65 V und –1,4 V) leicht zu oxidierende Thiokethylradikal lassen sich unter anderem verschiedene tautomere Formen formulieren, so daß von einer Stabilisierung des Radikals ausgegangen werden kann (Grabarse et al. 2001a; Grabarse et al. 2001b). Neben einer Strukturisomerie könnte auch die *cis*-*trans*-Stereoisomerie der Thiopeptidbindung von relevanter Bedeutung für die Funktion des Thioglycins im aktiven Zentrum sein. Allgemein herrschen in Proteinstrukturen fast ausschließlich *trans*-Peptidbindungen vor. Theoretische Berechnungen zeigten jedoch, daß das Energieminimum im Falle des Thioketylradikals tatsächlich eher in der *cis*-Form der Peptidbindungen liegt (Bernhard Jaun, persönliche Mitteilung). Eine Rolle als treibende Kraft für eine Konformationsänderungen im Reaktionszentrum des Enzyms ist aufgrund der niedrigen freiwerdenden Energie bei einer *trans*→*cis*-Isomerisation allerdings auszuschließen. Umgekehrt ist jedoch nicht auszuschließen, daß eine durch die Bindung von Coenzym B induzierte Konformationsänderung zur Ausbildung der *cis*-Thiopeptidbindung beiträgt. Bereits erwähnt wurde die Hypothese, daß der MCR-ox1-Zustand ein inaktives Intermediat des Katalysezyklus darstellt, mutmaßlich aufgrund einer veränderter Konformation. Weitergehend könnte somit ein denkbarer Zusammenhang bestehen zwischen einer wie oben beschriebenen Konformation bzw. Konformationsänderung und der Tatsache, ob MCR im aktiven red1- oder im inaktiven ox-Zustand vorliegt. Die geänderte Konformation selbst und/oder das Thioketylradikal würde den Faktor F_{430} oder dessen axialen Liganden in eine andere räumliche Konformation zwingen und somit eine Erklärung z. B. für das unterschiedliche EPR-Spektum liefern. Wie das Thioketylradikal die Ligandenhülle von F_{430} beeinflussen könnte, ist jedoch unklar.

Somit wäre es möglich, MCR-ox1 über eine durch Energiezufuhr ausgelöste Konformationsänderung zu reaktivieren, womit früher beobachtete „spontane“ Aktivierungen von MCR-ox1-Präparationen (nicht gezeigt) erklärt werden könnten. Gestützt wird diese Hypothese dadurch, daß MCR-ox1 als postuliertes Ni(II)/Thiylradikal oder Ni(III)/Thiolat (Duin et al. 2004) und Ni(I)F_{430} plus Heterodisulfid isoelektronische Formen darstellen. Experimentell könnte diese Theorie mit Hilfe von Photoisomerisationsversuchen gefestigt werden. An Thioamiden wie beispielsweise *N*-5-Triflouromethyl-6-Methoxy-1-Thionaphthoyl-*N*-Methylglycin (Shim and Lee 1988) sind solche Experimente bereits erfolgreich durchgeführt worden. Dazu werden Thiamide mit energiereichem Licht bestrahlt und dadurch eine *trans*→*cis*-Isomerisation induziert. Im Falle von MCR könnte die Bestrahlung von MCR-ox1 mit UV-Licht eine gezielte Aktivierung des Enzyms und Überführung in den MCR-red1-Zustand auslösen.

Fraglich ist allerdings, ob UV-Bestrahlung alleine ausreicht, um die Thiopeptidbindung trotz Einbindung in die Proteinstruktur von MCR zu beeinflussen. Interessanterweise wurde bereits von Olson et al. (1991) eine Methode beschrieben, bei der aerob gereinigte und daher vollständig inaktive MCR aus *M. thermoautotrophicus* ΔH in Gegenwart des Reduktionsmittels Ti(III)Citrat durch Einstrahlung von Licht einer Wellenlänge zwischen 400-515 nm in sehr geringem Umfang reaktiviert wurde (Olson et al. 1991). Unter der Annahme, daß das gereinigte Enzym im MCR-silent-Zustand wahrscheinlich Spuren von nicht detektiertem MCR-ox1 enthält, könnte es sich bei dieser Teilaktivierung sogar um eine Reaktion im Sinne der oben beschriebenen handeln.

Ein weiterer Schwerpunkt dieser Arbeit beschäftigte sich mit einem MCR-Zustand, der augenscheinlich zunächst in keinem Zusammenhang mit einem Reaktionsmechanismus steht. MCR-red2, welches sich durch ein rhombisches EPR-Signal auszeichnet, wird sowohl *in vivo* als auch *in vitro* in Gegenwart der beiden Thiole Coenzym M (HS-CoM) und Coenzym B (HS-CoB) nur in Abwesenheit von Methyl-Coenzym M induziert (Mahlert et al. 2002a). In Experimenten mit ^{33}S-markiertem Coenzym M wurde die axiale Koordinierung des Ni(I) aus F_{430} mit dem Thioetherschwefel von Coenzym M eindeutig bewiesen (diese Arbeit). Jedoch ist Methyl-Coenzym M und nicht Coenzym M das eigentliche Substrat von MCR. Dennoch können Untersuchungen an MCR-red2 zum Verständnis des Enzyms wesentlich beitragen. Die Versuche mit H^{33}S-CoM zeigten beispielweise keine Linienverbreitung der EPR-Spektren von MCR im ox1- oder red1-Zustand. Das bedeutet, daß in diesen Fällen die Interaktion des Nickels mit ^{33}S verglichen mit der Auflösung der EPR-Spektren sehr klein ist. Diese Ergebnisse lassen vermuten, daß Coenzym B kein zweites Substrat darstellt (Horng et al. 2001), aber eine Änderung hervorruft, die dazu führt, daß Ni(I) und das eigentliche Substrat Methyl-Coenzym M miteinander interagieren können. Unterstützt wird diese Interpretation durch Versuchsreihen zur Inaktivierung von MCR durch 2-Bromoethansulfonat (BES). Diese haben gezeigt, daß die Gegenwart von Coenzym B die Reaktivität des Ni(I) um das 10-fache steigert. Interessanterweise kann MCR-red2 ausgehend von MCR-red1c auch von den beiden Coenzym B-Analoga *N*-6-Mercaptohexanoylthreoninphosphat (HS-CoB_6) und *N*-7-(Methylthio)heptanoylthreoninphosphat (CH_3-S-CoB) induziert werden (diese Arbeit; Mahlert et al. 2002b) (Abb. 14). Beide Analoga sind bereits in der Literatur als potente Inhibitoren mit einem K_i von 0,1 µM für HS-CoB_6 (Ellermann et al. 1988; Horng et al. 2001) und einem K_i von 6 µM für CH_3-S-CoB (Ellermann et al. 1987) beschrieben worden. Im Vergleich zu HS-CoB besitzt MCR mit HS-CoB_6 als Substrat weniger als 1% der Aktivität (Horng et al. 2001). Im

Falle von HS-CoB_6 wurde zudem, bezogen auf die Spinkonzentration pro mol F_{430}, etwa 2/3 weniger an MCR-red2-Signal induziert verglichen mit den induzierten MCR-red2-Signalen durch HS-CoB oder CH_3-S-CoB. HS-CoB-Analoga wie *N*-8-Mercaptooctanoylthreoninphosphat (HS-CoB_8) oder *N*-Nonanoylthreoninphosphat (CH_3-CH_2-CoB; kurz: Desulfamethyl-CoB) können bezüglich einer Induktion des MCR-red2-Zustandes nicht für HS-CoB substituieren (diese Arbeit; Mahlert et al. 2002b) (Abb. 14). Zusammenfassend zeigt sich damit, daß zumindest für die Induktion des MCR-red2-Zustandes die freie Thiolgruppe von Coenzym B nicht benötigt wird. Statt dessen könnte die Position des Schwefels im aliphatischen Arm eine Rolle spielen. Dagegen scheint eine freie Thiolgruppe an einer geeigneten Position essentiell zu sein, sowohl für die Reduktion von Methyl-Coenzym M zu Methan, als auch für die Umwandlung von MCR-red2 in den MCR-ox3-Zustand nach Sauerstoffexposition. Dies würde eine Erklärung dafür liefern, warum ein durch CH_3-S-CoB induziertes MCR-red2-Signal nach Inkubation mit O_2 in den EPR-silent- und nicht in den ox3-Zustand übergeht (Mahlert et al. 2002b).

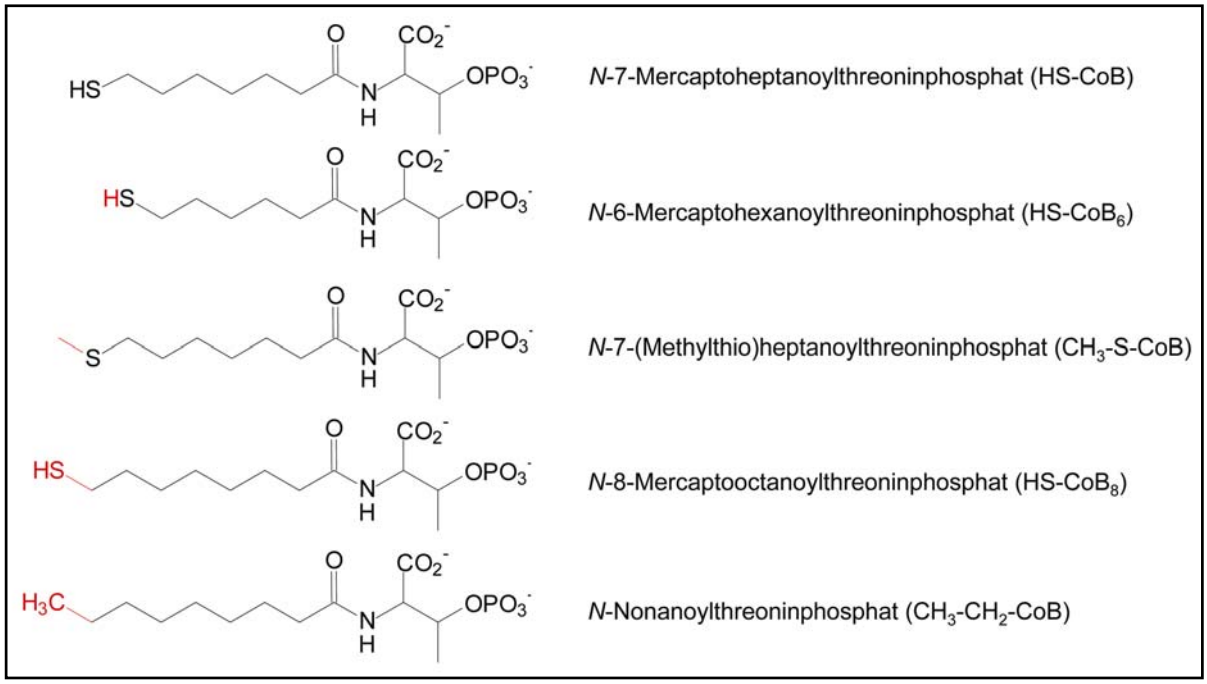

Abb. 14: Strukturen von Coenzym B und dessen in dieser Arbeit erwähnten Analoga. Von Coenzym B abweichende Bereiche wurden mit Rot gekennzeichnet.

Bereits erwähnt wurde auch die für einen makrozyklischen Ni(I)-Komplex eher ungewöhnliche Rhombizität des MCR-red2-Signals. Rhombische Ni(I)-EPR-Signale wurden aber beispielsweise für 5- oder 6-fach koordinierte Ni(I)-Thiaporphyrine nachgewiesen (Chmielewski et al. 1989). Sowohl das rhombische MCR-red2- als auch das axiale MCR-ox1-

Signal basieren auf hexakoordinierten Nickel. Ihre spektroskopischen Unterschiede können sich dadurch erklären lassen, daß die MCR-red2-Form um 1 Elektron stärker reduziert ist und der Makrozyklus möglicherweise signifikant verzerrt ist, entweder elektronisch oder geometrisch (Duin et al. 2004). In MCR-red2 könnte also die Konformation von Ni(I)F_{430} nach Bindung von Coenzym B unsymmetrisch werden, wodurch der g-Tensor rhombische Eigenschaften bekommen würde. Abgeleitet aus der festen Bindung von F_{430} in den Ni(II)-Kristallstrukturen (Ermler et al. 1997; Grabarse et al. 2000; Grabarse et al. 2001b) sind jedoch größere konformelle Änderungen am Nickelporphinoidsystem eher nicht zu erwarten. Vielmehr lassen ^{14}N- und ^{1}H-ENDOR-Daten (Finazzo et al. 2003b) zusammen mit dem Nachweis des Thioetherschwefels als axialer Ligand von Ni(I) vermuten, daß die untypischen g-Werte die Konsequenz einer Mischung aus verschiedenen Grundzuständen, in welchem das ungepaarte Elektron aufgrund der axialen Koordinierung des Nickels zu einem hohen Prozentsatz im d_{z2}-Orbital lokalisiert vorliegt.

Einen weiteren Aspekt zum MCR-red2-Signal bietet das Ausmaß der Induktion durch Coenzym M und Coenzym B. Hier beschriebene Untersuchungen zeigten, daß lediglich 50% des ursprünglichen MCR-red1-Signals in das MCR-red2-Signal umgewandelt werden. Dies könnte verschieden Ursachen haben: (i) in 50% aller MCR-Moleküle befinden sich beide aktive Zentren im red1- oder im red2-Zustand; (ii) alle MCR-Moleküle besitzen jeweils ein aktives Zentrum im red1- und das andere im red2-Zustand. Die Tatsache, daß bei Temperaturen über 20°C keine Änderung des 50:50 Verhältnisses von red1 und red2 stattfindet, spricht eher für letzteres. Demnach befinden sich nach Zugabe von Coenzym M und Coenzym B alle MCR-Moleküle im red1/2-Zustand, was auf eine Halbseitenreaktivität von MCR schließen läßt (Levitzki et al. 1971). Die aktive Beteiligung von nur einer Hälfte der zur Verfügung stehenden Reaktionszentren an der Katalyse ist bereits für zahlreiche multimere Enzyme bekannt. Beispiele hierfür sind die Cytidintriphosphat(CTP)-Synthase, 5-Phosphoribose-1-diphosphat(PRPP)-Aminotransferase und Glutamin-Synthase (Walsh 1979), der Pyruvat-Dehydrogenasecomplex (Khailova and Korochkina 1985) und Aldehyd-Dehydrogenase (Zhou and Weiner 2000; Weiner et al. 2001). Entgegen der Definition einer Halbseitenreaktivität scheint jedoch der red1-Anteil (g_z = 2,27; g_y = 2,08; g_x = 2,07) im MCR-red1/2-Zustand nicht mit dem red1 (g_z = 2,25; g_y = 2,07; g_x = 2,06) im MCR-red1/1-Zustand vor Zugabe des Coenzym B zu entsprechen. Neben leichten Differenzen in den g-Werten der Signale oder den MCD-Spektren vor allem im Bereich von 800 nm (Duin et al. 2004) zeigen beide red1-Formen ein unterschiedliches Verhalten bei Oxidation durch Polysulfid, Sulfit und O_2. Während das red1-Signal des MCR-red1c-Zustandes

in allen drei Fällen EPR-silent wird, wandelt sich MCR-red1/2 bis zu 80% in die MCR-Zustände ox1, ox2 oder ox3 um (Mahlert et al. 2002b). Dies führt zu dem Schluß, daß sowohl der red1-, als auch der red2-Anteil in MCR-red1/2 in die ox-Zustände überführt wird. Eine nicht 100%ige Umwandlung von MCR-red1/2 in MCR-ox ließe sich nachvollziehen, wenn ein Gleichgewicht zwischen MCR-red1/1 und MCR-red1/2 vorläge, wobei eben MCR-red1/1 in Gegenwart der Oxidanten in MCR-silent übergeht.

Aus den bislang erhältlichen Kristallstrukturen von MCR wird deutlich, daß die Reduktion von Methyl-Coenzym M mit Coenzym B innerhalb einer hydrophoben Tasche unter vollständigem Ausschluß von Wasser stattfindet (Ermler et al. 1997; Grabarse et al. 2001b). Im Anschluß an die Reaktion muß das entstandene Heterodisulfid, das am unteren Ende des Substratkanals über die Sulfonatgruppe mit dem Nickelatom von F_{430} koordiniert ist und am oberen Ende immer noch mit seiner Threoninphosphatgruppe an der Proteinmatrix gebunden ist, in die Wasserphase außerhalb des Enzyms freigesetzt werden. Unter anderem kann dazu die Abstoßung zwischen Ni(I) und der Sulfonatfunktion bis zu einem gewissen Grad genutzt werden. Zusätzlich ist möglicherweise eine konformelle Änderung der Enzymstruktur nötig, welche im Katalysemechanismus einen der exergonen Schritte darstellen würde (Pelmenschikov et al. 2002; Pelmenschikov and Siegbahn 2003). Solch eine Konformationsänderung betrifft entweder direkt das aktive Zentrum, in welchem die exergone Reaktion stattfindet, oder aber durch eine Übertragung über die α-Untereinheit des Enzyms das zweite aktive Zentrum. Die zuvor beschriebene Halbseitenreaktivität von MCR würde letzteres befürworten. Damit ließe sich für MCR ein Modell definieren, das nach dem Prinzip eines Zweitaktmotors funktioniert: Die Bindung von Methyl-Coenzym M und Coenzym B in einem Reaktionszentrum führt zur Induktion einer Konformationsänderung, welche nötig ist, um das Produkt CoM-S-S-CoB im anderen Reaktionszentrum in die Wasserphase zu entlassen (Abb. 15). Zweitaktmotormechanismen wurden bereits für das Chaperonsystem GroEL/GroES (Lorimer 1997) und für das 20S Proteasom (Hutschenreiter et al. 2004) beschrieben.

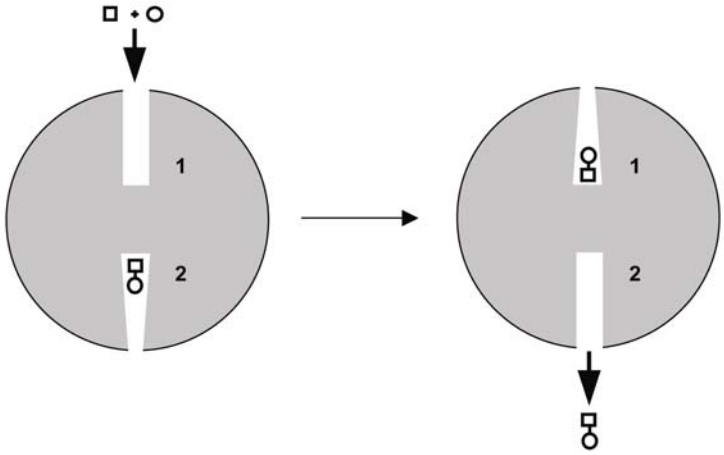

Abb. 15: Zweitaktmotor-Modell für MCR. Das Schema zeigt die beiden aktiven Zentren (1) und (2) des Enzymmoleküls. Die Bindung von Methyl-Coenzym M (□) und Coenzym B (○) in einem aktiven Zentrum induziert eine Konformationsänderung, die im zweiten aktiven Zentrum zur Entlassung des Produkts Heterodisulfid (○-□) in die Wasserphase führt.

Sogenannte Stopped-flow/freeze-quench-Experimente, die zeigen könnten, daß die Konzentration der Intermediate im Katalysezyklus mit einer doppelt so hohen Frequenz wechseln wie die Umsatzrate des Enzyms, sollten ein solches Zweitaktermodell festigen. Möglicherweise aufgrund der Schnelligkeit der Enzymreaktion sind Versuche zur Identifizierung der Intermediate bislang fehlgeschlagen. So könnten zukünftige Ansätze in Anlehnung an die Befunde dieser Arbeit niedrige Temperaturen, sowie Ethyl-Coenzym M und HS-CoB_6 als Substrate nutzen, um eine verringertere Umsatzrate des Enzyms zu erreichen.

Die Identifizierung von Intermediaten würde zur entgültige Aufklärung des Katalysemechanismus von MCR maßgeblich beitragen. Die aktuell diskutierten Mechanismen konnten bislang weder eindeutig bestätigt noch widerlegt werden, sie dürften aber teilweise dem tatsächlichen Reaktionsmechanismus schon sehr nahe kommen. Die in dieser Arbeit erzielten Ergebnisse lassen sich jedoch überwiegend mit Mechanismus I vereinbaren. Weitere Erkenntnisse zum Reaktionsmechanismus sollten vor allem mit zeitlich hochauflösende Methoden möglich sein.

VI Literaturverzeichnis

Aasa R, Vanngard T, Dunford HB (1975) EPR studies on compound I of horseradish peroxidase. Biochim Biophys Acta **391**:259-264

Ahn Y, Krzycki JA, Floss HG (1991) Steric course of the reduction of ethyl coenzyme M to ethane catalyzed by methyl-coenzyme M reductase from *Methanosarcina barkeri*. J Am Chem Soc **113**:4700-4701

Albracht SPJ, Ankel-Fuchs D, van der Zwaan JW, Fontijn RD, Thauer RK (1986) A new EPR signal of nickel in *Methanobacterium thermoautotrophicum*. Biochim Biophys Acta **870**:50-57

Albracht SPJ, Ankel-Fuchs D, Böcher R, Ellermann J, Moll J, van der Zwaan JW, Thauer RK (1988) Five new EPR signals assigned to nickel in methyl-coenzyme M reductase from *Methanobacterium thermoautotrophicum,* strain Marburg. Biochim Biophys Acta **955**:86-102

Ankel-Fuchs D, Hüster R, Mörschel E, Albracht SPJ, Thauer RK (1986) Structure and function of methyl-coenzyme M reductase and of factor F_{430} in methanogenic bacteria. System Appl Microbiol **7**:383-387

Ankel-Fuchs D, Thauer RK (1986) Methane formation from methyl-coenzyme M in a system containing methyl-coenzyme M reductase, component B and reduced cobalamin. Eur J Biochem **156**:171-177

Becker DF, Ragsdale SW (1998) Activation of methyl-SCoM reductase to high specific activity after treatment of whole cells with sodium sulfide. Biochemistry **37**:2639-2647

Beinert H, Albracht SPJ (1982) New insights, ideas and unanswered questions concerning iron-sulfur clusters in mitochondria. Biochim Biophys Acta **683**:245-277

Bobik TA, Olson KD, Noll KM, Wolfe RS (1987) Evidence that the heterodisulfide of coenzyme M and 7-mercaptoheptanoyl threonine phosphate is a product of the methylreductase reaction in *Methanobacterium*. Biochem Biophys Res Commun **149**:455-460

Boetius A, Ravenschlag K, Schubert CJ, Rickert D, Widdel F, Gieseke A, Amann R, Jorgensen BB, Witte U, Pfannkuche O (2000) A marine microbial consortium apparently mediating anaerobic oxidation of methane. Nature **407**:623-626

Bonacker LG, Baudner S, Thauer RK (1992) Differential expression of the two methyl-coenzyme M reductases in *Methanobacterium thermoautotrophicum* as determined immunochemically via isoenzyme-specific antisera. Eur J Biochem **206**:87-92

Bonacker LG, Baudner S, Mörschel E, Böcher R, Thauer RK (1993) Properties of the two isoenzymes of methyl-coenzyme M reductase in *Methanobacterium thermoautotrophicum*. Eur J Biochem **217**:587-595

Bradford MM (1976) A rapid and sensitive method for the quantitation of microgram quantities of protein utilizing the principle of protein-dye binding. Anal Biochem **72**:248-254

Brenner MC, Zhang H, Scott RA (1993) Nature of the low activity of S-methyl-coenzyme M reductase as determined by active site titrations. J Biol Chem **268**:18491-18495

Bult CJ, White O, Olsen GJ, Zhou L, Fleischmann RD, Sutton GG, Blake JA, FitzGerald LM, Clayton RA, Gocayne JD, Kerlavage AR, Dougherty BA, Tomb JF, Adams MD, Reich CI, Overbeek R, Kirkness EF, Weinstock KG, Merrick JM, Glodek A, Scott JL, Geoghagen NS, Venter JC (1996) Complete genome sequence of the methanogenic archaeon *Methanococcus jannaschii*. Science **273**:1058-1073

Chmielewski P, Grzeszczuk M, Latos-Grazynski L, Lisowski J (1989) Studies of the reduction of the nickel(II) complex of 5,10,15,20-tetraphenyl-21-thiaporphyrin to form corresponding nickel(I) complexes. Inorg Chem **28**:3546-3552

Conrad R (1996) Soil microorganisms as controllers of atmospheric trace gases (H_2, CO, CH_4, OCS, N_2O, and NO). Microbiol Rev **60**:609-640

Craft JL, Horng YC, Ragsdale SW, Brunold TC (2004a) Nickel oxidation states of F_{430} cofactor in methyl-coenzyme M reductase. J Am Chem Soc **126**:4068-4069

Craft JL, Horng YC, Ragsdale SW, Brunold TC (2004b) Spectroscopic and computational characterization of the nickel-containing F_{430} cofactor of methyl-coenzyme M reductase. J Biol Inorg Chem **9**:77-89

Daas PJ, Keltjens JT, Hagen WR, van der Drift C (1995) The electrochemistry of 5-hydroxybenzimidazolylcobamide. Arch Biochem Biophys **319**:244-249

Diekert G, Jaenchen R, Thauer RK (1980) Biosynthetic evidence for a nickel tetrapyrrole structure of factor F_{430} from *Methanobacterium thermoautotrophicum*. FEBS Lett **119**:118-120

Duin EC, Signor L, Piskorski R, Mahlert F, Clay MD, Goenrich M, Thauer RK, Jaun B, Johnson MK (2004) Spectroscopic investigation of the nickel-containing porphinoid cofactor F_{430}. Comparison of the free cofactor in the +1, +2 and +3 oxidation states with the cofactor bound to methyl-coenzyme M reductase in the silent, red and ox forms. J Biol Inorg Chem **9**:563-576

Ekberg M, Potsch S, Sandin E, Thunnissen M, Nordlund P, Sahlin M, Sjoberg BM (1998) Preserved catalytic activity in an engineered ribonucleotide reductase R2 protein with a nonphysiological radical transfer pathway. The importance of hydrogen bond connections between the participating residues. J Biol Chem **273**:21003-21008

Ellefson WL, Wolfe RS (1981) Component C of the methylreductase system of *Methanobacterium*. J Biol Chem **256**:4259-4262

Ellefson WL, Whitman WB, Wolfe RS (1982) Nickel-containing factor F_{430}: Chromophore of the methylreductase of *Methanobacterium*. Proc Natl Acad Sci USA **79**:3707-3710

Ellermann J, Kobelt A, Pfaltz A, Thauer RK (1987) On the role of *N*-7-mercaptoheptanoyl-*O*-phospho-*L*-threonine (component B) in the enzymatic reduction of methyl-coenzyme M to methane. FEBS Lett **220**:358-362

Ellermann J, Hedderich R, Böcher R, Thauer RK (1988) The final step in methane formation. Investigations with highly purified methyl-CoM reductase (component C) from *Methanobacterium thermoautotrophicum* (strain Marburg). Eur J Biochem **172**:669-677

Ermler U, Grabarse W, Shima S, Goubeaud M, Thauer RK (1997) Crystal structure of methyl-coenzyme M reductase: the key enzyme of biological methane formation. Science **278**:1457-1462

Färber G, Keller W, Kratky C, Jaun B, Pfaltz A, Spinner C, Kobelt A, Eschenmoser A (1991) Coenzyme F_{430} from methanogenic bacteria: Complete assignment of configuration based on an X-ray analysis of 12,13-diepi-F_{430} pentamethyl ester and on NMR spectroscopy. Helv Chim Acta **74**:697-716

Ferry JG (1999) Enzymology of one-carbon metabolism in methanogenic pathways. FEMS Microbiol Rev **23**:13-38

Finazzo C, Harmer J, Bauer C, Jaun B, Duin EC, Mahlert F, Goenrich M, Thauer RK, Van Doorslaer S, Schweiger A (2003a) Coenzyme B induced coordination of coenzyme M via its thiol group to Ni(I) of F_{430} in active methyl-coenzyme M reductase. J Am Chem Soc **125**:4988-4989

Finazzo C, Harmer J, Jaun B, Duin EC, Mahlert F, Thauer RK, Van Doorslaer S, Schweiger A (2003b) Characterization of the MCR_{red2} form of methyl-coenzyme M reductase: a pulse EPR and ENDOR study. J Biol Inorg Chem **8**:586-593

Ghosh A, Wondimagegn T, Ryeng H (2001) Deconstructing F_{430}: quantum chemical perspectives of biological methanogenesis. Curr Opin Chem Biol **5**:744-750

Goenrich M, Mahlert F, Duin EC, Bauer C, Jaun B, Thauer R. K (2004) Probing the reactivity of Ni in the active site of methyl-coenzyme M reductase with substrate analogues. J Biol Inorg Chem **im Druck**

Goubeaud M, Schreiner G, Thauer RK (1997) Purified methyl-coenzyme M reductase is activated when the enzyme-bound coenzyme F_{430} is reduced to the nickel(I)oxidation state by titanium(III) citrate. Eur J Biochem **243**:110-114

Grabarse W, Mahlert F, Shima S, Thauer RK, Ermler U (2000) Comparison of three methyl-coenzyme M reductases from phylogenetically distant organisms: Unusual amino acid modification, conservation and adaptation. J Mol Biol **303**:329-344

Grabarse W, Mahlert F, Duin EC, Goubeaud M, Shima S, Thauer RK, Lamzin V, Ermler U (2001a) On the mechanism of biological methane formation: Structural evidence for conformational changes in methyl-coenzyme M reductase upon substrate binding. J Mol Biol **309**:315-330

Grabarse W, Shima S, Mahlert F, Duin EC, Thauer RK, Ermler U (2001b) Methyl-coenzyme M reductase. John Wiley & Sons, Chichester, pp 897-914

Gunsalus RP, Romesser JA, Wolfe RS (1978) Preparation of coenzyme M analogues and their activity in the methyl-coenzyme M reductase system of *Methanobacterium thermoautotrophicum*. Biochemistry **17**:2374-2377

Hallam SJ, Girguis PR, Preston CM, Richardson PM, DeLong EF (2003) Identification of methyl-coenzyme M reductase A (mcrA) genes associated with methane-oxidizing archaea. Appl Environ Microbiol **69**:5483-5491

Hartzell PL, Wolfe RS (1986) Requirement of the nickel tetrapyrrole F_{430} for *in vitro* methanogenesis: Reconstitution of methylreductase component C from its dissociated subunits. Proc Natl Acad Sci USA **83**:6726-6730

Hedderich R, Thauer RK (1988) *Methanobacterium thermoautotrophicum* contains a soluble enzyme system that specifically catalyzes the reduction of the heterodisulfide of

coenzyme M and 7-mercaptoheptanoylthreonine phosphate with H_2. FEBS Lett **234**:223-227

Hogenkamp HPC, Bratt GT, Sun S (1985) Methyl transfer from methylcobalamin to thiols. A reinvestigation. Biochemistry **24**:6428-6432

Holliger C, Kengen SW, Schraa G, Stams AJ, Zehnder AJ (1992) Methyl-coenzyme M reductase of *Methanobacterium thermoautotrophicum* Δ H catalyzes the reductive dechlorination of 1,2-dichloroethane to ethylene and chloroethane. J Bacteriol **174**:4435-4443

Holliger C, Pierik AJ, Reijerse EJ, Hagen WR (1993) A spectrochemical study of factor F_{430} nickel (II/I) from methanogenic bacteria in aqueous solution. J Am Chem Soc **115**:5651-5656

Holmgren A (1988) Thioredoxin and glutaredoxin – small multi-functional redox proteins with active-site disulfide bonds. Biochem Soc Trans **16**:95-96

Horng YC, Becker DF, Ragsdale SW (2001) Mechanistic studies of methane biogenesis by methyl-coenzyme M reductase: evidence that coenzyme B participates in cleaving the C-S bond of methyl-coenzyme M. Biochemistry **40**:12875-12885

Hutschenreiter S, Tinazli A, Model K, Tampe R (2004) Two-substrate association with the 20S proteasome at single-molecule level. EMBO J **23**:2488-2497

Jaun B (1990) Coenzyme F_{430} from methanogenic bacteria: oxidation of F_{430} pentamethyl ester to the Ni(III) form. Helv Chim Acta **73**:2209-2217

Jaun B (1993) Methane formation by methanogenic bacteria: redox chemistry of coenzyme F_{430}. In: Sigel H, Sigel A (eds) Metal ions in biological systems. Marcel Dekker, New York, pp 287-337

Jaun B, Pfaltz A (1986) Coenzyme F_{430} from methanogenic bacteria: reversible one-electron reduction of F_{430} pentamethyl ester to the nickel(I) form. J Chem Soc, Chem Commun:1327-1329

Jaun B, Pfaltz A (1988) Coenzyme F_{430} from methanogenic bacteria: methane formation by reductive carbon-sulphur bond cleavage of methyl sulphonium ions catalysed by F_{430} pentamethyl ester. J Chem Soc, Chem Commun:293-294

Jetten MSM, Stams AJM, Zehnder AJB (1990) Purification and some properties of the methyl-CoM reductase of *Methanothrix soehngenii*. FEMS Microbiol Lett **66**:183-186

Kandror II, Kopylova BV, Freidlina RK (1984) Radical reactions of thioamides, thioureas, and related compounds. Sulfur Reports **3**:289-320

Khailova LS, Korochkina LG (1985) Half-of-the-site reactivity of the decarboxylating component of the pyruvate dehydrogenase complex from pigeon breast muscle with respect to 2-hydroxyethyl thiamine pyrophosphate. Biochem Int **11**:509-516

Klimmek O, Kroeger A, Steudel R, Holdt G (1991) Growth of *Wolinella succinogenes* with polysulfide as terminal acceptor of phosphorylative electron transport. Arch Microbiol **155**:177-182

Kobelt A, Pfaltz A, Ankel-Fuchs D, Thauer RK (1987) The L-form of *N*-7-mercaptoheptanoyl-*O*-phosphothreonine is the enantiomer active as component B in methyl-CoM reduction to methane. FEBS Lett **214**:265-268

Kolberg M, Strand KR, Graff P, Andersson KK (2004) Structure, function, and mechanism of ribonucleotide reductases. Biochim Biophys Acta **1699**:1-34

Krüger M, Meyerdierks A, Glockner FO, Amann R, Widdel F, Kube M, Reinhardt R, Kahnt J, Bocher R, Thauer RK, Shima S (2003) A conspicuous nickel protein in microbial mats that oxidize methane anaerobically. Nature **426**:878-881

Lehmacher A, Klenk HP (1994) Characterization and phylogeny of mcrII, a gene cluster encoding an isoenzyme of methyl coenzyme M reductase from hyperthermophilic *Methanothermus fervidus*. Mol Gen Genet **243**:198-206

Levitzki A, Stallcup WB, Koshland DE (1971) Half-of-sites reactivity and conformational states of cytidine triphosphate synthetase. Biochemistry **10**:3371

Lexa D, Saveant JM (1983) The electrochemistry of vitamin B_{12}. Acc Chem Res **16**:235-243

Lin S-K, Jaun B (1991) Coenzyme F_{430} from methanogenic bacteria: detection of a paramagnetic methylnickel(II) derivative of the pentamethyl ester by ^{2}H-NMR spectroscopy. Helv Chim Acta **74**:1725-1738

Lin S-K, Jaun B (1992) Coenzyme F_{430} from methanogenic bacteria: mechanistic studies on the reductive cleavage of sulfonium ions catalyzed by F_{430} pentamethyl ester. Helv Chim Acta **75**:1478-1490

Lind J, Shen X, Eriksen TE, Merenyi G (1990) The one-electron reduction potential of 4-substituted phenoxyl radicals in water. J Am Chem Soc **112(2)**: 479-482

Lorimer G (1997) Protein folding. Folding with a two-stroke motor. Nature **388**:720-721, 723

Mahlert F, Grabarse W, Kahnt J, Thauer RK, Duin EC (2002a) The nickel enzyme methyl-coenzyme M reductase from methanogenic archaea: *in vitro* interconversions among the EPR detectable MCR-red1 and MCR-red2 states. J Biol Inorg Chem **7**:101-112

Mahlert F, Bauer C, Jaun B, Thauer RK, Duin EC (2002b) The nickel enzyme methyl-coenzyme M reductase from methanogenic archaea: In vitro induction of the nickel-based MCR-ox EPR signals from MCR-red2. J Biol Inorg Chem **7**:500-513

Nauhaus K, Boetius A, Kruger M, Widdel F (2002) *In vitro* demonstration of anaerobic oxidation of methane coupled to sulphate reduction in sediment from a marine gas hydrate area. Environ Microbiol **4**:296-305

Noll KM, Donnelly MI, Wolfe RS (1987) Synthesis of *N*-7-mercaptoheptanoylthreonine phosphate and its activity in the methylcoenzyme M methylreductase system. J Biol Chem **262**:513-515

Nölling J, Pihl TD, Vriesema A, Reeve JN (1995) Organization and growth phase-dependent transcription of methane genes in two regions of the *Methanobacterium thermoautotrophicum* genome. J Bacteriol **177**:2460-2468

Nordlund P, Aberg A, Uhlin U, Eklund H (1993) Crystallographic investigations of ribonucleotide reductase. Biochem Soc Trans **21**(3):735-738

Nordlund P, Sjoberg BM, Eklund H (1990) Three-dimensional structure of the free radical protein of ribonucleotide reductase. Nature **345**:593-598

Olson KD, McMahon CW, Wolfe RS (1991) Photoactivation of the 2-(methylthio)ethanesulfonic acid reductase from *Methanobacterium*. Proc Natl Acad Sci USA **88**:4099-4103

Palmer G (2000) Electron paramagnetic resonance of metalloproteins. In: Que L (ed) Physical methods in bioinorganic chemistry. University science books, Sausalito, pp 121-185

Pelmenschikov V, Blomberg MR, Siegbahn PE, Crabtree RH (2002) A mechanism from quantum chemical studies for methane formation in methanogenesis. J Am Chem Soc **124**:4039-4049

Pelmenschikov V, Siegbahn PE (2003) Catalysis by methyl-coenzyme M reductase: a theoretical study for heterodisulfide product formation. J Biol Inorg Chem **8**:653-662

Pfaltz A, Jaun B, Fässler A, Eschenmoser A, Jaenchen R, Gilles HH, Diekert G, Thauer RK (1982) Zur Kenntnis des Faktors F_{430} aus methanogenen Bakterien; Struktur des porphinoiden Ligandsystems. Helv Chim Acta **65**:828-865

Piskorski R, Jaun B (2003) Direct determination of the number of electrons needed to reduce coenzyme F_{430} pentamethyl ester to the Ni(I) species exhibiting the electron paramagnetic

resonance and ultraviolet-visible spectra characteristic for the MCR_{red1} state of methyl-coenzyme M reductase. J Am Chem Soc **125**:13120-13125

Rospert S, Linder D, Ellermann J, Thauer RK (1990) Two genetically distinct methyl-coenzyme M reductases in *Methanobacterium thermoautotrophicum* strain Marburg and ΔH. Eur J Biochem **194**:871-877

Rospert, S (1991) ESR-Eigenschaften der Methyl-CoM-Reduktase aus *Methanobacterium thermoautotrophicum* und ihre Korrelation zur Enzymaktivität. **Dissertation**, Philipps-Universität Marburg

Rospert S, Böcher R, Albracht SPJ, Thauer RK (1991a) Methyl-coenzyme M reductase preparations with high specific activity from H_2-preincubated cells of *Methanobacterium thermoautotrophicum*. FEBS Lett **291**:371-375

Rospert S, Breitung J, Ma K, Schwörer B, Zirngibl C, Thauer RK, Linder D, Huber R, Stetter KO (1991b) Methyl-coenzyme M reductase and other enzymes involved in methanogenesis from CO_2 and H_2 in the extreme thermophile *Methanopyrus kandleri*. Arch Microbiol **156**:49-55

Rospert S, Voges M, Berkessel A, Albracht SPJ, Thauer RK (1992) Substrate-analogue-induced changes in the nickel EPR spectrum of active methyl-coenzyme-M reductase from *Methanobacterium thermoautotrophicum*. Eur J Biochem **210**:101-107

Schauder R, Mueller E (1993) Polysulfide as a possible substrate for sulfur-reducing bacteria. Arch Microbiol **160**:377-382

Schönheit P, Moll J, Thauer RK (1980) Growth parameters (K_S, μ_{max}, Y_S) of *Methanobacterium thermoautotrophicum*. Arch Microbiol **127**:59-65

Segel IH (1993) Enzyme kinetics: behavior and analysis of rapid equilibrium and steady-state enzyme systems. John Wiley & Sons, Chichester

Selmer T, Kahnt J, Goubeaud M, Shima S, Grabarse W, Ermler U, Thauer RK (2000) The biosynthesis of methylated amino acids in the active site region of methyl-coenzyme M reductase. J Biol Chem **275**:3755-3760

Shim SC, Lee SJ (1988) Rotational photoisomerization of a thioamide, *N*-5-trifluoromethyl-6-methoxy-1-thionaphthoyl-*N*-methylglycine. B Kor Chem Soc **9**:236-240

Smith DR, Doucette-Stamm LA, Deloughery C, Lee H, Dubois J, Aldredge T, Bashirzadeh R, Blakely D, Cook R, Gilbert K, Harrison D, Hoang L, Keagle P, Lumm W, Pothier B, Qiu D, Spadafora R, Vicaire R, Wang Y, Wierzbowski J, Gibson R, Jiwani N, Caruso A, Bush D, Reeve JN (1997) Complete genome sequence of *Methanobacterium thermoautotrophicum* ΔH: functional analysis and comparative genomics. J Bacteriol **179**:7135-7155

Stubbe J, van der Donk WA (1998) Protein radicals in enzyme catalysis. Chemical Reviews **98**:705-762

Stubbe J, Nocera DG, Yee CS, Chang MC (2003) Radical initiation in the class I ribonucleotide reductase: long-range proton-coupled electron transfer? Chem Rev **103**:2167-2201

Surdhar PS, Armstrong DA (1987) Reduction potentials and exchange-reactions of thiyl radicals and disulfide anion radicals. J Phys Chem **91(26)**:6532-6537

Tang Q, Carrington PE, Horng YC, Maroney MJ, Ragsdale SW, Bocian DF (2002) X-ray absorption and resonance Raman studies of methyl-coenzyme M reductase indicating that ligand exchange and macrocycle reduction accompany reductive activation. J Am Chem Soc **124**:13242-13256

Telser J, Horng YC, Becker DF, Hoffman BM, Ragsdale SW (2000) On the assignment of nickel oxidation states of the ox1, ox2 forms of methyl-coenzyme M reductase. Am Chem Soc **122**:182-183

Telser J, Davydov R, Horng YC, Ragsdale SW, Hoffman BM (2001) Cryoreduction of methyl-coenzyme M reductase: EPR characterization of forms, MCR_{ox1} and MCR_{red1}. J Am Chem Soc **123**:5853-5860

Thauer RK (1998) Biochemistry of methanogenesis: a tribute to Marjory Stephenson. Microbiology **144**:2377-2406

Uhlin U, Eklund H (1994) Structure of ribonucleotide reductase protein R1. Nature **370**:533-539

Wackett LP, Honek JF, Begley TP, Shames SL, Niederhoffer EC, Hausinger RP, Orme-Johnson WH, Walsh C (1988) Methyl-S-coenzyme-M reductase: A nickel-dependent enzyme catalyzing the terminal redox step in methane biogenesis. In: Lancaster J, JR (ed) The bioinorganic chemistry of nickel. VCH Publishers Inc., Weinheim, pp 249-274

Wackett LP, Honek JF, Begley TP, Wallace V, Orme-Johnson WH, Walsh CT (1987) Substrate analogues as mechanistic probes of methyl-S-coenzyme M reductase. Biochemistry **26**:6012-6018

Walsh C (1979) Enzymatic reaction mechanisms. In: Bartlett AC, McCombs LW (eds) Enzymatic reaction mechanisms. W. H. Freeman and Company, San Francisco

Wasserfallen A, Nolling J, Pfister P, Reeve J, Conway de Macario E (2000) Phylogenetic analysis of 18 thermophilic *Methanobacterium* isolates supports the proposals to create a new genus, *Methanothermobacter* gen. nov., and to reclassify several isolates in three species, *Methanothermobacter thermautotrophicus* comb. nov., *Methanothermobacter wolfeii* comb. nov., and *Methanothermobacter marburgensis* sp. nov. Int J System Evol Microbiol **50**(1):43-53

Weil JA, Bolton JR, Wertz JE (1994) Electron Paramagnetic Resonance: Elementary Theory and Practical Applications. John Wiley & Sons, Chichester

Weiner H, Wei B, Zhou J (2001) Subunit communication in tetrameric class 2 human liver aldehyde dehydrogenase as the basis for half-of-the-site reactivity and the dominance of the oriental subunit in a heterotetramer. Chem Biol Interact **130-132**:47-56

Wolfe RS (2004) Pistola di Volta. ASM News **70**:15-18

Wondimagegn T, Ghosh A (2001) Theoretical modeling of putative Ni(III)-F_{430} intermediates of methylcoenzyme M reductase. J Am Chem Soc **123**:1543-1544

Zhou J, Weiner H (2000) Basis for half-of-the-site reactivity and the dominance of the K487 oriental subunit over the E487 subunit in heterotetrameric human liver mitochondrial aldehyde dehydrogenase. Biochemistry **39**:12019-12024

VII Anhang

Weitere Ergebnisse, die in dieser Dissertation nicht aufgegriffen wurden, sind in folgenden Publikationen veröffentlicht worden:

Goenrich M, Bartoschek S, Hagemeier CH, Griesinger C, Vorholt JA (2001) A glutathione-dependent formaldehyde activating enzyme Gfa from *Paracoccus denitrificans* detected and purified via 2D proton exchange NMR spectroscopy. J Biol Chem **277**(5): 3069-3072

Goenrich M, Bursy J, Hübner E, Linder D, Schwartz AC, Vorholt JA (2001) The methylene tetrahydromethanopterin dehydrogenase MtdB and the methylene tetrahydrofolate dehydrogenase FolD from *Hyphomicrobium zavarzinii* ZV580. Arch Microbiol **177**(4): 299-303

Acharya P, Goenrich M, Hagemeier CH, Demmer U, Vorholt JA, Thauer RK, Ermler U (2004) How an enzyme binds the C_1-carrier tetrahydromethanopterin: Structure of the tetrahydromethanopterin-dependent formaldehyde-activating enzyme Fae from *Methylobacterium extorquens* AM1. EMBO J **eingereicht**

Accelerated Publication

THE JOURNAL OF BIOLOGICAL CHEMISTRY
Vol. 277, No. 5, Issue of February 1, pp. 3069–3072, 2002

A Glutathione-dependent Formaldehyde-activating Enzyme (Gfa) from *Paracoccus denitrificans* Detected and Purified via Two-dimensional Proton Exchange NMR Spectroscopy*[S]

Received for publication, October 5, 2001, and in revised form, December 3, 2001
Published, JBC Papers in Press, December 10, 2001,
DOI 10.1074/jbc.C100579200

Meike Goenrich‡§, Stefan Bartoschek‡§¶‖, Christoph H. Hagemeier‡, Christian Griesinger¶, and Julia A. Vorholt‡ ‡‡**

From the ‡Max-Planck-Institut für terrestrische Mikrobiologie, Karl-von-Frisch-Strasse, 35043 Marburg, Germany, the ¶Institut für Organische Chemie der Universität Frankfurt, Marie-Curie-Strasse 11, 60439 Frankfurt a.M., Germany, and the Max-Planck-Institut für biophysikalische Chemie, Am Fassberg 11, 37077 Göttingen, Germany

The formation of *S*-hydroxymethylglutathione from formaldehyde and glutathione is a central reaction in the consumption of the cytotoxin formaldehyde in some methylotrophic bacteria as well as in many other organisms. We describe here the discovery of an enzyme from *Paracoccus denitrificans* that accelerates this spontaneous condensation reaction. The rates of *S*-hydroxymethylglutathione formation and cleavage were determined under equilibrium conditions via two-dimensional proton exchange NMR spectroscopy. The pseudo first order rate constants k_1* were estimated from the temperature dependence of the reaction and the signal to noise ratio of the uncatalyzed reaction. At 303 K and pH 6.0 k_1* was found to be 0.02 s^{-1} for the spontaneous reaction. A 10-fold increase of the rate constant was observed upon addition of cell extract from *P. denitrificans* grown in the presence of methanol corresponding to a specific activity of 35 units mg^{-1}. Extracts of cells grown in the presence of succinate revealed a lower specific activity of 11 units mg^{-1}. The enzyme catalyzing the conversion of formaldehyde and glutathione was purified and named glutathione-dependent formaldehyde-activating enzyme (Gfa). The gene *gfa* is located directly upstream of the gene for glutathione-dependent formaldehyde dehydrogenase, which catalyzes the subsequent oxidation of *S*-hydroxymethylglutathione. Putative proteins with sequence identity to Gfa from *P. denitrificans* are present also in *Rhodobacter sphaeroides*, *Sinorhizobium meliloti*, and *Mesorhizobium loti*.

Formaldehyde is a highly toxic compound due to nonspecific reactivity with proteins and nucleic acids (1). It is liberated as a result of demethylation reactions in mammals (2) or from environmental sources (3), and it is a central intermediate upon growth of methylotrophic bacteria on one-carbon substrates like methanol or methane (4). The most widespread enzymatic system for the conversion of formaldehyde is the glutathione (GSH)[1]-linked oxidation pathway, which has been found in bacteria, mammals, and plants. In autotrophic methylotrophic bacteria like *Paracoccus denitrificans* and *Rhodobacter sphaeroides* as well as methylotrophic yeasts, it is involved in the complete oxidation of methanol to carbon dioxide (5–8). In higher organisms, as well as non-methylotrophic bacteria, such as *Escherichia coli*, glutathione-linked formaldehyde oxidation serves to detoxify the one-carbon unit (9, 10).

The glutathione-dependent formaldehyde conversion to formate starts with the adduct formation, formaldehyde reacts with the SH group of glutathione producing *S*-hydroxymethylglutathione (Reaction 1) (11). This reaction is considered to proceed *in vivo* uncatalyzed by a specific enzyme (6, 7, 10, 11). The product of this reaction, *S*-hydroxymethylglutathione, is oxidized by glutathione-dependent formaldehyde dehydrogenase (GS-FDH) (Reaction 2), which belongs to the class III alcohol dehydrogenases and has been characterized from various organisms (6, 7, 9, 12). The enzyme has been shown to be induced upon formaldehyde stress in different microorganisms (10, 13). In the subsequent enzymatic reaction, *S*-formylglutathione hydrolase (FGH) regenerates glutathione and forms formate (Reaction 3) (14), which can be further oxidized to carbon dioxide.

$$GSH + HCHO \rightleftharpoons GSCH_2OH$$

REACTION 1

$$GSCH_2OH + NAD^+ \rightleftharpoons GSCHO + NADH + H^+ \text{ (GS-FDH)}$$

REACTION 2

$$GSCHO + H_2O \rightleftharpoons GSH + HCOOH \text{ (FGH)}$$

REACTION 3

In this study, we investigated whether the condensation of formaldehyde and glutathione (Reaction 1) proceeds indeed only non-enzymatically *in vivo*. We have chosen *P. denitrificans* as a model organism, since it is a facultative methylotroph and converts high amounts of formaldehyde during energy metabolism upon

* This work was supported by the Max-Planck-Gesellschaft, the Deutsche Forschungsgemeinschaft and the Fonds der Chemischen Industrie. All NMR measurements were conducted at the European Large Scale Facility for Biomolecular NMR (ERBCT95–0034) at the University of Frankfurt. The costs of publication of this article were defrayed in part by the payment of page charges. This article must therefore be hereby marked "*advertisement*" in accordance with 18 U.S.C. Section 1734 solely to indicate this fact.

[S] The on-line version of this article (available at http://www.jbc.org) contains Supplemental Figs. 2 and 3.

§ These authors contributed equally to this work.

‖ Supported by a Kekulé stipend of the Fonds der Chemischen Industrie.

** Supported by the Peter and Traudl Engelhorn Stiftung.

‡‡ To whom correspondence should be addressed: INRA/CNRS, BP27 Chemin de Borde Rouge, 31326 Castanet-Tolosan, France. Tel.: 33-5-61-28-54-58; Fax: 33-5-61-28-50-61; E-mail: vorholt@toulouse.inra.fr.

[1] The abbreviations used are: GSH, glutathione; Gfa, glutathione-dependent formaldehyde-activating enzyme; GS-FDH (or GD-FALDH), glutathione-dependent formaldehyde dehydrogenase; FGH, *S*-formylglutathione hydrolase; Fae, tetrahydromethanopterin-dependent formaldehyde-activating enzyme; EXSY, proton exchange NMR spectroscopy.

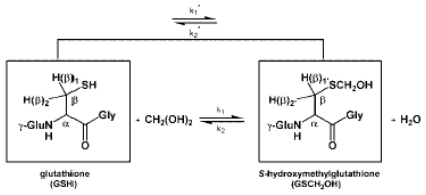

FIG. 1. **Formation of *S*-hydroxymethylglutathione ($GSCH_2OH$) from formaldehyde and GSH (γ-L-glutamyl-L-cysteinyl-glycine).** Two diasteriotopic protons at C_β have different chemical shifts and were used for the analysis of EXSY (see Fig. 2).

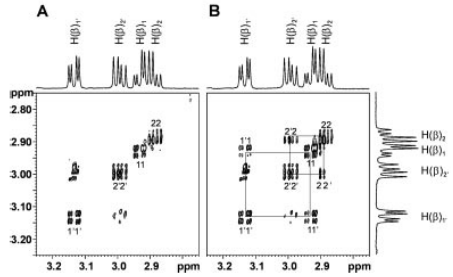

FIG. 2. **Aliphatic region of the one-dimensional and two-dimensional EXSY NMR spectra of the C_β protons of glutathione and *S*-hydroxmethylglutathione at equilibrium without (*A*) and with (*B*) cell extract from *P. denitrificans* at 303 K and pH 6.0.** Two-dimensional ^1H homonuclear EXSY NMR spectra (400 ms mixing time) are shown in the center and one-dimensional proton NMR spectra above and lateral. The signals $H(\beta)_1$ and $H(\beta)_2$ of the one-dimensional spectra are from protons of glutathione and the signals $H(\beta)_{1'}$ and $H(\beta)_{2'}$ from protons of *S*-hydroxymethylglutathione (Fig. 1). Diagonal peaks of the glutathione and *S*-hydroxymethylglutathione protons in chemical exchange are labeled with 11 and 1′1′ or 22 and 2′2′. Off-diagonal cross-peaks arising from chemical exchange are labeled with 1′1 and 11′ or 2′2 and 22′. These exchange cross-peaks are clearly visible in the presence of cell extract of *P. denitrificans* (1.04 mg), whereas in the absence of cell extract they are hardly detectable because of the signal to noise ratio (*B*). The NMR spectra were acquired at a ^1H frequency of 600.13 MHz on a DRX600 spectrometer (Bruker) and processed as described under "Experimental Procedures." The NMR tube (ϕ 5 mm) contained 0.6 ml of a reaction mixture made up of 10.8 mM glutathione, 5 mM formaldehyde, 60 μl of D_2O, 1.04 mg of cell extract protein of methanol grown *P. denitrificans* (*B*) in 120 mM potassium phosphate buffer, pH 6.0.

growth on methanol by glutathione-linked enzymes. Glutathione-dependent formaldehyde dehydrogenase and *S*-formylglutathione hydrolase have been shown to be essential for growth of the autotrophic bacterium in the presence of methanol (6, 14).

To determine *S*-hydroxymethylglutathione formation from formaldehyde and glutathione in *P. denitrificans*, we used proton exchange NMR spectroscopy (15). The method is based on the finding that the protons at the C_β atom of the thiol group of the cysteine part in glutathione and *S*-hydroxymethylglutathione exhibit different chemical shifts and that the saturation transfer kinetics of these protons can be followed by proton exchange NMR spectroscopy (EXSY) (Fig. 1). We used the two-dimensional EXSY approach to detect the activity of an previously unknown enzyme and used it for purification of the enzyme from cell extracts. To our knowledge this is the first time that EXSY has been successfully applied to find a previously unknown enzyme.

EXPERIMENTAL PROCEDURES

NMR Measurements—Rates of *S*-hydroxymethylglutathione formation from formaldehyde and glutathione were determined under equilibrium conditions via EXSY (16). NMR spectra were acquired at a ^1H frequency of 600.13 MHz on a DRX600 spectrometer (Bruker) and processed with the program XWINNMR (Bruker). The assays were performed in NMR tubes (ϕ 5 mm) with 0.6 ml of reaction mixture. Standard assays contained 10.8 mM GSH and 5 mM formaldehyde in 120 mM potassium phosphate buffer pH 6.0 (H_2O/D_2O = 9:1) if not otherwise noted. Exchange rates $v_1 = k_1^*[GSH] = v_2 = k_2^*[GSCH_2OH]$ (see Fig. 1) were calculated from the concentrations of GSH and $GSCH_2OH$ in equilibrium which were obtained by integration of one-dimensional spectra yielding the $[GSH]/[GSCH_2OH]$ ratio (see Fig. 2). From the ratios, the relative populations $p_{GSH} = [GSH]/([GSH] + [GSCH_2OH])$ and $p_{GSCH2OH} = [GSCH_2OH]/([GSH] + [GSCH_2OH])$ were calculated, whereby $[GSH] + [GSCH_2OH]$ equals the GSH concentration added. GSH was considered to be fully protonated, since measurements were performed between pH 5.5 and 6.5 and the pK_a of GSH is 9.12. The second order rate constants k_1 and k_2 were defined from k_1^* and k_2^* and the equilibrium concentration of formaldehyde: $v_1 = k_1[GSH][HCHO] = v_2 = k_2[GSCH_2OH][H_2O]$. $[H_2O]$ was considered to be constant, since measurements were performed in aqueous solution. The exchange rates v_1 and v_2 were calculated from the concentration of GSH, HCHO, and $GSCH_2OH$, and the rate constants k_1 and k_2, which are related to the relative populations p_{GSH} and $p_{GSCH2OH}$, and the peak volumes V_{ij} and the mixing time τ_m by the expression $V_{ij} = (\exp(-R\tau_m))_{ij}$. For definition of V_{ij} and R, see Ref. 16. The enzyme activities were calculated from the exchange rates v_1 of the $GSCH_2OH$ formation and converted from the unit mM s^{-1} to μmol min^{-1} (=1 unit).

Bacterial Growth and Enzyme Purification—*P. denitrificans* (DSM413), *E. coli* DH5α, and *Methylobacterium extorquens* AM1 were cultivated as described previously (4, 10). For enzyme purification from methanol-grown *P. denitrificans*, 20 g of wet cells were resuspended in 120 mM potassium phosphate buffer and broken by a French press. Purification of Gfa was performed by four chromatographic steps at 4 °C. The soluble fraction of the cell extract was loaded onto a DEAE-Sephacel (Sigma) column equilibrated with 50 mM potassium phosphate, pH 7.0. Protein was eluted with the following gradient steps of NaCl in this buffer: 60 ml of 0 mM, 60 ml of 150 mM, 60 ml of 200 mM, 60 ml of 250 mM, and 60 ml of 500 mM. Gfa was eluted at 150 mM NaCl. Active fractions were diluted 1:2 in 10 mM potassium phosphate buffer, pH 7.0, and loaded onto a hydroxyapatite column (Bio-Rad) equilibrated in the same buffer. Protein was eluted with a stepwise increasing potassium phosphate gradient (10–250 mM in 275 ml). Gfa was recovered in the flow-through of the column, which was subjected to chromatography on Q-Sepharose (Amersham Biosciences, Inc.) in 120 mM potassium phosphate buffer. Protein was eluted with an increasing gradient of NaCl (0–300 mM in 450 ml). Gfa was eluted at 60 mM NaCl. Active fractions were pooled and diluted 1:2 in 50 mM potassium phosphate buffer, pH 7.0, and loaded onto a Mono Q column (Amersham Biosciences, Inc.). Protein was eluted with an increasing gradient of NaCl in this buffer (0–500 mM in 100 ml). Gfa was eluted at 400 mM NaCl. GS-FDH was measured photometrically and purified as described previously (6).

RESULTS

In most organisms, the conversion of exogenous or endogenous formaldehyde proceeds by addition to glutathione prior to oxidation by GS-FDH. To address the question of whether an enzyme exists which catalyzes the formation of *S*-hydroxymethylglutathione from formaldehyde and glutathione, we analyzed cell extracts of *P. denitrificans* grown under methylotrophic conditions. The rates of formaldehyde-glutathione condensation were determined by one-dimensional and two-dimensional proton exchange NMR spectroscopy. Recording of the standard spectra was performed at pH 6.0, 303 K (30 °C) and under aerobic conditions, since *P. denitrificans* is an aerobic mesophilic bacterium. To increase the accuracy of the analysis, a product/educt ratio of 1:1 was aspired and achieved by using a ratio of glutathione to formaldehyde of 2:1 (10.8 mM glutathione, 5 mM formaldehyde). This ratio was used throughout this study.

In Fig. 2, the aliphatic regions of a one-dimensional proton NMR spectrum and a two-dimensional ^1H homonuclear EXSY NMR spectrum of glutathione and *S*-hydroxymethylglutathione at equilibrium, in the absence (*A*) and in the presence (*B*) of cell extract from methanol grown *P. denitrificans*, are shown. From the one-dimensional spectra, the relative populations p_{GSH} = 0.52 and $p_{GSCH2OH}$ = 0.48 were obtained by integration of the signals 1 and 1′ (Fig. 2, *A* and *B*). Integration of the signals 2 and 2′ yields the same values for both species. From the two-dimensional spectrum in the presence of cell extract (Fig. 2*B*) the peak volumes of the protons 1 and 2 were obtained and k_1^* = 0.24

TABLE I

Effect of cell extracts of different organisms on the rate of S-hydroxymethylglutathione formation in 120 mM potassium phosphate buffer, pH 6.0, and 303 K (30 °C)

The rates of *S*-hydroxymethylglutathione formation were determined under equilibrium conditions by EXSY and one-dimensional NMR spectroscopy. The experiments were performed in NMR tubes (∅ 5 mm). The 0.6-ml reaction mixture contained 10.8 mM glutathione, 5 mM formaldehyde, 60 μl of D_2O, and 1.04 mg of cell extract protein if not otherwise noted. Where indicated, denatured cell extract protein was applied, which was boiled for 5 min at 95 °C and centrifuged. A unit of enzyme activity was defined as the formation of 1 μmol of *S*-hydroxymethylglutathione from formaldehyde and glutathione per min minus the spontaneous reaction rate without enzyme added. The activity of GS-FDH is given as a control and was measured photometrically with NAD as electron acceptor to exclude an effect of the dehydrogenase on the exchange rates (6). For definition of k_1* and calculation of the activities, see "Experimental Procedures." LB, Luria-Bertani medium; ND = not detectable.

Conditions	$10^{-2}\ k_1$*	Activity	Specific activity	Specific activity GS-FDH
	s^{-1}	*units*	*units* mg^{-1}	*units* mg^{-1}
−Protein	2[a]	5		
+Cell extract				
P. denitrificans, grown on methanol	20	41	35	1.1
P. denitrificans, grown on methanol, ½ × protein	11	23	35	1.1
P. denitrificans, denatured	3[a]	6		
P. denitrificans, grown on succinate	8	16	11	<0.04
E. coli DH5α, grown on LB + formaldehyde (250 μM)	5	10	5	0.55
E. coli DH5α, grown on LB	4	9	4	0.05
M. extorguens AM1, grown on methanol	3[a]	6		ND

[a] Estimated from signal to noise ratio.

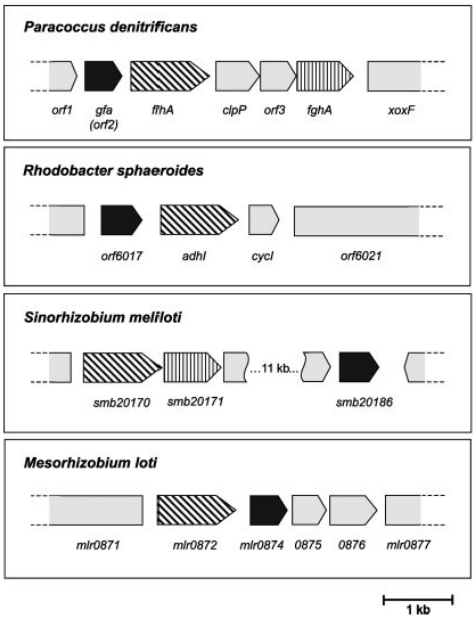

FIG. 3. **Comparison of the genomic arrangement of Gfa from *P. denitrifians* and putative proteins from the complete genomes of *R. sphaeroides*[2] and the symbiotic nitrogen-fixing bacteria *S. meliloti* (19) and *M. loti* (20).** The open reading frames for proteins with sequence identity to each other are marked with the same pattern. In *P. dentitrificans*, *gfa*, formerly *orf2* (6,14), encodes Gfa (this work); *flhA* encodes GS-FDH (or GD-FALDH) (6); and *fghA* encodes FGH (14). In *R. sphaeroides*, *adhI* was shown to encode GS-FDH (7) and is located downstream of an open reading frame with sequence identity to Gfa.[2] Putative proteins with sequence identity to Gfa from *P. denitrificans* could also be found in the currently unfinished genomes of *T. ferrooxidans* and *S. putrefaciens* (not shown).[3]

s^{-1} and k_2* = 0.21 s^{-1} calculated (16). From the data, an exchange rate v_1 was obtained corresponding to 41 units for the rate in the presence of cell extract of methanol grown *P. denitrificans*, which has 35 units mg^{-1} cell extract protein (Table I). Without cell extract (Fig. 2A) a spontaneous rate of only 5 units was determined. No increase in the spontaneous rate was observed if supernatant of denatured and centrifuged cell extract from *P. denitrificans* was applied, indicating that the observed activity is the result of enzyme catalysis. Addition of purified GS-FDH from *P. denitrificans*, which oxidizes *S*-hydroxymethylglutathione (Reaction 2), did not result in higher *S*-hydroxymethylglutathione formation from formaldehyde and glutathione (Table I). This shows that the observed acceleration is catalyzed by a separate enzyme distinct from GS-FDH. Analysis of cell extract of *P. denitrificans* grown in the presence of succinate revealed that enzymatic formaldehyde conversion is still clearly detectable with an activity of 11 units mg^{-1} amounting to one-third of the activity in comparison to cells grown in the presence of the one-carbon substrate. Activity of GS-FDH, which was measured as a control enzyme, was not detectable upon growth in the presence of succinate and shows a more pronounced effect of induction (Table I; Ref. 6).

The influence of temperature and pH upon the rate of *S*-hydroxymethylglutathione formation from formaldehyde and glutathione was analyzed. The rate of the spontaneous reaction *versus* the accelerated rate in the presence of cell extract of methanol-grown *P. denitrificans* was determined between 293 and 333 K (20–60 °C). In both cases, the rate of *S*-hydroxymethylglutathione formation increased about 3-fold when the temperature was raised from 293 K to 303 K (20 and 30 °C). The increase of the spontaneous rate was linear up to 333 K (60 °C), whereas determination of the enzyme-promoted rates, by addition of cell extract, above 323 K (50 °C) was not possible due to protein denaturation. Dependence of the pH on the rate of *S*-hydroxymethylglutathione formation was determined between pH 5.5 and 6.5. The spontaneous rate increased with higher pH; the rate k_1* without cell extract was only 0.03 s^{-1} at pH 5.5 and 0.45 s^{-1} at pH 6.5. In the presence of cell extract from *P. denitrificans* the rate was always higher. At pH values higher than 6.5 the determination was rather difficult due to instability of *S*-hydroxymethylglutathione *in vitro* (17).

The enzyme that catalyzes the formation of *S*-hydroxymethylglutathione, glutathione-dependent formaldehyde-activating enzyme, Gfa, was purified from *P. denitrificans* as described under "Experimental Procedures." The enzyme activity was detected via NMR measurements. After four chromatographic steps, preparations contained only one polypeptide with an apparent molecular mass of 21 kDa, as revealed by SDS-PAGE and exhibited a specific activity of 350 units mg^{-1}. Purification was about 24-fold with a yield of 6%. UV/visible spectroscopy did not reveal the presence of a chromophoric prosthetic group. The N-terminal amino acid sequence of the 21-kDa polypeptide was determined (MVDTSGVKIHPAVDNG; terminal methionine cleaved off to 90%) and matched exactly that predicted for the *orf2* gene product (6, 14). We now assign this gene as *gfa*. Gfa from *P. denitri-*

ficans shows high sequence identity to putative proteins known from the complete genome sequences of the α-proteobacteria *R. sphaeroides* (72%),[2] *Sinorhizobium meliloti* (75%) (19), and *Mesorhizobium loti* (61%) (20). Putative proteins with sequence identities of about 63% could also be identified in the currently unfinished genome sequences of the γ-proteobacteria *Thiobacillus ferrooxidans* and *Shewanella putrefaciens*.[3]

Interestingly, *gfa* from *P. denitrificans* is located directly upstream from *flhA* coding for GS-FDH (or GD-FALDH) (6) (Fig. 3). In *R. sphaeroides* (7)[2] and *T. ferrooxidans*,[3] the same arrangement of genes for the putative glutathione-dependent proteins could be found, whereas in *M. loti* the arrangement of the two genes is inverted (20). In *S. meliloti*, the genes for a putative Gfa and a putative GS-FDH are located about 13 kb apart on the pSymB megaplasmid (Fig. 3). This genome region also includes a putative methanol dehydrogenase structural gene (19). In *S. putrefaciens*, the gene for a protein with sequence identity to Gfa is located directly downstream of a putative iron containing alcohol dehydrogenase.[3] No more additional putative proteins with sequence identity to Gfa from *P. denitrificans* could be identified. Therefore Gfa is not conserved in all organisms that have been shown to contain GS-FDH, *i.e. E. coli* (10).

DISCUSSION

In this study, we detected and purified a novel glutathione-dependent formaldehyde-activating enzyme Gfa from the facultative methylotrophic bacterium *P. denitrificans*. The condensation of formaldehyde and glutathione to *S*-hydroxymethylglutathione is the first step in the widespread glutathione-linked conversion of formaldehyde and was thought to occur without enzymatic catalysis *in vivo*.

Gfa is not the first example of a protein that catalyzes the condensation of formaldehyde and a cofactor to form an adduct in the process of energy metabolism. It was recently shown that the methylotrophic proteobacterium *M. extorquens* AM1 possesses a tetrahydromethanopterin-linked formaldehyde-activating enzyme, Fae, which catalyzes the condensation of formaldehyde and tetrahydromethanopterin producing methylene tetrahydromethanopterin (22). Fae is present in all heterotrophic methylotrophic proteobacteria we tested that contain tetrahydromethanopterin-dependent enzymes.[4] Both formaldehyde-converting enzymes, Gfa and Fae, are composed of one type of subunit of about 20 kDa and lack a chromophoric prosthetic group. In addition, both enzymes are encoded next to genes for enzymes involved in further oxidation of the cofactor-bound one-carbon unit to carbon dioxide (6, 22). The primary sequences of Gfa and Fae do not reveal any sequence identity to each other and have obviously evolved independently, which is not too surprising, since the cofactors are very different, and binding of formaldehyde occurs either to the sulfur atom of glutathione or the N^5,N^{10} nitrogen atoms of tetrahydromethanopterin.

Tetrahydromethanopterin-dependent enzymes are restricted to methylotrophic proteobacteria and methanogenic archaea, whereas the glutathione-linked formaldehyde dehydrogenase is widespread in procarya and eucarya (6, 7, 9, 12). Nevertheless, the presence of Gfa appears to be limited. It might be that Gfa is present only in organisms that produce and consume large amounts of intracellular formaldehyde, whereas the spontaneous formation of *S*-hydroxymethylglutathione would be sufficient for detoxification of exogenous formaldehyde, which may occur in the environment. In this respect it is interesting to discuss the bacteria that contain a Gfa homolog. Methanol consumption of the nitrogen-fixing bacteria *S. meliloti* and *M. loti* appears likely, since they contain open reading frames for putative proteins with high sequence identity to Gfa as well as putative proteins for *S*-hydroxymethylglutathione oxidation and methanol dehydrogenase structural genes (19, 20). A functional active Gfa homolog could also be expected in *R. sphaeroides* where the role of glutathione-linked formaldehyde dehydrogenase has been shown under both photosynthetic and aerobic respiratory conditions (8). *S. putrefaciens* is able to grow anaerobically in the presence of formate and proposed to form free formaldehyde intracellulary (21). A *Thiobacillus* species, *Thiobacillus thioparus*, also forms formaldehyde upon growth on methyl mercaptan (18). The same might be true for *T. ferrooxidans*, which possesses putative proteins for Gfa and glutathione-linked formaldehyde dehydrogenase.

We cannot rule out that another glutathione-linked formaldehyde-activating enzyme might have evolved that is shared by other organisms. We observed a slight increase in *S*-hydroxymethylglutathione formation in cell extracts of *E. coli*, which was, however, not induced by formaldehyde stress like GS-FDH so that the presence of glutathione-linked formaldehyde activation could not be demonstrated.

At present it is not clear whether Gfa serves solely as an enzyme or can also serve as a formaldehyde scavenger to prevent unspecific binding of the toxin. In this respect, it is interesting to note that in *P. denitrificans*, Gfa activity could also be detected in cells grown in the absence of methanol, whereas activity of GS-FDH is not detectable under these growth conditions. Therefore it is likely that the corresponding genes are under the control of different promotors.

Acknowledgment—We thank Jochen Junker for revealing discussions.

REFERENCES

1. Grafstrom, R. C., Fornace, A. J. Jr., Autrup, H., Lechner, J. F., and Harris, C. C. (1983) *Science* **220,** 216–218
2. Jones, D. P., Thor, H., Andersson, B., and Orrenius, S. (1978) *J. Biol. Chem.* **253,** 6031–6037
3. Zimmerman, P. R., Chatfield, R. B., Fishman, J., Crutzen, P., and Hanst, P. L. (1978) *Geophys. Res. Lett.* **5,** 679–682
4. Vorholt, J. A., Chistoserdova, L., Stolyar, S. M., Thauer, R. K., and Lidstrom, M. E. (1999) *J. Bacteriol.* **181,** 5750–5757
5. Fernandez, M. R., Biosca, J. A., Norin, A., Jornvall, H., and Pares, X. (1995) *FEBS Lett.* **370,** 23–26
6. Ras, J., van Ophem, P. W., Reijnders, W. N., van Spanning, R. J., Duine, J. A., Stouthamer, A. H., and Harms, N. (1995) *J. Bacteriol.* **177,** 247–251
7. Barber, R. D., Rott, M. A., and Donohue, T. J. (1996) *J. Bacteriol.* **178,** 1386–1393
8. Barber, R. D., and Donohue, T. J. (1998) *Biochemistry* **37,** 530–537
9. Shafqat, J., Elahmad, M., Danielsson, O., Martinez, M. C., Persson, B., Pares, X., and Jornvall, H. (1996) *Proc. Natl. Acad. Sci. U. S. A.* **93,** 5595–5599
10. Gutheil, W. G., Kasimoglu, E., and Nicholson, P. C. (1997) *Biochem. Biophys. Res. Commun.* **238,** 693–696
11. Mason, R. P., Sanders, J. K., Crawford, A., and Hunter, B. K. (1986) *Biochemistry* **25,** 4504–4507
12. Uotila, L., and Koivusalo, M. (1981) *Methods Enzymol.* **77,** 314–320
13. van Ophem, P. W., and Duine, J. A. (1994) *FEMS Microbiol. Lett.* **116,** 87–94
14. Harms, N., Ras, J., Reijnders, W. N., van Spanning, R. J., and Stouthamer, A. H. (1996) *J. Bacteriol.* **178,** 6296–6299
15. Schleucher, J., Schwörer, B., Thauer, R. K., and Griesinger, C. (1995) *J. Am. Chem. Soc.* **117,** 2941–2947
16. Bartoschek, S., Vorholt, J. A., Thauer, R. K., Geierstanger, B. H., and Griesinger, C. (2000) *Eur. J. Biochem.* **267,** 3130–3138
17. Naylor, S., Mason, R. P., Sanders, J. K. M., Williams, D. H., and Monetti, G. (1988) *Biochem. J.* **249,** 573–579
18. Gould, W. D., and Kanagawa, T. (1992) *J. Gen. Microbiol.* **138,** 217–221
19. Finan, T. M., Weidner, S., Wong, K., Buhrmester, J., Chain, P., Vorhölter, F. J., Hernandez-Lucas, I., Becker, A., Cowie, A., Gouzy, J., Golding, B., and Pühler, A. (2001) *Proc. Natl. Acad. Sci. U. S. A.* **98,** 9889–9894
20. Kaneko, T., Nakamura, Y., Sato, S., Asamizu, E., Kato, T., Sasamoto, S., Watanabe, A., Idesawa, K., Ishikawa, A., Kawashima, K., Kimura, T., Kishida, Y., Kiyokawa, C., Kohara, M., Matsumoto, M., Matsuno, A., Mochizuki, Y., Nakayama, S., Nakazaki, N., Shimpo, S., Sugimoto, M., Takeuchi, C., Yamada, M., and Tabata, S. (2000) *DNA Res.* **7,** 331–338
21. Scott, J. H., and Nealson, K. H. (1994) *J. Bacteriol.* **176,** 3408–3411
22. Vorholt, J. A., Marx, C. J., Lidstrom, M. E., and Thauer, R. K. (2000) *J. Bacteriol.* **182,** 6645–6650

[2] Sequence data was obtained from the Oak Ridge National Laboratory webpage at genome.ornl.gov/microbial/rsph/.

[3] Preliminary sequence data was obtained from The Institute for Genomic Research website at www.tigr.org.

[4] M. Goenrich and J. A. Vorholt, unpublished results.

Arch Microbiol (2002) 177:299–303
DOI 10.1007/s00203-001-0394-y

ORIGINAL PAPER

Meike Goenrich · Jan Bursy · Eva Hübner
Dietmar Linder · Arnold C. Schwartz · Julia A. Vorholt

Purification and characterization of the methylene tetrahydromethanopterin dehydrogenase MtdB and the methylene tetrahydrofolate dehydrogenase FolD from *Hyphomicrobium zavarzinii* ZV580

Received: 29 August 2001 / Revised: 16 November 2001 / Accepted: 12 December 2001 / Published online: 31 January 2002.

Abstract Recently, it has been shown that heterotrophic methylotrophic Proteobacteria contain tetrahydrofolate (H_4F)- and tetrahydromethanopterin (H_4MPT)-dependent enzymes. Here we report on the purification of two methylene tetrahydropterin dehydrogenases from the methylotroph *Hyphomicrobium zavarzinii* ZV580. Both dehydrogenases are composed of one type of subunit of 31 kDa. One of the dehydrogenases is NAD(P)-dependent and specific for methylene H_4MPT (specific activity: 680 U/mg). Its N-terminal amino acid sequence showed sequence identity to NAD(P)-dependent methylene H_4MPT dehydrogenase MtdB from *Methylobacterium extorquens* AM1. The second dehydrogenase is specific for NADP and methylene H_4F (specific activity: 180 U/mg) and also exhibits methenyl H_4F cyclohydrolase activity. Via N-terminal amino acid sequencing this dehydrogenase was identified as belonging to the classical bifunctional methylene H_4F dehydrogenases/cyclohydrolases (FolD) found in many bacteria and eukarya. Apparently, the occurrence of methylene tetrahydrofolate and methylene tetrahydromethanopterin dehydrogenases is not uniform among different methylotrophic α-Proteobacteria. For example, FolD was not found in *M. extorquens* AM1, and the NADP-dependent methylene H_4MPT dehydrogenase MtdA was present in the bacterium that also shows H_4F activity.

Keywords C_1-metabolism · Methylotrophic bacteria · Methanogenic archaea · Tetrahydromethanopterin · Tetrahydrofolate

Abbreviations *H_4MPT* Tetrahydromethanopterin · *H_4F* Tetrahydrofolate

Introduction

Cell extracts of heterotrophic methylotrophic Proteobacteria of the α, β, and γ-group exhibit tetrahydromethanopterin (H_4MPT)- and tetrahydrofolate (H_4F)-dependent enzyme activities (Chistoserdova et al. 1998; Vorholt et al. 1999). It has been proposed that the enzymes form two independent pathways of formaldehyde oxidation to CO_2, which allows the α-proteobacterium *Methylobacterium extorquens* AM1 to grow on methanol and methylamine as sole carbon and energy source (Chistoserdova et al. 1998; Vorholt et al. 1998). The H_4MPT-dependent pathway consists of enzymes with sequence identity to those involved in methanogenesis, and it has been suggested that ancestral bacteria acquired these enzymes from an ancestral archaeon (Pomper et al. 1999; Vorholt et al. 1999; Pomper and Vorholt 2001). In addition, *M. extorquens* AM1 contains two novel types of dehydrogenases, an NADP-dependent methylene H_4MPT dehydrogenase (MtdA), and an NAD(P)-dependent methylene H_4MPT dehydrogenase (MtdB) (Vorholt et al. 1998; Hagemeier et al. 2000, 2001). Whereas MtdB is specific for methylene H_4MPT, MtdA also catalyzes the dehydrogenation of methylene H_4F, albeit with lower catalytic efficiency. The latter exhibits a sequence identity of only 15% to classical methylene H_4F dehydrogenases/cyclohydrolases FolD. A separate methylene H_4F dehydrogenase could not be detected on the protein level, in agreement with the apparent absence of *folD* in the genome of *M. extorquens* AM1 (L. Chistoserdova, University of Washington, personal

M. Goenrich · J. Bursy · J.A. Vorholt (✉)
Max-Planck-Institut für terrestrische Mikrobiologie,
Karl-von-Frisch-Strasse, 35043 Marburg, Germany
e-mail: vorholt@toulouse.inra.fr,
Tel.: +33-5-61-285458, Fax: +33-5-61-285061

E. Hübner · A.C. Schwartz
Kirschallee 1, 53115 Bonn, Germany

D. Linder
Biochemisches Institut des Fachbereichs Humanmedizin,
Justus von Liebig-Universität,
Friedrichstrasse 24, 35392 Giessen, Germany

Present address:
J.A. Vorholt
Laboratoire de Biologie Moléculaire
des Relations Plantes-Microorganismes, INRA/CNRS,
Chemin de Borde Rouge, BP 27, 31326 Castanet-Tolosan, France

communication). This is in contrast to *Methylobacterium* sp. strain CM4, which contains a gene for a methylene H_4F dehydrogenase FolD (Vannelli et al. 1999) and is able to grow on chloromethane as carbon and energy source. Currently it is not known whether one or two pyridine-nucleotide-dependent methylene H_4MPT dehydrogenases are present in *Methylobacterium* sp. strain CM4.

We have now analyzed another α-proteobacterium, *Hyphomicrobium zavarzinii* ZV580, for the occurrence of methylene-H_4MPT-dependent and methylene-H_4F-dependent dehydrogenases to learn more about their distribution, function, and possible evolution. The *Hyphomicrobium* species is able to metabolize a range of substrates by the transfer of one-carbon units. These substrates include methanol and methylamine (Harder and Attwood 1978; Stackebrandt et al. 1988), methane sulfonic acid (Kelly and Murrell 1999), chloromethane (Doronina and Trotsenko 1997; McAnulla et al. 2001; McDonald et al. 2001), dichloromethane (Kohlerstaub et al. 1995), and dimethyl sulfonic acid (Borodina et al. 2000).

Materials and methods

Growth of bacteria

Hyphomicrobium zavarzinii ZV580 was grown on methanol (100 mM) at 30 °C in the minimal medium described previously (Fulton et al. 1984). The cells were cultivated in 10-l glass fermenters containing 8 l medium. The fermenters were inoculated with 800 ml of a culture grown in Erlenmeyer flasks. The glass fermenter was stirred at 500 rpm and gassed with air (2 $l \cdot min^{-1}$). The cultures were harvested in the late-exponential phase at an OD_{578} of 1.4. Cells were pelleted by centrifugation at 5,000×*g* and stored at –20 °C.

Preparation of cell extracts

Frozen cells (15 g) of *H. zavarzinii* ZV580 were suspended in 50 mM Mops/KOH, pH 7.0, for the purification of methylene H_4MPT dehydrogenase, and 10 g of frozen cells were resuspended in 50 mM Tris/HCl, pH 8.5, for the purification of methylene H_4F dehydrogenase at 4 °C. Cell suspensions were passed three times through a French pressure cell at 120 MPa. Cell debris, whole cells, and the membrane fractions, which were shown not to contain methylene H_4F dehydrogenase or methylene H_4MPT dehydrogenase activity were removed by centrifugation at 150,000×*g* for 1 h.

Protein was determined according to Bradford (1976) using the Bio-Rad reagent with bovine serum albumin as standard.

Determination of enzyme activities

Enzyme activities were routinely assayed at 30 °C in 1-ml cuvettes (path length 1 cm) in a total volume of 0.7 ml. The reactions were monitored photometrically by measuring the increase in absorbance at 340 nm as described previously (Vorholt et al. 1998). The cofactors utilized in the assays were from Sigma (H_4F) or purified from *Methanothermobacter marburgensis* (Shima and Thauer 2001) (H_4MPT).

Purification of NAD(P)-dependent methylene H_4MPT dehydrogenase from *H. zavarzinii* ZV580

NAD(P)-dependent methylene H_4MPT dehydrogenase was purified from *H. zavarzinii* ZV580 by four chromatographic steps at 4 °C under oxic conditions. All chromatographic materials were from Amersham Pharmacia Biotech. The soluble fraction, consisting of the supernatant after ultracentrifugation (42 ml), was loaded onto a DEAE-Sephacel column (2.6×10 cm) equilibrated with 50 mM Mops/KOH, pH 7.0. Protein was eluted with NaCl gradients in this buffer: 60 ml 0 M NaCl, 290 ml 0–0.5 M NaCl, 70 ml 0.5–2 M NaCl, 100 ml 2 M NaCl. NAD(P)-dependent methylene H_4MPT dehydrogenase was recovered at about 0.1 M NaCl. Active fractions (36 ml) were pooled and diluted 1:4 with 50 mM Mops/KOH, pH 7.0, and applied to a Q-Sepharose column (1.6×10 cm) using the same buffers as described for the DEAE column. Protein was eluted with 40 ml 0 M NaCl, 240 ml 0–0.4 M NaCl, 20 ml 0.4–2 M NaCl, 40 ml 2 M NaCl. NAD(P)-dependent methylene H_4MPT dehydrogenase was eluted at about 50 mM NaCl. Combined active fractions (16 ml) were pooled, washed and concentrated using Centricon 30 microconcentrators (Millipore) and 10 mM potassium phosphate buffer. Protein was loaded onto a hydroxyapatite column (1.6×10 cm) equilibrated with 10 mM potassium phosphate. Protein was eluted stepwise with 10, 50, 100, 150, 200, 250, 300, and 500 mM potassium phosphate (25 ml each). The dehydrogenase eluted at 250 mM potassium phosphate. Active fractions (18 ml) were pooled, washed, and concentrated using Centricon 30 microconcentrators and 50 mM Mes/NaOH, pH 5.5. The enzyme was further purified by cation-exchange chromatography on a Mono S column (0.5×5 cm) with a linear gradient from 0 to 0.4 M NaCl in 50 mM Mes/NaOH, pH 5.5 (60 ml). The dehydrogenase was recovered at 120 mM NaCl and concentrated using Centricon 30 microconcentrators.

Purification of NADP-dependent methylene H_4F dehydrogenase

NADP-dependent methylene H_4F dehydrogenase was purified by three chromatographic steps at 4 °C under oxic conditions. The soluble fraction, consisting of the supernatant after ultracentrifugation (24 ml), was loaded onto a DEAE-Sephacel column (2.6×10 cm) equilibrated with 50 mM Tris/HCl, pH 8.5. Protein was eluted with NaCl gradients in this buffer: 80 ml 0 M NaCl, 220 ml 0–0.5 M NaCl, 50 ml 2 M NaCl. The enzyme activity was recovered in the flow-through of the column. Active fractions (19 ml) were pooled, and 15 ml of a saturated ammonium sulfate in 50 mM Tris/HCl, pH 7.5, was added to a final concentration of 44%. After 30 min of stirring, the precipitated protein was removed by centrifugation at 27,000×*g* for 30 min. The supernatant was applied to a phenyl-Sepharose column (2.6×10 cm) equilibrated with 1.8 M ammonium sulfate in 50 mM Tris/HCl, pH 7.5. With a linear gradient decreasing from 1.8 to 0 M $(NH_4)_2SO_4$ (380 ml), the dehydrogenase was eluted at about 0.4 M $(NH_4)_2SO_4$. Combined active fractions (10 ml) were diluted 1:6 with 10 mM potassium phosphate buffer, pH 7.0, and subjected to chromatography on hydroxyapatite (1.6×10 cm) equilibrated in 10 mM potassium phosphate buffer, pH 7.0. Protein was eluted stepwise with 60 ml of 10 mM, 20 ml 100 mM, 20 ml 125 mM, 20 ml 150 mM, and 40 ml 500 mM potassium phosphate buffer, pH 7.0. Methylene H_4F dehydrogenase was recovered at 125 mM potassium phosphate and concentrated with Centricon 30 microconcentrators.

Determination of the N-terminal amino acid sequences

Electrophoresis of the purified enzymes in the presence of SDS was followed by electroblotting onto a poly(vinyl trifluoride) membrane (Applied Biosystems). The N-terminus was sequenced on a 477A protein/peptide sequencer from Applied Biosystems.

Results

Cell extracts of *H. zavarzinii* ZV580 grown on methanol exhibited NADP-dependent methylene H_4MPT dehydrogenase activity of 2.3 U/mg, NAD-dependent methylene

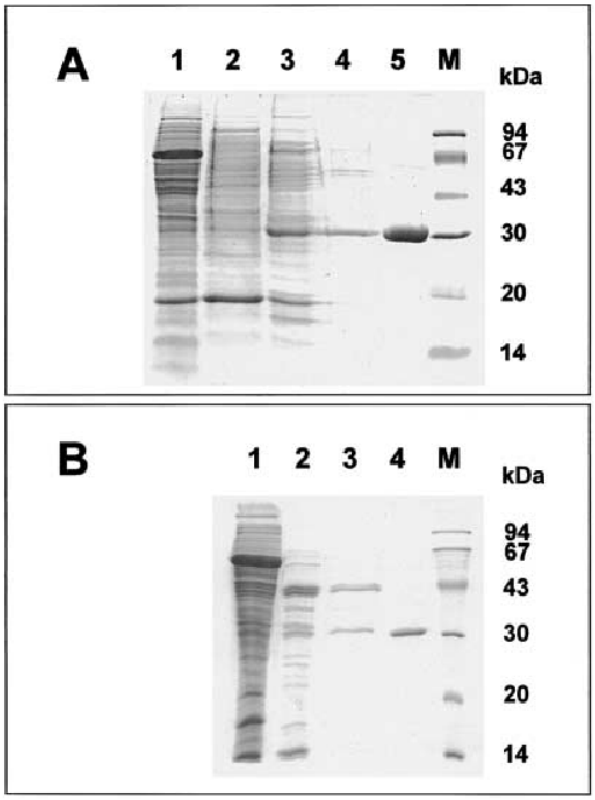

Fig. 1 SDS-PAGE analysis of purified NAD(P)-dependent methylene H_4MPT dehydrogenase MtdB (**A**) and NADP-dependent methylene H_4F dehydrogenase FolD (**B**) from *Hyphomicrobium zavarzinii* ZV580. Protein was separated on a 16% polyacrylamide gel, which was subsequently stained with Coomassie brilliant blue R250 (Laemmli 1970). **A** *Lane 1* 20 µg of cell extract protein, *lane 2* 8 µg protein after DEAE-Sephacel, *lane3* 4 µg protein after Q-Sepharose, *lane 4* 1 µg protein after hydroxyapatite, *lane 5* 3.5 µg protein after Mono-S, *lane M* standards (Amersham Pharmacia Biotech). **B**. *Lane 1* 25 µg of cell extract protein, *lane 2* 2.5 µg protein after DEAE-Sephacel, *lane 3* 1.0 µg protein after phenyl-Sepharose, *lane 4* 1.2 µg of protein after hydroxyapatite, *lane M*, molecular mass standards as in **A**

H_4MPT dehydrogenase activity of 0.4 U/mg, and NADP-dependent methylene H_4F dehydrogenase activity of 0.4 U/mg. NAD-dependent methylene H_4F dehydrogenase could not be detected.

In this study two different dehydrogenases were found to be responsible for these enzyme activities. Their purification and characterization is described below.

NAD(P)-dependent methylene H_4MPT dehydrogenase

NAD(P)-dependent methylene H_4MPT dehydrogenase was purified by four chromatographic steps to apparent homogeneity. In every step, the NAD- and NADP-dependent activities co-purified. Analysis by SDS/PAGE (Fig. 1A) revealed the presence of only one polypeptide with an apparent molecular mass of 31 kDa. Purification was about 300-fold with 15% yield (Table 1). After this purification procedure, the preparation contained only one polypeptide of an apparent molecular mass of 31 kDa.

Table 1 Purification of NAD(P)-dependent methylene H_4MPT dehydrogenase MtdB from *H. zavarzinii* ZV580. Enzyme activities were determined at 30 °C under standard assay conditions with NADP as cosubstrate

Purification step	Protein (mg)	Activity (U)	Specific activity (U/mg)	Purification (-fold)	Yield (%)
Cell extract	464	1075	2.3	1	100
DEAE-Sephacel	113	1004	8.9	3.9	93
Q-Sepharose	8.1	855	106	46	80
Hydroxyapatite	1.0	535	535	233	50
Mono-S	0.24	163	678	295	15

The N-terminal amino acid sequence was determined to be (S)EATPILHMLSPQK?MS. An alignment of the sequence with the N-terminal amino acid sequences of MtdA and MtdB from *M. extorquens* AM1 is shown in Fig. 2A. The N-terminal amino acid sequences of methylene H_4MPT dehydrogenase from *H. zavarzinii* ZV580 and MtdB from *M. extorquens* AM1 have 11 identical residues (out of 16) whereas the former and MtdA from *M. extorquens* AM1 have only four identical residues. Therefore, methylene H_4MPT dehydrogenase from H. *zavarzinii* ZV580 might be more closely related to MtdB from *M. extorquens* AM1, although the small amount of sequence information is not sufficient to validate this with confidence.

The ultraviolet/visible spectrum of the enzyme indicated that the protein does not contain a chromophoric prosthetic group.

The rate of methylene H_4MPT dehydrogenation with NADP showed a pH dependence in which the activity increased by a factor of 5 between pH 5 and 6. A slow decrease in activity was observed above pH 6 and was measured up to pH 9.

No enzymatic activity was observed upon addition of methylene H_4F in place of methylene H_4MPT, i.e., the methylene H_4F could not be dehydrogenated. Also the methylene H_4MPT dehydrogenase did not display any methenyl H_4MPT cyclohydrolase activity, and is therefore monofunctional. As mentioned before, both NADP and NAD can serve as cosubstrates. The apparent K_m values for methylene H_4MPT with NADP and NAD, respectively, were 12 µM and 42 µM. A K_m of 0.8 mM was determined for NAD with a V_{max} of 200 U/mg. The apparent K_m for NADP was 15 µM (V_{max} 735 U/mg).

The initial rates of methylene H_4MPT dehydrogenation with NADP were not dependent on the order of substrate addition, in contrast to observations with MtdB from *M. extorquens* AM1 (Hagemeier et al. 2000). Addition of NADPH or NADH to the enzymatic reaction had no influence on the rate of the catalyzed reaction.

302

A

B

Fig. 2 Alignment of the N-terminal amino acid sequence of NAD(P)-dependent methylene H_4MPT dehydrogenase MtdB (**A**) and NADP-dependent methylene H_4F dehydrogenase FolD (**B**) from *H. zavarzinii* ZV580. N-terminal amino acid sequences of the dehydrogenases from *H. zavarzinii* ZV580 were determined by Edman degradation. The sequence of NAD(P)-dependent methylene H_4MPT dehydrogenase was compared to MtdA (P55818) and MtdB (AF032114) from *M. extorquens* AM1 (**A**).The sequence of NADP-dependent methylene H_4F dehydrogenase was compared to FolD proteins from *Pisum sativum* (AC084218), *Photobacterium phosphoreum* (U34207), *Caulobacter crescentus* (AE005798), and *Escherichia coli* (M74789) (**B**)

Table 2 Purification of NADP-dependent methylene H_4F dehydrogenase FolD from *H. zavarzinii* ZV580. Enzyme activities were determined at 30 °C under standard assay conditions

Purification step	Protein (mg)	Activity (U)	Specific activity (U/mg)	Purification (-fold)	Yield (%)
Cell extract	270	97	0.4	1	100
DEAE-Sephacel	7.2	48	6.7	18.6	49
Phenyl-Sepharose	0.7	22	31	86	23
Hydroxyapatite	0.06	10.7	178	445	11

NADP-dependent methylene H_4F dehydrogenase/cyclohydrolase

The NADP-dependent methylene H_4F dehydrogenase was purified as described in Table 2. After three chromatographic steps, preparations contained only one polypeptide, with an apparent molecular mass of 31 kDa, as revealed by SDS-PAGE (Fig. 1B), the same value as determined for MtdB. The purified protein had a specific activity of about 180 U/mg. Purification was about 450-fold with a 10% yield. The N-terminal amino acid sequence of the purified enzyme (AAQIIDGKAIAA(H/D)VRKQVAADVKALQASHGLTPGLAVVLVG) indicates that the enzyme from *H. zavarzinii* ZV580 belongs to the classical bifunctional dehydrogenases (FolD) from Bacteria and Eukarya. The sequence identity with other FolD proteins is 60% or more (Fig. 2B).

The ultraviolet/visible spectrum of the purified enzyme was very similar to that of bovine serum albumin, indicating the absence of a chromophoric prosthetic group.

The optimum pH for methylene H_4F dehydrogenation was found to be between 5.5 and 6.5. The purified enzyme did not catalyze the reduction of NAD. Determination of substrate binding resulted in apparent K_m values of 24 µM (V_{max}=510 U/mg) for methylene H_4F and 130 µM for NADP.

The purified enzyme also showed methenyl H_4F cyclohydrolase activity of 67 U/mg. This confirms that the enzyme is a bifunctional "FolD" enzyme as indicated by the N-terminal amino acid sequence.

Discussion

Analysis of *H. zavarzinii* ZV580 revealed that the methylotrophic proteobacterium grown in the presence of methanol expresses two distinct methylene tetrahydropterin dehydrogenases. An NADP-dependent methylene H_4F dehydrogenase/cyclohydrolase FolD similar to those found in many bacteria and eukarya is expressed as well as a novel type of NAD(P)-dependent methylene H_4MPT dehydrogenase with sequence identity to MtdB from *M. extorquens* AM1 (Hagemeier et al. 2000, 2001).

Presumably, NAD(P)-dependent methylene H_4MPT dehydrogenase from *H. zavarzinii* ZV580 has a catabolic role in formaldehyde oxidation to CO_2, as has been suggested for methylene H_4MPT dehydrogenases from *M. extorquens* AM1 (Vorholt et al. 1998; Hagemeier et al. 2000). A nearly irreversible reaction, favoring the oxidation of the one-carbon unit, is predicted on the basis of thermodynamics (ΔG°=–13 kJ/mol). A conversion of most of the formaldehyde to methylene H_4MPT and not methylene H_4F could be accomplished by the formaldehyde-activating enzyme (Fae) (Vorholt et al. 2000). Fae accelerates the condensation of formaldehyde and H_4MPT and was found to be present in cell extracts of *H. zavarzinii* ZV580, showing an activity of 0.8 U/mg (this study). NAD(P)-dependent methylene H_4MPT dehydrogenase MtdB from *H. zavarzinii* ZV580 could reduce either NAD or NADP. The enzyme exhibited a higher apparent affin-

ity for NADP than for NAD, consistent with what was observed with MtdB from *M. extorquens* AM1 (Hagemeier et al. 2000). Since the internal concentration of NAD is presumably higher than that of NADP, the majority of reducing equivalents in vivo may be used in the reduction of NAD to NADH (for a detailed discussion see Hagemeier et al. 2000).

Methylene H_4F dehydrogenase FolD from *H. zavarzinii* ZV580 is most likely essential for the biosynthesis of thymidylate, purines, and formyl methionine-tRNA (MacKenzie 1984). A methylene H_4MPT dehydrogenase with a side activity for H_4F, as found for MtdA from *M. extorquens* AM1, is apparently absent in *H. zavarzinii* ZV580. This finding supports the hypothesis that MtdA from *M. extorquens* AM1 operates in H_4F-linked metabolism rather than in H_4MPT-linked metabolism. Most likely, MtdA from *M. extorquens* AM1 and "FolD" from *H. zavazinii* ZV580 are functionally equivalent.

It is tempting to speculate that the precursor of MtdA and MtdB was a methylene H_4MPT-dependent enzyme. In some methylotrophic bacteria, such as *M. extorquens* AM1, the acquisition of an enzyme able to convert either H_4F or H_4MPT and the acquisition of H_4F-dependent cyclohydrolase activity may have precluded the need for classical FolD-type enzymes. In the future, three-dimensional analysis of enzymes from all the different classes of tetrahydropterin dehydrogenases and a broader set of sequences of these enzymes from the different organisms may help to elucidate how pterin dehydrogenases evolved.

Acknowledgements This work was supported by the Max-Planck-Gesellschaft. We thank Johanna Moll, Marburg, for the preparation of H_4MPT.

References

Borodina E, Kelly DP, Rainey FA, Ward-Rainey NL, Wood AP (2000) Dimethylsulfone as a growth substrate for novel methylotrophic species of *Hyphomicrobium* and *Arthrobacter*. Arch Microbiol 173:425–437

Bradford MM (1976) A rapid and sensitive method for the quantitation of microgram quantities of protein utilizing the principle of protein-dye binding. Anal Biochem 72:248–254

Chistoserdova L, Vorholt JA, Thauer RK, Lidstrom ME (1998) C_1 transfer enzymes and coenzymes linking methylotrophic bacteria and methanogenic archaea. Science 281:99–102

Doronina NV, Trotsenko YA (1997) Isolation and characterization of aerobic degraders of methyl chloride. Microbiology 66:57–64

Fulton GL, Nunn DN, Lidstrom ME (1984) Molecular cloning of a malyl coenzyme A lyase gene from *Pseudomonas* sp. strain AM1, a facultative methylotroph. J Bacteriol 160:718–723

Hagemeier CH, Chistoserdova L, Lidstrom ME, Thauer RK, Vorholt JA (2000) Characterization of a second methylene tetrahydromethanopterin dehydrogenase from *Methylobacterium extorquens* AM1. Eur J Biochem 267:3762–3769

Hagemeier CH, Bartoschek S, Griesinger C, Thauer RK, Vorholt JA (2001) Re-face stereospecificity of NADP dependent methylenetetrahydromethanopterin dehydrogenase from *Methylobacterium extorquens* AM1 as determined by NMR spectroscopy. FEBS Lett 494:95–98

Harder W, Attwood MM (1978) Biology, physiology and biochemistry of Hyphomicrobia. Adv Microb Physiol 17:303–359

Kelly DP, Murrell JC (1999) Microbial metabolism of methanesulfonic acid. Arch Microbiol 172:341–348

Kohlerstaub D, Frank S, Leisinger T (1995) Dichloromethane as the sole carbon source for *Hyphomicrobium* sp. strain DM 2 under denitrification conditions. Biodegradation 6:229–235

Laemmli UK (1970) Cleavage of structural proteins during the assembly of the head of bacteriophage T4. Nature 227:680–685

MacKenzie RE (1984) Biogenesis and interconversion of substituted tetrahydrofolates. In: Blakley RL, Benkovic SJ (eds) Folates and pterins. Chemistry and biochemistry of folates. Wiley, New York, pp 256–306

McAnulla C, Woodall CA, McDonald IR, Studer A, Vuilleumier S, Leisinger T, Murrell JC (2001) Chloromethane utilization gene cluster from *Hyphomicrobium chloromethanicum* strain CM2(T) and development of functional gene probes to detect halomethane-degrading bacteria. Appl Environ Microbiol 67:307–316

McDonald IR, Doronina NV, Trotsenko YA, McAnulla C, Murrell JC (2001) *Hyphomicrobium chloromethanicum sp. nov.* and *Methylobacterium chloromethanicum sp. nov.*, chloromethane-utilizing bacteria isolated from a polluted environment. Int J Syst Evol Microbiol 51:119–122

Pomper BK, Vorholt JA (2001) Characterization of the formyltransferase (Ftr) from *Methylobacterium extorquens* AM1. Eur J Biochem 269:4769–4775

Pomper BK, Vorholt JA, Chistoserdova L, Lidstrom ME, Thauer RK (1999) A methenyl tetrahydromethanopterin cyclohydrolase and a methenyl tetrahydrofolate cyclohydrolase in *Methylobacterium extorquens* AM1. Eur J Biochem 261:475–480

Shima S, Thauer RK (2001) Tetrahydromethanopterin-specific enzymes from *Methanopyrus kandleri*. Methods Enzymol 331:317–353

Stackebrandt E, Fischer A, Roggentin T, Wehmeyer U, Bomar D, Smida J (1988) A phylogenetic survey of budding, and/or prosthecate, non-phototrophic eubacteria: membership of *Hyphomicrobium, Hyphomonas, Pedomicrobium, Filomicrobium, Caulobacter* and "*Dichotomicrobium*" to the alpha-subdivision of purple non-sulfur bacteria. Arch Microbiol 149:547–556

Vannelli T, Messmer M, Studer A, Vuilleumier S, Leisinger T (1999) A corrinoid-dependent catabolic pathway for growth of a *Methylobacterium* strain with chloromethane. Proc Nat Acad Sci. USA 96:4615–4620

Vorholt JA, Chistoserdova L, Lidstrom ME, Thauer RK (1998) The NADP-dependent methylene tetrahydromethanopterin dehydrogenase in *Methylobacterium extorquens* AM1. J Bacteriol 180:5351–5356

Vorholt JA, Chistoserdova L, Stolyar SM, Thauer RK, Lidstrom ME (1999) Distribution of tetrahydromethanopterin-dependent enzymes in methylotrophic bacteria and phylogeny of methenyl tetrahydromethanopterin cyclohydrolases. J Bacteriol 181:5750–5757

Vorholt JA, Marx CJ, Lidstrom ME, Thauer RK (2000) Novel formaldehyde-activating enzyme in *Methylobacterium extorquens* AM1 required for growth on methanol. J Bacteriol 182:6645–6650

The EMBO Journal (2004), submitted for publication on 17 september 2004

How an enzyme binds the C_1-carrier tetrahydromethanopterin:

Structure of the tetrahydromethanopterin dependent formaldehyde-activating enzyme (Fae) from *Methylobacterium extorquens* AM1

Priyamvada Acharya[1,2,4], Meike Goenrich[2,4], Christoph H. Hagemeier[2], Ulrike Demmer[1], Julia A. Vorholt[2,3], Rudolf K . Thauer[2] and Ulrich Ermler[1,*]

[1]Max-Planck-Institut für Biophysik, Frankfurt am Main, Germany. [2]Max-Planck-Institut für terrestrische Mikrobiologie, Marburg, Germany. [3]INRA/CNRS, Castanet-Tolosan, France

Tetrahydromethanopterin (H_4MPT) is a tetrahydrofolate (H_4F) analogue involved as C_1-carrier in the metabolism of various groups of microorgansims. How H_4MPT is bound to the respective C_1-unit converting enzymes remained elusive. We describe here the structure of the homopentameric formaldehyde-activating enzyme (Fae) from *Methylobacterium extorquens* AM1 established at 2.0 Å without and at 1.9 Å with methylene-H_4MPT bound. Methylene-H_4MPT is bound in a 'S'-shaped conformation into the cleft formed between two adjacent subunits. Coenzyme binding is accompanied by side chain rearrangements up to 5 Å and leads to a rigidification of the C-terminal arm, a formation of a new hydrophobic cluster and an inversion of the amide side chain of Gln88. Methylene-H_4MPT in Fae shows a characteristic kink between the tetrahydropyrazine and the imidazolidine rings of 70° that is more pronounced than that reported for free methylene-H_4MPT in solution (50°). Fae is an essential enzyme for energy metabolism and formaldehyde detoxification of this bacterium and catalyses the formation of methylene-H_4MPT from H_4MPT and formaldehyde. The molecular mechanism of this reaction involving His22 as acid catalyst is discussed.

Keywords: Crystal structure; Formaldehyde-activating enzyme; Tetrahydromethanopterin; Tetrahydrofolate; C_1-metabolism

*Corresponding author. Max-Planck-Institut für Biophysik, Marie-Curie-Strasse 15, 60439 Frankfurt am Main, Germany. Tel. +4969 6306 1054; Fax +49 69 6303 1002; E-mail: Uli.Ermler@mpibp-frankfurt.mpg.de

[4] Both authors contributed equally

Abbreviations: H_4MPT, tetrahydromethanopterin; H_4F, tetrahydrofolate; Fae, formaldehyde-activating enzyme

Introduction

Tetrahydromethanopterin (H_4MPT) and tetrahydrofolate (H_4F) are coenzymes of analogous structure (Maden 2000) (Fig. 1). Both coenzymes are involved in the interconversion of C_1-units at the oxidation level of formate (N^5-formyl, N^{10}-formyl, N^5,N^{10}-methenyl and N^5,N^{10}-methylene), formaldehyde (N^5,N^{10}-methylene) and methanol (N^5-methyl). Whereas the universal distribution of H_4F is well documented since a long time, the presence of H_4MPT in various groups of archaea and bacteria is just emerging. Originally, after the discovery of H_4MPT (van Beelen *et al,* 1984, Escalante-Semerena *et al,* 1984) it was thought to be restricted to methanogenic archaea where it respresents the essential cofactor of a series of enzymes that form the integral part of the process of methane formation from H_2 and CO_2 (Thauer 1998). However, in the last decade, its much wider occurrence and importance became evident: H_4MPT was found in sulfate-reducing archaea that are phylogenetically closely related to methanogenic archaea (Gorris *et al,* 1991, Thauer and Kunow 1995). More surprisingly, H_4MPT was later found to be present also outside the archaea and shown to be an essential cofactor of the central metabolism of many methylotrophic α-, β-, and γ-proteobacteria (Chistoserdova *et al,* 1998, Vorholt *et al,* 1999), a group of bacteria that also comprises methanotrophic bacteria. Very recently, it was found that not only aerobic methane oxidation relies on H_4MPT but also anaerobic oxidation of methane is likely to depend on H_4MPT (Krueger *et al,* 2003), a process catalysed by a group of archaea closely related to the *Methanosarcinales* (Boetius *et al,* 2000, Michaelis *et al,* 2002). All these organisms are highly specialised in C_1-metabolism and are of great ecological importance in the global carbon cycle (Hogan *et al,* 1991; Hinrichs *et al,* 1999). The recent documentation of functional H_4MPT-dependent enzymes in the enigmatic bacterial group of *Planctomycetes* re-opened the debate of the evolution of H_4MPT and H_4MPT-dependent enzymes since phylogenetic analysis places the *Planctomycetes* sequences as distantly from the archaeal counterparts as

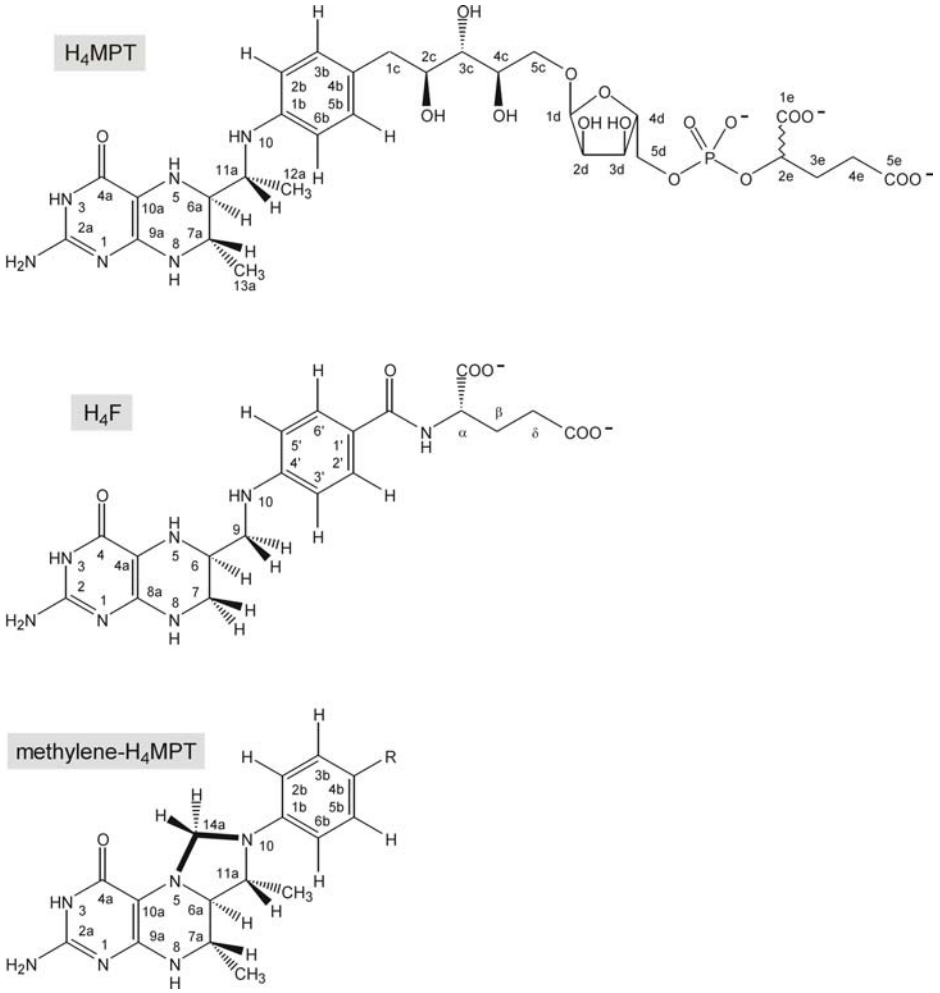

Figure 1 Structures of tetrahydromethaneopterin (H_4MPT), of tetrahydrofolate (H_4F) and of methylene-H_4MPT. The numbering scheme for H_4MPT was adopted from van Beelen *et al,* (1984) and for H_4F from Poe and Benkovic (1980). H_4MPT is similar to H_4F in that both compounds consist of a reduced pterin linked to an arylamine via a methylene group, with C_1-units binding at N^5,N^{10} or both N^5 and N^{10}. In methylene-H_4MPT the C_1-unit bridges N^5 and N^{10} forming an imidazolidine ring, which is condensed to the tetrahydropyrazine ring of the reduced pterin. To the left of the phenyl ring the structure is referred to as head group and to the right of the phenyl ring as tail of H_4MPT and H_4F, respectively.

from their proteobacterial counterparts (Chistoserdova *et al,* 2004).

Functionally the most important difference between H_4MPT and H_4F is the electron donating methylene group of H_4MPT in position 1c (Fig. 1), which is conjugated to N^{10} through the aromatic ring whereas H_4F has an electron withdrawing carbonyl group in this position (Thauer *et al,* 1996; Maden 2000). One consequence is that the redox potentials of the N^5,N^{10}-methenyl-H_4MPT$^+$/N^5,N^{10}-methylene-H_4MPT couple (-390 mV) and of the N^5,N^{10}-methylene-H_4MPT/N^5-methyl-H_4MPT couple (-310 mV) are almost 100 mV more negative than the corresponding H_4F couples. The structural and functional differences between H_4MPT and H_4F are reflected in the finding that most of the enzymes catalysing the interconversion of their C_1-derivatives are highly specific for H_4MPT or H_4F exceptions being N^5-methyl-H_4MPT: coenzyme M methyltransferase (Mtr) from *Methanosarcina mazei* (Lienard *et al,* 1996*)*, serine hydroxymethyltransferase (GlyA) from *Methanosarcina barkeri* (Buchenau and Thauer 2004) and NADP-dependent methylene-H_4MPT dehydrogenase (MtdA) from *Methylobacterium extorquens* AM1 (Vorholt *et al,* 1998).

Despite the fact that H_4MPT and H_4F specific enzymes catalyse analogous reactions their primary structures indicate that most of them have evolved separately (Shima *et al,* 2000; Maden 2000). This is also true for most of the enzymes involved in the biosynthesis of H_4MPT and of H_4F (White 2001; Graham and White 2002). The two C_1-carriers thus appear to be products of convergent evolution.

The crystal structure of six H_4MPT specific enzymes have been determined: formylmethanofuran: H_4MPT formyltransferase (Ftr) (Ermler *et al,* 1997; Mamat *et al,* 2002); methenyl-H_4MPT cyclohydrolase (Mch) (Grabarse

et al, 1999); F_{420}-dependent methylene-H_4MPT dehydrogenase (Mtd) (Hagemeier *et al,* 2003); NADP-dependent methylene-H_4MPT dehydrogenase (MtdA) (Ermler *et al,* 2002); H_2-forming methylene-H_4MPT dehydrogenase (Hmd) (Mamat 2002) and F_{420}-dependent methylene-H_4MPT-reductase (Mer) (Shima *et al,* 2000). So far none of these enzymes could be crystallised with H_4MPT or one of its C_1-derivatives bound. Only the conformation of methylene-H_4MPT bound to Hmd was determined by two-dimensional NMR spectroscopy (Bartoscheck *et al,* 2001).

Here we describe the structure of the formaldehyde-activating enzyme Fae from *M. extorquens* AM1 with and without methylene-H_4MPT bound. The enzyme catalyses the condensation of formaldehyde with H_4MPT to methylene-H_4MPT (Vorholt *et al,* 2000). This reaction also proceeds spontaneously but only at a lower rate. Fae was discovered in *M. extorquens* AM1, which grows aerobically at the expense of methanol oxidation to CO_2 involving N^5,N^{10}-methylene-H_4MPT, N^5,N^{10}-methenyl-H_4MPT$^+$ and N^5-formyl-H_4MPT as intermediates (Vorholt 2002). Fae appears to be specific for H_4MPT, no formaldehyde-H_4F condensing activity could be found with purified Fae (Vorholt *et al,* 2000). Fae minus mutants of *M. extorquens* AM1 are no longer capable of growth on methanol and are inhibited by trace amounts of formaldehyde indicating that Fae additionally has a function in formaldehyde detoxification (Vorholt *et al*, 2000). Fae has been found to be present in other methylotrophic bacteria (Vorholt 2002). Functional orthologs of Fae are also present in some methanogenic archaea (Vorholt *et al,* 2000) and in *Planctomyces* species (Chistoserdova *et al,* 2004). The widespread occurrence of Fae orthologs suggests that formaldehyde may play an unknown but important role in a broad group of prokaryotes.

In all the experiments only H_4MPT was used that was isolated from *Methanothermobacter marburgensis*. It has the structure shown in Figure 1. H_4MPT from *M. extorquens* AM1 differs from that in *M. marburgensis* by lacking the phosphate and hydroxyglutarate group. It has been shown, however, that enzymes from *M. extorquens* AM1 are equally active with H_4MPT and with the dephospho form (Vorholt et al 1998).

Results and Discussion

Structure of Fae with and without methylene-H_4MPT bound

Formaldehyde-activating enzyme Fae in the absence and presence of H_4MPT was structurally characterised in two crystal forms at a resolution of 2.0 Å and 1.9 Å, respectively (Table 1). The crystals formed in the presence of H_4MPT contained methylene-H_4MPT rather than H_4MPT, which can be explained by the facts that polyethyleneglycols are contaminated with formaldehyde and that methylene-H_4MPT forms spontaneously and enzyme catalysed from formaldehyde and H_4MPT under the crystallisation conditions. Attempts to obtain a crystal structure, in which only the substrate formaldehyde was bound, failed.

Fae is organized as homopentameric protein complex with dimensions of about 70 Å x 70 Å x 40 Å (Figure 2A). Each monomer consists of one compact domain that belongs to the class of α/β proteins. The central sheet contains five strands (β1-β5) joined in the order β1, β2, β5, β4 and β3, only β4 and β5 being oriented parallelly. Helix α1 arranged after strand β2 packs against one side of the sheet, helices α2 (after strand 4) and α3 (after strand 5) pack against the other (Figure 2B).

Table 1: Data statistics

	Fae				Fae with H_4MPT bound
	Native	Se-methionine (peak)	Se-methionine (inflection)	Se-methionine (remote)	
Data collection					
Space group	$P4_32_12$	$P4_32_12$	$P4_32_12$	$P4_32_12$	$P2_1$
Completeness (%)	98.6 (95.4)	98.6 (98.8)	99.9 (99.9)	99.5 (99.3)	93.5 (76.1)
R_{sym} (%)	5.4 (40)	6.0 (25)	6.1 (45.6)	7.3 (68.6)	8.2 (40)
Redundancy	3.5	3.3	4.6	4.0	3.1
Refinement statistics					
No. of protein residues	802				840
No. of water molecules	610				642
No. of H_4MPT molecules	0				5
No. of monomers in a.u.	5				5
Resolution range (Å)	50-2.0				50-1.9
Reflections ($F > 0\sigma$)	100903				59380
$R_{working}$ (%)	24				24
R_{free} (%)	20				21
rmsd from ideal values					
Bond lengths (Å)	0.023				0.011
Bond angles (deg.)	2.3				1.7

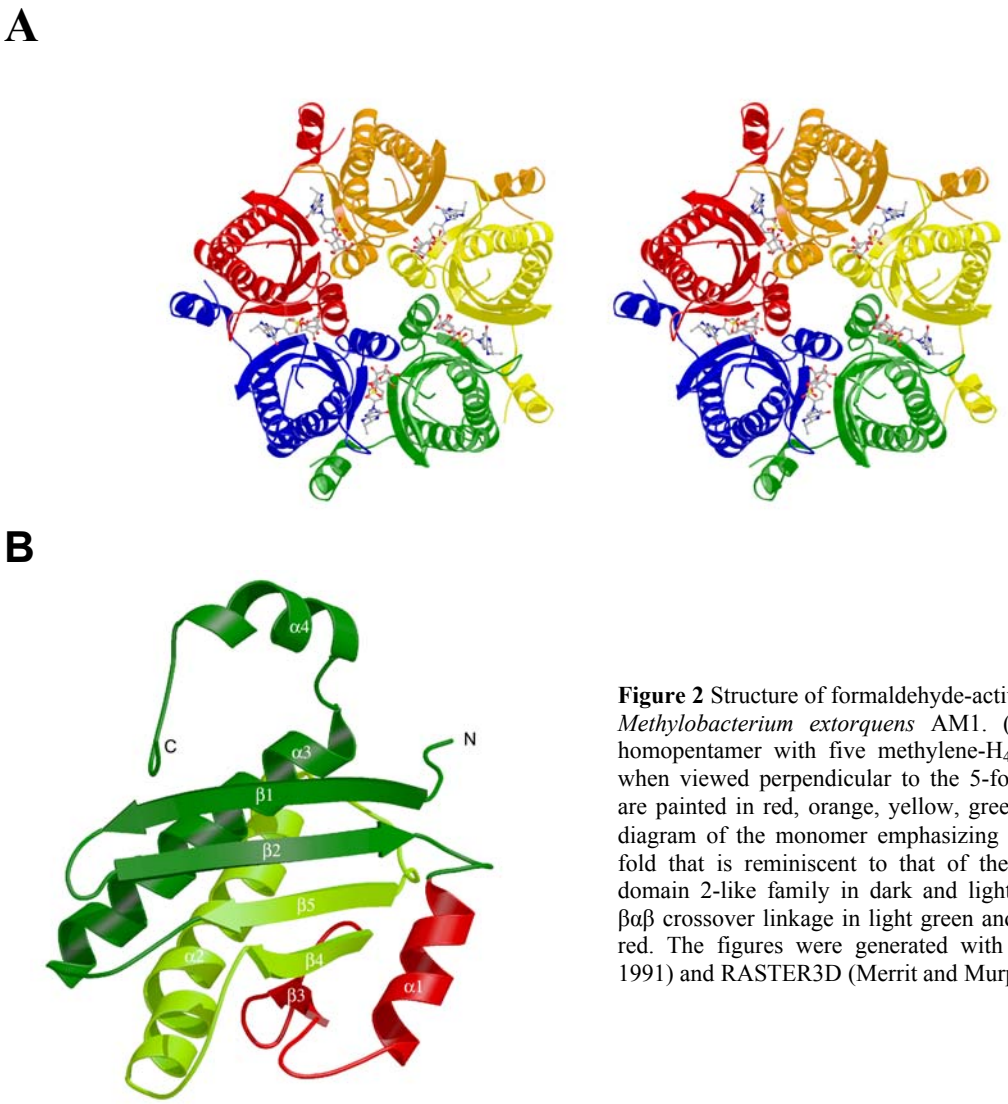

Figure 2 Structure of formaldehyde-activating enzyme Fae from *Methylobacterium extorquens* AM1. (**A**) Stereoview of the homopentamer with five methylene-H_4MPT molecules bound when viewed perpendicular to the 5-fold axis. The monomers are painted in red, orange, yellow, green and blue. (**B**) Ribbon diagram of the monomer emphasizing the segment of the α/β fold that is reminiscent to that of the ribosomal protein S-5 domain 2-like family in dark and light green, the left-handed βαβ crossover linkage in light green and the insertion region in red. The figures were generated with MOLSCRIPT (Kraulis 1991) and RASTER3D (Merrit and Murphy 1994)

This architecture is somehow reminiscent to that of the ribosomal protein S-5 domain 2-like family to which for example the elongation factor G (al-Karadaghi *et al,* 1996), the ribosomal protein S-5 (Ramakrishnan and White, 1992) and some kinases like phosphomevalonate kinase (Romanowski *et al,* 2002) belong. According to Dali (Holm and Sander, 1993), the rms deviations between Fae and elongation factor G and phosphomevalonate kinase are 2.7 Å and 3.1 Å using about 60% of the C_α positions for calculation. In comparison, the rms deviation between the five monomers in the asymmetric unit is around 0.15 Å that between the pentamers of the two crystal forms is 0.6 Å. A rare topological feature of this fold is the β4α2β5 left-handed crossover linkage that appears to be crucial for the integrity of the fold (Figure 2B). Compared to the other family members helix α2 in Fae is prolonged and part of the H_4MPT binding site. The major difference between Fae and the other family members is an insertion between strand β2 and β4 (Figure 2B) consisting of helix α1, strands β3 and an unusual protrusion at the end of strand β3 (see below).

The pentamer can be subdivided into three circular layers built up of an α-helical, a β-sheet and again an α-helical region (Figure 2A). The inner ring is formed by the five tightly linked helices α1 of the insertion indicating its importance for pentamerisation. The outer layer is formed by helices α2, α3 and α4 the latter being connected to helix α2 of the next monomer. The central ring consists of the five 5-stranded β-sheets each of them being oriented roughly perpendicular to the neighbouring sheet. The hydrophobic core of each sheet is enlarged by helices α1 of the next monomer at the inner side and of the C-terminal segment of the previous monomer at the outer side. A channel crosses the entire pentamer along the 5-fold axis (Figure 2A) and is occupied with several solvent molecules and extra electron density that could not be assigned.

The binding site for methylene-H_4MPT is located in a 20 Å long, 8 Å wide and 12 Å deep cleft at the interface

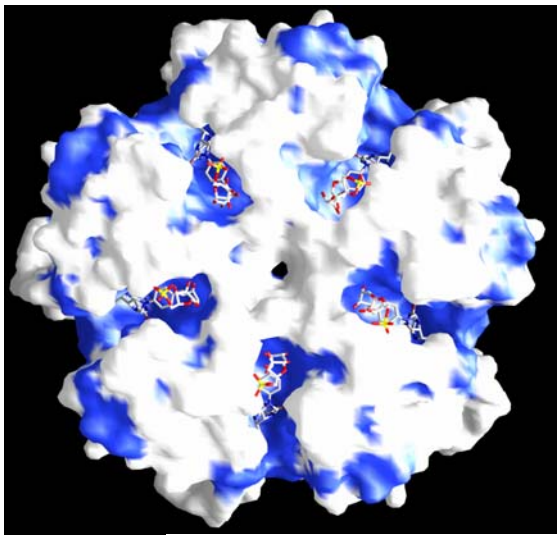

Figure 3 Conservation of amino acid residues in Fae. (**A**) Molecular surface representation of the Fae pentamer highlighting the five methylene-H_4MPT binding clefts. The surface was coloured in blue when the equivalent residues in at least eight of the nine aligned sequences (Figure 3B) were identical to Fae from *M. extorquens* AM1. The figure was generated with GRASP (Nicholls *et al,* 1993) (**B**) Alignment of the primary structures of Fae from α-proteobacterium *M. extorquens* AM1 and of related proteins from the genomes of the β-proteobacterium *Burkholderia fungorum* (Marx *et al,* 2004), the γ-proteobacterium *Methylomicrobium* sp. AMO1 (Chistoserdova *et al,* 2004), the planctomycete *Gemmata* sp. Wa1-1 (Chistoserdova *et al,* 2004), the methanogenic archaea *Methanosarcina acetivorans* (Galagan *et al,* 2002), *Methanobacterium thermoautotrophicus* ΔH (Smith *et al,* 1997), *Methanopyrus kandleri* (Slesarev *et al,* 2002) and of the sulfate-reducing archaeon *Archeoglobus fulgidus* (Klenk *et al,* 1997). A blue background indicates residues with high sequence conservation. Light blue indicates highly conserved residues located in the active site cleft and responsible for methylene-H_4MPT binding. The active site His22 is printed in red. The secondary structure assignment on the basis of the structure of the *M. extorquens* AM1 enzyme is shown above the sequence alignment in the colours used in Figure 2B. In some methanogenic archaea Fae is fused at the C-terminus to a domain (not shown) that shows sequence similarity to 3-hexulose-6-phosphate synthase (Hps) (Vorholt *et al*, 2000).

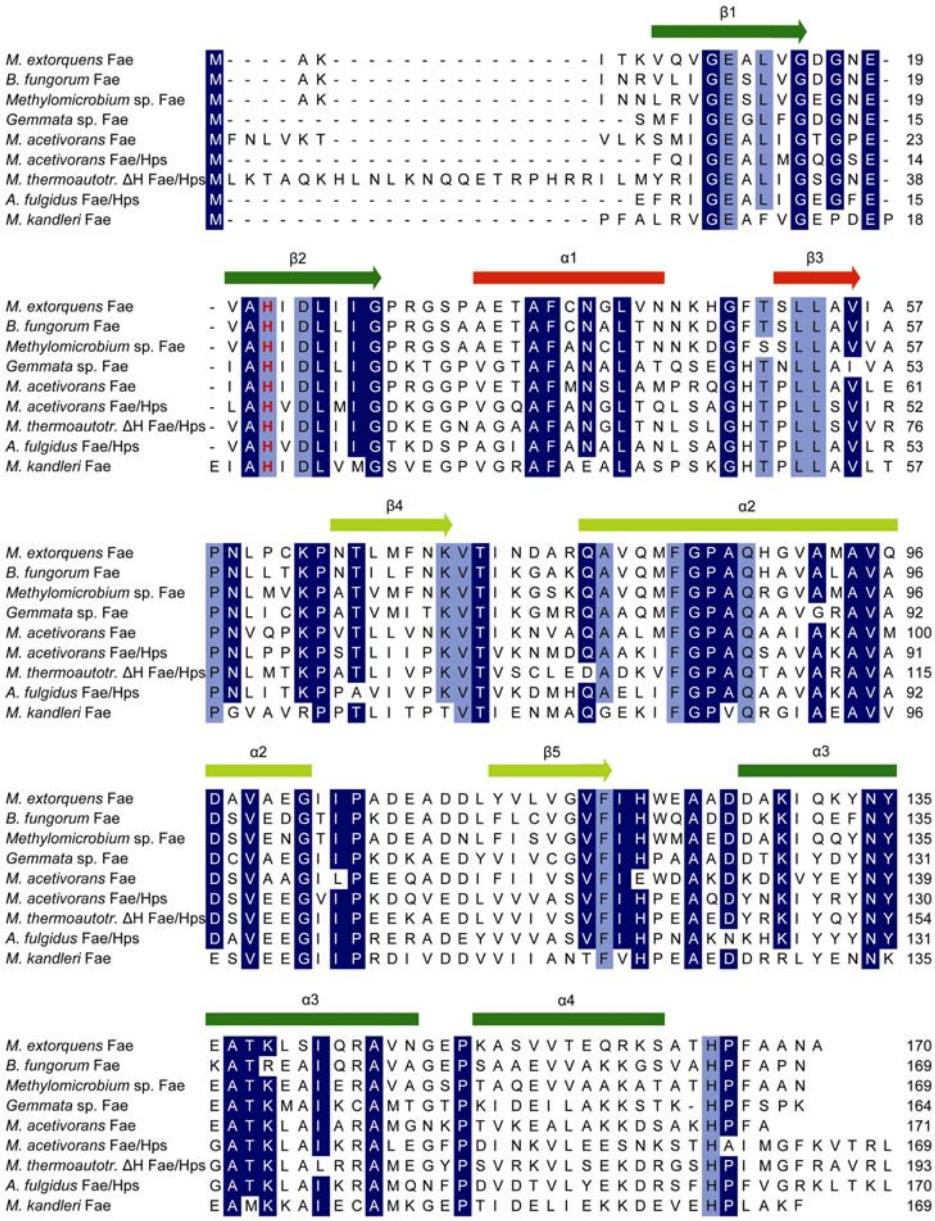

between two adjacent subunits called A and B (Figures 2 and 3A). The amino acid residues forming the cleft are highly conserved (Figure 3A and B). The bottom of this cleft is composed of strands β2 and β4 of subunit A and strand β3 of subunit B. The wall of the cleft constituted by subunit A is built up by strands β1, β2 and β5 and the loop following strand β4, whereas the wall made by subunit B consists essentially of helix α2 and the following loop (Figure 2A). The roof of the cleft is built up by the mentioned protrusion at the end of strand β3 of subunit B and of the C-terminal segment of subunit A. Upon methylene-H_4MPT binding the width of the cleft is slightly decreased due to a rotation of helix α2 of about 5° and to a displacement of strands β1, β2 and β5 in the range 0.3 - 0.5 Å. Additionally, the flexible C-terminal arm of subunit A (A160-A166) is rigidified and the protrusion of subunit B is shifted around 2 Å towards the coenzyme.

Conformation of methylene-H_4MPT when bound to Fae

Methylene-H_4MPT binds to the binding cleft with a high occupancy (about 80%), derived from comparison between the temperature factors of the pterin ring and surrounding side chains. However, the temperature factor increased dramatically from the pterin and imidazolidine rings (30 $Å^2$), via the benzene ring (38 $Å^2$), the ribitol group (50 $Å^2$), the ribose group (68 $Å^2$) to the phosphate group (78 $Å^2$) indicating an excellent electron density of the functionally relevant head group and partially of the ribitol group. The 2-hydroxyglutarate group is located in the bulk solvent and is not visible in the electron density map (Figure 4). Note that Fae from *M. extorquens* AM1 was crystallised together with H_4MPT from *M. marburgensis* rather than with H_4MPT from *M. extorquens* AM1, which lacks the phosphate and the 2-hydroxyglutarate group (Chistoserdova *et al,* 1998).

Methylene-H_4MPT is accommodated into its binding site in an 'S'-shaped conformation, the 'S' being positioned perpendicular to the front side of the cleft (Figure 4). The pterin ring points towards the channel bottom, the imidazolidine ring and the phenyl ring are attached roughly parallel to the length of the cleft and the ribose and phosphate groups are directed towards the bulk solvent. The 'S'-shape of methylene-H_4MPT is the result of two kinks (Figure 4). The first sharp kink of about 70° is located between the pterin and the imidazolidine rings around the N^5-C^{6a} bond. An additional small rotation between the imidazolidine and the phenyl rings results in a nearly perpendicular orientation between the pterin and the phenyl ring. The second kink of roughly 90° is performed within the ribitol group. This conformation of methylene-H_4MPT implicates that solely the pterin ring is shielded from bulk solvent by the described roof. The rest of the methylene-H_4MPT inclusive the imidazolidine ring is at least partly solvent accessible.

The conformation of methylene-H_4MPT in the Fae-methylene-H_4MPT complex (this work) is different from the conformations of methylene-H_4MPT in solution or when bound to H_2-forming methylene-H_4MPT dehydrogenase (Hmd), which have previously been determined by two-dimensional NMR spectroscopy (Bartoschek *et al,* 2001). The major conformational surprise of methylene-H_4MPT in Fae is the large kink angle of about 70° between the pterin and the imidazolidine ring that is in solution only 50° and when bound to Hmd only 40° (Figure 5). This remarkable change necessitates a different conformations of the *sp3* configurated C^{6a} and C^{7a} atoms of the tetrahydropyrazine ring. The C^{6a} atom has to point to the *Si*-face in Fae but

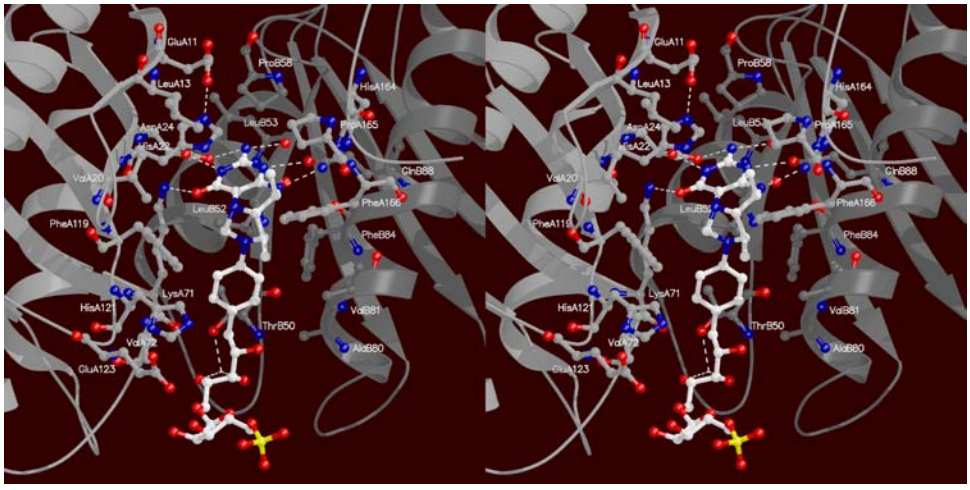

Figure 4 Stereoview of the polar interactions between the protein scaffold of Fae and methylene-H_4MPT. The model is depicted in a ball-and-stick representation (carbons of methylene-H_4MPT in white, carbons of the polypeptide of subunit A in light grey, carbons of the polypeptide of subunit B in grey, oxygen in red, nitrogen in blue, and phosphorus in yellow). Specific polar contacts between the protein and the H_4MPT tail are only formed to the ribitol OH^{3c} and OH^{4c} groups but not to the ribose OH^{3d} group and the phosphate This figure was generated with MOLSCRIPT (Kraulis 1991) and RASTER3D (Merrit and Murphy 1994).

to the *Re*-face in solution and when bound to Hmd. Consequently, atom C^{7a} of methylene-H_4MPT bound to Fae is oriented to the *Re*-face orientation that leads to a conformation of the C^{13a} atom perpendicular to the pterin ring whereas the *Si*-face orientation leads to an equatorial position as found in the free and Hmd bound form (Figure 5). Obviously, the protein scaffold of Fae substantially influences the conformation of methylene-H_4MPT upon binding. For example, methylene-H_4MPT in the conformation found in solution would interfer with PheA166 of Fae that could not evade due to its contact to ValB81. A related conformational variability of the kink is expected for methylene-H_4F dependent enzymes, although an enzyme-methylene-H_4F complex is, so far, not structurally characterized.

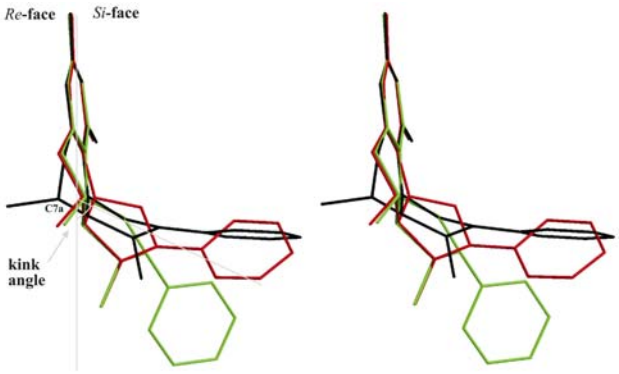

Figure 5 Conformational diversity of methylene-H_4MPT. Structural alignment of methylene-H_4MPT bound to Fae (black), to H_2-forming methylene-H_4MPT dehydrogenase (green) and in solution (red). The superposition is based on the pyrimidine ring and atoms N^5 and N^8 of the piperidine ring.

In the crystal structure of Fae the imidazolidine ring of methylene-H_4MPT deviates only slightly from planarity and therefore the electron density at 1.9 Å resolution is not sufficient to unequivocally distinguish between different conformations. The electron density suggests a flap of N^{10} above the ring plane that is agreement with the conformation of the imidazolidine ring in the Hmd (Bartoscheck *et al,* 2001). In solution the flap at N^{10} is below the ring plane (Bartoscheck *et al,* 2001) (Figure 5).

H_4MPT from *M. marburgensis* contains 11 asymmetric carbons (Figure 1). The stereoconfiguration of five of these, of 7a, 6a, 11a, 2c and 3c (Figure 1), could be deduced from the 1.9 Å crystal structure and agreed well with stereoconfiguration of these carbons determined previously by two-dimensional NMR spectroscopy (Schleucher *et al,* 1992 and 1994). Due to the increasing flexibility between the head and the tail of methylene-H_4MPT when bound to Fae, the stereoconfiguration of the four ribose carbons and of carbon 2e (Figure 1) could not be resolved.

Interactions between Fae and methylene-H_4MPT

The increasing flexibility along the elongated molecule is reflected in a parallel decrease of the protein-cofactor interactions. Only two hydrogen bonds and a few van der Waals contacts are formed between the protein matrix and the tail groups of H_4MPT (Figure 4). In other words binding is essentially based on interactions between the polypeptide chain and the catalytically relevant head groups. The conserved residues AspA24, LysA71, LeuB53 and GlnB88 form specific hydrogen bond interactions towards the N^1, NH_2^{2a}, N^3H and O^{4a} atoms (Figure 4). The head groups including the imidazole group of HisA22 are encircled by two hydrophobic belts one above and the other below the pterin ring. The first belt includes PheA119, ValA20, LeuA13, ProB58, ProA165 and PheA166; the second belt contains ValA72, PheA119, the hydrophobic portions of LysA71 and ThrB50, LeuB52, PheB84, ValB81 and AlaB80. The two belts partly touch each other and are opened at the frontside of the cleft, the shortest distances of about 7.5 Å being between PheA119 and PheA166 and between ValA72 and AlaB80. This entrance provides access to the catalytically relevant N^5, N^{10} and C^{14a} atoms of the imidazolidine ring. Of particular importance for the adjustment of the ring conformations are HisA22 and LeuB52 sandwiching the pterin ring and LeuB52 and PheB84 that are positioned in the groove between the pterin, imidazolidine and phenyl rings (Figure 4). Interestingly, the methyl groups of methylene-H_4MPT not present in methylene-H_4F (Figure 1) mainly interact with invariant hydrophobic side chains of the C-terminal arm. Atom C^{12a} is in contact with PheA166 and atom C^{13a} with HisA164, PheA166 and ProB58 the latter protruding from the described protrusion at the end of strand β3.

Interestingly, the binding site of methylene-H_4MPT can not be considered as prebuilt. In the empty enzyme PheA119, PheB84 and HisA22 point into the coenyzme binding site but evade the arriving methylene-H_4MPT by movements up to 5 Å thereby inducing many additional conformational changes. For example, the rotation of PheA119 induces substantial rearrangements of the side chains of HisA121 and GluA123 and allows LysA71 to partially fill out the generated free place. Likewise, PheB84 swings towards the channel bottom accompanied by a shift of LeuB52 to the *Re*-side of the pterin ring that induce a movement of ThrB50 of 1.9 Å. The Oγ1 atom is now connected to the ribitol oxygens OH^{3c} and OH^{4c} via a water molecule. Upon H_4MPT binding HisA22 moves about 2Å up towards the described protrusion accompanied by a conformational change of LeuA13. Due to these complex side chain rearrangements a modeling of methylene-H_4MPT is not possible.

Selectivity of Fae for methylene-H_4MPT rather than for methylene-H_4F

Fae catalyses the reaction of formaldehyde with H_4MPT. Using the same assay a formation of methylene-H_4F from formaldehyde and H_4F was not observed (Vorholt *et al,* 2000). Fae activity was measured by following the formation of methylene-H_4MPT from formaldehyde and H_4MPT spectrophotometrically exploiting the fact that methylene-H_4MPT and H_4MPT have different UV spectra. The difference is much smaller in case of methylene-H_4F and H_4F, which is why it is difficult to exclude via the photometric assay that Fae can catalyse methylene-H_4F formation at low catalytic efficiency. The specificity of Fae for H_4MPT is, however, indicated by the finding that the rate of condensation of formaldehyde and H_4MPT was not inhibited by the addition of an excess of H_4F (unpublished results).

This finding needs discussion as except for two methyl groups H_4MPT and H_4F only differ in their tail groups but, as described, the ribitol, ribose and phosphate groups of methylene-H_4MPT appears to contribute only slightly to binding (Figures 4). Although these few interactions as well as an interference between the protein and the formylglutamate tail groups in H_4F might be crucial for selectivity the structural data support a binding mechanism that attributes a key function to the additional methyl groups (Figure 6). Accordingly, three of four van der Waals contacts between the methyl groups are formed to side chains of the C-terminal arm that might contribute to its partial fixation. A simultaneous conformational change of several side chains at the *Re*-side of H_4MPT generates a hydrophobic cluster composed of the tetrahydropyrazine and the imidazolidine rings, LeuA13, HisA164, ProA165, PheA166 and ProB58 and most interestingly triggers an inversion of the amide group of GlnB88. This exchange of the amide oxygen and amine groups is the prerequisite to form two hydrogen bonds to methylene-H_4MPT and one hydrogen bond to HisA164 of the C-terminal arm (Figure 6). Thus, preferred binding of H_4MPT against H_4F is not only accomplished by the quantitatively small van der Waals interactions between the methyl groups and the protein but by an induced cooperative process that enhances both methylene-H_4MPT binding and the fixation of the C-terminal arm. The interactions between the C-terminal arm and the methyl groups of methylene-H_4MPT might additionally influence the kink angle between the pterin and imidazolidine rings and thus the binding energy between methylene-H_4MPT and Fae.

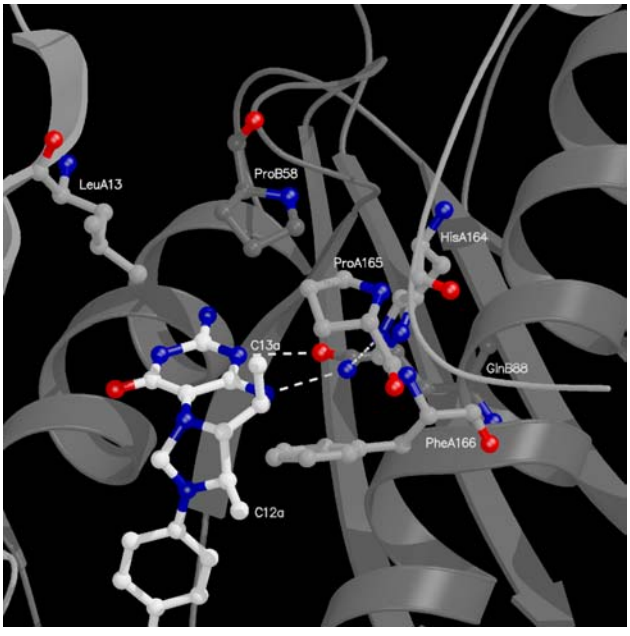

Figure 6 View into the active site of Fae highlighting the interactions between the methyl groups 12a and 13a of methylene-H_4MPT and the protein. For details of representation see the legend to Figure 4.

Formaldehyde binding site and enzymatic mechanism

Attempts to determine a structure of Fae in complex with formaldehyde failed but an attractive binding site of the substrate is offered by the structure of the Fae-methylene-H_4MPT complex. At first glance, an activation of formaldehyde by the amine group of LysA171 appears to be chemically plausible as a conformational change of the side chain could bring the bound formaldehyde in front of the N^5 atom (Figure 4). However, a structural analysis rejects this possibility as LysA171 is fixed in its position by a large number of hydrogen bonds and van der Waals interactions and no space is available for formaldehyde binding without pushing H_4MPT out of its binding site. More attractively, a site either occupied with a solvent molecule or an unknown molecule (depending on the considered cleft of the asymmetric unit) is positioned parallel to the imidazolidine ring and accessible from bulk solvent. Furthermore, the oxygen atom of formaldehyde can be modeled into the site of the solvent molecule or into a protrusion of the electron density of the unknown molecule being about 4 Å apart from the N^5 atom of methylene-H_4MPT and 3 Å apart from the Nδ1 atom of the highly conserved HisA22. Despite of its fairly hydrophobic environment HisA22 is probably protonated as its Nε2 atom donates a hydrogen bond to the negatively charged Oε1 atom of GluA11 (Figure 4). Assuming the oxygen atom as fixed, the methylene group of formaldehyde can be placed in front of the N^5 atom the distance of 3 Å being optimal for a nucleophilic attack. In this way the formaldehyde binding site is approximately defined.

On the basis of the proposed formaldehyde position and of an assumed similarity between the conformation of H_4MPT and the observed methylene-H_4MPT a catalytic mechanism was outlined that essentially consists of a nucleophilic addition and a nucleophilic substitution reaction (Figure 7). First, the nucleophilic N^5 atom attacks the carbonyl carbon of formaldehyde thereby forming a tetrahedral anionic intermediate state that become

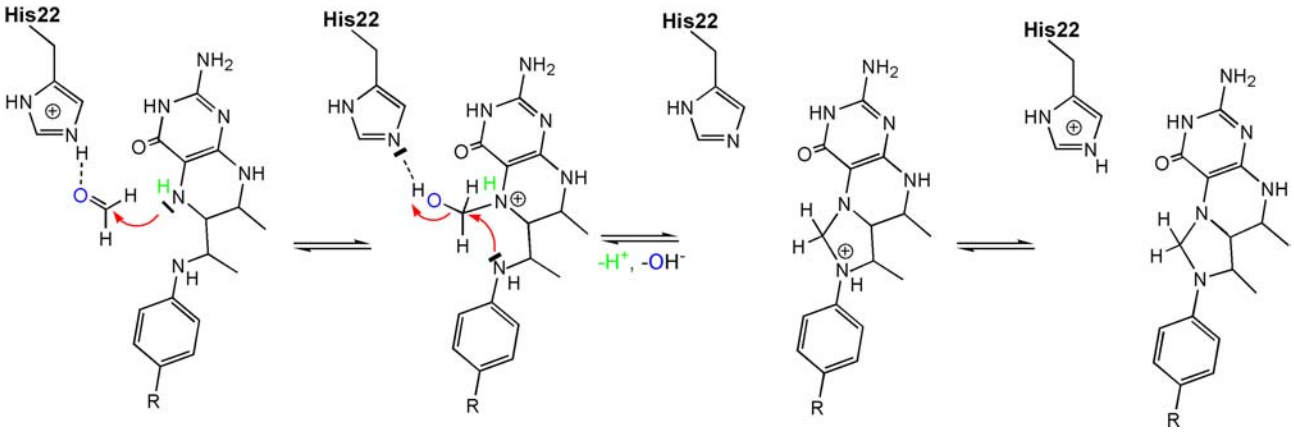

Figure 7 Proposed mechanism of methylene-H_4MPT formation from formaldehyde and H_4MPT. The reaction can be subdivided in a nucleophilic addition and a nucleophilic substitution process. A key function in formaldehyde activation and catalysis is attributed to HisA22, which is highly conserved (see Figure 3B).

protonated by HisA22. The positively charged HisA22 enhances the electrophilic properties of the carbonyl carbon of formaldehyde and serves as general acid catalyst thereby playing a key role in the formaldehyde activation process. After formation of the hydroxymethylene-H_4MPT adduct the N^5 nitrogen become presumably deprotonated (Figure 7). Second, the N^{10} atom nucleophilically attacks the hydroxymethylene carbon atom and the hydroxylate group is concomitantly released. HisA22 might be already reprotonated prior to hydroxylate release and acts again as hydrogen donor. After deprotonating of the N^{10} atom the product methylene-H_4MPT is generated. This mechanism is in agreement with the results of kinetic experiments of spontaneous methylene-H_4F formation from H_4F and formaldehyde (Kallen and Jencks 1966a, b and c). The spontaneous reaction proceeds optimally under acidic conditions indicating that a protonation step is involved. Most likely, in the enzyme, the proton for this step is provided by protonated HisA22.

Conclusions

In conclusion, we can state that we have not only determined the first structure of an enzyme with the cofactor H_4MPT bound to it, but also obtained insights into the mechanism of how the highly toxic intermediate formaldehyde is converted and thus detoxified. Formaldehyde is an intermediate in methylotrophic metabolism and Fae an essential enzyme for growth in the presence of C_1-substrates in *M. extorquens* AM1. The importance of Fae for methylotrophy is also reflected by its high abundance in the cytoplasm of the cell (Laukel *et al,* 2004). A paralog of Fae with a sequence identity of 26% to Fae has also been found to be expressed in the methylotroph, evoking the question of whether the corresponding reaction of condensation of formaldehyde and H_4F might also be enzyme catalysed (Laukel *et al,* 2004).

In the crystal structure of Fae the C_1-carrier is bound in a cleft formed by two adjacent subunits of the homopentamer. Binding is characterized by several hydrogen bonds to the buried pyrimidine ring and by hydrophobic layers around the imidazolidine and phenyl rings. There are indications that this binding mode is also used in other H_4MPT specific enzymes (i.e. Grabarse *et al*, 1999). The contacting side chains of Glu11, Leu13, Val20, His22, Lys71, Val72, Phe119, Pro165 and Phe166 from the one subunit and of Thr50, Leu52, Pro58, Ala80, Val81, Phe84 and Gln88 from the adjacent subunit are conserved in Fae from different organisms (Figure 3b) but not in any of the other H_4MPT specific enzymes. A common binding motif for the C_1-carrier was not found. This was also not to be expected since the known H_4MPT specific enzymes are not similar neither on the level of their primary structure nor on the level of their secondary-, tertiary- and quarternary structures. This also holds true for the different H_4F specific enzymes, which also do not show a common H_4F binding motif.

Materials and Methods

Methylobacterium extorquens AM1 is the strain deposited under DSM 1338 in the Deutsche Sammlung von Mikroorganismen und Zellkulturen (Braunschweig).

Heterologous expression of the fae gene in E. coli

Amplification of the *fae* gene was achieved with Expand-DNA-polymerase (Roche Diagnostics), the primers (MWG) 5'-GAGACCCCATATGGCAAAAATCACCAAGGTTC-3' (sense; the *Nde*I site is underlined) and 5'-CTGCCCAGGAATTCCTCCGATCTAAGCGTT-3' (antisense; the *Eco*RI site is underlined), and chromosomal DNA of *M. extorquens* AM1 as a template. The PCR product was digested with *Nde*I and *Eco*RI and ligated into the pET17b expression vector previously digested with the same restriction enzymes, and then introduced into *E. coli* BL21 (DE3) pLysS. Sequencing

of the *fae* gene cloned into pET17b revealed no mutation. Each transformant of *E. coli* BL21 (DE3) pLysS was grown aerobically at 37°C on minimal medium M9 (Sambrook *et al,* 1989) supplemented with ampicillin (100 µg ml^{-1}) and chloramphenicol (50 µg ml^{-1}). When the ΔOD_{600} of the culture reached 0.5, cells were induced by 2 mM isopropyl-β-D-thiogalactopyranoside. After 4 h, the cells were harvested by centrifugation at 4200*g* at 4°C.

Selenomethionine-labeled protein was produced using the method of metabolic inhibition as described in Doublie (1997) and van Duyne *et al,* (1993).

Purification

Non-labeled Fae and selenomethionine-labeled protein were purified under aerobic conditions as described in Vorholt *et al,* (2000) for formaldehyde-activating enzyme (Fae) from *M. extorquens* AM1. Protein concentrations were determined by the Bradford assay (Bradford 1976) by using the BioRad reagent with bovine serum albumin as a standard. Fae activity was performed at 30°C and pH 8 as described in Vorholt *et al,* (2000).

H_4MPT was purified from *Methanothermobacter marburgensis* (DSM 2133) (Breitung *et al,* 1992). Anoxic stock solutions of H_4MPT were prepared in 10 mM MOPS/KOH buffer pH 7.

Crystallisation and data collection

Crystallisation trials were performed with non-labeled and selenomethionine-labeled Fae at 4°C under aerobic conditions and with enzyme in the presence of H_4MPT at 8ºC under strictly anaerobic conditions. Within a hanging drop experiment each drop consisted of 1 µl of enzyme solution (13 mg/ml) and 1 µl of reservoir solution. Crystals of non-labeled Fae as well as selenomethionine-labeled Fae grew in a reservoir solution composed of 0.2 M calciumchloride x $2H_2O$, 0.1 M sodium acetate x $3H_2O$ pH 4.6 and 10-20% (v/v) isopropanol. Their space group was $P4_32_12$ and the lattice parameters were a = b = 120.8 Å and c = 206.8 Å indicating the presence of 5 to 10 monomers in the asymmetric unit. For crystallisation in the presence of H_4MPT, the enzyme solution (13 mg/ml) was supplemented with 5 mM H_4MPT and then combined with the reservoir solution containing 0.1 M HEPES/NaOH pH 7.5 and 20% (w/v) polyethyleneglycol 10,000. The space group was $P2_1$ and the lattice parameters were a = 48.9 Å, b = 112.6 Å, c = 72.0 Å and $\alpha,\gamma = 90^{\circ}$, $\beta = 91.6^{\circ}$, which is most compatible with 5 monomers per asymmetric unit.

Data were collected at ID14-4 and ID29 beamlines at the European Synchrotron Radiation Facility (ESRF), Grenoble (Table 1). Processing and scaling were performed with XDS (Kabsch 1988) and Denzo/Scalepack (Otwinowski and Minor 1997).

Phase determination and refinement

Phases were determined using the multiple anomalous wavelength dispersion method with selenium as anomalous scatterer. The selenium sites were found using SHELXD (Schneider and Sheldrick 2002) and further refined using SHARP (de la Fortelle and Bricogne 1997). The phases were calculated with SHARP and improved by solvent flattening (Abrahams and Leslie 1996) assuming a solvent content of 70%. Fivefold molecular averaging within DM (Cowtan 1994) resulted in an excellent electron density map where about 80% of the chain could be traced by the automated model building program MAID (Levitt 2001). Except for 10 residues at the C-terminal end the residual model could be manually incorporated using O (Jones *et al*, 1991). Iterative cycles of refinement and manual model building were carried out using the programs in CNS (Brünger *et al*, 1998) and O. The refinement statistics are given in Table 1. The structure of the H_4MPT-bound enzyme was solved by molecular replacement using the program EPMR (Kissinger *et al*, 1999) with the coordinates of Fae without bound substrate as the search model. After initial refinement the C-terminal amino acids disordered in the coenzyme free structure and H_4MPT later replaced by methylene-H_4MPT were modelled into the density. The results of the refinement are listed in Table 1. The quality of the models was checked with PROCHECK (Laskowski *et al,* 1993).

Acknowledgements

This work was supported by the Max-Planck-Gesellschaft, by the DFG and by the Fonds der Chemischen Industrie. Meike Goenrich thanks the Claussen-Simon-Stiftung for a graduate fellowship. We thank Hartmut Michel for continuous support and the staff of the beamlines ID29 and ID14-4 at ESRF for help during data collection.

References

Abrahams JP, Leslie, AGW (1996) Methods used in the structure determination of bovine mitochondrial F_1 ATPase. *Acta Crystallogr D* **52**: 30-42

Al-Karadaghi S, Aevarsson A, Garber M, Zheltonosova J, Liljas A (1996) The structure of elongation factor G in complex with GTP: conformational flexibility and nucleotide exchange. *Structure* **5**: 555-565

Bartoschek S, Buurman G, Thauer RK, Geierstanger BH, Weyrauch JP, Griesinger C, Nilges M, Hutter MC, Helms V (2001) Re-face stereospecificity of methylenetetrahydromethanopterin and methylenetetrahydrofolate dehydrogenases is predetermined by intrinsic properties of the substrate. *Chembiochem* **2**: 530-541

Boetius A, Ravenschlag K, Schubert CJ, Rickert D, Widdel F, Gieseke A, Amann R, Jorgensen BB, Witte U, Pfannkuche O (2000) A marine microbial consortium apparently mediating anaerobic oxidation of methane. *Nature* **407**: 623-626

Bradford MM (1976) A rapid and sensitive method for the quantitation of microgram quantities of protein utilizing the principle of protein-dye binding. *Anal Biochem* **72**: 248-254.

Breitung J, Börner G, Scholz S, Linder D, Stetter KO, Thauer RK (1992) Salt dependence, kinetic properties and catalytic mechanism of *N*-formylmethano-furan:tetrahydromethanopterin formyltransferase from the extreme thermophile *Methanopyrus kandleri*. *Eur J Biochem* **210**: 971-981

Brünger AT, Adams PD, Clore GM, DeLano WL, Gros P, Grosse-Kunstleve RW, Jiang JS, Kuszewski J, Nilges M, Pannu NS, Read RJ, Rice LM, Simonson T, Warren GL (1998) Crystallography & NMR system: A new software suite for macromolecular structure determination. *Acta Crystallogr D* **54**: 905-921

Buchenau B, Thauer RK (2004) Tetrahydrofolate-specific enzymes in *Methanosarcina barkeri* and growth dependence of this methanogenic archaeon on folic acid or *p*-aminobenzoic acid. *Arch Microbiol* **in press**

Bult CJ, White O, Olsen GJ, Zhou L, Fleischmann RD, Sutton GG, Blake JA, FitzGerald LM, Clayton RA, Gocayne JD, Kerlavage AR, Dougherty BA, Tomb JF, Adams MD, Reich CI, Overbeek R, Kirkness EF, Weinstock KG, Merrick JM, Glodek A, Scott JL, Geoghagen NS & Venter JC (1996) Complete genome sequence of the methanogenic archaeon, *Methanococcus jannaschii*. *Science* **273**: 1058-1073

Chistoserdova L, Jenkins C, Kalyuzhnaya MG, Marx CJ, Lapidus A, Vorholt JA, Staley JT, Lidstrom ME (2004) The enigmatic planctomycetes may hold a key to the origins of methanogenesis and methylotrophy. *Mol Biol Evol* **21**: 1234-1241

Chistoserdova L, Vorholt JA, Thauer RK, Lidstrom ME (1998) C_1 transfer enzymes and coenzymes linking methylotrophic bacteria and methanogenic archaea. *Science* **281**: 99-102

Cowtan KD (1994) 'DM': an automated procedure for phase improvement by density modification. *Joint CCP4 and ESF-EACBM Newsletter on Protein Crystallography* **31**: 83-91

De la Fortelle E, Bricogne G (1997) Maximum-likelihood heavy-atom parameter refinement for multiple isomorphous replacement and multiwavelength anomalous diffraction methods. *Methods Enzymol* **276**: 472-494

Doublie S (1997) Preparation of selenomethionyl proteins for phase determination. *Methods Enzymol.* **276**: 523-530

Ermler U, Hagemeier CH, Roth A, Demmer U, Grabarse W, Warkentin E, Vorholt JA (2002) Structure of methylene-tetrahydromethanopterin dehydrogenase from *Methylobacterium extorquens* AM1. *Structure* **10**: 1127-1137

Ermler U, Merckel M, Thauer RK, Shima S (1997) Formylmethanofuran: tetrahydromethanopterin formyltransferase from *Methanopyrus kandleri* - new insights into salt-dependence and thermostability. *Structure* **5**: 635-646

Escalante-Semerena JC, Rinehart KL Jr., Wolfe RS (1984) Tetrahydromethanopterin, a carbon carrier in methanogenesis. *J Biol Chem* **259**: 9447-9455

Esnouf RM (1999) Further additions to MolScript version 1.4, including reading and contouring of electron-density maps. *Acta Crystallogr D* **55**: 938-940

Galagan JE, Nusbaum C, Roy A, Endrizzi MG, MacDonald P, FitzHugh W, Calvo S, Engels R, Smirnov S, Atnoor D, Brown A, Allen N, Naylor J, Stange-Thomann N, DeArellano K, Johnson R, Linton L, McEwan P, McKernan K, Talamas J, Tirrell A, Ye WJ, Zimmer A, Barber RD, Cann I, Birren B (2002) The genome of *M. acetivorans* reveals extensive metabolic and physiological diversity. *Genome Res* **12**: 532-542

Gorris LGM, Voet ACWA, van der Drift C (1991) Structural characteristics of methanogenic cofactors in the non-methanogenic archaebacterium *Archaeoglobus fulgidus*. *Biofactors* **3**: 29-35

Grabarse W, Vaupel M, Vorholt JA, Shima S, Thauer RK, Wittershagen A, Bourenkov G, Bartunik HD, Ermler U (1999) The crystal structure of methenyltetrahydromethanopterin cyclohydrolase from the hyperthermophilic archaeon *Methanopyrus kandleri*. *Structure* **7**: 1257-1268

Graham DE, White RH (2002) Elucidation of methanogenic coenzyme biosyntheses: from spectroscopy to genomics. *Nat Prod Reports* **19**: 133-147

Hagemeier CH, Shima S, Thauer RK, Bourenkov G, Bartunik HD, Ermler U (2003) Coenzyme F_{420}-dependent methylenetetrahydro-methanopterin dehydrogenase (Mtd) from *Methanopyrus kandleri*: A methanogenic enzyme with an unusual quarternary structure. *J Mol Biol* **332**: 1047-1057

Hinrichs KU, Hayes JM, Sylva SP, Brewer PG, DeLong EF (1999) Methane-consuming archaebacteria in marine sediments. *Nature* **398**: 802-805

Hogan KB, Hoffman JS, Thompson AM (1991) Methane on the greenhouse agenda. *Nature* **354**: 181-182

Holm L, Sander C (1993) Protein structure comparison by alignment of distance matrices. *J Mol Biol* **233**: 123-138

Jones TA, Zou JY, Cowan SW, Kjeldgaard M (1991) Improved methods for binding protein models in electron density maps and the location of errors in these models. *Acta Crystallogr A* **47**: 110-119

Kabsch W (1988*)* Evaluation of single-crystal X-ray diffraction data from a position-sensitive detector. *J Appl Cryst* **21**: 916-924

Kallen RG, Jencks WP (1966a) The dissociation constants of tetrahydrofolic acid. *J Biol Chem* **241**: 5845-5850

Kallen RG, Jencks WP (1966b) The mechanism of the condensation of formaldehyde with tetrahydrofolic acid. *J Biol Chem* **241**: 5851-5863

Kallen RG, Jencks WP (1966c) Equilibria for the reaction of amines with formaldehyde and protons in aqueous solution. A re-examination of the formol titration. *J Biol Chem* **241**: 5864-5878

Kissinger CR, Gehlhaar DK, Fogel DB (1999) Rapid automated molecular replacement by evolutionary search. *Acta Crystallogr D* **55**: 484-491

Klenk HP, Clayton RA, Tomb JF, White O, Nelson KE, Ketchum KA, Dodson RJ, Gwinn M, Hickey EK, Peterson JD, Richardson DL, Kerlavage AR, Graham DE, Kyrpides NC, Fleischmann RD, Quackenbush J, Lee NH, Sutton GG, Gill S, Kirkness EF, Dougherty BA, McKenney K, Adams MD, Loftus B, Venter JC (1997) The complete genome sequence of the hyperthermophilic, sulphate-reducing archaeon *Archaeoglobus fulgidus*. *Nature* **390**: 364-70

Kraulis PJ (1991) MOLSCRIPT: a program to produce both detailed and schematic plots of protein structures. *J Appl Cryst* **24**: 946-950

Krüger M, Meyerdierks A, Glockner FO, Amann R, Widdel F, Kube M, Reinhardt R, Kahnt J, Bocher R, Thauer RK, Shima S (2003) A conspicuous nickel protein in microbial mats that oxidize methane anaerobically. *Nature* **426**: 878-881

Laskowski RA, MacArthur MW, Moss DS, Thornton JM (1993) PROCHECK: a program to check the stereochemical quality of protein structures. *J Appl Cryst* **26**: 283-291

Laukel M, Rossignol M, Borderies G, Völker U, Vorholt JA (2004) Comparison of the proteome of *Methylobacterium extorquens* AM1 grown under methylotrophic and nonmethylotrophic conditions. *Proteomics* **4**: 1247-1264

Levitt DG (2001) A new software routine that automates the fitting of protein X- ray crystallographic electron-density maps. *Acta Crystallogr D* **57**: 1013-1019

Lienard T, Becher B, Marschall M, Bowien S, Gottschalk G (1996) Sodium ion translocation by N-5-methyltetrahydromethanopterin-coenzyme M methyltransferase from *Methanosarcina mazei* GO1 reconstituted in ether lipid liposomes. *Eur J Biochem* **239**: 857-864

Maden BEH (2000) Tetrahydrofolate and tetrahydromethanopterin compared: functionally distinct carriers in C_1 metabolism. *Biochem J* **350**: 609-629

Mamat B, (2002) Ph.D. thesis. Johann Wolfgang Goethe-Universität, Frankfurt/Main (Germany)

Mamat B, Roth A, Grimm C, Ermler U, Tziatzios C, Schubert D, Thauer RK, Shima S (2002) Crystal structures and enzymatic properties of three formyltransferases from archaea: environ-mental adaptation and evolutionary relationship. *Prot Science* **11**: 2168-2178

Marx CJ, Miller JA, Chistoserdova L, Lidstrom ME (2004) Multiple formaldehyde oxidation/detoxification pathways in *Burkholderia fungorum* LB400. *J Bacteriol* **186**: 2173-2178

Merritt EA, Murphy MEP (1994) Raster3d Version-2.0 - a Program for Photorealistic Molecular Graphics. *Acta Crystallogr D* **50**: 869-873

Michaelis W, Seifert R, Nauhaus K, Treude T, Thiel V, Blumenberg M, Knittel K, Gieseke A, Peterknecht K, Pape T, Boetius A, Amann R, Jorgensen BB, Widdel F, Peckmann J, Pimenov NV, Gulin MB (2002) Microbial reefs in the Black Sea fueled by anaerobic oxidation of methane. *Science* **297**: 1013-1015

Nicholls A, Bharadwaj R, Honig B (1993) GRASP: graphical representation and analysis of surface properties. *Biophys J* **64**: 166-170

Otwinowski Z, Minor W (1997) Processing of X-ray diffraction data collected in oscillation mode. *Methods Enzymol* **276**: 307-326

Poe M, Benkovic SJ (1980) 5-Formyl- and 10-formyl-5,6,7,8-tetrahydrofolate. Conformation of the tetrahydropyrazine ring and formyl group in solution. *Biochemistry* **19**: 4576-4582

Ramakrishnan V, White SW (1992) The structure of ribosomal protein S5 reveals sites of interaction with 16S rRNA. *Nature* **358**: 768-771

Romanowski MJ, Bonanno JB, Burley SK (2002) Crystal structure of the *Streptococcus pneumoniae* phosphomevalonate kinase, a member of the GHMP kinase superfamily. *Proteins* **47**: 568-571

Schleucher J, Griesinger C, Schworer B, Thauer RK (1994) H_2 forming N^5,N^{10} -methylenetetrahydromethanopterin dehydrogenase from *Methanobacterium thermoautotrophicum* catalyzes a stereoselective hydride transfer as determined by 2-dimensional NMR spectroscopy. *Biochemistry* **33**: 3986-3993

Schleucher J, Schwörer B, Zirngibl C, Koch U, Weber W, Egert E, Thauer RK, Griesinger C (1992) Determination of the relative configuration of 5,6,7,8-tetrahydromethanopterin by two-dimensional NMR spectroscopy. *FEBS Let* **314**: 440-444.

Sambrook J, Fritsch EF, Maniatis TL (1989) *Molecular Cloning: A Laboratory Manual.* Cold Spring Harbour Press, Cold Spring Harbour, New York, USA

Schneider TR, Sheldrick GM (2002) Substructure solution with SHELXD. *Acta Crystallogr D* **58**: 1772-1779

Shima S, Warkentin E, Grabarse W, Sordel M, Wicke M, Thauer RK, Ermler U (2000) Structure of coenzyme F_{420}-dependent methylenetetrahydro-methanopterin reductase from two methanogenic archaea. *J Mol Biol* **300**: 935-950

Slesarev AI, Mezhevaya KV, Makarova KS, Polushin NN, Shcherbinina OV, Shakhova VV, Belova GI, Aravind L, Natale DA, Rogozin IB, Tatusov RL, Wolf YI, Stetter KO, Malykh AG, Koonin EV, Kozyavkin SA (2002) The complete genome of hyperthermophile *Methanopyrus kandleri* AV19 and monophyly of archaeal methanogens. *Proc Natl Acad Sci* USA **99**: 4644-4649

Smith DR, Doucette-Stamm LA, Deloughery C, Lee H, Dubois J, Aldredge T, Bashirzadeh R, Blakely D, Cook R, Gilbert K, Harrison D, Hoang L, Keagle P, Lumm W, Pothier B, Qiu D, Spadafora R, Vicaire R, Wang Y, Wierzbowski J, Gibson R, Jiwani N, Caruso A, Bush D, Reeve JN (1997) Complete genome sequence of *Methanobacterium thermoautotrophicum* ΔH: functional analysis and comparative genomics. *J Bacteriol* **179**: 7135-7155

Thauer RK (1998) Biochemistry of methanogenesis: a tribute to Marjory Stephenson. *Microbiology* **144**: 2377-2406

Thauer RK, Klein AR, Hartmann GC (1996) Reactions with molecular hydrogen in microorganism – evidence for a purely organic hydrogenation catalyst. *Chem Rev* **96**: 3031-3042

Thauer RK, Kunow J (1995) Sulfate-Reducing Archaea. In *Sulfate Reducing Bacteria*, Barton LL (ed) pp 33–48. Plenum Press New York and London

van Beelen P, van Neck JW, de Cock RM, Vogels GD, Guijt W, Haasnoot CAG (1984) 5,10-Methenyl-5,6,7,8-tetrahydromethanopterin, a one-carbon carrier in the process of methanogenesis. *Biochemistry* **23**: 4448-4454

van Duyne GD, Standaert RF, Karplus PA, Schreiber SL, Clardy J (1993) Atomic structures of the human immunophilin FKBP-12 complexes with FK506 and rapamycin. *J Mol Biol* **229**: 105-124

Vorholt JA (2002) Cofactor-dependent pathways of formaldehyde oxidation in methylotrophic bacteria. *Arch Microbiol* **178**: 239-249

Vorholt JA, Chistoserdova L, Lidstrom ME, Thauer RK (1998) The NADP-dependent methylene tetrahydromethanopterin dehydrogenase in *Methylobacterium extorquens* AM1. *J Bacteriol* **180**: 5351-5356

Vorholt JA, Chistoserdova L, Stolyar SM, Thauer RK, Lidstrom ME (1999) Distribution of tetrahydromethanopterin-dependent enzymes in methylotrophic bacteria and phylogeny of methenyl tetrahydromethanopterin cyclohydrolases. *J Bacteriol* **181**: 5750-5757

Vorholt JA, Kunow J, Stetter KO, Thauer RK (1995) Enzymes and coenzymes of the carbon monoxide dehydrogenase pathway for autotrophic CO_2 fixation in *Archaeoglobus lithotrophicus* and the lack of carbon monoxide dehydrogenase in the heterotrophic *A. profundus*. *Arch Microbiol* **163**: 112-118

Vorholt JA, Marx CJ, Lidstrom ME, Thauer RK (2000) Novel formaldehyde-activating enzyme in *Methylobacterium extorquens* AM1 required for growth on methanol. *J Bacteriol* **182**: 6645-6650

Vorholt JA, Thauer RK (1997) The active species of CO_2 utilized by formylmethanofuran dehydrogenase from methanogenic archaea. *Eur J Biochem* **248**: 919-924

White RH (2001) Biosynthesis of the methanogenic cofactors. Vitamins and hormones – Advances in research and applications. Cofactor biosynthesis: a mechanistic perspective. **61**: 299-337

Danksagung

Mein besonderer Dank gilt vor allem Prof. Dr. Rudolf K. Thauer für die Überlassung des interessanten Themas, die fachliche und persönliche Betreuung und für das mir geschenkte Vertrauen.

Assist. Prof. Dr. Evert Duin und Dr. Felix Mahlert danke ich für die hervorragende Zusammenarbeit am MCR-Projekt. Gerade zu Beginn der Arbeit waren sie eine wertvolle Hilfe, um mir den Einstieg in die komplexe Thematik zu ermöglichen. Darüber hinaus hätte die Arbeit ohne deren tatkräftige Unterstützung und die vielen Diskussionen in dieser Form nicht entstehen können.

Bei Prof. Dr. Bernhard Jaun, Prof. Dr. Arthur Schweiger, Dr. Carsten Bauer, Dr. Jeffrey Harmer, Rafal Piskorski und Cinzia Finazzo von der ETH-Zürich möchte ich mich nicht nur für die Synthese zahlreicher Substratanaloga und der Messung von ENDOR- und HYSCORE-Spektren, sondern auch für die Vermittlung der chemischen Sichtweise auf das MCR-Projekt und die stete Diskussionsbereitschaft bedanken.

Einen besonderen Dank auch an PD Dr. Ulrich Ermler, Dr. Priyamvada Acharya und Ulrike Demmer am Max-Planck-Institut für Biophysik in Frankfurt/Main, durch deren beständigen Einsatz bei der röntgenspektroskopischen Aufklärung der Kristallstrukturen von Fae aus *Methylobacterium extorquens* AM1 dieses Projekt nach fast vier Jahren zu einem erfolgreichen Abschluß gebracht werden konnte.

Im Rahmen dieses Fae-Projekts und darüber hinaus danke ich Dr. Christoph Hagemeier für die vielen fachlichen Ratschläge und die Hilfsbereitschaft bei Fragen und Problemen jeder Art.

Bedanken möchte ich mich bei PD Dr. Julia A. Vorholt-Zambelli und Dr. Markus Laukel für den stetigen Fluß an Fae-relevanten Informationen und dem großen Interesse am Vorankommen der diesbezüglichen Projekte.

Großer Dank gebührt Reinhard Böcher, Horst Henseling, Dr. Manfred Irmler, Jörg Kahnt, Manuela Kauß, Jürgen Koch, Steffi Lindow, Johanna Moll, Dr. Antonio Pierik und Monika Schmidt, die mir alle immer wieder bei vielen kleinen und großen Problemen hilfreich zur Seite standen.

Insbesondere Bärbel Buchenau, Andrea Graff und allen Mitgliedern der Arbeitsgruppen Thauer, Hedderich und Shima danke ich für die freundschaftliche Unterstützung und das angenehme Arbeitsklima.

Bei der Claussen-Simon-Stiftung bedanke ich mich für die finanzielle Förderung dieser Arbeit.

Herzlich danken möchte ich meinen Eltern, Geschwistern und Freunden, die mich immer unterstützt haben und jederzeit für mich da waren.

Thomas danke ich für die liebevolle Begleitung durch alle Höhen und Tiefen während der Doktorarbeit.

Lebenslauf

Persönliche Daten:

Name:	Meike Maria Goenrich
Geburtstag:	11. Mai 1977
Geburtsort:	Hanau
Familienstand:	ledig

Schulbildung:

08/1983 bis 06/1987	Grund- und Hauptschule Gründau/Rothenbergen
07/1987 bis 07/1993	Kreisrealschule Gelnhausen
07/1993 bis 06/1996	Grimmelshausen Gymnasium Gelnhausen

Hochschulbildung:

10/1996 bis 09/2004	Philipps-Universität Marburg (Fachrichtung Biologie)
10/2000	Diplomprüfung in den Fächern Mikrobiologie, Genetik und Virologie/Biochemie
11/2000 bis 07/2001	Anfertigung der Diplomarbeit am Max-Planck-Institut für terrestrische Mikrobiologie in Marburg unter Anleitung von Dr. J. A. Vorholt-Zambelli. Thema: „Die Formaldehyd-aktivierenden Enzyme Fae und Gfa in methylotrophen Proteobakterien“
10/2001 bis 09/2004	Anfertigung der Doktorarbeit am Max-Planck-Institut für terrestrische Mikrobiologie in Marburg unter Anleitung von Prof. Dr. R. K. Thauer (Stipendium der Claussen-Simon-Stiftung). Thema: „Untersuchungen zum Katalysemechanismus von Methyl-Coenzym M Reduktase aus methanogenen Archaea“

Hiermit versichere ich, daß ich die vorliegende Arbeit selbstständig verfasst, keine anderen als die angegebenen Hilfsmittel verwendet und sämtliche Stellen, die im Wortlaut oder Sinn nach anderen Werken entnommen sind, mit Quellenangaben kenntlich gemacht habe. Diese Versicherung schliesst Zeichnungen und Skizzen mit ein.

Marburg, den 21. September 2004